Author:
Law, S. S

Title:
Structural integrity assessment of reinforced concrete bridge decks.

DEPARTMENT OF CIVIL ENGINEERING
UNIVERSITY OF BRISTOL

STRUCTURAL INTEGRITY ASSESSMENT OF REINFORCED CONCRETE BRIDGE DECKS

A Thesis submitted for the Degree of
Doctor of Philosophy

at

The University of Bristol
Department of Civil Engineering

by
S.S. Law, B Sc., M Ph.

April 1992

THANKS TO MY DEAR WIFE CONNIE LAM

FOR HER UNFAILING SUPPORT

WITHOUT WHICH NONE OF THIS WOULD HAVE BEEN ACHIEVED.

ABSTRACT

Recent work on the problem of localization of damage in a structure based on frequency response functions has been extended to include the phase angle as an observable parameter in the identification problem. A set of sensitivity equations has been derived to predict, from changes in the measured phase difference between response at two points of a structure, the current value of the structural stiffness in each finite element of the structure under study. This technique has been implemented with some success in the damage identification of a cantilever beam with a slot, and in the identification of a cracked diaphragm of a model reinforced concrete bridge deck.

An optimal finite element model of grillage beams representing the bridge deck has been developed. A parametric study on the effects of boundary conditions of bridge deck on the dynamic response has been carried out.

Field measurement on seventeen full-scale reinforced concrete bridge decks have been carried out for their vibrational response from traffic-generated excitation, and their modal frequencies have been studied.

A 3.2m long small scale reinforced concrete bridge deck was tested incrementally to destruction, and the vibrational response to ambient excitation at different stages of damage was studied.

A method capable of assessing the load carrying capacity of a Tee-beam and slab bridge deck was developed based on the test results of the model bridge deck. This method required only the a priori information on the geometric dimensions and the fundamental modal frequency of the structure. This method can also be used alternatively to assess the general condition of a bridge deck. Different potential sources of error in this strategy were discussed. It has been evaluated against the test results of the model bridge deck and a database of seventeen full-scale bridge decks. Good results were obtained with a maximum error in the estimate of steel percentage of -16.2%.

ACKNOWLEDGEMENTS

The author wishes to thank a number of people and parties that have helped in various ways in the completion of this research.

To Dr P Waldron and Dr C Taylor, Reader and Lecturer of the Civil Engineering Department, for providing facilities, encouragement, and support from their department.

To Dr H S Ward, former Associate Director (Research & Development) of the Hong Kong Polytechnic, a special word of thanks for his endless support and learned advice throughout.

The author is indebted to the Guangdong Communication Science Research Institute, and Mr G B Shi and Mr R Z Chen, for their support in carrying out the field measurements, providing technical drawings of the bridges and most of all, their useful discussion.

The author is indebted to Mr. Li Xun of South China University of Technology for his discussion and assistance in the field measurements and laboratory works.

Strong appreciations of the financial support given by the Research Sub-Committee of the Hong Kong Polytechnic is truly expressed.

The author wishes to thank all the technical staff of the Civil and Structural Engineering Department of the Hong Kong Polytechnic for their assistance in the laboratory work.

MEMORANDUM

The accompanying dissertation entitled "Structural Integrity Assessment of Reinforced Concrete Bridge Decks" is submitted for the degree of Doctor of Philosophy in the Faculty of Engineering at the University of Bristol.

The dissertation is based on independent work carried out by the author between June 1987 and June 1992 except the field test of full-scale bridge decks, under the supervision of Dr P Waldron and Dr C Taylor. The work and ideas are original and all contributions from others are duly acknowledged in the text by references.

This dissertation has not previously been submitted for a degree or diploma at this, or any other University of Examining Board. A part of the work has form the basis of four Conference papers and one Journal paper submitted for publication.

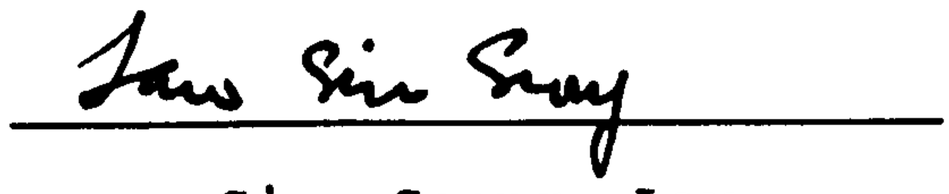

Siu Seong Law

(April 1992)

LIST OF PUBLICATION SUPPORTING THIS THESIS

The following papers basing on the work developed in this thesis have been published/submitted for publication:

1. **Law S S, Shi G B, Chen R Z and Ward H S**
   "The Vibrational Response of Reinforced Concrete Bridge Deck Before and After Rehabilitation", Proceedings of the Federation Internationale de la Precontrainte FIP '92 Symposium, Vol.1, Budapest, May 1992, pp 339-346

2. **Law S S, Ward H S, Shi G B, Chen R Z, Waldron P and Taylor C**
   "Load Carrying Capacity of Bridge Deck from Vibrational Response", Journal of Structural Engineering, ASCE, (under review)

3. **Law S S, Waldron P and Taylor C**
   "Damage Detection of a Reinforced Concrete Bridge Deck using the Frequency Response Function", Proceedings of the Tenth International Modal Analysis Conference, San Diego, California, February 1992

4. **Law S S, Ward H S, Waldron P and Taylor C**
   "Condition Monitoring of a Model Reinforced Concrete Bridge Deck in its Failure Process", Proceedings of the International Workshop on Technology for Hong Kong Infrastructure Development, Hong Kong, December 1991

5. **Law S S, Waldron P and Taylor C**
   "Phase Component of the FRF as a Tool in Structural Fault Diagnosis", Proceedings of the Asia-Pacific Vibration Conference '91, Vol. 1, Melbourne, Australia, November 1991, pp 7.22-7.29

CONTENTS

NOTATIONS

FACTORS

α Structural Damage Factor;

α_m the Reference Factor, which is the mean value of the Structural Damage Factor α of a group of bridge deck of the same span length;

β Load Carrying Capacity Factor;

β_{LS} the Reference Factor, which is the statistical average of the Load Carrying Capacity Factor β of a number of bridge decks such that the square errors in the estimates of the percentage of reinforcement of the bridge decks are minimized;

DIMENSIONS AND SECTION PROPERTIES

I_{nom} nominal cracked moment of inertia of a cross-section;

I_{max} moment of inertia of an uncracked composite beam section;

I_{est} estimate of cracked moment of inertia of a cross-section from simulation of the measured first modal frequency of the structure, and is assumed constant over the whole length of member;

I_{o1} moment of inertia of the cracked section at ultimate strength state about the neutral axis;

I_2, I_3 moment of inertia about local axis 2 and 3 of a secton;

I_t torsional moment of inertia of a section;

$[EI]_i$ flexural stiffness of the ith beam;

W_2, W_3 section modulus at centroid of tension steel and edge of flange of beam;

S_2, S_3 shear area in local axis 2 and 3 of a section;

A_1 axial area of a cross-section;

A_g area of tension reinforcement;

A'_g area of compression reinforcement;

a'_g distance between the compression reinforcement and the top of section;

b width of section or rib of Tee-beam;

b_1 effective width of flange;

b' distance between two adjacent diaphragms;

b_i width of flange on tension edge;

c outstand of flange of precast beam;

d equivalent diameter of tension reinforcement;

h overall height of section;

h_o effective height of section;

h_1 distance between the tension reinforcement to compression edge;

h_b overall height of precast section;

h_i thickness of flange on tension edge;

n modular ratio;

L span of structure;

L' distance between two adjacent beams;

t average thickness of flange;

t_o effective depth of cast-in-situ deck of beam in stiffness calculation;

$\bar{x}$ neutral axis depth;

FORCE AND MATERIAL STRENGTH

μ percentage of tension reinforcement;

μ_1 Poisson's ratio;

γ_c safety factor on concrete, taken as 1.25;

γ_s safety factor on reinforcement, taken as 1.25;

σ_g service stress on tension reinforcement;

ξ_{jg} factor on compression zone of section, taken as 0.55 for Class II and III reinforcement in the Chinese Design Code;

δ_1 deflection at midspan of the ith beam;

C_1 factor on surface condition of reinforcement, taken as 1.4 for plain steel and 1.0 for high yield bars;

C_2 factor on load duration, taken as 1.0 for short-term loading;

C_3 factor on shape of bending element, taken as 1.0 for member with ribs and 1.15 for slab;

x displacement;

P_1 fraction of applied load on the ith beam;

M bending moment under service load;

M_g the moment due to self weight of beam;

M_j the moment resistance to ultimate strength limit requirement;

M_{1c} the moment resistance to deflection limit requirement;

M_{cc} the moment resistance to crack width limit requirement;

R_a compressive strength of concrete;

R_g tensile strength of tension reinforcement;

R'_g compressive strength of compression reinforcement;

E_g elastic modulus of tension reinforcement;

E_h elastic modulus of concrete;

E_s static modulus of elasticity;

FREQUENCY ANALYSIS

ε specified error;

ε_b normalized bias error;

ε_r normalized random error;

ϕ statistical parameter;

$\hat{\phi}$ estimate of statistical parameter;

$E[\phi]$ mean of statistical parameter;

$b[\phi]$ bias error of the statistical parameter;

$\sigma[\phi]$ random error of the statistical parameter;

$\hat{\mu}_x$ mean estimate;

$\hat{\mu}_x^2$ mean square value of estimate;

$\hat{\sigma}_x$ standard deviation of estimate;

$\hat{\psi}_x$ root mean square value of estimate;

$\hat{\sigma}_x^2$ variance of estimate;

$\hat{\psi}_x^2$ mean square value of estimate;

$\hat{p}(x)$ probability density function of estimate;

$\hat{R}_{xy}(\tau)$ cross-correlation function of estimate;

$\hat{G}_{xx}(f)$ auto-spectral density function of estimate;

$\rho_{xy}(\tau)$ cross coherence;

ψ_i ith mode shape;

λ_i ith characteristic root of equation;

ζ_n damping ratio at nth mode;

f_c cutoff frequency of filter;

f_n nth modal frequency;

f_{NY} Nyquist frequency;

f_s sampling rate;

f(t) forcing function;

B total bandwidth occupied by data;

B_r half-power bandwidth of spectral peak;

B_e frequency resolution in spectrum;

h(τ) a weighting function defined as the output of the system at any time to a unit impulse input applied a time τ before;

m number of modes;

n(t) measurement noise;

n_d number of segment of time history in the overlap process;

N number of averages required in spectral analysis;

T analyzer measurement time;

T_r total required record length;

W width of data window;

x(t) time history record;

[Z(ω)] impedance matrix;

[H(ω)] frequency response function matrix;

$\bar{[H(\omega)]}$ modified frequency response function matrix;

[R] diagonal matrix with its elements equal to the inverse of the corresponding diagonal elements of the frequency response function matrix;

ΔH small change in frequency response function;

$\Delta|H|$ small change in the modulus of frequency response function;

H^* conjugate of frequency response function H

$\Delta\theta$ small change in phase angle;

$\partial m, \partial k, \partial c$ small change in elemental mass, stiffness and damping;

$\eta|H/m|, \eta|H/k|, \eta|H/c|$ sensitivity of frequency response function to small changes in elemental mass, stiffness and damping constant;

ω circular frequency;

ω_d damped circular modal frequency;

ω_n circular modal frequency;

$\bar{\omega}$ ratio of circular frequency to circular modal frequency;

VECTORS AND MATRICES

{ε} error matrix;

b_i damage parameter which may be any of the elastic constants of material or geometrical dimensions of the element;

[A] sensitivity matrix;

$\{a_{K+1}\}$ (κ+1)th row of matrix $[A_{K+1}]$;

{B} vector of measurable parameters;

b_{K+1} (κ+1)th element of vector {B};

[M] mass matrix;

[K] stiffness matrix;

[C] damping matrix;

$\{H_r\}$ the rth column vector of the frequency response matrix [H];

$[K_{ab}]$ partitioned stiffness matrix of coordinates a and b;

$[\bar{K}]$ reduced stiffness matrix;

[L] gain matrix;

[P] error variance matrix;

[V] measurement noise matrix;

[X] damage state vector;

$\{X_k\}$ estimate of damage state vector at (k+1)th step;

RANGES AND DOMAINS

Re(..),Im(..) Real and imaginary parts of (..)

R real number domain;

C complex number domain;

r,s points of measurement;

p,q points in the geometric range of the structure to be diagnosis.

LIST OF FIGURES

LIST OF TABLES

CHAPTER ONE

INTRODUCTION

1.1 RATIONALE OF THE RESEARCH

This Thesis addresses three aspects in the area of maintenance of bridge engineering: (i) a quick and simple means of damage diagnosis; (ii) a scientific method to classify damages of a bridge deck; and (iii) a method to assess the load carrying capacity of bridge decks with no design information. The type of structure under study is confined to simply supported reinforced concrete Tee-beam and slab bridge decks which is most common in the People's Republic of China. The first bridge of this type was built in the fifties and more are being constructed in the nineties with span up to 50 metres. Many of these bridges are deteriorating due to ageing, inadequate maintenance and increasing load spectra, and there are problems with the assessment of damage and the load carrying capacity of such structures.

1.2 THE PROBLEMS

Damage in a bridge deck is most commonly revealed in the periodic checking of the structure which involves closure of the bridge or limiting access. While most damage can be visually inspected, some more obscure faults require heavy equipment to be used in their identification. A quick and simple means of damage diagnosis would mean less out-of-service time for the structure and lower maintenance cost.

The location of damage is usually identified visually, but the evaluation of the magnitude depends on the experience of

the inspector. Its effect on the safety of the bridge deck is often descriptively noted down in adjectival terms such as "good", "fair", "bad" and "dangerous" against a check list. A more objective classification based on scientific study of the structure is required.

Many of the bridges built in the fifties in the People's Republic of China do not have complete design information. The structural behaviour and the load carrying capacity of the structure may be calculated from the estimated values of the basic properties of the structure. A more deterministic approach is required however to assess more accurately the actual load carrying capacity.

1.3 THE PROPOSED SOLUTIONS AND RESEARCH STRATEGY

A damage detection technique is developed based on the measurements of angle phase difference between the dynamic response at two measuring stations in a structure due to small change in its stiffness. A set of simultaneous equations is derived relating the measured change of phase difference to a set of damage parameters in the suspected finite elements of the structure. Solution of this set of equations gives the magnitudes of the damage parameters.

The type of bridge deck under study fails primarily in tension failure due to loading only, with sufficient detailing and design provision to prevent other types of failure, like shear and compression failures.

The cracked moment of inertia of the bridge deck is estimated from simulation of the vibrational response of the structure with a finite element model. The uncracked composite moment of inertia of the beam is also calculated. The ratio of the cracked to the uncracked moment of inertia gives a Structural Damage (SD) Factor α, which is an indication of the cracked condition in the bridge deck. This

factor varies over the life span of the bridge deck, and it can serve as a tool in periodic surveillance of the structure.

For a reinforced concrete bridge deck under load, there is a likely or "nominal" cracked moment of inertia in the beam section to resist the bending moment. This nominal moment of inertia is a characteristic of the structure dependent on the steel percentage of the section. A relationship is derived relating the steel percentage of the bridge beam with this nominal moment of inertia of the beam section. The Load Carrying Capacity (LCC) can then be estimated from the different limiting requirements of the design code. A LCC Factor β is calculated which is a characteristic of a span group of bridge decks.

Random error in the estimate of the steel percentage of the bridge beams is minimized by including a Reference Factor β_{LS} in the calculation. This Reference Factor is a statistical average of the LCC Factor of a group of bridge decks of equal span length.

1.4 DEVELOPMENT OF THE PROPOSED TECHNIQUE AND STRATEGY

The proposed damage detection technique has been implemented in the damage identification of a steel cantilever beam with a slot under narrow-band excitation, and in the identification of a cracked diaphragm of a model reinforced concrete bridge deck under ambient excitation. The accuracy of the technique is investigated and compared with those obtained using other measurable vibrational parameters.

The method of damage classification and LCC assessment of bridge decks is evaluated against the test results of the model bridge deck obtained in a controlled environment, and a database of seventeen full-scale reinforced concrete bridge decks.

The accuracy of the proposed technique and method depends on the correct dynamic testing and signal analysis, and a correct finite element modelling of the structure. Hence, the following pieces of work have been completed in the development of this research: (i) optimal dynamic testing techniques have been developed; and (ii) programmes on static and dynamic data acquisition and a Fast Fourier Transform (FFT) based signal processing programme are written; and (iii) optimal signal processing method is developed; and (iv) an iterative optimization programme is written; and (v) parametric study on the effect of boundary conditions on the modal frequencies is completed.

1.5 THE GENERAL LAYOUT OF THE THESIS

Following this introductory Chapter, Chapter Two presents a literature review on damage detection techniques and methods of damage classification and LCC assessment of bridge decks. Chapter Three gives an introduction on dynamic testing techniques and signal processing with particular emphasis on the special considerations applicable to this research. Chapter Four presents the proposed damage detection technique with a linear least-squares algorithm for optimal solution. Chapter Five presents the development of an optimal finite element modelling of the bridge deck together with a parametric study on the effects of boundary conditions on the dynamic response of the structure. Chapter Six describes the laboratory test of a steel cantilever beam and a small scale reinforced concrete bridge deck. Chapter Seven describes the proposed method in damage classification and LCC assessment. The method is developed using the test results of the model bridge deck. Chapter Eight gives an account of the field testing of seventeen prototype bridge decks with detailed discussion of Yuan Dun Bridge as a case study. Chapter Nine evaluates the proposed method in damage classification and LCC assessment against a database of

prototype bridge decks. Chapter Ten gives the conclusions drawn from all aspects of this research and a final discussion on the proposed damage detection technique and method for damage classification and LCC assessment, together with their limitations and areas requiring further research.

CHAPTER TWO

LITERATURE REVIEW

2.1 REVIEW OF DAMAGE ASSESSMENT TECHNIQUES

Much work has been done on the damage assessment of structures. Mitsuru et al (1983) have presented the process in the form of a chart which is shown in Fig.2.1. As a first step, the existing condition of the structure is determined mainly through review of design and construction documents, determination of existing geometry, determination of the nature, quality and amounts of construction materials, visual evaluation of damage including areas of concrete crushing, the extent of any cracking, crack width measurements, crack pattern mapping, visible reinforcement corrosion, and simple in-situ tests on the structure for the static and dynamic properties.

The results obtained should contain sufficient information to quantify the load carrying capacity of the structure with the assistance of a finite element model as described by Baker and Edwards (1985). Otherwise the more conventional in-situ load testing has to be considered.

Vibration techniques have developed rapidly over the last two decades as a tool for damage assessment. The use of dynamic response as a diagnostic measure of structural performance gives a rapid and simple means to assess the condition of a structure. Much literature has been published on the complementary modelling of a damaged structure by finite element models, modal models, time domain response models and static test measurements. A simple classification of the different techniques of damage assessment is shown in Fig.2.2.

2.1.1 Modal Parameter Comparison

The modal parameters obtained from the analysis of the vibrational response of a structure are functions of the physical stiffness, damping and mass of the structure. Any change in the system matrices would induce changes in the modal parameters. Work in this area is related to the identification of the more sensitive modal parameter for small damage in a structure.

Damping, modal frequency, mode shape and mechanical impedance have been evaluated by Salane et al (1981) in a full-scale bridge test for their effectivensss in performance monitoring. The changes in modal frequencies with stiffness degradation of the structure have been studied in a bridge model of Mazurek and DeWolf (1990), and in a full-scale bridge deck of Kato and Shimada (1986) and Salane and Baldwin (1990). Jeary and Ellis (1984) suggested that the modal damping is not directly related to the change in stiffness of the structure and there is a region of higher and relatively constant value close to the ultimate failure of the structure. However, Salane et al (1981) showed that the damping ratio increases and later decreases with increasing damage in the structure.

The use of modal assurance criteria, which is a DOT product of two modal vectors, was successfully applied in the identification of damage in a bridge model by Biswas et al (1990a; 1990b), and in an analytical study of a simply supported plate by Kim et al (1992). A modal confidence factor developed by Ibrahim (1978) was successfully employed in the identification of damage in a model bridge deck by Law et al (1991b). The effectiveness of mode shape, modal assurance criteria and nodal line were discussed by Wolff and Richardson (1989), and later Natke and Cempel (1991) have given proof on the sensitivity of nodal line to damage in a structure. Curvature mode shape, which is a function of

the stiffness of the structural element, was proposed by Pandey et al (1991) to detect the presence of damage.

The use of relative transmissibility across a structure under sinusoidal excitation was investigated by Akgun et al (1985) and the pseudo-nodes on the deflected shapes of the structure were identified as the more sensitive sites of measurement for damage detection.

The receptance was expressed by Afolabi (1987) in rational fractions from which the anti-resonance frequencies were obtained. The anti-resonance frequencies are selectively sensitive to changes in system parameters, and the shift of these frequencies at different measuring points were used successfully to detect the location and extent of damage in a portal frame.

Springer et al (1988) suggested that the frequency response function would be a sensitive parameter to damage in a structure, while Natke and Yao (1988) identified the dynamic stiffness matrix to be a more sensitive parameter than frequency response function as it contains the higher modes which are more sensitive to damage.

Tsai et al (1985) used the random decrement technique to compute a reference signature for the undamaged structure and compared it with the signature from later recording.

Freeman's chain code, which is a technique of pattern recognition, was used by Samman et al (1991) in the structural pattern recognition of a model bridge deck to accentuate the difference of measured frequency response function in the undamaged and damaged states.

2.1.2 Compliance Approach Using the Modal Parameters

Work has been done by Minami (1987) and Vandeurzen et al (1987) using a finite element model to simulate the change of mass and stiffness in a structure from frequency changes. Attempts have been made to use the change of modal frequencies, modal damping and a finite element model to identify structural damage in offshore platforms by Lock and Jones (1976); Wojnarowskim et al (1977); Kenley and Dodds (1980); Shahrivar and Bouwkamp (1980); Vandiver (1985) and Staalduinen and Brederode (1987). The deterioration of a full-scale bridge deck was simulated by Katyo and Shimada (1986) with a finite element model by matching the measured modal frequencies.

2.1.3 System Matrices Identification Approach

Much work has been published on the identification of the system matrices, i.e. the stiffness, mass and damping matrices of a structure using dynamic measurements. Such identification is made in the periodic testing of the structure, the difference between the identified system matrices in the undamaged and damaged states showing the location and extent of the damage. This is an indirect way of damage assessment and representative works are those of Luk (1987); Han and Yang (1987); Tai et all (1988); Roemer and Mook (1990); Mannan and Richardson (1990); and Lim (1991b).

The composition of the stiffness matrix depends on the elastic and geometric properties of the structure as well as on the element connectivity. A given element of the matrix therefore has contributions from several members sharing the same node, making it difficult to identify the precise location of damage using this approach.

2.1.4 Analytical Approach

Various analytical theories have been developed to relate the damage in a structural element with the change in modal frequencies and other parameters. Most of these theories are applicable to one-dimensional structures only.

The location and stiffness of a spring simulating damage in a beam were expressed by Adams et al (1978) as a function of the receptance at a point. The spring stiffness was assumed to be independent of the excitation frequency. The two unknowns (location and severity of the crack) were determined by known changes in the frequencies of two modes. Correction due to temperature effects was also discussed. A three element model of a cracked beam was later proposed by Springer et al (1988). The receptance concept was later applied to a non-uniform beam by Liang et al (1992) in the determination of location and depth of a crack.

A theory was developed by Ju et al (1984) and Ju and Mimovich (1987) based on the analytical theory of a spring-loaded "fracture-hinge". In this method the change in modal frequency was expressed as a function of the spring constant and "sensitivity number" of the crack which were analogously related to the damage parameters, the stiffness and location of the crack.

A non-linear characteristic equation was established by Rizos and Aspragathos (1990) based on the continuity conditions at an open crack. The location and depth of the crack were determined with the measured amplitude of vibration at two points of the structure vibrating at any one of its modal frequencies. Further work by Liang et al (1992) has led to the development of a relationship between the change in modal frequencies with the location and depth of cracking.

A compliance matrix was developed by Papaeconomou and Dimarogonas (1989) in the vicinity of a crack based on a strain energy formulation which led to the development of a transfer matrix of the cracked beam element. Solution of the set of transfer matrices of the beam gives the location and extent of cracking.

A theory of crack detection was developed by Akgun and Ju (1987a) using the analogy of electrical T-circuits. The individual beam segments were represented by T-circuits, and the cracks by resistors. Further work by Akgun and Ju (1987b) was published using Π-circuits and fracture hinges in which each elastic beam element was analogous to a 3-terminal circuit.

An elemental stiffness matrix of a cracked beam element was derived by Qian et al (1990a) from an integration of stress intensity factors. The equation of motion was expressed in terms of strain, which was proved to be more sensitive to damage than displacement. A new and effective criterion for optimization in the damage detection problem was proposed. Later Qian et al (1990b) determined the crack position based on the relationship between the crack and the eigenpair of the beam.

2.1.5 Perturbation Approach

The perturbation study of a dynamic system involves an investigation of the effect of a small change in the system matrices on the eigenvalues, eigenvectors and other modal parameters. Pioneer work was undertaken by Fox and Kappor (1968), and later by Wolf (1987; 1988); Orr (1990); Wang (1991) and many others contributing to this area. Useful relationships between the physical damage and change in the modal parameters have been derived.

Sensitivity of the various modal parameters to change in

elemental stiffness, damping and mass have been discussed in the literature. A general sensitivity theory was proposed by Ju and Xu (1989) and later by Natke and Cempel (1991). The sensitivities of the modal frequency, frequency response function and spectral density function were derived by Brandon (1987); Wang (1987); Wang and Zhang (1987) and later extended by Gu et al (1989) and Zhang et al (1990). The sensitivity of the mode shape was discussed by Natke and Cempel (1991). The sensitivity of the eigenvalue and eigenvector to a small change in stiffness of a structure was again derived by Chondros and Dimarogonas (1989) using the Rayleigh principle. Higher order terms on the sensitivity of modal parameters was given by Ju and Xu (1989).

The ratio of frequency change in two modes was expressed by Cawley and Adams (1979) as a function of the damage location. An error function was computed for the sensitivity at different points to define the location of damage. Directional damage can also be identified by giving different weights to the modes.

Agbabian et al (1990) expressed the same ratio of frequency change as a function of the relative strain energy contribution of the damaged element for the different modes. Later Hearn and Testa (1991) developed the same relationship based on the initial member stiffnesses, masses and mode shapes, each member having a characteristic influence on the natural frequency of vibration modes. To monitor the condition of a structure, the set of ratios of frequency change has to be compared to the various member characteristic ratios.

Similar work was undertaken by Lim (1991a) using system submatrices (elemental stiffness matrices). The modal strain energy of each submatrix was calculated and the fractional modal strain energy of each submatrix formed a good

indicator of damage.

A damage diagnostic technique was developed by Law et al (1990b) based on the eigenvalue problem of the system and the shift in the measured modal frequencies. It was proved that there is no need of an exact description of the structure in the eigenvalue problem. The set of algebraic equations was solved by a non-linear programming method.

A theory was developed by Chen and Garba (1988a; 1988b) to express the vector of small changes in stiffness as a function of the modal displacement vector. The change in kinetic energy was used to locate the damage based on a minimum deviation approach with the underlying assumption that the mass matrix does not change with damage. This approach of minimizing the changes in the parameters of the analytical model is not particularly applicable as significant variation can be introduced in these parameters. Besides, the total kinetic energy is a global measure, and it is not sensitive to damage involving small local changes of the structure.

The sensitivity of the entire structural system was expressed by Stubbs (1985) and Stubbs and Osegueda (1990) as the summation of sensitivity to change in stiffness, damping and mass of the structure. Expressions relating variations in the stiffness of structural elements to the variation in modal stiffness were derived. A vector of changes in modal stiffness was given as a function of the unknowns of changes in member stiffness. Solution of the system of algebraic equations identified the location and magnitude of damage in the structure.

2.1.6 Error Output Approach

In this approach different types of error functions and error matrices are computed between either the measured

response of a structure and the analytical model, or the measured response of an undamaged and damaged structure. Their differences are used to quantify the damage in a structure.

Cawley and Adams (1979) computed the change in modal frequencies due to damage in a structure, and the errors in the pattern of frequency shifts between the measured and calculated values were calculated. The defected area was then identified by comparing the normalized errors throughout the whole structure. Further, some weights were given to the errors to ease detection of directional damage. A disadvantage of this method is that it requires very accurate measurement of frequency change.

He and Ewins (1986) introduced the error matrix to expedite analytical model correction with measured eigenproperties by localizing the region of errors in the model stiffness and mass matrices. Since all the elements of the stiffness matrix can be interpreted as the local stiffness of corresponding members of the structure, the changes in stiffness matrix can give valuable information for locating damaged elements.

Later Park et al (1988) showed that only large stiffness faults can be identified through the error-matrix technique. He used a weighted-error matrix to magnify the damages in the error matrix. The weighted-error matrix was constructed by adding the measured-modal-property change patterns and the analytical sensitivity characteristics into the conventional error matrix.

Chen and Garba (1988a; 1988b) used the minimum deviation approach in which changes in the system parameters from initial assumed values were minimized, subject to the constraints that the system equations be satisfied. The Euclidian norm of the matrix representing the perturbation

of the analytical stiffness matrix due to the structural damage was minimized. Since entries in the stiffness matrix depend on the elastic and geometric properties of the structure as well as on the element connectivity, a given element of the matrix may have contributions from several members sharing the same node, making it difficult to identify the precise location of damage. Furthermore, this minimum deviation approach results in small deviations from an a priori model which is not realistic in the case of significant damage in a structure.

Some system characteristic responses were selected as the entity for which the analytical model was refined to minimize the difference between the analytical prediction and experimental measurements, Hajela and Soeiro (1990a; 1990b). Damage was represented by reductions in the elastic moduli of the elements which were designated as the design variables of the problem. Static structural displacement was used as the measured response, and iterative nonlinear programming methods were employed to solve the unconstrained optimization problem. The inclusion of eigenmodes was used as additional measured response in an attempt to identify damage in elements less affected by static load.

Hajela and Soeiro (1990a); Sanayei and Onipede (1991) and Sanayei and Scampoli (1991) discussed an equation error method in which equations describing the system response were explicitly stated. This avoided an explicit decomposition of the system matrix in the solution process. The system parameters, which were typically coefficients in such equations, were then selected to minimize the error in satisfying the system equations with a set of measured data. The design variables for the optimization were the same as in the output error approach. In the case of incomplete measured data, the system of equilibrium equations could be partitioned which required a matrix inversion in its solution. This approach is particularly useful in problems

where the region of damage is known, and can result in a significant reduction in the number of design variables.

Masri et al (1987a; 1987b); and Agbabian et al (1991) demonstrated the equation error method in time domain. The differential equations of motion of a multi-degree-of-freedom linear system was converted into a set of algebric equations with a vector of measured responses related to a vector of excitation through a vector containing all the unknown influence coefficients of the system, which were the system matrices. When a sufficient number of measurements had been taken in the time domain, the problem was solved using least-square procedures.

A similar approach using a random decrement technique in the time domain was presented by Qi et al (1990). Errors in the identified parameters were discussed, and a criterion for damage identification was recommended.

2.1.7 Static Test Approach

This classification of damage detection techniques is based on a simple and quick static test not requiring sophisticated equipment very different from that employed for conventional load testing of a structure.

Since dynamic parameter identification requires the use of the mass, stiffness, and damping properties, it is more complicated than a static method which only uses the stiffness properties of the structure. Basically a linear elastic structure is assumed. If there is non-linearity in some of its elements, only a small force is applied to ensure the displacement is in a linear range.

Work in this area has been reported by Hajela and Soeiro (1990a; 1990b); Sanayei and Onipede (1991) and Sanayei and Scampoli (1991). A short description of them have been

presented previously in section 2.1.6.

2.2 REVIEW OF THE DAMAGE CLASSIFICATION METHODS

2.2.1 Types of Damages

Damage can be broadly classified into that caused by material defects and that due to structural deficiencies. Examples of the former are corrosion of steel and material voids. Those belonging to the latter category may be cracks in concrete, cracks in welds, fatigue cracks, spalling of material, loss of bond between two composite materials, loosening of connecting bolts and rusty joints.

The damage developed in reinforced concrete structures involves a number of damage modes, including tensile cracking, shear cracking, spalling, bond failure of steel reinforcement, or various combinations of these mechanisms. Both shear cracking and bond failure are usually associated with the final stages of catastrophic failure of reinforced concrete. On the other hand, tensile cracking occurs early enough in the overall failure process that detection would allow early implementation of remedial measures.

2.2.2 Existing Practices

Overstress indices were calculated by Cabrera (1988) to simplify the comparison of a large number of structures and gauge how much reserve is in hand. This comparison is based on the ratio of experimental and theoretical ultimate load effects which may be stresses or deformations of the structure. This overstress index should be unity or less for code compliance.

If the actual loading matches the calculated strength in service such that the overstress index exceeds unity, collapse is not necessarily imminent. The reserves of

strength have simply been reduced from those allowed for by the code. Design codes tend to use simplified methods of analysis having additional conservatism which is appropriate for design but not for assessment. A further factor is that design codes may prohibit the use of conservative features or simply ignore outdated construction techniques which may nevertheless be present in existing bridges.

A "Performance Index" was proposed by Cabrera (1988) for the evaluation of concrete bridges which was based on the observation of signs of distress and their quantification using weightings based on frequency and extent. Numerical values were obtained by weighting the three main signs of distress, i.e., leaks, cracks and surface defects, and a tentative scale of weights was proposed.

Deterioration affects various structural parts differently. Damage in horizontal/expansion joints between simply supported decks does not present a direct threat to bridge safety. Vehicles passing over the damaged joint may induce large dynamic load on the bridge deck instead. Fatigue and corrosion of the superstructure may cause a considerable reduction of capacity. Changes in member stresses and geometric properties are associated with a loss of material. This loss may be on a local or microscopic level, such as rusting and pitting, or in a general area, such as surface spalling and cracking.

Existing practice is to separate the various structural components of the bridge deck into different categories according to their importance to safety. Different weights are then given to damage observed in the different categories. Damage identified is checked against a check list for the bridge. The classification of each occurrence of damage is entirely dependent on the experience of the inspector with no scientific basis on the actual behaviour of the structure.

The United States of America is using a rating system of 0 to 9 as reported by Lauer (1991) as a damage classification system for concrete structures. It involves adjectivial ratings summarizing the condition of individual bridge components into four general categories of good, fair, poor or critical. The People's Republic of China uses a similar system in the inspection and classification of concrete bridges. It involves four classes which use adjectivial terms along with crack width limitations, Ministry of Communication (1986).

2.3 REVIEW OF LOAD CARRYING CAPACITY ASSESSMENT TECHNIQUES

2.3.1 Load Carrying Capacity from Design

In the past, load testing has been more important than it is today, and the development of load testing practice has gone on in parallel with the development of mathematical models for design. The successful use of load testing has been accompanied by advances in analytical techniques, that in turn have led to a reduced need for testing. This process has led to the present situation with design by calculation favoured over design by testing, when possible. The load carrying capacity of a structure therefore comes off the design desk.

It has been concluded by Bakht and Csagoly (1981) and Bakht and Jaeger (1990) that most existing bridges possess substantial load carrying capacities above their originally designed strengths. These reserves of strength exist for a variety of reasons, namely simplified methods of force analysis, variations between actual and design strength values of structural materials, errors in the strength analysis, conservative basic assumptions and unaccounted component interaction. The true load carrying capacity in turn relies on the rational evaluation procedures such as

load testing.

In practice, the effect of damage is simulated with a "damaged" finite element in a finite element model to assess its effect on the structural behaviour and load carrying capacity of the structure. This approach requires a detailed knowledge of the design and construction of the bridge deck.

2.3.2 Load Carrying Capacity from Proof Load Testing

In "proof load testing", a structure is tested at a fixed load, and if it survives the load, its resistance is demonstrated to be greater than the proof load. This type of test is a strength verification test, a resistance test performed at the member or system level, usually with loading similar to actual service loading. It is a non-ageing test intended to be nondestructive. The information measured by the test is not merely the test load, but the observation that the structure performed successfully under it, and by inference has resistance greater than or equal to the proof load. Full-scale bridge tests provide very useful information about structural behaviour. However, it is very costly and involves closure of the bridge to traffic or restrictions on use.

2.3.3 The Existing Evaluation Philosophy

The most common approach is to employ the same calculations for evaluation as for design. If a component is found to be weaker than required by design calculations, the bridge is declared substandard. This philosophy has been adopted in the reanalysis of structures based on measured damage, and in the more sophisticated proof load testing.

Since the introduction of limit state concepts in design, the levels of safety against collapse have been set by calibrating a representative range of designs to each code

against another range of designs to the previous codes which have been shown by experience to give satisfactory performance. The partial factors in CP110 (1972), BS8110 (1985) and BS5950 (1982) were determined by deterministic calibration over a range of structures; whereas in BS5400:Part 3 (1982) a fully probabilistic procedure using reliability theory was adopted, Flint et al (1981). As a result of these considerations, an assessment version of the concrete Bridge Design Code BS5400:part 4 (1984) is being prepared by the Department of Transport to determine the need for any adjustment to the partial safety factors originally proposed, Tilly (1990).

2.4 CONCLUSION

The evaluation of bridges is an increasingly important topic in the effort to deal with the deteriorating infrastructure in the People's Republic of China. Many bridges constructed in the fifties are suspected of their serviceability, and some of them are in need of rehabilitation and replacement. The major factors that have contributed to the present situation are: age, inadequate maintenance, increasing load spectra and environmental contamination. To minimize the high costs of replacement or repair, the evaluation must accurately reveal the present load carrying capacity of the structure for a certain period of time.

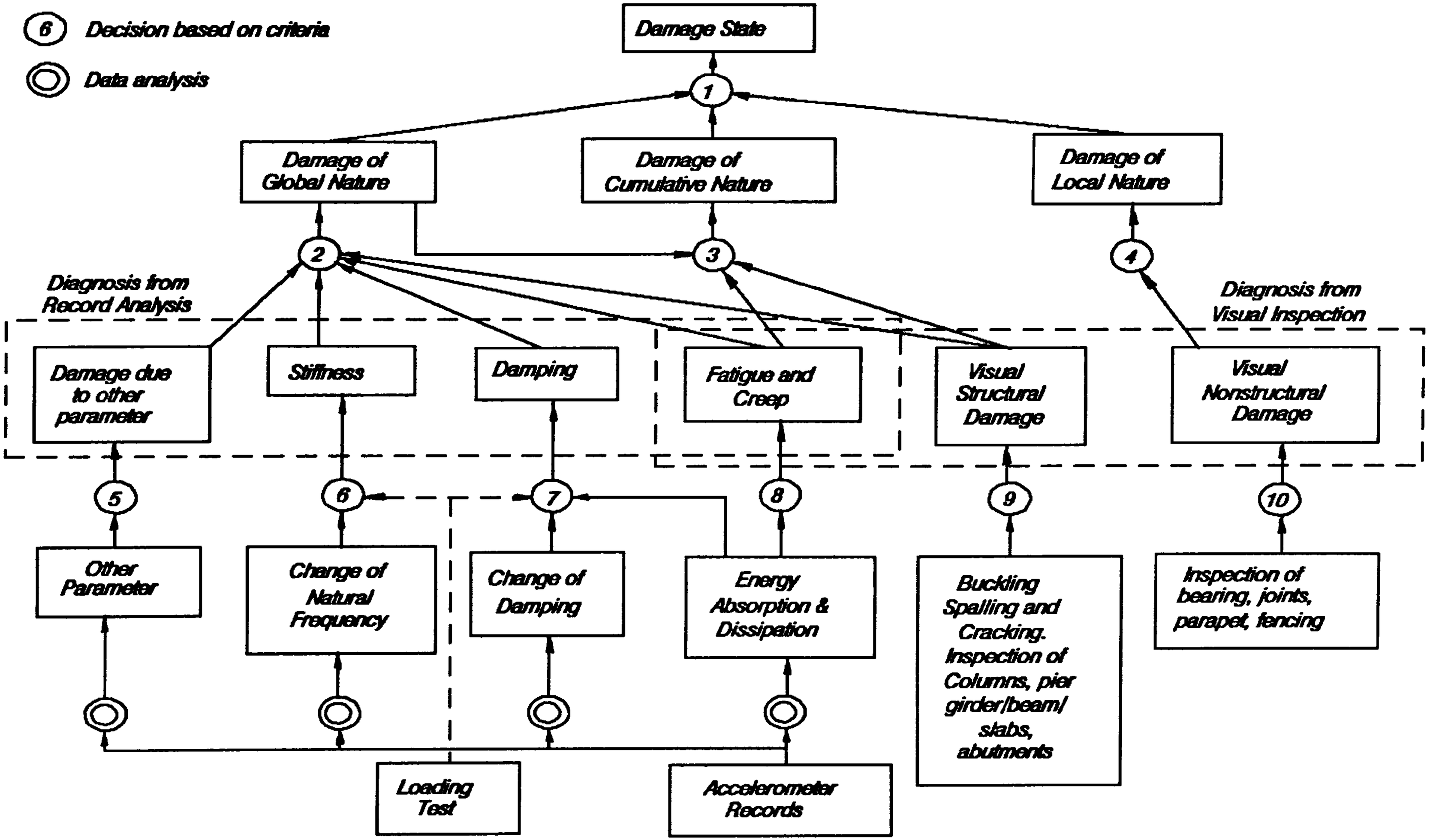

FIG.2.1-Damage Assessment Process, Mitsuru et al (1983)

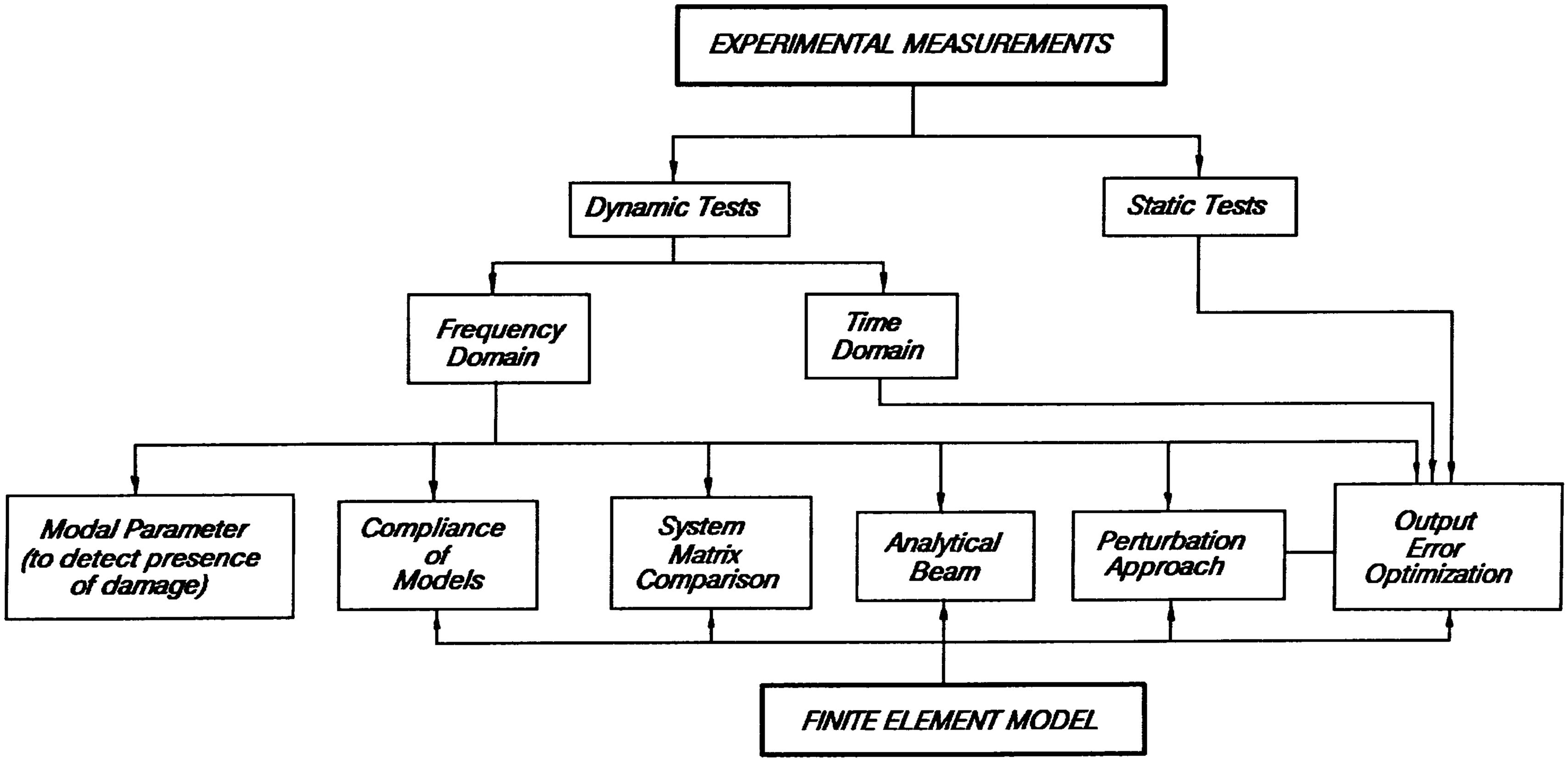

FIG.2.2-Classification of Damage Detection Techniques

CHAPTER THREE

DYNAMIC TESTING TECHNIQUES AND SIGNAL PROCESSING

The general aim of a modal test or dynamic test on a structure is to determine its modal frequencies, damping, and modal vectors which are its basic dynamic properties. The success of a modal test depends on the correct selection of excitation for the structure, and the correct acquisition and analysis of data. This Chapter gives a brief description of these three aspects in modal testing with particular emphasis on the requirements of this research.

Two terms need to be discussed before going further into dynamic testing. They are Stationary Random Process and Ergodic Random Process, Bendat and Piersol (1986). A stationary random process is a collection of time-history records having statistical properties that are invariant with respect to translations in time. Statistical averages computed over an ensemble of time-history records are not a function of the times being analysed. An ergodic random process is a stationary random process involving a collection of time-history records where time-averaged results are the same for every record. It follows that these time-averaged results from any single record will then be equal to the average results of the corresponding ensemble over the collection of records.

Dynamic testing may be classified according to the way the test is conducted. It may be conducted as a single-input and multi-output exercise or as a multi-input and multi-output exercise. The former can be done with proper equipment like an exciter, which inputs a signal at a specific frequency at a single point on the structure, while the response is monitored at different points. The latter method makes use

of several exciters working at the same frequency at several locations on the structure. The response of the structure is again measured at different points. If the source of excitation is from the environment, the input excitations are at the points of connection of the structure with the environment. These excitations are assumed to come from the same natural sources.

3.1 EXCITATION TECHNIQUES

Dynamic testing may be classified according to the type of excitation involved in the test, e.g. steady state, random, periodic, transient or ambient excitation.

3.1.1 The Steady State Signal

The steady state signal type is typically a slowly swept sine or stepped sine sweep of the structure under test with the sweep slow enough such that the structure always reaches steady state response. The principal advantages of this technique are (i) the extremely good signal to noise ratios using a narrow bandpass tracking filter and averaging over many cycles of the driving frequency, and (ii) the ability to characterize non-linear systems with different excitation levels. The disadvantage of it is that it is extremely slow, especially if the structure under test is lightly damped or the bandwidth in the tracking filter is small. This method is still very popular however due to the relatively inexpensive equipment required.

3.1.2 The Periodic Signal

A periodic signal is any waveform that is periodic within the analyzer measurement time T. This could be a sine wave with an integer number of cycles in T, or a complex waveform that repeats every T seconds. Any signal that is periodic within the analyzer measurement time T can be Fourier

transformed without "leakage" errors. Examples are fast sine sweep, pseudo random and periodic random. The main advantage of this type of signal is that it eliminates the leakage errors and the associated distortion introduced by the use of a window function.

3.1.3 The Random Signal

A random signal, in general, is a non-deterministic signal that can be characterized by a Power Spectral Density Function and by an Amplitude Probability Density Function. This is one of the easier type of excitation to utilize with a Fourier Transform based analyzer. However, a true random signal is not periodic within the analyzer measurement time T, and it requires the use of a window function to reduce the leakage errors, Beauchamp and Yuen (1979). A typical weighting function used is a Hanning window which will usually reduce the leakage errors to an acceptable value. However, there is an increase in the variance of the spectral peaks with the use of windows. This statistical information can be effectively recovered by a process called overlap processing. For a linear system there is a minimum number of averages required to recover the statistical information lost by the use of windows as discussed in Section 3.4.5, Bendat and Piersol (1986). Furthermore overlap processing is a means of reducing the measurement time required to achieve a low variance in the measurement.

3.1.4 The Transient Signal

A transient signal type is one which changes dramatically as a function of time but typically decays away over some time interval. A special example of this is the response to a hammer blow where data is obtained just before the hit and continues until the response effectively dies out. This signal is also "leakage" free when Fourier transformed, provided the entire history of the response signal is

captured within the analyzer measurement time T. Examples are impact excitation, swept sine bursts and burst random excitation. This type of signal has the advantages of being fast and leakage free, and relatively easy to use. The disadvantages are poor signal to noise ratio and limited control of the frequency content.

3.1.5 The Ambient Signal

The ambient signal type corresponds to input forces occurring naturally while the structure under test is operating. Examples are wind-generated excitation, micro-tremors from the earth and traffic-generated excitation. The characteristic of this type of excitation is independent of the time sample obtained. The response of a structure to this type of excitation may be considered as a stationary process or, more generally, as a ergodic stationary process. If there is a sufficiently long record of the response, the statistical properties of the ensemble averages may be calculated by performing corresponding time averages on the response. The advantage of relying on this type of input is that the test procedure is considerably simplified, as the only equipment required during the test is that for data acquisition. The main disadvantage is that the excitation is a non-stationary random process, and extraction of modal properties is made difficult by the varying and sometimes negligible participation of some structural response modes, as well as by the appearance of responses at frequencies highly characteristic of the excitation but not of the structure. Nevertheless, results from ambient tests have shown their validity by comparison with forced vibration response measurements as reported in the works of Hudson (1977); Bao (1981) and Brownjohn et al (1987). Ambient testing is therefore becoming very popular among structural dynamicists.

3.2 DATA ACQUISITION

The excitation and response time histories must be acquired and stored for subsequent analysis. Where many measurement stations are involved and the measurement system consists of only a few sensors, it is necessary to repeat excitations in order to measure all responses. In the case of random signal excitation, one measurement station is unchanged for each of the repeated measurements to serve as a link between responses from stations for different measurements. By using this method, two sensors can cover several dozen measurement stations by repeated measurement. Once measurements are completed, the data are recalled for time-domain analysis or Fourier transformation.

The arrangement of instruments for data acquisition is shown in Fig.3.1. The sensors are placed on top of the structure. The vibrational response signal in the form of acceleration is recorded on tape recorder. The vibration signal can be inspected on site by digitizing the signal via A/D conversion and analysed by a standard FFT subroutine. Alternatively it can be analysed back in the laboratory using a spectrum analyzer.

3.3 SIGNAL PROCESSING

3.3.1 Frequency Domain Analysis

3.3.1.1 Frequency-Domain Curvefit (FDC)

This procedure involves systematic selection of modal parameters in the analytic functions such that they are best matched to measured frequency response functions (FRFs).

Pioneer work of this approach was Kennedy and Pancu (1947). They observed that, for a single-mode response, the real or coincident response (i.e. the component of response that is

in phase with excitation) peaks as it approaches resonance then moves quickly through zero at resonance and that the imaginary or quadrature response (i.e. the response component that leads the excitation by 90°) peaks sharply at resonance.

If these data are plotted in the real and imaginary plane, the locus of data points forms a circle centered on the imaginary axis and tangent to the real axis with its diameter equal to the modal amplitude. Frequency varies around the circle and the modal frequency corresponds to the maximum path-length derivative with respect to frequency. For multimode response, each mode forms a separate loop. The procedure is to search for a local maximum of path-length derivative and fit a circle to that part of the plot determining the modal amplitude. Damping is estimated from a formula based on rate of change of phase.

Stahle (1962) introduced the phase-separation method where modal frequencies are identified from peaks of quadrature responses and modal damping is estimated from peaks of the coincident responses. The mode shape component can be determined by simply equating it to the magnitude of quadrature response. This becomes the simplest form of application of FDC. A single-mode circle fit includes all the complex data values in the calculations. A multimode model is required to fit a broad frequency band containing two or more modes.

3.3.1.2 Simultaneous Frequency Domain (SFD)

This method developed by Coppolino (1981) is based on the concept that the total response of a structure, represented by a large number of measured FRFs, can be represented as a linear combination of a smaller set of generalized response functions (GRFs) which are themselves linear combinations of all the FRFs. A linear transformation between the FRFs and

the GRFs is systematically established by a rank-ordering process. Next, reduced damping and stiffness matrices are established by a least-squares fit to the reduced set of measured GRFs. Then, modal frequency, damping, and generalized mode shapes are found by eigensolution of the reduced matrices. Finally, the total modes are found by linear transformation.

3.3.2 Time-domain Analysis

The basic idea of time domain identification makes use of the differential equations of motion of a lumped parameter system,

$$[M](\ddot{x}) + [C](\dot{x}) + [K](x) = (f(t)) \tag{3.1}$$

as an identification model. The solution of the equation is often used in the identification especially in cases when there is no input force.

The impulse response functions, or simply the free decay response time functions, are linear combinations of the system's eigensolutions.

$$(x(t)) = \sum_{i=1}^{2m} (\psi_i) e^{\lambda_i t} + (n(t)) \tag{3.2}$$

where (ψ_i) are the mode shapes, and

λ_i are the characteristic roots defined as

$\lambda_i = \sigma_i + j\omega_i$, where σ_i is the damping factor and ω_i is the modal frequency of the system under consideration.

$(n(t))$ is the noise associated with the measurements.

m is the number of modes included in the measurements.

The problem of modal identification then becomes the

solution of the mode shapes ψ and characteristic roots λ from the measurements {x}.

The random decrement technique, Cole (1973) was initially developed to obtain a single signature of one single measurement. It was later generalised by Ibrahim (1977a) to multi-measurement multi-mode responses, not to generate signatures but rather to produce free decay response time functions that could be used in the time domain modal identification of structures.

The major problems associated with using Eqn.(3.2) as the identification model are:

1. The equations are nonlinear and require elaborate, mostly iterative, algorithms to solve.
2. The rank of the system (the number of modes m) is unknown.
3. Solutions are usually sensitive to measurement noise.

The different time domain analysis methods are aiming for an effective solution to these problems.

3.3.2.1 The Complex Exponential Algorithm (CEA)

Stroud (1985) has reported that Prony converted Eqn.(3.2) into a polynomial problem whose coefficients are computed by equating them to a measured response history then extracting the roots which yield the eigenvalues. The CEA uses a time sequence that has four times as many values as there are modes present.

In a least-squares version of CEA by Brown et al (1984), the Prony method is replaced by a least-squares procedure to find the polynomial coefficients and another least-squares process to estimate the modal amplitudes. This approach allows the use of more data values and does not require

precise matching of measured and estimated histories thereby reducing noise effects.

An advantage of the CEA is that it requires little interaction. No initial estimates of the eigenvalues are necessary, and only an estimate of the number of modes present is required. However, determining an appropriate estimate for the number of modes to include is a major problem with both versions of CEA, and the solution is affected by this selection.

3.3.2.2 Ibrahim Time Domain (ITD) Analysis

Ibrahim and Mikulcik (1973) introduced the time-domain method and refined it later, Ibrahim and Mikulcik (1976; 1977). The original formulation was derived from free-response equations written in state-variable form. It was shown that the eigensolution of a matrix, which is itself formed by combining a matrix of the state-vector history and another matrix containing the corresponding history of the state vector's first time derivative, yields the modal parameters.

This formulation was abandoned because of several practical considerations. The procedure requires a matrix inversion which in turn requires a square matrix having exactly twice as many rows (and columns) as the number of modes present (which is unknown). This formulation also presents experimental difficulties because it requires measurements of the state vector and its derivatives (i.e. acceleration, velocity and displacement).

The improved formulations involve measurement of only one parameter, usually acceleration. ITD uses oversized matrices to accommodate the unknown number of modes and to reduce noise effects, Ibrahim and Mikulcik (1977); Ibrahim and Pappa (1982). The procedure is to form two large matrices

containing discrete measurements of free-response histories. Each matrix must have, at least, twice as many rows (or measurement locations) as there are suspected modes. In practice, the number of rows is many times the number of suspected modes. The number of columns (or measurement stations) must be equal to or greater than the number of rows. Another similar matrix is formed from data collected some known increment of time later. These two matrices are combined to form another matrix whose eigensolution provides the estimated modal parameters.

If there are fewer measurement locations than needed for the number of modes assumed, pseudostations can be created by entering response-history rows that are previously used histories shifted by a known time interval. In fact, this concept is used to provide Modal Confidence Factors, which is a criterion used to separate the structural modes from computational modes arising from the use of an oversized identification model, Ibrahim (1978). To accomplish this, the bottom halves of the aforementioned matrices contain the same response records as the top halves, all delayed by the same time increment. This produces double-length eigenvectors whose second halves are the first halves multiplied by a known complex exponential. Modal Confidence Factors are based on a comparison of these complex quantities.

The ITD method requires little interaction. It is effective for closely spaced and/or highly damped modes. It offers modal confidence factors to verify its results. The disadvantages are that it requires significant computing capacity, and noisy data tends to yield unconservative damping estimates.

3.3.2.3 The Polyreference Analysis

This method was developed by Vold and Rocklin (1982) and later extended by Deblauwe et al (1987). It is a multidimensional extension of the least-squares CEA. It simultaneously analyses multiple free responses to excitation at several locations. It implements free decay responses except for responses obtained from the inverse FFT of the transfer functions. This latter approach is chosen to take advantage of the possible averaging of the FFT functions, thus reducing the noise levels in the computed time functions. Such a reduction in noise levels will require smaller identification models and in turn less computer storage and execution time.

Also two response matrices are used to compute a matrix of eigenvalues. To conserve memory, only the eigenvalues are computed from which the modal frequencies and damping factors are determined. Then the mode shapes are calculated from Eqn.(3.2), using the least-squares method.

Polyreference analysis has the advantage of requiring little interaction. It provides a consistent set of modal parameters for all drive points. It is effective for closely spaced and/or highly damped modes. However, it is sensitive to non-ideal data, and user judgment is required to assess validity of results.

3.3.2.4 The Eigensystem Realization Algorithm (ERA)

Like ITD, ERA uses two matrices whose rows are discrete measurements of free response taken at many locations, Juang and Pappa (1984). These matrices are formed as described in Section 3.3.2.2 and combined to formulate an eigensystem whose solution contains estimates of the modal parameters. It uses singular-value decomposition to solve for the modal parameters instead of least-squares method used by ITD. The

decomposition approach provides information on the rank of the matrix, thereby offering the opportunity to reduce the order of the eigensystem. However, with noisy measurements, using singular value decomposition to determine the system's order is inconclusive, and an oversized identification model has to be used.

ERA offers quality checks in the form of "modal amplitude coherence" and "modal phase colinearity". These quantities (like ITD's modal confidence factor) are based on a comparison of the first and last halves of double-length eigenvectors containing a repeated solution.

3.4 ASPECTS OF DATA ACQUISITION AND ANALYSIS PARTICULAR TO THIS RESEARCH

In random vibration analysis, the basic assumption is that the signal represents an ergodic random process. However, in some cases the sampled data includes spurious trends or low-frequency components with a wavelength longer than the record length. Common sources of spurious trends are instrumentation drift and signal integration operations. If such trends are not removed from the data, large distortion can occur in the low frequency components. They can be removed by fitting a low-order polynomial to the data using the least-squares procedures.

3.4.1 General Criteria for Acceptance of Spectral Estimates

This paragraph gives the definitions of some terms commonly used in modal analysis. In the case of forced or sinusoidal excitation, the transfer function between the point of measurement and the point of excitation is obtained as the ratio of their vibration levels at a given frequency. The phase angle is the difference in phase in the vibration signal at two measuring points at a given frequency. The auto-power spectrum is a measure of the power of vibration at a specified point and is an indirect measure of the

magnitude of vibration. All these parameters are usually obtained through the Fourier Transform which transforms a time-history record into a frequency-based representation from which the vibration components of a structure at different frequencies are identified. From inspection of the magnitude of vibration at the modal frequencies and the phase angle between different signals, the vibration mode shape of the structure can be easily obtained.

In random vibration measurement, since there is no distinct point of excitation on the structure, the transfer function between two stations which is called the frequency response function in this case, is obtained by treating the signal at the first point as input and that at the second point as output.

The following are the general criteria for accepting the spectral estimates from the Fourier Transform.

1. A peak must appear at the same frequency in the spectra from all the measurement locations, except those which are closed to stationary points in that mode. Such deviations are observed usually within one or two resolution frequencies of the spectrum.

2. The relative phase difference between the signals from any two measurement points must be close to 0° or 180°. However, phase differences as much as $\pm 20^{\circ}$ from 0° or 180° can be accepted for the identification of a natural mode, particularly if one of the signals is small.

3. A peak in a cross-spectrum indicates that there is some correlation between the two signals at that frequency. This correlation is measured by a coherence function which varies between 0 and 1 and is dependent on frequency. In practice, coherence as low as 0.7 would

be acceptable.

3.4.2 The Sampling Rate and Aliasing

The analogue-to-digital conversion of the recorded responses leads to some errors by representing a continuous waveform as a series of discrete numbers. If there are insufficient points used to represent the waveform, i.e. if the sampling rate is too low, a process called "aliasing" occurs whereby the data above a certain frequency appears at lower frequencies (a process called fold back) thus contaminating the data. The frequency that is equal to one-half the sampling rate f_s is called the Nyquist frequency, f_{NY}. This is the theoretical maximum frequency at which the waveform can be represented by the discrete series. One way to avoid aliasing error is to choose a sampling rate high enough so that the energy content of the data above the Nyquist frequency is negligible. However, this would require more computation time as well as a larger memory size in the data processing equipment. A better method is to use an analogue "anti-aliasing" filter which pre-filters out data above the upper frequency limit of interest before data reduction. The sampling rate will then depend on the filter cut-off frequency, f_c, as well as the filter roll-off characteristic.

3.4.3 The Fourier Analysis, Windowing and Overlap Process

The time series after digitization is converted into the frequency domain by Fourier transformation. One requirement for the Fourier transformation of a time series is that the record is periodic, otherwise, an infinite duration of the time record will be required. In practice, neither of the two requiremnts above can be met. The truncation of the time series results in a "leakage" error which causes unrealistic negative power spectra and distorts the true shape of the spectral curves, Otnes and Enochson (1978). A Hanning

(cosine bell function) window with a more gentle slope is applied to the window of data to correct this problem. The use of a Hanning window, however, increases the half-power bandwidth of the main spectral peak by 60% as reported by Bendat and Piersol (1986), and this will affect the measured damping ratios of the structures.

Furthermore, the time series tapering operation also causes an increase in the variability of the resulting spectral estimates. To counteract this effect, overlap processing technique are used. Specifically, instead of dividing a time record x(t) into n_d independent segments, the record is divided into overlap segments covering the time intervals. A 50% overlapping will retrieve about 90% of the stability lost due to the tapering operation, Bendat and Piersol (1986).

3.4.4 The Resolution Requirements

Resolution means the frequency interval B_e of the discrete points representing the continuous transformed functions such as the auto-spectrum. Resolution is governed by the finite memory size of the Fourier analyzer, as well as the Nyquist frequency. For example, if the size of the Fourier Transform is 1024 and a Nyquist frequency of 256 Hz is chosen, then since the transformed data in general are complex, only 512 points are available to represent the real part of the transformed data, resulting in a resolution of 0.5 Hz.

For auto-spectra, cross-spectra and transfer functions containing narrowband data such as those showing moderately damped structural modes, the frequency resolution must be fine enough to define the amplitude of the peak. The normalized bias error, ε_b, in the estimate of the amplitude of a peak due to insufficient frequency resolution is estimated by Bendat and Piersol (1986) as

$$\varepsilon_b = -\frac{1}{3}\left(\frac{B_e}{B_r}\right)^2 \qquad (3.3)$$

where B_r is the true (not measured) half-power bandwidth of the peak.

It is noted that the bias error is always negative, i.e. the actual amplitude of the peak is higher than the measured amplitude due to this error.

3.4.5 The Statistical Accuracy and Record Length Requirements

It is obvious that the more data points that are included in the analysis, the more accurate will be the estimate of the spectral results. This is related to the total length of time record available, as well as the frequency resolution used in the analysis.

In random vibration data analysis, the statistical parameters are obtained only as estimates of the continuous time-history records of record length T seconds and in the form of discrete independent observations of sample size N. Statistical errors exist between the estimates and the real value. The bias error b, describing the systematic error in the experiment is shown as

$$b[\hat{\phi}\,] = E[\hat{\phi}] - \phi \qquad (3.4)$$

where $\hat{\phi}$ is the estimate of statistical parameter, and

ϕ is the statistical parameter.

Random error σ, as its name suggests, describes the random error in the data as

$$\sigma[\hat{\phi}] = \sqrt{E[\hat{\phi}^2] - E^2[\hat{\phi}]} \qquad (3.5)$$

For $\phi \neq 0$, the normalized random and bias errors are given by:

$$\text{normalized bias error} = \varepsilon_b = \frac{b[\hat{\phi}]}{\phi} = \frac{E[\hat{\phi}]}{\phi} - 1 \qquad (3.6)$$

$$\text{normalized random error} = \varepsilon_r = \frac{\sigma[\hat{\phi}]}{\phi} = \frac{\sqrt{E[\hat{\phi}^2] - E^2[\hat{\phi}]}}{\phi} \qquad (3.7)$$

These error expressions could be used to predict the accuracy of parameter estimates, or to establish the record length required to obtain a predetermined degree of accuracy. Details of the record lengths and averages requirements for different estimates as from Bendat and Piersol (1986) are listed in Table 3.1.

The various error expressions involve either a BT_r product or B_eT_r product where T_r (in place of T) is the total record length, B is the total bandwidth occupied by the data, W is the window width, and B_e is the resolution bandwidth for spectral estimates. From inspection of Table 3.1, it is seen that spectral estimates are the most demanding of the various parameter estimates from the viewpoint of required record length for a given error.

Suppose the power spectrum of the random vibration response of the structure is to be estimated with a maximum random error of $\varepsilon_r = 0.1$. The natural frequencies of the structure are of interest up to 10 Hz and the damping ratio ζ_n for the resonance is about 0.01. The calculation proceeds by using the approximation for the half-power bandwidth B_r of a system resonance as:-

$$B_r = 2\ \zeta_n\ f_n \qquad (3.8)$$

For the worst case when $f_n = 10$ Hz, then B_r will be 0.2 Hz. For a maximum bias error of 0.1, Eqn.(3.3) gives

$$B_e \simeq 0.5\ B_r \text{ Hz} \tag{3.9}$$

Substituting in value of B_r, $B_e = 0.1$ Hz.
The required record length T is given by:-

$$T = (B_e \varepsilon_r^2)^{-1} \text{ seconds} \tag{3.10}$$

Substituting in value of B_e and ε_r,

$$T = ((0.1)\ (0.1)^2)^{-1} \text{ seconds}$$

$$T = 1 \times 10^3 \text{ seconds or } 16.7 \text{ minutes}$$

Thus records of minimum length of approximately 17 minutes should be used in the analysis.

Table 3.1 Record Lengths and Averages for Basic Estimates

Estimates	Symbol	Required Total Record Length	Required No. of Averages
Mean value	$\hat{\mu}_x$	$T_r = \frac{1}{2B\varepsilon^2}\left(\frac{\sigma_x}{\mu_x}\right)^2$	$N = \frac{1}{\varepsilon^2}\left(\frac{\sigma_x}{\mu_x}\right)^2$
Mean square value	$\hat{\mu}_x^2$	$T_r = \frac{1}{B\varepsilon^2}\left(\frac{\sigma_x}{\mu_x}\right)^2$	$N = \frac{4}{\varepsilon^2}\left(\frac{\sigma_x}{\mu_x}\right)^2$
Standard deviation and root mean square value	$\hat{\sigma}_x, \hat{\psi}_x$	$T_r = \frac{1}{B\varepsilon^2}$	$N = \frac{1}{2\varepsilon^2}$
Variance and mean square value	$\hat{\sigma}_x^2, \hat{\psi}_x^2$	$T_r = \frac{1}{B\varepsilon^2}$	$N = \frac{2}{\varepsilon^2}$
Probability density function	$\hat{p}(x)$	$T_r = \frac{1}{WBp(x)\varepsilon^2}$	$N = \frac{2}{Wp(x)\varepsilon^2}$
Cross-correlation function	$\hat{R}_{xy}(\tau)$	$T_r = \frac{1}{2B\varepsilon^2}[1+\rho_{xy}^{-2}(\tau)]$	$N = \frac{1}{\varepsilon^2}[1+\rho_{xy}^{-2}(\tau)]$
Auto-spectral density function	$\hat{G}_{xx}(f)$	$T_r = \frac{1}{B_e\varepsilon^2}$	$n_d = \frac{1}{\varepsilon^2}$

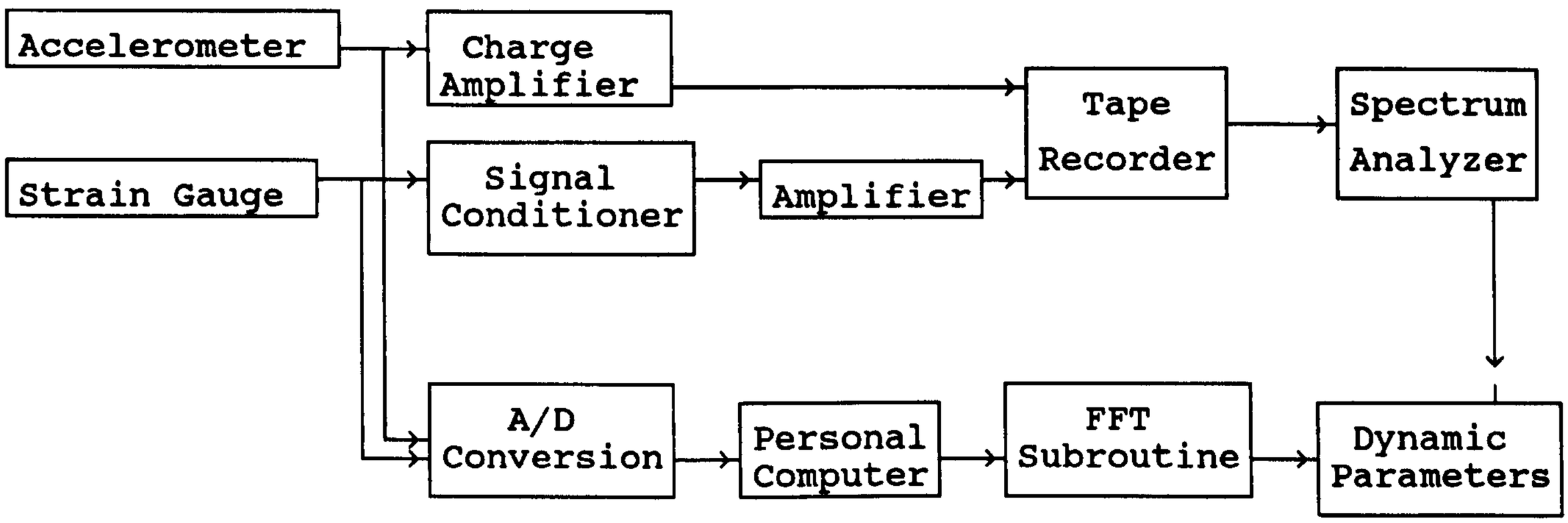

FIG.3.1-Arrangement of Instruments for Dynamic Data Acquisition

CHAPTER FOUR

THE DAMAGE DETECTION TECHNIQUE BASED ON MODAL TESTING

A damage detection technique is discussed in this Chapter which requires the measurement of response to narrow-band excitation or ambient excitation at points of interest on the structure at the undamaged state to form the sensitivity matrix of the basic identification equations. Measurement of response at only two points of the structure are required in later periodic inspection to detect any occurrence of damage in the interval.

The dynamic characteristics of a constant parameter linear system can be described by a weighting function $h(\tau)$, which is defined as the output of the system at any time to a unit impulse input applied a time τ before. For any arbitrary input $x(t)$, the system output $y(t)$ is given by the convolution integral

$$y(t) = \int_{-\infty}^{\infty} h(\tau)\, x(t-\tau)\, d\tau \qquad (4.1)$$

That is, the value of the output $y(t)$ is given as a weighted linear (infinite) sum over the entire history of the input $x(t)$.

The Frequency response function $H(f)$, is defined as the Fourier transform of $h(\tau)$, Bendat and Piersol (1986),

$$H(f) = \int_{0}^{\infty} h(\tau)\, e^{-j2\pi f\tau}\, d\tau \qquad (4.2)$$

Let $X(f)$ be the Fourier transform of an input $x(t)$ and $Y(f)$ be the Fourier transform of the resulting output $y(t)$. By taking the Fourier transform of both sides of Eqn.(4.1),

$$Y(f) = H(f)\ X(f) \qquad (4.3)$$

4.1 THE ORIGINAL WORK

Wang and Zhang (1987) and later Gu et al (1989) have discussed the sensitivity of various modal parameters such as auto and cross spectral density functions, modal frequency, frequency response function and its modulus to small changes in mass, damping and stiffness. An implementation of a damage diagnosis technique based on these sensitivity equations was presented using a frequency response function and its modulus as measured data in the damage assessment of a cantilever beam with a slot.

4.2 THE EXTENSION TO THE ORIGINAL WORK

Phase difference has been proved numerically by Dharaneepathy (1984) and Tsai et al (1985) to be more sensitive to changes in elemental stiffness of a structure than the modal frequencies especially close to resonance. In this Chapter, the sensitivity equations are developed relating the changes in the phase difference of response at two measuring stations to small changes in the elemental mass, damping and stiffness. Damage is defined as a reduction in one of the physical parameters in the elemental stiffness of a finite element, which may be any of the elastic constants or the geometrical dimensions of the element. One of these parameters is selected to be the damage parameter. The phase difference is related to the value of the damage parameter of each element in the structure through the sensitivity equation. This phase difference is expanded in a Taylor's series in terms of the damage parameter to form a set of simultaneous equations, the solution of which gives the magnitude of the damage parameter, the larger values indicate greater damage.

4.3 SENSITIVITY TO DAMAGE

The three basic problems in damage assessment are: (i) what characteristic is most sensitive for detecting the damage; (ii) where is the best place to put the transducer; and (iii) in frequency domain identification, which bandwidth of the response contains the most information about the damage. The following sensitivity analysis aims to provide answers to these problems.

Assuming that the structure mass, damping and stiffness matrix are denoted by [M], [C] and [K], respectively (the elements of which are real) the sensitivity of function $Y=Y(X_1X_2X_3....X_i)$ to argument X_i is

$$\eta(Y/X_i) = \lim_{\Delta X_i \to 0} \frac{\Delta Y/Y}{\Delta X_i/X_i} = \frac{X_i}{Y}\frac{\partial Y}{\partial X_i} \qquad (4.4)$$

where $(X \varepsilon R,\ Y \varepsilon C)$ $\qquad (i = 1,2,.....,n)$

$X_i \neq 0$ and $Y \neq 0$

where R and C represent the real number domain and complex number domain, respectively.

This equation gives the rate between the ratio of the change ∂X_i over X_i before modification and the ratio of the change ∂Y over Y before modification. The larger is $\eta(Y/X_i)$, the greater is the sensitivity.

Usually, the increment in the vibration characteristic is caused by the increment of m parameters simultaneously. The gross relative change is given by

$$\frac{\Delta Y}{Y} = \sum_{i=1}^{m} \eta(Y/X_i)\frac{\Delta X_i}{X_i} \qquad (4.5)$$

4.4 SENSITIVITY OF MODAL FREQUENCIES TO STRUCTURAL DAMAGE

The linear differential equation of a single-DOF system is written as

$$m\ddot{x} + c\dot{x} + kx = f(t) \tag{4.6}$$

The sensitivity of the damped circular frequency ω_d due to variation of mass, stiffness and damping coefficient are given by Wang (1987) as

$$\eta|\omega_d/k| = \frac{1 - 2\zeta^2}{2(1-\zeta^2)} \tag{4.7}$$

$$\eta|\omega_d/m| = \frac{1}{2(1-\zeta^2)} \tag{4.8}$$

$$\eta|\omega_d/c| = -\frac{\zeta^2}{(1-\zeta^2)} \tag{4.9}$$

The absolute values of the sensitivities are plotted in Fig.4.1. It is noted that all the values are less then 1 in the usual cases of damping for which ζ is less than 0.707. Therefore the damped modal frequency is not sensitive to variation in mass, damping and stiffness.

Further it has also been proved by Wang (1987) that the modal frequency for a multi-DOF system is also not sensitive to damages.

4.5 SENSITIVITY OF FREQUENCY RESPONSE FUNCTION, ITS MODULUS AND THE PHASE DIFFERENCE TO DAMAGE

For a n DOF system characterized with mass, stiffness and damping matrices given by [M], [K] and [C] respectively, the equation of motion is given by

$$[M]\{\ddot{x}\} + [C]\{\dot{x}\} + [K]\{x\} = \{F\} \tag{4.10}$$

When the force vector and displacement vector are written as

$$\{F(t)\} = \{F\}\, e^{j\omega t}, \quad \text{and} \tag{4.11}$$

$$\{x(t)\} = \{x\}\, e^{j\omega t}, \tag{4.12}$$

the equation of motion becomes,

$$(-\omega^2\,[M] + j\omega\,[C] + [K])\,\{x\}\, e^{j\omega t} = \{F\}\, e^{j\omega t} \tag{4.13}$$

Taking the Fourier transform of both sides of Eqn.(4.13), the receptance matrix is then written as

$$[Z(\omega)] = [K] - \omega^2\,[M] + j\omega\,[C] \tag{4.14}$$

and the receptance frequency response function matrix as

$$[H(\omega)] = [Z(\omega)]^{-1} \tag{4.15}$$

Taking the first differential with respect to k_{ij}

$$\frac{\partial [H(\omega)]}{\partial k_{ij}} = -\,[H(\omega)]\,\frac{\partial [Z(\omega)]}{\partial k_{ij}}\,[H(\omega)]$$

$$= -\,[H(\omega)]\,\frac{\partial [K]}{\partial k_{ij}}\,[H(\omega)]$$

$$= -\,[H(\omega)]\,\begin{bmatrix} \vdots \\ i \\ \vdots \\ j \end{bmatrix}_i\,[H(\omega)] \tag{4.16}$$

For any element H_{rs} in matrix $H(\omega)$,

$$\frac{\partial H_{rs}(\omega)}{\partial k_{ij}} = -\,H_{ri}(\omega)\;H_{js}(\omega) \tag{4.17}$$

where i,j are any row and column in the system matrices;
r,s are the points of measurements;

p,q are the geometric range of the structure to be diagnosis.

Rewriting Eqn.(4.17), and also for small change in mass and damping, the sensitivity equations are derived by Wang (1987) as

$$\frac{\partial H_{rs}}{\partial k_{pq}} = - H_{rp} H_{qs} \tag{4.18}$$

$$\frac{\partial H_{rs}}{\partial m_{pq}} = \omega^2 H_{rp} H_{qs} \tag{4.19}$$

$$\frac{\partial H_{rs}}{\partial c_{pq}} = - j \omega H_{rp} H_{qs} \tag{4.20}$$

where k_{pq}, m_{pq} and c_{pq} are the elements of the stiffness, mass and damping.

Similarly, for the modulus of FRF, $|H_{rs}|$, the sensitivity equations by Wang (1987) are given without derivation:

$$\frac{\partial |H_{rs}|}{\partial k_{pq}} = - \frac{Re(H_{rp} H_{qs} H_{rs}^*)}{|H_{rs}|} \tag{4.21}$$

$$\frac{\partial |H_{rs}|}{\partial m_{pq}} = \omega^2 \frac{Re(H_{rp} H_{qs} H_{rs}^*)}{|H_{rs}|} \tag{4.22}$$

$$\frac{\partial |H_{rs}|}{\partial c_{pq}} = \omega \frac{Im(H_{rp} H_{qs} H_{rs}^*)}{|H_{rs}|} \tag{4.23}$$

In the above equations, all other terms except ∂k_{pq}, ∂m_{pq} and ∂c_{pq} can be determined by experimental modal analysis.

By expressing the frequency response function H_{rs} as

$$H_{rs} = |H_{rs}|\ e^{j\theta}$$

the phase difference sensitivity equations are derived by the author as an extension to the original work:

$$\frac{\partial\theta_{rs}}{\partial k_{pq}} = j\ \frac{H_{rp}H_{qs}}{H_{rs}} - j\ \frac{Re(H_{rp}H_{qs}H_{rs}^{*})}{|H_{rs}|^{2}} \qquad (4.24)$$

$$\frac{\partial\theta_{rs}}{\partial m_{pq}} = -\ j\ \omega^{2}\ \frac{H_{rp}H_{qs}}{H_{rs}} + j\ \omega^{2}\ \frac{Re(H_{rp}H_{qs}H_{rs}^{*})}{|H_{rs}|^{2}} \qquad (4.25)$$

$$\frac{\partial\theta_{rs}}{\partial c_{pq}} = -\ \omega\ \frac{H_{rp}H_{qs}}{H_{rs}} + j\ \omega\ \frac{Im(H_{rp}H_{qs}H_{rs}^{*})}{|H_{rs}|^{2}} \qquad (4.26)$$

where $\partial\theta_{rs}$ is the change in phase difference between response at two measuring stations r and s due to change in stiffness, mass or damping in elements of coordinates p and q.

In deriving Eqns.(4.20,4.23,4.26), proportional damping is assumed.

For a single-degree-of-freedom system, sensitivity of the different parameter to small changes in stiffness, mass and damping are given as

$$\eta|H/k| = -\ \frac{(1-\bar{\omega}^{2}) - (j2\zeta\bar{\omega})}{(1-\bar{\omega}^{2})^{2} + (2\zeta\bar{\omega})^{2}} \qquad (4.27)$$

$$\eta|H/m| = -\ \bar{\omega}^{2}\left[\frac{(1-\bar{\omega}^{2}) - (j2\bar{\zeta}\omega)}{(1-\bar{\omega}^{2})^{2} + (2\zeta\bar{\omega})^{2}}\right] \qquad (4.28)$$

$$\eta|H/c| = - \frac{(2\zeta\bar{\omega})^2 + j(1-\bar{\omega}^2)2\zeta\bar{\omega}}{(1-\bar{\omega}^2)^2 + (2\zeta\bar{\omega})^2} \tag{4.29}$$

$$\eta||H|/k| = - \frac{(1-\bar{\omega}^2)}{(1-\bar{\omega}^2)^2 + (2\zeta\bar{\omega})^2} \tag{4.30}$$

$$\eta||H|/m| = \frac{(1-\bar{\omega}^2)\bar{\omega}^2}{(1-\bar{\omega}^2)^2 + (2\zeta\bar{\omega})^2} \tag{4.31}$$

$$\eta||H|/c| = - \frac{(2\zeta\bar{\omega}^2)}{(1-\bar{\omega}^2)^2 + (2\zeta\bar{\omega})^2} \tag{4.32}$$

$$\eta|\theta/k| = \frac{1}{\theta} \frac{2\zeta\bar{\omega}}{[(1-\bar{\omega}^2)^2 + (2\zeta\bar{\omega})^2]} \tag{4.33}$$

$$\eta|\theta/m| = - \frac{1}{\theta} \frac{2\zeta\bar{\omega}^3}{[(1-\bar{\omega}^2)^2 + (2\zeta\bar{\omega})^2]} \tag{4.34}$$

$$\eta|\theta/c| = - \frac{1}{\theta} \frac{(1-\bar{\omega}^2)2\zeta\bar{\omega}}{[(1-\bar{\omega}^2)^2 + (2\zeta\bar{\omega})^2]} \tag{4.35}$$

with $\bar{\omega} = \frac{\omega}{\omega_n}$, and ω_n is the modal frequency

where Eqns.(4.33 to 4.35) have been derived by the author.

The phase sensitivity can be explained as the difference between the original phase value of the frequency response function and the modified value when a small change in [K], [M] or [C] occurs.

Eqns.(4.27) to (4.35) are plotted in Fig. 4.2 for $\zeta = 0.05$. It is noted that phase difference is more sensitive to small changes in [K], [M] and [C], especially in the case of a small phase difference between the response of two measurement stations.

It has also been proved by Wang (1987) that for a multi-DOF system the shape of the sensitivity curve when close to the modal frequency, is similar to that of a single-DOF system, and, in general, there exist multi-sensitive ranges in the frequency response function.

4.6 RELATIONSHIP BETWEEN THE DYNAMIC SENSITIVITY AND ELEMENTAL STIFFNESS

Expanding $\Delta\theta$ as a Taylor's series

$$\Delta\theta_{rs} = \sum_{i} \frac{\partial\theta_{rs}}{\partial b_i} \Delta b_i - \sum_{m,n} \frac{\partial^2\theta_{rs}}{\partial b_m \partial b_n} \frac{\Delta b_m \Delta b_n}{2!} + \ldots.$$

$$(r,s=1,2,\ldots\ldots,n) \qquad (4.36)$$

where b_i is the damage parameter which may be any of the elastic constants of material or geometrical dimensions of the element.

For a small change in the elemental stiffness k_{pq}

$$\frac{\partial\theta_{rs}}{\partial b_i} = \sum_{p,q} \frac{\partial\theta_{rs}}{\partial k_{pq}} \cdot \frac{\partial k_{pq}}{\partial b_i} \qquad (4.37)$$

Putting Eqn.(4.24) into (4.37),

$$\frac{\partial\theta_{rs}}{\partial b_i} = j \sum_{p,q} \left[\frac{H_{rp} H_{qs}}{H_{rs}} - \frac{\mathrm{Re}(H_{rp} H_{qs} H_{rs}^*)}{|H_{rs}|^2} \right] \frac{\partial k_{pq}}{\partial b_i} \qquad (4.38)$$

Taking the first term in Eqn.(4.36) and neglecting the higher derivatives, we have

$$\Delta\theta_{rs} = \sum_i \left(j \sum_{p,q} \left(\frac{H_{rp} H_{qs}}{H_{rs}} - \frac{Re(H_{rp} H_{qs} H_{rs}^*)}{|H_{rs}|^2} \right) \frac{\partial k_{pq}}{\partial b_i} \right) \Delta b_i$$

$$= j \left\{ \frac{1}{H_{rs}} (H_r)^T \left[\frac{\partial K}{\partial b_i} \right] (H_s) - \frac{1}{|H_{rs}|^2} Re((H_r)^T \left[\frac{\partial K}{\partial b_i} \right] (H_s)) H_{rs}^* \right\} \{\Delta b_i\}$$

$$= j \left\{ \frac{Im((H_r)^T \left[\frac{\partial K}{\partial b_i} \right] (H_s)) H_{rs}^*}{|H_{rs}|^2} \right\} \{\Delta b_i\} \qquad (4.39)$$

where $\{H_r\}$ is the rth column vector in the frequency response matrix H.

Eqn.(4.39) gives the relationship between the damage vector $\{\Delta b_i\}$ and the measurable parameter $\Delta\theta_{rs}$ through the frequency response function of the undamaged structure.

A point on the frequency response function constitutes one Eqn.(4.39). In practice, as many points as possible around one or more modal frequencies within the sensitive range as given in Eqn.(4.33) are taken to form a set of Eqn.(4.39) written in the following form:

$$\{B\} = [A] \{X\} \qquad (4.40)$$

where $\{B\}$ is the vector of the measurable parameter $\Delta\theta_{rs}$ at different frequencies and $\{X\}$ is the damage vector $\{\Delta b_i\}$. The vector on the left hand side can be determined experimentally, and the elements in the sensitivity matrix [A] are calculated from Eqn.(4.39). The set of simultaneous Eqn.(4.40) can then be solved to obtain values of the damage parameters Δb_i.

4.7 ITERATIVE PROBLEM OPTIMIZATION

Eqn.(4.40) will only yield a unique solution if the number of damage parameters considered is equal to the number of equations available. If the number of equations is less than the number of damage parameters, some mathematical procedure has to be applied to determine the best estimates of the parameters. In fact, the set of Eqn.(4.40) is derived from the frequency response function and it usually contains more equations than unknowns, in which case no exact solution exists. An approximate solution exists in the least squares sense in which the Euclidian norm of the error ε is minimized.

For the set of Eqn.(4.40),

$$\underset{M\times 1}{\{B\}} = \underset{M\times N}{[A]}\ \underset{N\times 1}{\{X\}} \qquad \text{where } M > N \qquad (4.41)$$

Let $\{\varepsilon\} = ([A]\ \{X\} - \{B\})$

The optimization problem is to minimize the Euclidian norm $\{\varepsilon\}^T\{\varepsilon\}$, i.e.

$$|([A]\ \{X\} - \{B\})^T([A]\ \{X\} - \{B\})| \qquad (4.42)$$

with $A \in R$ and $B \in R$ and $M > N$.

The preceding analysis is entirely deterministic. In practice, however, the experimentally determined quantities are really random variables. By including the measurement noise in practice, Eqn.(4.40) can be rewritten into the following state equations:

$$\{B\} = [A]\{X\} + \{V_K\}$$

and $$\{B_{K+1}\} = [A_{K+1}]\{X\} + \{V_{K+1}\}$$

$$= \begin{pmatrix} [A_K] \\ \{a_{K+1}\} \end{pmatrix} \{X\} + \{V_{K+1}\} \qquad (4.43)$$

where $[A_K]$ is the matrix formed from data of κ measurements,

$\{V_{K+1}\}$ is the measurement noise vector from $(\kappa+1)$ measurements,

and $\{a_{K+1}\}$ is the $(\kappa+1)$th row of the matrix $[A_{K+1}]$.

The optimization problem now becomes to minimize

$$\left(\{B_{K+1}\} - [A_{K+1}]\{\hat{X}_{K+1}\}\right)^T \left(\{B_{K+1}\} - [A_{K+1}]\{\hat{X}_{K+1}\}\right) \qquad (4.44)$$

The problem is usually solved by an iterative algorithm, and the $(\kappa+1)$th estimate of $\{X\}$ in the iterative optimization is given by

$$\{\hat{X}_{K+1}\} = \left([A_{K+1}]^T[A_{K+1}]\right)^{-1}[A_{K+1}]^T\{B_{K+1}\} \qquad (4.45)$$

A recursive linear least-squares algorithm described by He (1987) and shown in Eqn.(4.46) is adopted for computer implementation of this optimization problem.

$$\{\hat{X}_{K+1}\} = \{\hat{X}_K\} + \{L_{K+1}\}\left(b_{K+1} - \{a_{K+1}\}\{\hat{X}_K\}\right)$$

$$\{L_{K+1}\} = [P_{K+1}]\{a_{K+1}\}^T$$

$$[P_{K+1}] = [P_K] - \frac{[P_K]\{a_{K+1}\}^T\{a_{K+1}\}[P_K]}{1 + \{a_{K+1}\}[P_K]\{a_{K+1}\}^T} \qquad (4.46)$$

where b_{K+1} is the $(\kappa+1)$th element of vector $\{B\}$,

$[P_K] = ([A_K]^T[A_K])^{-1}$ and $\{L_K\}$ are called the error

variance matrix and gain vector respectively.

This algorithm takes in one linear equation from the set of Eqn.(4.40) as the new set of information of the system in each iteration, and it outputs the variance matrix and gain matrix before updating the estimate of the damage vector {X}. A large initial value has to be input for elements of $\{L_K\}$ which is usually of the order of 10^{+10}. Successful result is seen as convergence in the estimates of {X}.

4.8 CONCLUSION

A damage detection technique is presented which makes use of the phase angle difference between response at two points of a structure as a measurable parameter for the detection of damage occurred in the period between two sets of measurements. No comprehensive finite element modelling is required. Iterative optimization algorithm is used to solve the set of over-determined equations by treating each equation as a new set of information from measurement to solve for the damage parameters $\{\Delta b_1\}$.

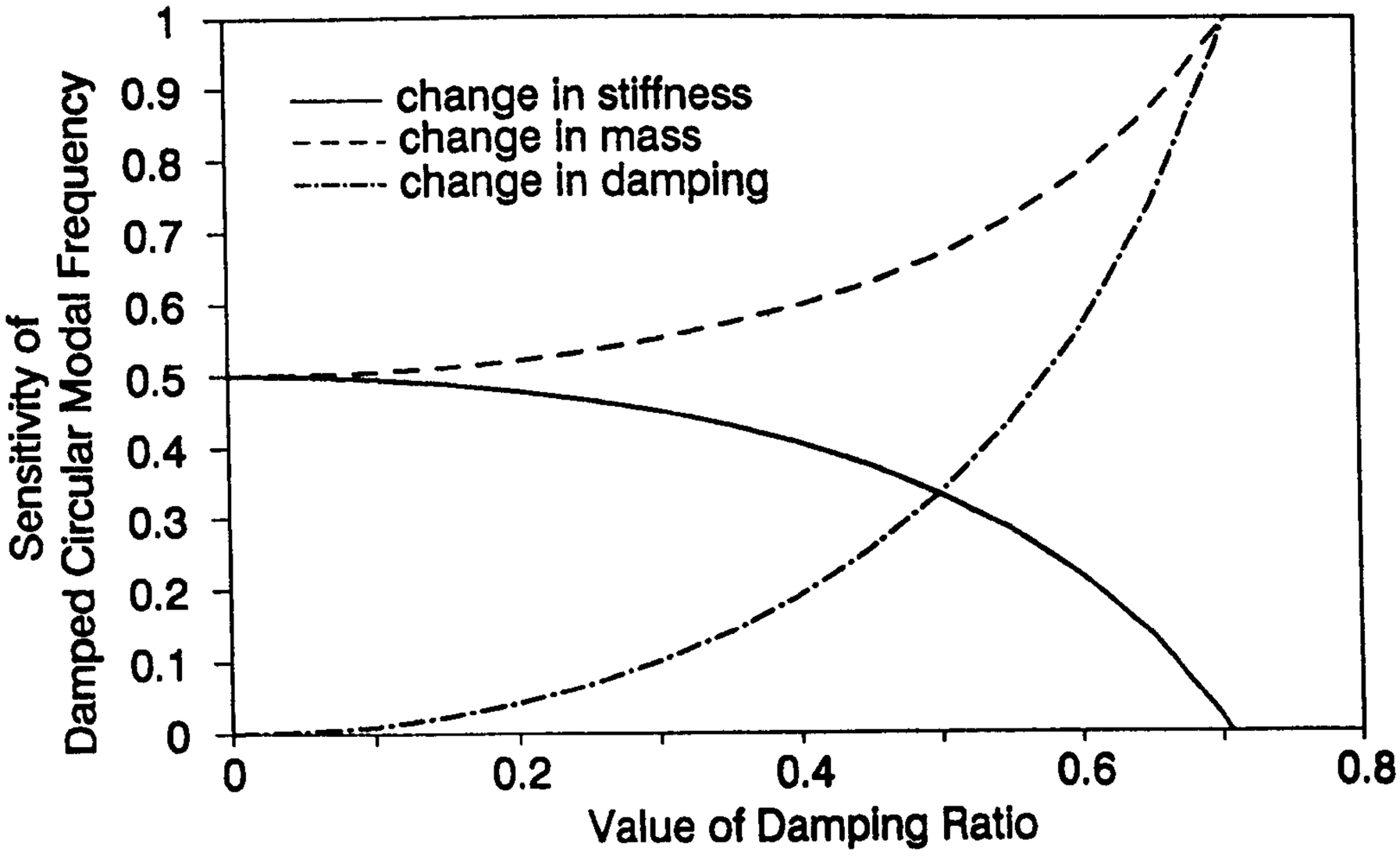

FIG.4.1-Sensitivity of Damped Circular Modal Frequency to small changes in Stiffness, Mass and Damping for a SDOF

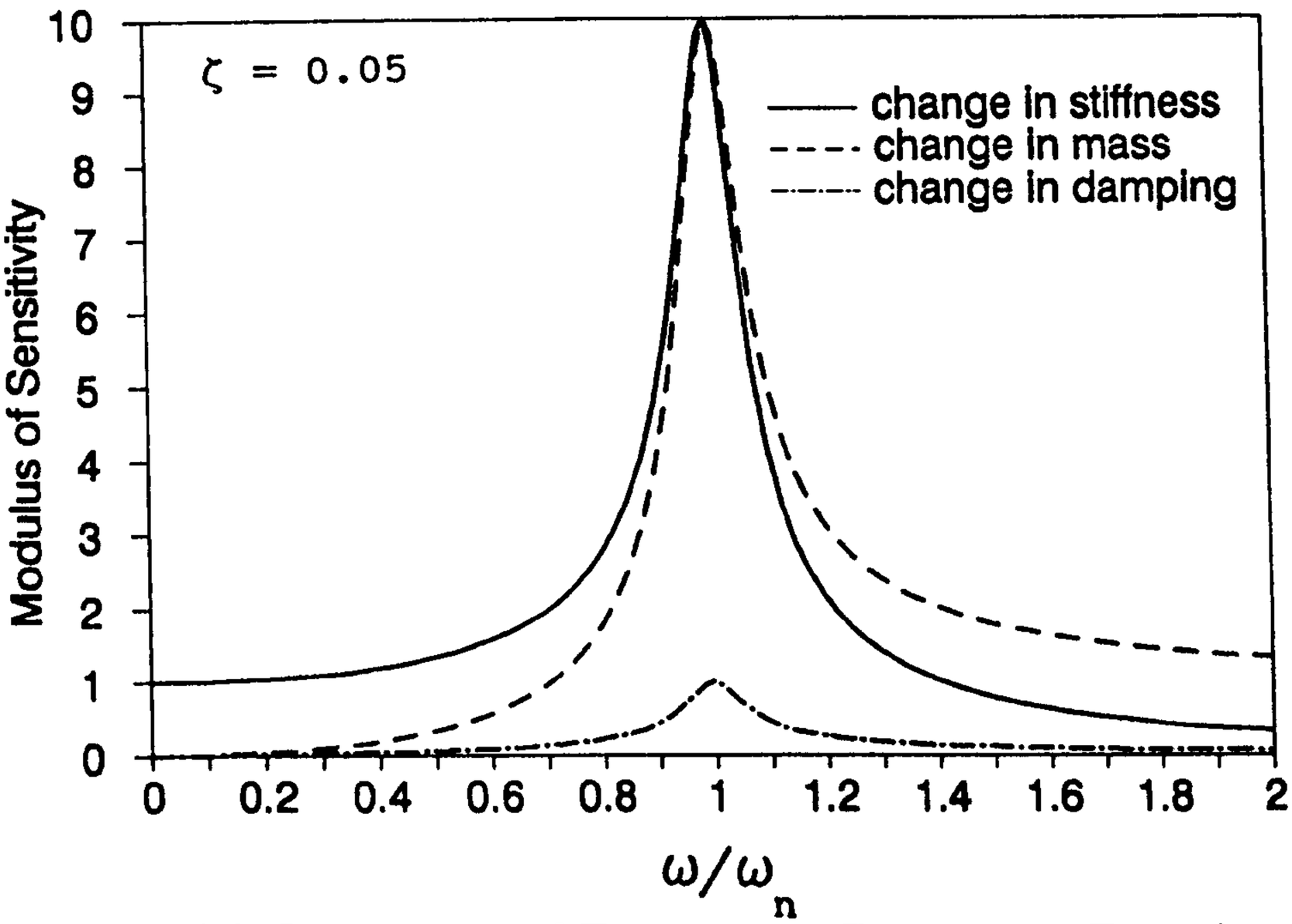

FIG.4.2(a)-Sensitivity of Frequency Response Function

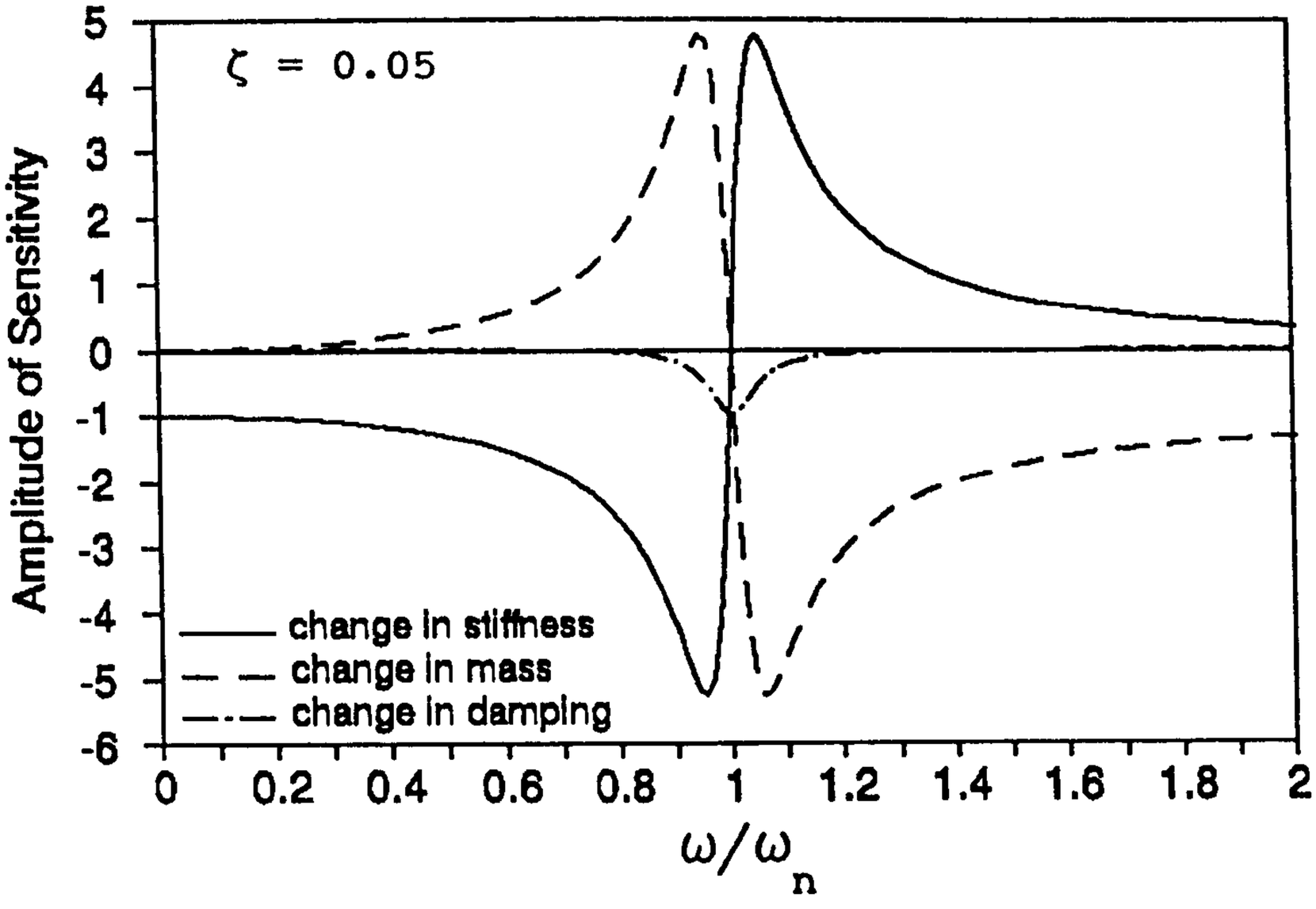

FIG4.2(b)-Sensitivity of the Modulus of Frequency Response Function

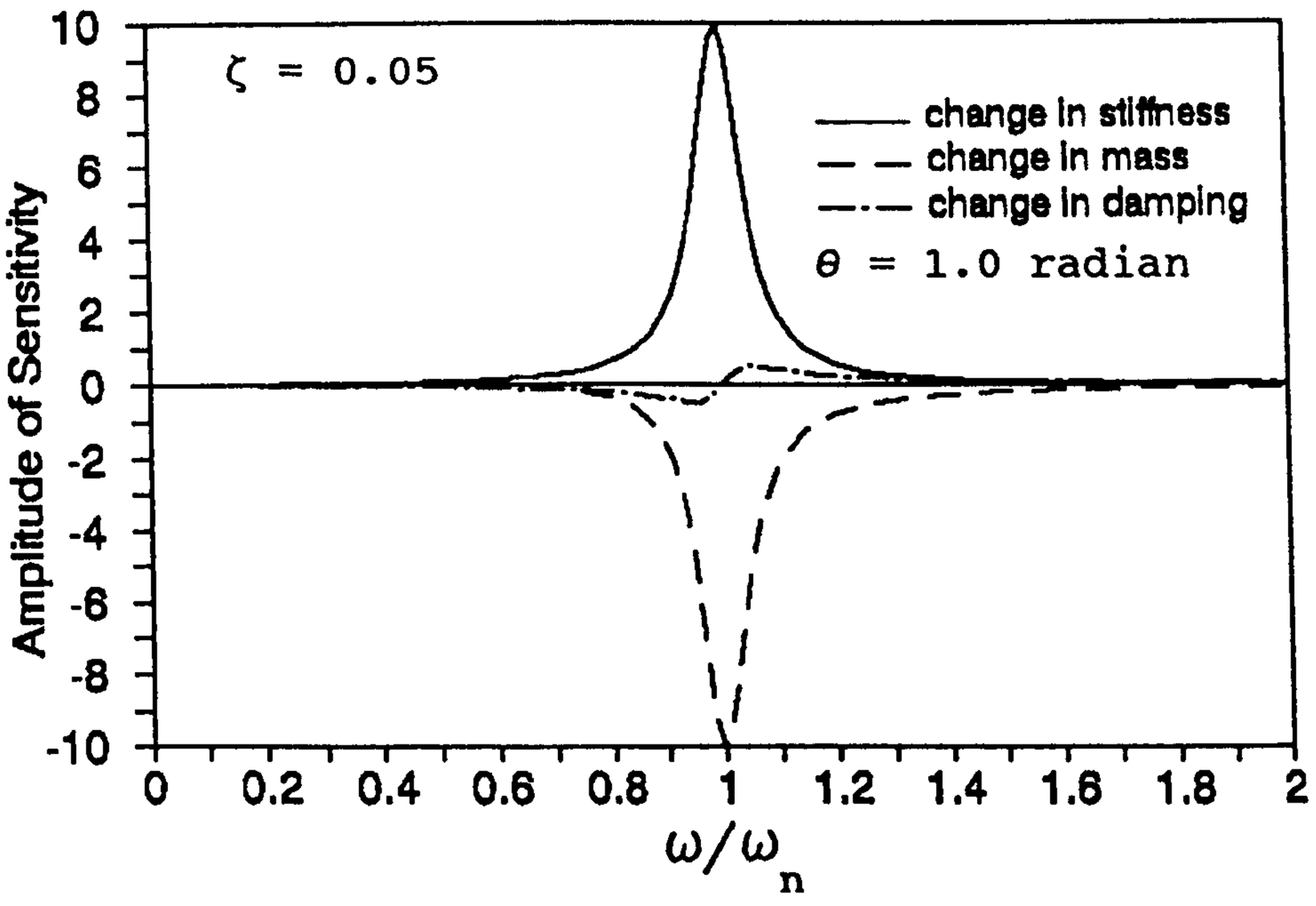

FIG.4.2(c)-Sensitivity of Phase Angle of Frequency Response Function

CHAPTER FIVE

THE DEVELOPMENT OF A FINITE ELEMENT MODEL FOR THIS RESEARCH

5.1 OBJECTIVE OF THIS STUDY

The principal objective of this Chapter is to investigate alternative finite element models and to determine the one that will give the best representation of the dynamic response of a bridge deck. The effect of different boundary conditions on the general dynamic behaviour of the bridge deck is then studied. The more significant factors are incorporated in the development of the proposed method.

5.2 THE OPTIMAL FINITE ELEMENT MODEL

Three different finite element models were investigated and their suitability was assessed by comparing the computed dynamic response with the measured response of a reference small scale reinforced concrete bridge deck.

5.2.1 The Reference Bridge Deck for Modelling

A simply supported reinforced concrete bridge deck 3.2 m long and 1.68 m wide was tested in the laboratory. A plan and elevation of the structure is shown in Fig.5.1. The deck consisted of five precast Tee-beams and five transverse diaphragms. A layer of concrete reinforced with wire mesh was cast on top of the beams to form an integral bridge deck. The physical properties of the materials were determined from material tests, and the geometry of the deck was found by measurement. The support condition was stiff with the beams resting on a block of well-founded precast concrete. Other details are given in Section 6.2.3 of this Thesis.

The measured static modulus of elasticity of concrete was used in the modelling. This decision was based on the tensile test results by Toner (1992) and compression test results by Watstein (1953) on 75 mm diameter cylinders. The tension tests on samples of 52 N/mm^2 characteristic compressive strength indicated a 1.4% increase in the modulus of elasticity with a loading rate 100 times of that specified by BS1881 (1983). Compression tests on samples of 19 N/mm^2 and 44 N/mm^2 characteristic compressive strength indicated 2% and 6% increase respectively in the modulus of elasticity when the loading rate was 86 times and 204 times respectively of that specified by BS1881 (1983).

The loading rate in vibration problem depends on two factors: the magnitude of load and the vibration frequency. In the practical case of a bridge deck under ambient excitation or traffic-generated excitation, the amplitude of vibration at the modal frequencies is small and the modal frequencies are usually below 100 Hz. None of these factors supports the need to use a higher modulus of elasticity in the analysis.

5.2.2 The Finite Element Models

Model 1 - Three-dimensional, mixed beam, plate and membrane elements;

The ribs of the Tee-beams and diaphragms were discretized into beam elements. The flange of the beams together with the cast-in-situ deck were discretized into triangular bending plate elements and rectangular membrane elements. A lump-mass model was used in which the contributions to each modal point by the bridge slab, beams, parapet and kerbstones were considered to be concentrated at the nodal points. Damping was neglected in this study. All 6 degrees-of-freedom (DOF) were unrestrained and the model was

analysed by a finite element software package DDJ-W developed by Dalien University of Technology.

Model 2 - Three-dimensional, mixed beam, plate and membrane elements but with the horizontal DOF restrainted;

The second model was the same as the first except horizontal DOF were restrained. This was to suppress the generation of horizontal modes by the computer software. It was again analysed by software package DDJ-W.

Model 3 - Three-dimensional, all beam elements.

Both the longitudinal beams and transverse diaphragms together with the deck slab were treated as beam elements. The bridge deck was represented by a grid structure. Full composite action was assumed between the slab and the beam. Effective width of the flange was considered in forming the equivalent beam section. Details of the calculation of the effective width can be found in Appendix 5.1. This model was analysed by software package SAP IV on a VAX 850 machine.

The finite element mesh for Models 1 and 2 is shown in Fig.5.1(a).

Model 1 is currently commonly used to evaluate the effectiveness of beam and slab elements. Model 2 is a simplification of Model 1 achieved by removing the unfavourable horizontal modes from the responses. Model 3 measures the effect of representing the beam and slab as an orthogonal grid structure with composite action of the deck on the system.

5.2.3 Comparison of Results

The calculated frequencies and the measured frequencies are shown in Table 5.1. The following notation is used to denote

the modes of vibration of the bridge deck as shown in Fig.5.2.

1B ----- First Bending Mode
1B,1T -- First Bending and First Torsional Mode
1B,2T -- First Bending and Second Torsional Mode
2B ----- Second Bending Mode
2B,1T -- Second Bending and First Torsional Mode

In Model 2, by imposing restriction on the horizontal DOF in Model 1, a significantly larger value for the higher modal frequencies is observed.

The assumption of an orthogonal grid structure for the bridge deck gives very good results up to the fourth modal frequency. The results differ slightly from that of Model 1 and yet the modelling of the bridge deck is much simpler by using only beam elements representing the composite action of the beam and slab.

Model 3 gives the closest results to the measured frequencies. Model 2 is worst and model 1 gives slightly better results. It is concluded that a grid structure best represents the dynamic response of this type of bridge deck.

5.3 PARAMETRIC STUDY OF THE EFFECT OF BOUNDARY CONDITIONS ON THE DYNAMIC RESPONSE

A prototype bridge deck is under ambient excitation and traffic-generated excitation. The mass of a vehicle crossing over the bridge is small when compared with that of the bridge deck which is usually over 100 Tonnes. Hence it could reasonably be assumed that the response of the bridge deck is linear under normal traffic-generated excitation.

Kinnier and McKeel (1965) has studied the effect of substructure on the vibrational response of composite bridge decks. The effect of bearing stiffness was investigated by Moody and Mansell (1980). The following section presents a

systematic investigation into the variation of modal frequency with changes in the support stiffness, cross-section of the bridge deck, configuration of the supporting pier and stiffness of the fencing and kerbstones.

5.3.1 The Bridge Deck for the Parameter Study

A full-scale bridge deck of Ni Zi Bridge was used in this parameter study where the effect of variation of different parameters on the modal frequencies was studied. The bridge deck carried a dual-lane single carriageway with footpath on either side. A cross-section is shown in Fig.5.3. The deck consists of seven precast reinforced concrete Tee-beams 16 metres long with five diaphragms one at either end and the others equally spaced along its length. The diaphragms are precast together with each beam and they are joined together by welding steel plates located at the top and bottom of the diaphragms from adjacent beams. The cast-in-situ reinforced concrete slab is 60 mm minimum thickness with 1.5% slope from the middle of the carriageway. Steel bars projecting from the edge of the precast beams are bent up and cast into the cast-in-situ slab for lateral continuity. More information is shown in Table 8.1.

The pedestrian pavement consists of precast panels resting on the kerbstones of the carriageway and on the edge of the outermost precast beam. The reinforced concrete fencing is supported on small cantilever beams supporting the precast panels.

The bridge deck is supported on 200x150x21 mm rubber pads underneath the ends of each beam. The vertical stiffness of the pads is 840.0E+3 kN/m and the horizontal shear stiffness is 2.1E+3 kN/m from manufacturer's information. The supporting pier consists of a crosshead beam and two circular columns 1.1 m diameter as shown in Fig.5.4. The columns are founded in deep layer of firm soil.

5.3.2 The Finite Element Model

The finite element analysis was carried out using software package DDJ-W. The bridge deck was represented by 14 x 12 four-node non-harmonic isoparametric plane stress elements and 28 x 12 triangular bending elements. Each beam was represented by 12 beam elements with rigid arms at either end connected to the slab nodes. This arrangement limits the local resonant of the beam elements. The nodes on the edge of slab were also rigidly connected to the adjacent slab nodes on top of the outermost beam to avoid local resonance. The rotational degree of freedom of the beams about the z-axis (perpendicular to the bridge deck) was released to reduce the computation time and memory requirement.

Values of Poisson's ratio and modulus of elasticity were taken from the Standard JTJ023-85 (1985).

5.3.3 Effect of Variations in the Vertical Support Stiffness

Moody and Mansell (1980) have investigated this effect on the vibrational response in the form of a stiffness ratio. This is defined as $K/(EI/L^3)$ where the numerator is the stiffness of support and the denominator is the relative stiffness of the bridge deck. A transition range was reported at around a value of 1000 below which there was a rapid increase in the amplification of the static response of the bridge deck. The ratio for a normal bearing-bridge combination was stated to be from 98 to 320.

In this study, the standard bridge deck was assumed to be supported on rubber pads on top of rigid supports. The range of vertical stiffnesses for the rubber pads under study was from 420.0E+3 kN/m to 840.0E+11 kN/m. The horizontal stiffness was kept as one four-hundredth of the vertical stiffness as in practice.

The variation of modal frequencies is plotted in Fig.5.5 which shows that there is little effect due to the variation of support stiffness.

For the most common 200x150 series elastomeric bearing in the People's Republic of China, the range of vertical stiffness is from 420.3E+3 kN/m to 1260.9E+3 kN/m. The change in modal frequencies in this range of vertical stiffness as shown in Fig.5.5 is small, and the effect of vertical support stiffness at the ends of bridge deck may be considered insignificant to the vibrational responses.

However the two ends of a bridge deck may be found on different types of supports and foundation. The structural form of the support may also give rise to a non-uniform distribution of support stiffness underneath each beam. This variation has not been studied further in this research.

5.3.4 Effect of Support Rotational Stiffness at the Beam Ends

Elastomeric bearings may induce rotational restraint at the beam ends such that the measured vibrational response is smaller than the theoretical value. In the present study, only rotational restraint in the plane of the bridge beam was studied. It was applied at the end of each beam, with a range of stiffness from 5.0 to 1.0E+11 kN-m/radian. The effect on modal frequencies is plotted in Fig.5.6.

When the rotational stiffness is small, the system behaves as simply supported. When the rotational restraint is large, the system behaves as with a fixed end condition. There is a transition region from 80.0E+3 to 530.0E+3 kN-m/radian. The ratio of fundamental frequency for a fixed end beam to a simply supported beam is 2.25 which is quite close to the value 2.04 shown in Fig.5.6.

For an elastomeric pad 200x150x21 mm, as the one used in

most of the bridge decks under investigation, the support rotational stiffness is 133.4E+3 kN-m/radian. For the 200x150 series elastomeric bearing, the range of rotational restraint is from 33.36E+3 to 300.2E+3 kN-m/radian. These are within the lower range of simply supported condition except at the higher end when it goes into the transition region as seen from the figure. In fact, their stiffnesses can always be quantified from site inspection and included in the FEM.

However, the rotational restraint at the end of a beam arises not only from the rubber bearing but also from a jammed bridge joint. A fully jammed bridge joint would induce large restraint similar to the fixed end condition. The actual condition has to be assessed on site.

5.3.5 Effect of Pier Height

The crosshead beam shown in Fig.5.4 is tapered where it cantilevers beyond the supporting columns. It was represented in the finite element model by beam elements of different depth. Each column was represented by five beam elements and was assumed to be fixed at the bottom. The rubber pads underneath the beams were represented by short columns with equivalent vertical and horizontal stiffnesses. In the finite element model, the height of column was varied from 4 meters to 12 meters in the study.

When the pier nodes were allowed to move laterally, the pier generated local resonant modes at frequencies far below that of the bridge deck. Hence there is little coupling between the modes of the bridge deck and the pier structure.

The finite element model was analysed by restraining the pier nodes in the lateral directions. The effect of pier height on the modal frequencies of the bridge deck is plotted in Fig.5.7.

There is little effect due to variation of pier height except in Mode 2B, the Second Bending Modal Frequency, where there is a slight decrease of 5% with pier height increases from 4m to 12m.

5.3.6 Effect of Bridge Deck Width

Bakht and Moses (1990) have demonstrated that the transverse diaphragm is very effective in distributing the applied load to adjacent longitudinal members. The bending moment diagram along individual longitudinal members approaches that of the beam under load with increasing numbers and stiffnesses of the diaphragms. A simple beam analogy would be quite sufficient for a superstructure with a large and effective transverse stiffness. This section investigates the suitability of a simple beam analogy in the calculation of vibrational response.

The effect of width/span ratio on the modal frequencies of the structure was studied. The Ni Zi bridge deck was again selected for this study.

The number of main beams in the FEM was reduced from 7 to 1, one beam at a time, and the first modal frequencies calculated for each case, are listed in Table 5.2. The mass of the diaphragm was assumed to be lumped on the corresponding nodal point of the beam. The maximum difference in the first modal frequency is less than 2%. It can be concluded that for a bridge deck with large and effective transverse stiffness, a simple beam analogy is sufficiently accurate for the calculation of the first modal frequency.

5.3.7 Effect of the Fencing and Kerbstones

Buckle (1985) has reported that the road fence or hand-rail contribute to the stiffness of the bridge deck when it is under the working load condition. Transverse static deformation distribution shows that barrier walls and kerbs, whether continuous or not, provide substantial stiffness under the service loading of a single truck, Billing (1984).

In the present study, the fencing and kerbstones were considered to be joined monolithically with the reinforced concrete deck. Some stiffness was being contributed by them giving rise to a set of higher modal frequencies. The modal frequencies are compared in Table 5.3.

The large differences in the modal frequencies shows that the stiffness from fencing and kerbstones has to be taken into account in the calculation of vibrational response.

5.3.8 Discussion on the Effect of Temperature

Richardson and Douglas (1987) has reported that the modal frequencies of a reinforced concrete bridge deck change during the course of a day's testing, and that this is suspected to be due to the diurnal temperature changes. This effect cannot easily be accommodated in a finite element model, and proper documentation of the temperature of the environment has to be made in the field measurement.

5.4 CONCLUSIONS

From the above observations, it can be concluded that in modelling this type of bridge deck for vibrational response, the variations in the substructure and support conditions have insignificant influence on the modal frequencies. In practice, the boundary conditions of the superstructure can be visually inspected and an appropriate stiffness can be

estimated for the rubber bearing and included in the calculation. The condition of the road joint can be assessed during the site visit, and any debris blocking the joint can be removed before carrying out the dynamic measurements.

The stiffness from fencing and kerbstones has to be taken into account in the numerical modelling. But since these structures are not structurally connected into the bridge deck, any part has become loose or disconnected may reduce greatly the additional stiffness. The best approach is to check the condition of the fencing and kerbstones before the dynamic measurement, and to model the detail correctly. Of course, if practicable, the best way is to remove all these additional features before dynamic measurement.

Table 5.1 Calculated and Measured Frequencies for the Model Reinforced Concrete Bridge Deck

Mode type	Measured	Model 1	Model 2	Model 3
1B	35.16	31.65	32.56	35.06
1B,1T	41.21	41.48	42.14	41.75
2B	114.06	112.23	124.22	113.30
2B,2T	139.84	140.25	145.35	137.30
1B,2T	182.81	204.08	209.21	202.10

Table 5.2 Modal Frequency of Bridge Deck with different Number of Main Beams

No. of beam	1	2	3	4	5	6	7
First Modal Frequency (Hz)	6.372	6.383	6.334	6.310	6.296	6.287	6.280

Table 5.3 Modal Frequencies of Bridge Deck with and without Fencing, etc.

Mode Type	Standard	Standard w. fencing, etc.
1B,1T	6.28	7.75
1B	6.42	7.12
1B,2T	18.34	18.73
2B,1T	20.97	26.85
2B	22.28	26.37
2B,2T	29.67	33.07

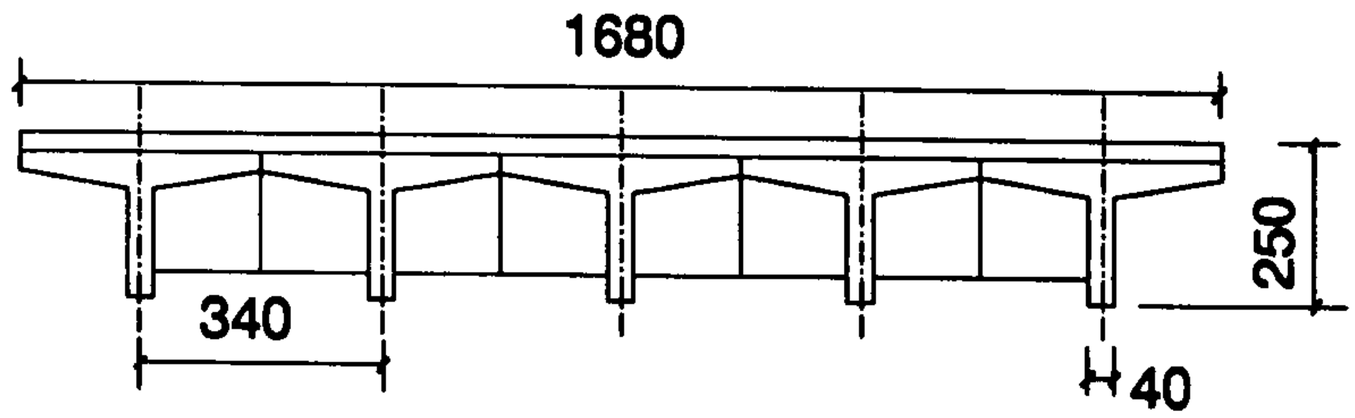

SECTION 1-1

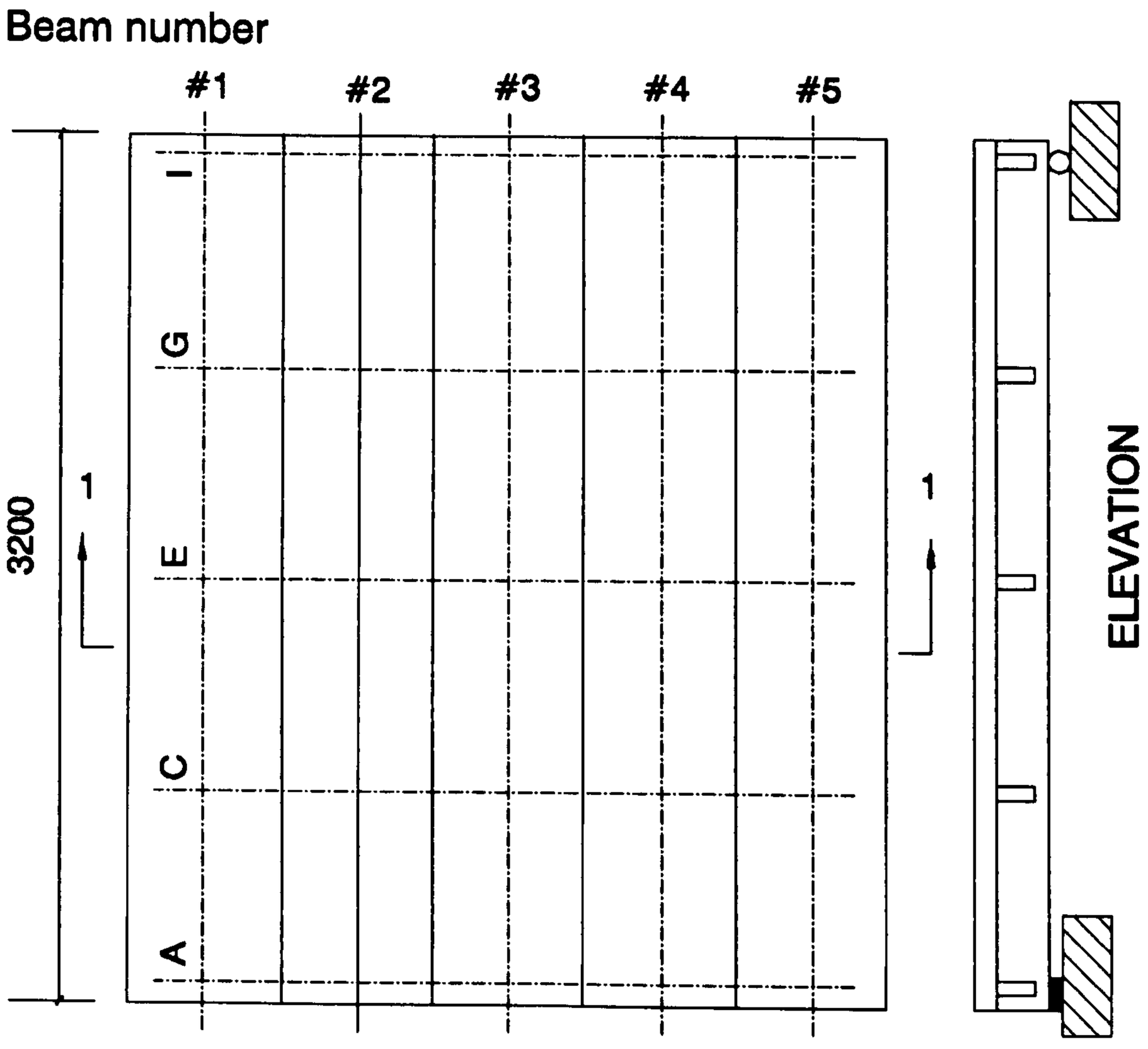

PLAN

FIG.5.1-Grid System and Dimensions of Model Bridge Deck

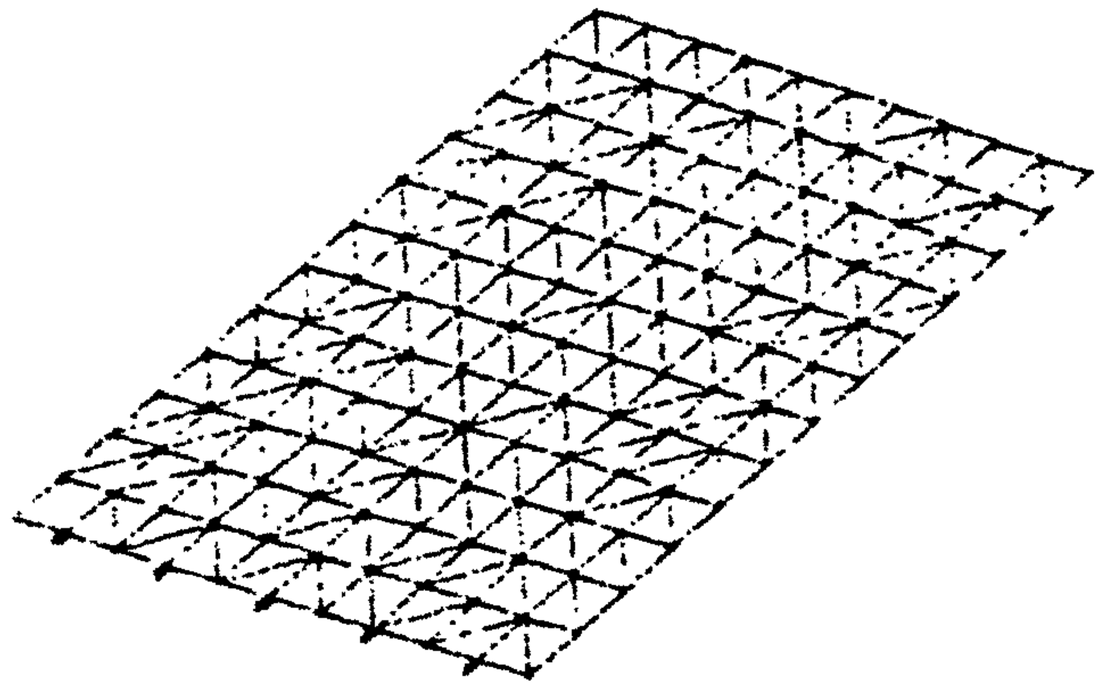

FIG.5.1(a)-Finite Element Mesh for Models 1 and 2

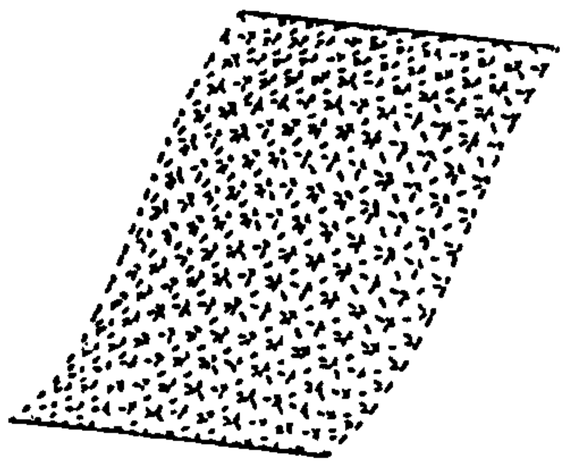

First Bending Mode

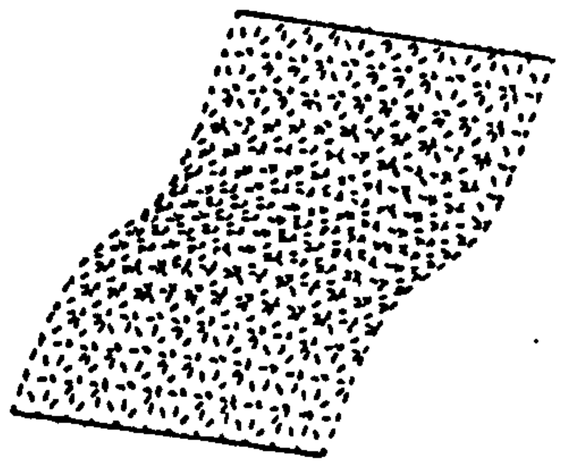

Second Bending Mode

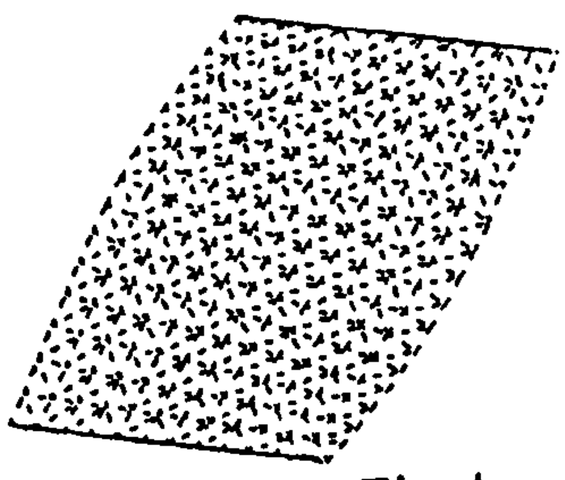

First Bending First Torsional Mode

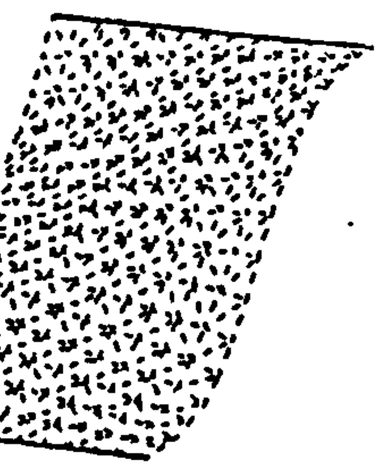

Second Bending First Torsional Mode

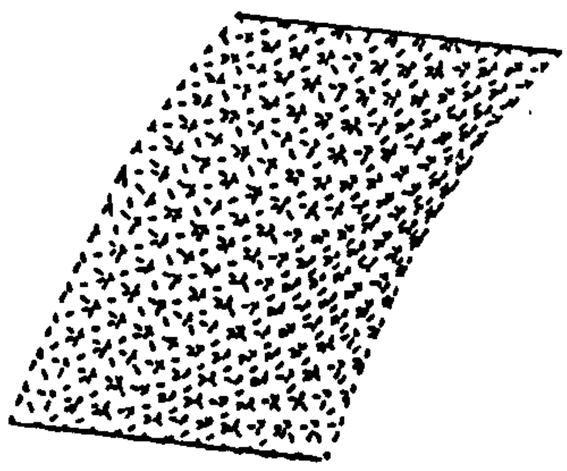

First Bending Second Torsional Mode

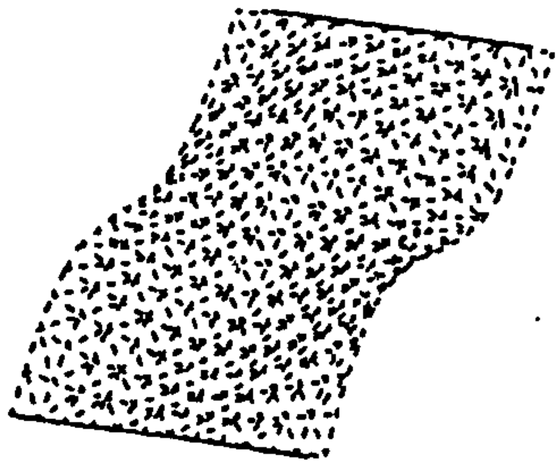

Second Bending Second Torsional Mode

FIG.5.2-Vibrational Mode Shapes of Simply Supported Bridge Deck

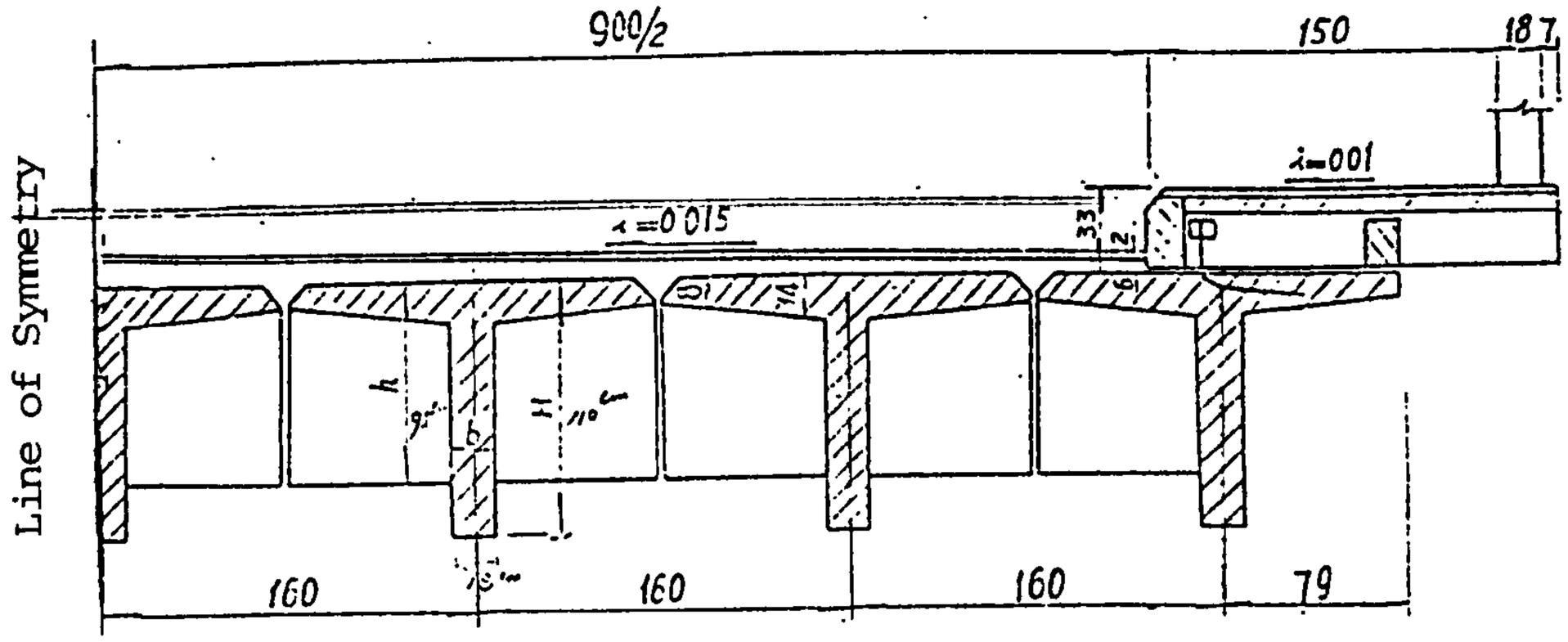

Note - Dimensions are in centimeters

FIG.5.3-Cross-section of Ni Zi Bridge Deck

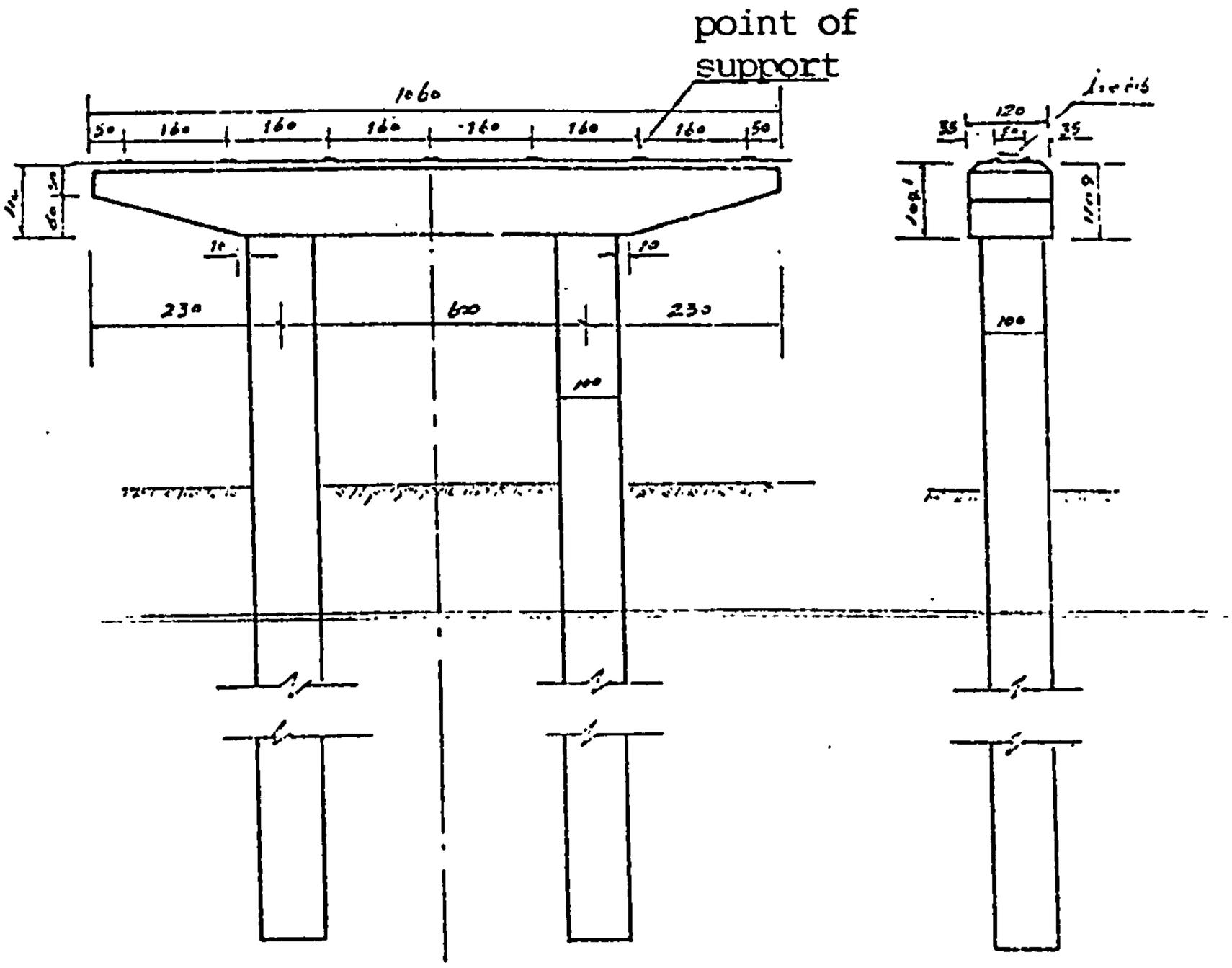

Note - Dimensions are in centimeters

FIG.5.4-Elevation Views of Pier of Ni Zi Bridge Deck

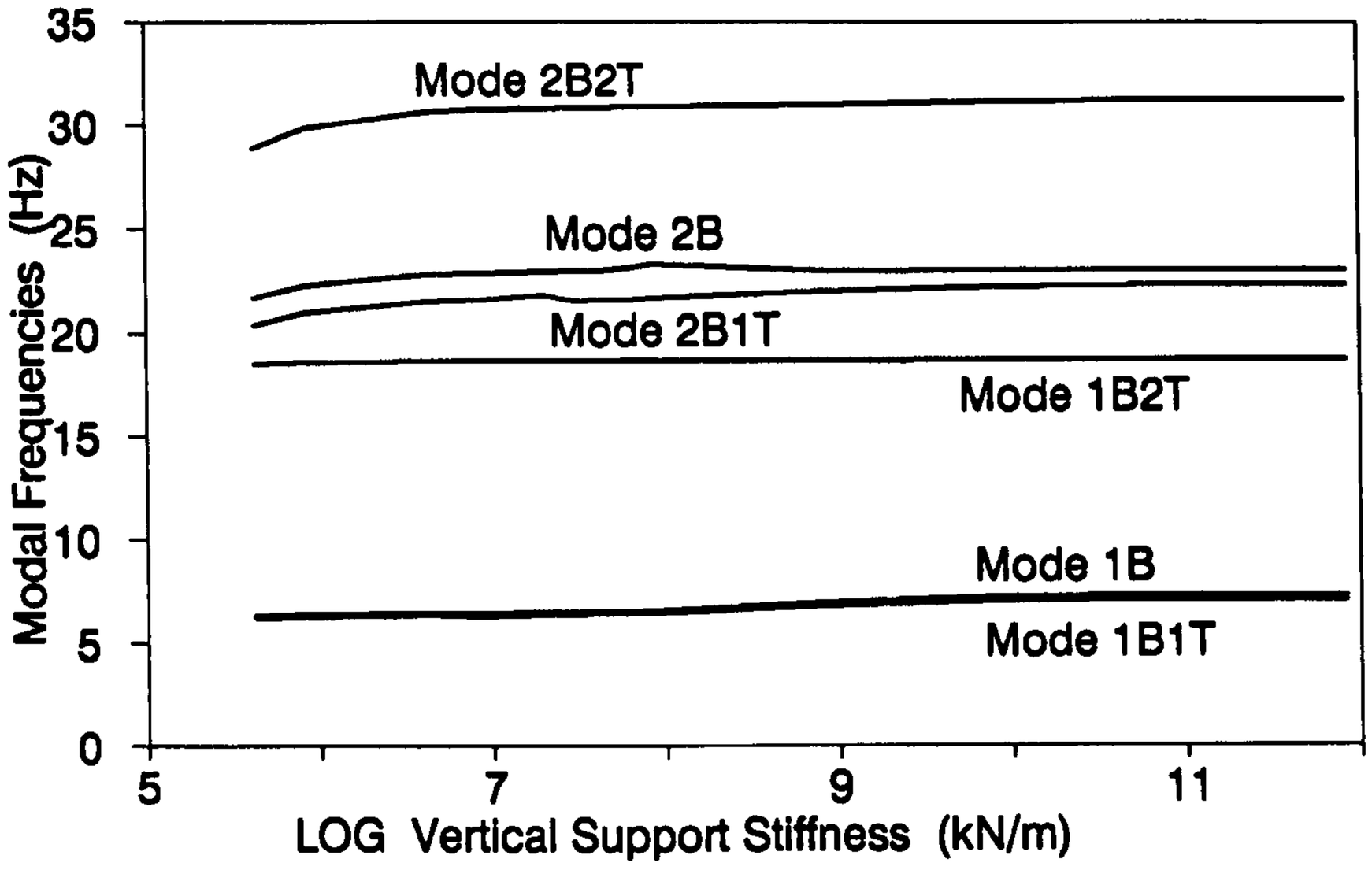

FIG.5.5-Effect of Support Vertical Stiffness on the Modal Frequencies of a Bridge Deck

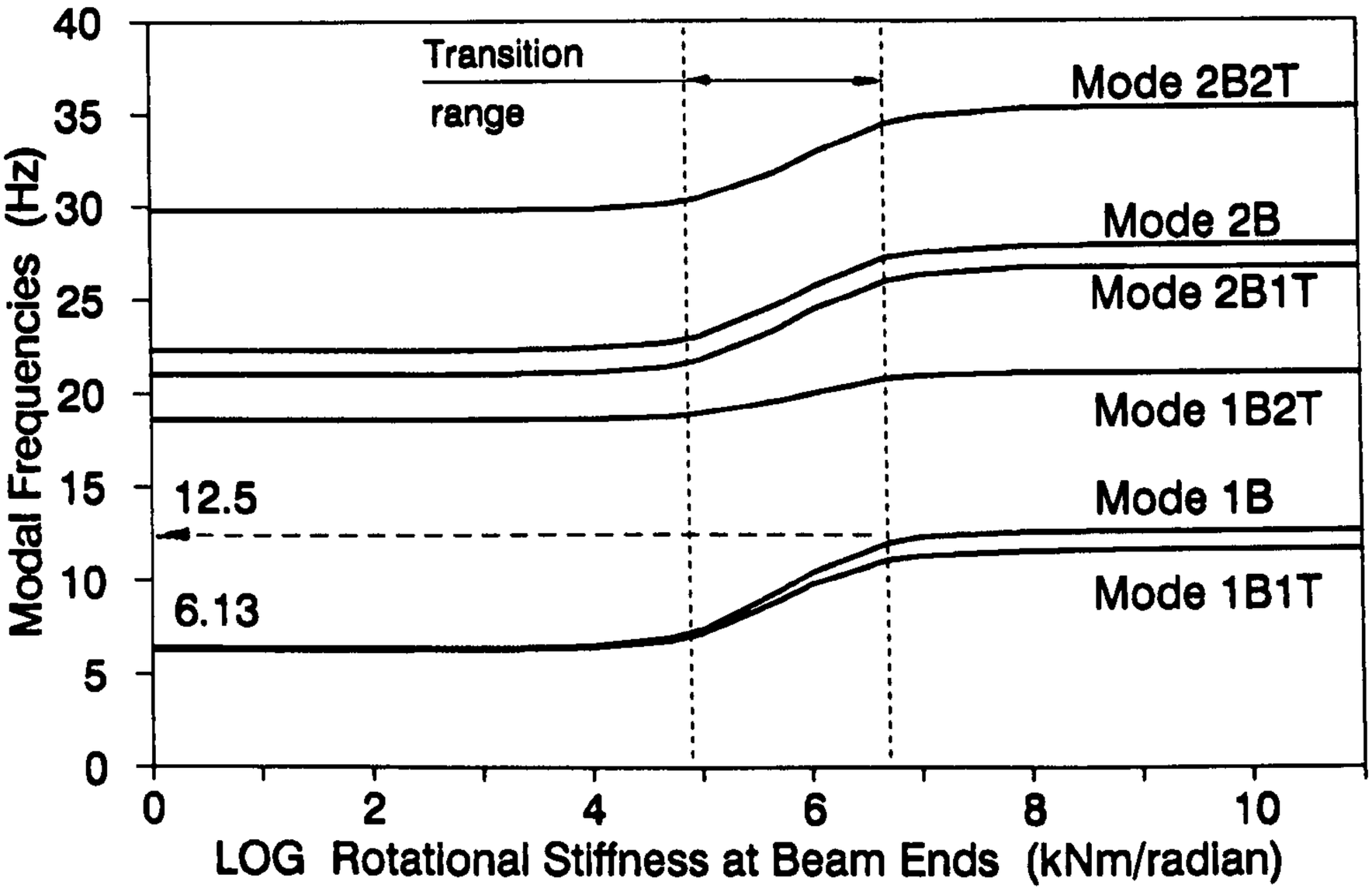

FIG.5.6-Effect of Support Rotational Restraint on the Modal Frequencies of a Bridge Deck

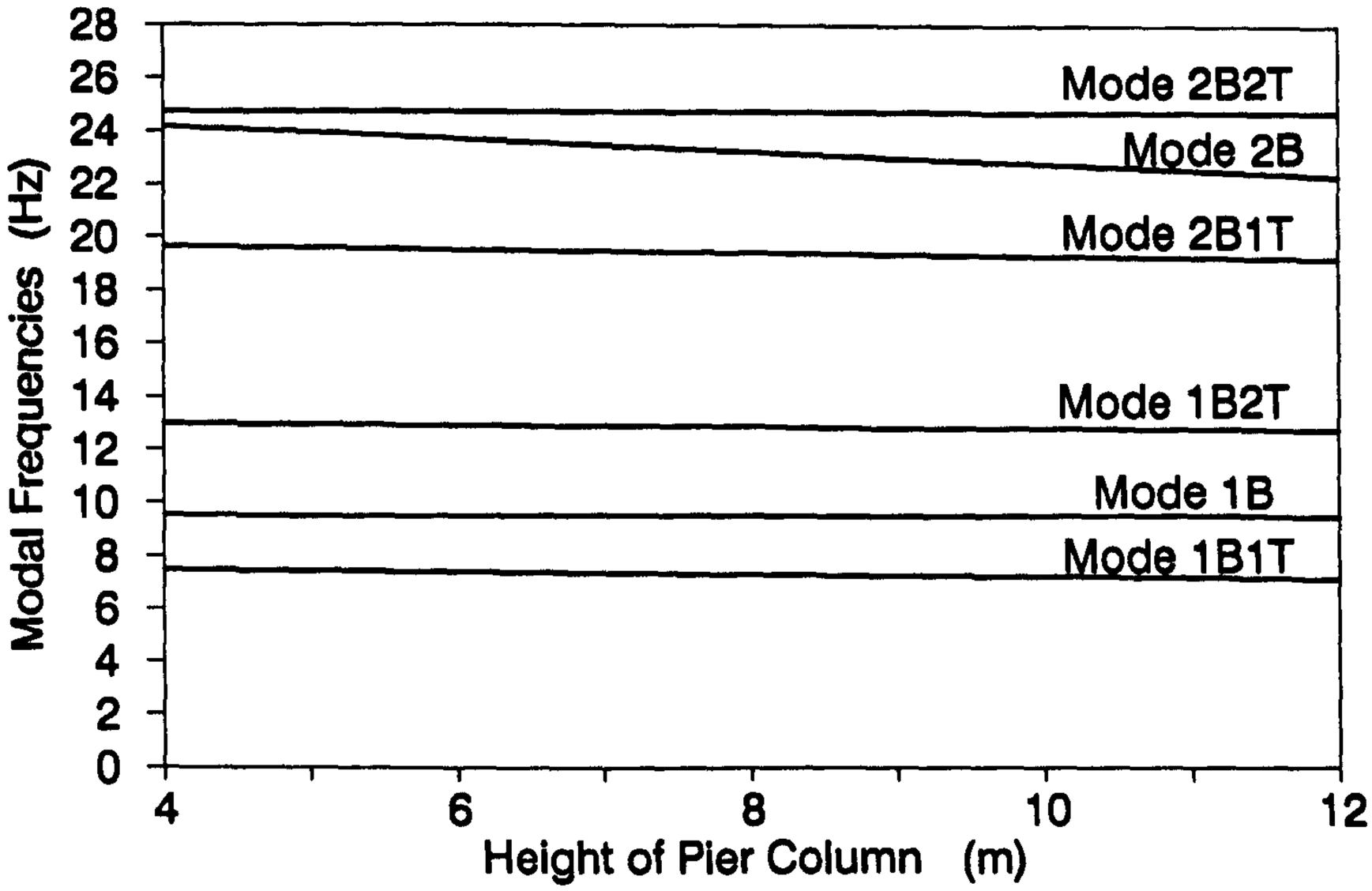

FIG.5.7-Effect of the Height of Pier Column on the Modal Frequencies of a Bridge Deck

CHAPTER SIX

LABORATORY TESTS

6.1 DYNAMIC TESTING OF A STEEL CANTILEVER BEAM

6.1.1 Objective of the Test

The proposed damage detection technique has been presented in Chapter Four. The implementation of the technique is discussed in this Section. The accuracy of the technique using phase difference as the measured parameter is compared, in a controlled environment, with those using the frequency response function and its modulus.

6.1.2 The Experimental Set Up and Instrumentation

A steel cantilever beam under sinusoidal excitation was set up as shown in Fig.6.1. The point of excitation was located 300 mm from the free end. Six B&K 4370 accelerometers were placed above and below the beam to pick up the vibrational responses. A narrow-band signal 31.6 Hz bandwidth generated from a B&K 1027 signal generator was amplified and passed onto a Ling V409 exciter to excite the beam. The responses were recorded on a TEAC-81 data recorder for ten minutes with the centre frequency at each of the first three modal frequencies. The experimental set up was dismantled. A slot 3.2 mm wide and 0.38 mm deep was cut on the top of the beam 200 mm from the fixed end to simulate the structural damage. The test assembly was set up again and another record of the responses of the beam was made.

6.1.3 Experimental Results

Experimental results are presented and discussed in Chapter Seven.

6.2 STATIC AND DYNAMIC TESTING OF A SMALL SCALE REINFORCED CONCRETE BRIDGE DECK

6.2.1 The Research Strategy

For a reinforced concrete bridge deck under load, there is a likely or "nominal" cracked moment of inertia in the beam sections to resist the bending moment. This nominal cracked moment of inertia of the structure is estimated from simulation of the vibrational response of the structure with a finite element model. The uncracked moment of inertia of the deck is also calculated. The ratio of the nominal to the uncracked composite moments of inertia gives a Structural Damage (SD) Factor α, which is an indication of the cracked condition in the structure. This factor varies with increased cracking indicating deteriorations in the bridge deck, and thus it serves as a tool in periodic surveillance of the structure. Furthermore, a Reference Factor α_m, which is an average value of the SD Factor for a group of good and serviceable bridge decks is calculated. Any SD Factor falling below this average value indicates worse than normal cracking in the structure.

For a given reinforced concrete beam section, a curve can be drawn with the nominal cracked moment of inertia against the steel percentage. The moment of resistance of a beam is expressed as a function of the steel percentage according to the limiting criteria of the Standard JTJ023-85 (1985). Hence the nominal cracked moment of inertia is directly related to the moment of resistance of a beam.

All the main beams in a bridge deck are assumed to have approximately the same distribution of cracked moment of

inertia throughout their working life.

The nominal cracked moment of inertia of the beam is then estimated from simulation of the vibrational response of the beam with a finite element model. The steel percentage of the beam is obtained from the graph plotted, and hence the moment of resistance of the beam is calculated. Further consideration on the transverse load distribution property of a bridge deck would give an estimate of the load carrying capacity of the bridge deck.

A Load Carrying Capacity (LCC) Factor β is calculated for each bridge deck which is a ratio of the estimated moment of inertia from dynamic testing to the nominal cracked moment of inertia.

Random error in the estimate of the steel percentage of the beam is minimized by including a Reference Factor β_{LS} in the calculation. This Reference Factor is a statistical average of the LCC Factor of a group of bridge decks of equal span length.

6.2.2 Objective of the Tests

The testing of this structure serves two purposes. It provides a chance to test the applicability of the proposed damage detection technique on a complicated structure like a bridge deck under ambient excitation only. This simulates the actual conditions during field measurement of a prototype bridge deck. It also provides the necessary information in a controlled environment for the development of the proposed method on damage classification and assessment of load carrying capacity of reinforced concrete bridge decks.

6.2.3 The Test Samples

The small scale bridge deck was modelled on the standard bridge deck as shown in the Standard JT/GQB011-73 (1973) to a linear scale of 1/5. No attempt was made to simulate the static stresses, deformation and dynamic responses of the prototype structure in this experiment. Hence model similitude did not need to be considered.

The structure has been briefly described in Section 5.2.1. It was 3.2 m long and 1.68 m wide consisting of five precast main beams connected transversely by five diaphragms. The precast beams were then placed side by side and the reinforcement projecting from the edge of the flanges were hooked together. An additional layer of reinforcement was placed on top and concrete was cast in-situ to form the integral deck. The diaphragms were precast together with the beams. Reinforcement of the diaphragms were welded together both at the top and bottom to simulate actual practice on site. A plan view and sectional elevations of the model has been shown in Fig.5.1. The reinforcement arrangement in the main beams and diaphragms are shown in Figs.6.2 and 6.3. Only 10 mm size aggregate and stone fines were used in the concrete mix.

Two additional precast Tee-beams were also cast. One was cast with the in-situ deck slab whereas the other was not. They are denoted Beam A and Beam B respectively and tested to obtain supplementary information on the behaviour of damaged single bridge beams. The cross-sections are given in Fig.6.4. The beams in the model bridge deck have a flange 20mm wider than for Beam A due to fabrication requirements and is called Beam C for convenience.

The model bridge deck and the two beams were supported on rigid concrete blocks well-founded on the concrete slab of the laboratory.

6.2.4 Instrumentation and Data Acquisition

6.2.4.1 The Static Test Instrumentation

For the model bridge deck, strain gauges were glued onto the concrete surfaces at the top and bottom of the precast beam, the top of the deck slab and on one of the lowest main steel reinforcement bars at midspan of each main beam. Displacements of the structure were monitored by five displacement transducers placed underneath the main beams at midspan. The arrangement of the sensors at midspan is shown in Fig.6.5. A similar arrangement was adopted for the two individual beams as shown in Fig.6.6.

The instruments used included a complete data-logging system to monitor signals from the strain gauge-based sensors. The arrangement of the data acquisition system is shown in Fig.6.7. The following is a list of the equipment forming the static data acquisition system.

1. Static Data Logger Model KYOWA-UCAM5BT
2. Personal Computer IBM/PC/AT
3. Displacement Transducers Model TML-CDP-25, 50 and 100
4. Load Cell Model TML-KC-50M
5. Strain gauge installation tester Model Measurement Group 1300

The strain gauges were connected to the data-logger via two 50 channel analogue scanners. The acquisition of strain gauge readings were controlled by an IBM/PC/AT microcomputer using a data acquisition programme developed by the author, Law and Kai (1991).

6.2.4.2 The Dynamic Test Instrumentation

The accelerometers were placed on top of the structure. The vertical vibrational response signals in the form of

accelerations were recorded on tape recorders. The arrangement of the equipment for dynamic measurement has been shown previously in Fig.3.1. The following is a list of the equipment forming the dynamic data acquisition system.

1. Personal Computer IBM/PC/AT
2. A/D - D/A Card Model Data Translation DT2801-A and DT2829
3. Accelerometer Model B&K 8306
4. Accelerometer Model B&K 4370
5. Accelerometer Model 6153
6. Charge Amplifier Model B&K 2635
7. RMS Voltmeter Model DATRON-1030
8. Dual Trace Oscilloscope Model Deltax DX 5015S
9. Data Tape Recorder Model KYOWA-RTP-800A
10. Data Tape Recorder Model TEAC R-81
11. Spectrum Analyzer Model HP-5420B

6.2.5 The Test Programme

The static and dynamic testing of this model bridge deck was carried out over two weeks in the laboratory with an ambient temperature of 28°C~33°C. This serves as a reference temperature range for comparison of case studies in the future.

6.2.5.1 The Static Test Programme

The static loading was applied in two ways. The first method was to load the middle of each beam in turn up to 20 kN to assess the load distribution property of the bridge deck. The second method was to load incrementally at the middle of Beam #2 to study the structural behaviour and failure mechanism. The deformation of the structure and the stresses in material were recorded during each loading cycle. The development of cracks in the structure was also recorded. The crack patterns of Beams #1 to #4 of the bridge deck are

shown in Fig.6.8 whereas the bottom view of the crack pattern of the bridge deck after test is shown in Fig.6.9. Only a few cracks are detected in Beam #5 and the crack pattern is therefore not shown. The different cycles of loading carried out are described as follows:

1. Dynamic tests.
2. Static load up to 10 kN was applied to the middle of each beam in turn to measure the transverse load distribution of the bridge deck, and then unloaded.
3. Beam #2 was loaded up to 60 kN when cracking occurred in Beams #1 and #2, and then unloaded.
4. Dynamic tests.
5. Beam #2 was loaded up to 70 kN, and then unloaded.
6 Static load up to 20 kN was applied to the middle of each beam in turn to measure the transverse load distribution of the bridge deck, and then unloaded.
7. Dynamic tests.
8. Beam #2 was loaded up to 86 kN, and then unloaded.
9. Dynamic tests.
10. Beam #2 was loaded up to 98 kN, and then unloaded.
11. Dynamic tests.
12. Beam #2 was loaded up to 115 kN, and then unloaded.
13 Dynamic tests.
14. Beam #2 was loaded up to 140 kN, and then unloaded.
15. Dynamic tests.
16. Static load up to 20 kN was applied to the middle of each beam in turn to measure the transverse load distribution of the bridge deck, and then unloaded.

The two individual beams were tested in a similar way with the static load applied at midspan. The different loading cycles carried out are summarized in Table 6.1. The stresses and deformations under loading were monitored at each stage, and the crack patterns for each beam after testing are shown in Fig.6.10.

6.2.5.2 The Dynamic Test Programme

Dynamic tests were carried out (i) before any static test was carried out, (ii) immediately after each static test, and (iii) after failure of the structure.

Response of the structure to ambient excitation was recorded. The excitation was provided from traffic outside the laboratory, laboratory apparatus, industrial plant on construction sites nearby, and mechanical plant in adjacent laboratories and other environmental excitation transmitted through the supports. The analogue vibrational signals were then passed through a low-pass filter and an A/D conversion, Law and Kai (1991), was made on the output to allow analysis by a FFT subroutine, Law (1991). The signal could be analysed also with a spectrum analyzer. A minimum record length of 25 minutes was adopted to ensure a maximum 10% random error and bias error in the spectral estimates as described in Bendat and Piersol (1986). The bridge deck was marked by grid lines as shown in Fig.5.1 to identify a total of 25 stations. A group of seven accelerometers was moved around to measure all 25 stations in the four different arrangements shown in Fig.6.11. One measurement station was unchanged for each of the repeated measurements to serve as a reference.

Beams A and B were tested in a similar way with the arrangement of accelerometers shown in Fig.6.12.

6.3 The Static Test Results

6.3.1 Material Properties

Three samples of the 16 mm diameter mild steel bar used as main reinforcement in the beams were tested providing an average yield strength of 350 N/mm^2 and yield strain of 1746 microstrain. This corresponds to Class II reinforcement of

the Standard JTJ023-85 (1985).

Results from six number 150x150x15 mm concrete cube tests gave an average concrete strength for the main beams and the in-situ deck slab of 28.1 N/mm^2 and 33.2 N/mm^2 respectively. These correspond to Grade 50 and 60 concrete of the Standard JTJ023-85 (1985). Average values of modulus of elasticity were 26.4 kN/mm^2 and 31.2 kN/mm^2 respectively. These were rather lower than expected for these grades of concrete probably because the concrete contained only 10 mm maximum size aggregate.

6.3.2 General Static Behaviour and Failure Mechanism

The load was applied at midspan of Beam #2 in all the loading cycles. The load corresponding to the onset of the plastic range of the steel was 115, 120 and 130 kN at approximately 1500 microstrain for Beams #2, #1 and #3 respectively. (There is residual strain after each loading cycle, and the total of which when added onto 1500 microstrain gives approximately 1700 microstrain which is close to the actual yield strain of the steel reinforcement obtained from tests). At a load lower than 115 kN, cracks which developed in the main beams did not cause any significant change in the patterns of transverse distribution of deflection and steel strain at midspan of each beam, as observed from Figs.6.13 to 6.16. At 115 kN, the main steel in Beam #2 yielded and Beams #1 and #3 resisted a higher proportion of further increases in load resulting in a large increase in steel strain in the other beams (Fig.6.16). A plot of deflection versus strain in the reinforcement shows the yielding of reinforcement very clearly in Figs.6.17 to 6.19 for Beams #1, #2 and #3. At 120 kN, steel in Beam #1 yielded and Beams #3 and #4 contributed more to the load resistance. At 130 kN, steel in Beam #3 yielded, and failure of the bridge deck was observed at 140 kN with a large increase in deflection for no increase in

the applied load.

Furthermore, Fig.6.9 shows a pattern of cracks in the deck soffit radiating from the point of load very similar to the yield line pattern in a plate. Most of the cracks in the flanges of beam occurred after 115 kN. This indicates that the diaphragms of the bridge deck are very effective in transmitting the load to adjacent beams throughout the loading ranges.

The tensile reinforcement in Beams A and B yielded at 32kN and 29kN respectively. The load versus deflection and strain in the reinforcement versus deflection curves are plotted in Figs.6.20 to 6.23. The curves show a very distinct failure load when the strain in the reinforcement reaches approximately 1500 microstrain. Again the addition of residual strain gives a yield strain of approximately 1700 microstrain, similar to that measured in tests.

6.3.3 The Transverse Load Distribution Properties Based on Strain in the Reinforcement

The bridge deck comprises five Tee-beams of equal cross-section. By its very nature, the bridge deck behaves as an integral structure to resist the applied bending moment. All the beams are assumed to be in the same cracked condition. (This is supported by the study on the neutral axis variation of the beams in Section 7.2.1.1). Hence it is assumed here that the section modulus at the level of the main reinforcement is the same for each of the five beams. The distribution of strain in the reinforcement of each beam is therefore proportional to the distribution of the applied loading. The strain when multiplied by the modulus of elasticity gives the stress, and when multiplied again by the section modulus at the main steel level provides an estimate of the bending moment at the cross-section.

The total elastic strain in the main reinforcement at

midspan of all the beams is first calculated. The transverse load distribution factors are then obtained by expressing the strain in each beam as a percentage of that total, and they are shown in Figs.6.24 and 6.25. The factors do not change with applied load up to 110 kN. When Beam #2 failed at 115 kN, the factor for Beam #2 became smaller and that for Beam #1 increased. After 120 kN when Beam #1 failed, the factor for Beam #1 became smaller and that for Beam #3 increased until Beam #3 failed at 130 kN. This failure sequence is clearly seen in Fig.6.25.

Similar load distribution factors have also been calculated based on longitudinal strain in the concrete on the top surface of the deck slab. The distribution factors are similar but do not show up the failure sequence as clearly as those calculated from steel strain. Values of the transverse load distribution factor before failure of Beam #1 are shown in Table 6.2.

6.3.4 The Transverse Load Distribution Properties Based on Deflection at Midspan of the Beams

When a concentrated load is applied at midspan of Beam #2, Beam #2 receives loading largely from the concentrated load. The other beams receive the load from a more uniform distribution of load from the adjacent beams through the deck slab and transverse beams. Furthermore, the distribution of load along the length of the beams is different, and therefore the deflection, bending moment and shear force in the beams at one cross-section do not have the same ratio as at another section.

Li and Shi (1987) have concluded that by replacing a single point load with an equivalent sine loading on the beam would satisfy the assumption that each beam has the same distribution of load along its length. The deflection then calculated is only 1.5% below that obtained from a single point load.

Hence by accepting this small error, the same distribution of load on each beam across a cross-section is assumed along the bridge deck, and the total deflection at midspan of all the beams is first calculated. The transverse load distribution factors are then obtained by expressing the deflection in each beam as a percentage of that total. These are given in Table 6.2 and Figs.6.26 and 6.27. The factors do not change with applied load up to 115 kN. After 115 kN, the factors for Beams #1 and #2 increase with load while those for Beams #4 and #5 decrease, as shown in Fig.6.27.

The difference between the factors calculated based on deflection and on steel strain is only 1.9% for Beam #1 and 3% for Beam #5. Since deflection at midspan of the beam is a more easily measurable parameter than strain in the reinforcement, the transverse load distribution factor based on deflection is therefore used in this study.

6.3.5 Variation of the Transverse Load Distribution Factors under Static Load

The transverse load distribution factors of the bridge deck were calculated when load was applied at the midspan of each beam in turn. These factors are shown in Figs.6.28 to 6.31. When the beam was first cracked after the 70 kN loading cycle, there was no observable difference in the factors when the 12kN load and then the 20kN load was applied to the beams. But after failure of the bridge deck at 140 kN, there were differences in the factors when 10kN and 20kN loads were applied to Beam #1. The changes for Beams #1, #2 and #3 were -4.5%, +23.0% and +30.0% respectively. This indicated damage in the transverse connection between Beams #1 and #2 and between Beams #2 and #3 had occurred which had an effect on the load distribution.

Next, the transverse load distribution factors for the bridge deck were calculated for each of the loads applied at

midspan of Beam #2. Only values for the first attainment of each load in the different loading cycles are selected and plotted in Figs.6.32 and 6.33. The factors are relatively constant from very small loads up to the first yield load of 115 kN. Fig.6.32, which is based on the strain in the reinforcement, shows a clear picture of the sequence of yielding of steel in Beams #2, #1 and then #3. This sequence does not show up in Fig.6.33 which is based on the deflection at midspan of the beams. It can be concluded that a significant change in the transverse load distribution factor occurs at the yielding of the reinforcement in any one of the beams. The history of strain in the reinforcement shows a clearer sequence of failure than the deflection at midspan of beams.

6.3.6 The Design Failure Load

Details of the calculations for the moment of resistance of a Tee-beam in accordance with the different limiting criteria in the Standard JTJ023-85 (1985) are given in Appendix 6.1.

The moment capacities of Beams A, B and C in the model bridge deck under the different limiting criteria are calculated and are listed in Tables 6.3 and 6.4. Since the neutral axis depth under the ultimate strength condition is within the depth of the in-situ deck slab, which is of a higher grade concrete, concrete of characteristic compressive strength 33.2 N/mm^2 as measured from controlled tests is used in the calculation for Beams A and C while a compressive strength of 28.1 N/mm^2 is adopted for Beam B. The yield strength of steel is 350 N/mm^2 as obtained from tests. A modulus of elasticity of 26.4 N/mm^2 is used for Beam B and 28 kN/mm^2 is used for Beams A and C in the calculation against defection criterion. The compression steel is neglected in the calculation. The moment due to the self weight of the beam is also calculated.

6.3.7 The Experimental Failure Load

The experimental failure load corresponding to 1746 microstrain in the main reinforcement (including residual strain) of Beam #2 is 115 kN. The failure load is divided by 1.25, the partial factor of safety for steel in the Chinese Code. It is multiplied by the transverse load distribution factor of the bridge deck in Table 6.2 and the resulting experimental failure loads are shown in Table 6.3. The experimental failure loads for the individual beams are shown in Table 6.4.

No record of crack width was taken, and therefore the history of crack width increases under load is not analysed here.

6.3.8 The Comparison of Failure Loads

The ratios of design to experimental failure load under different limiting conditions are calculated and listed in Tables 6.3 and 6.4. If we consider the strength criteria, the ratio is 0.717 and 0.665 for the individual Beams A and B. It is 0.85 for Beam C.

Failure is controlled by deflection criteria in both the individual beams and the bridge deck. Strength failure is defined by the strain in the reinforcement attaining the yield strain, which is the under-reinforced failure assumed in design.

The overall factor of safety of the structures based on the strength criterion is 1.17 for the bridge deck, 1.39 for Beam A and 1.50 for Beam B.

The use of 0.85 $E_h I_{o1}$ as stated in Appendix 6.1 from the Standard JTJ023-85 (1985) in calculating deflection is appropriate to give a similar factor of safety to that for

strength limit in all three structures.

6.4 THE DYNAMIC TEST RESULTS AND THE COMPUTER MODEL

The modal frequencies obtained from random vibration measurement are shown in Tables 6.5 to 6.7 for Beams A, B and the model bridge deck respectively. The general criteria for the acceptance of spectral estimates discussed in Section 3.4.1 were used to obtain these modal frequencies. Only a limited number of modal frequencies were found for each of the structures. There were strong noises in the frequency spectra and the level of vibration at the higher modal frequencies were small and mixed together with other spectral peaks originating from different sources of excitation. This made the determination of damping from the spectral peak difficult and in most of the cases impossible. No damping estimates were calculated from these spectra.

The computer model for the model bridge deck has been discussed in detail in Chapter Five. The bridge deck was represented by a simply supported orthogonal grid structure. Full composite action was assumed between the slab and the beams. The effective width of the flange was considered in forming the equivalent beam section. Simply supported beams were assumed for the individual Beams A and B. Modulus of elasticity was taken to be 28 kN/mm^2 for Beam A and the bridge deck, and 26.4 kN/mm^2 for Beam B. These models were analyzed by the software package SAP IV on a VAX 850 computer. The theoretical modal frequencies are shown in Tables 6.5 to 6.7 for comparison.

Table 6.1 Test Programme of Individual Beams			
	Beam A	Beam B	
1. Dynamic tests. 2. Loaded up to	10 kN beam cracked	11.5 kN	then unloaded
3. Dynamic tests. 4. Loaded up to	15 kN	14 kN beam cracked	then unloaded
5. Dynamic tests. 6. Loaded up to	20 kN	18 kN	then unloaded
7. Dynamic tests. 8. Loaded up to	23 kN	23 kN	then unloaded
9. Dynamic tests. 10. Loaded up to	26 kN	25.2 kN	then unloaded
11. Dynamic tests. 12. Loaded up to	28 kN	29 kN steel yielded	then unloaded
13. Dynamic tests. 14. Loaded up to	32 kN steel yielded	——	then unloaded
15. Dynamic tests.			

Table 6.2 Transverse Load Distribution Factor of the Model Bridge Deck before Yield of Steel

	Beam #1	Beam #2	Beam #3	Beam #4	Beam #5
Transverse Load Dist'n Factor from Steel Strain	0.279	0.286	0.241	0.131	0.064
Transverse Load Dist'n Factor from Concrete Strain	0.303	0.287	0.231	0.125	0.054
Transverse Load Dist'n Factor from Deflection	0.308	0.285	0.208	0.133	0.066

Table 6.3 Design and Experimental Moment Capacity of Main Beam C in the Model Bridge Deck (kN-m)

Limiting Criteria	Bending (M_j)	Deflection (M_{lc})	Cracking (M_{cc})	Moment due to Self weight (M_g)
Design	18.130	11.266	12.736	0.849
Experimental	20.320	13.752	——	0.849
$\frac{\text{Design} - (M_g)}{\text{Experimental}}$	0.850	0.757	——	——

Table 6.4 Design and Experimental Moment Capacity of Individual Beams A and B (kN-m)

Limiting Criteria	Bending (M_j)	Deflection (M_{lc})	Cracking (M_{cc})	Moment due to Self weight (M_g)
Design (Beam A)	18.106	11.234	12.898	0.813
Experimental (Beam A)	24.126	14.993	—	0.813
$\frac{\text{Design} - (M_g)}{\text{Experimental (Beam A)}}$	0.717	0.695	—	—
Design (Beam B)	15.826	8.610	12.651	0.525
Experimental (Beam B)	23.000	11.547	—	0.525
$\frac{\text{Design} - (M_g)}{\text{Experimental (Beam B)}}$	0.665	0.700	—	—

Table 6.5 Theoretical and Experimental Modal Frequencies of Beam A

Mode	Theory	After Loaded up to							
		kN	10 kN	15 kN	20 kN	23 kN	26 kN	28 kN	32 kN
First	33.80	33.88	33.00	32.88	32.38	32.75	32.13	32.00	31.63
Second	133.00	116.99	—	111.52	113.67	111.91	112.30	111.13	111.91
Third	290.20	286.16	277.34	275.00	274.57	277.73	282.03	277.73	272.27
Fourth	519.70	462.11	513.28	427.34	448.83	427.80	418.75	409.77	410.55

Table 6.6 Theoretical and Experimental Modal Frequencies of Beam B

Mode	Theory	After loaded up to					
		0 kN	14 kN	18 kN	23 kN	25 kN	29 kN
First	32.95	33.88	32.25	32.38	32.50	33.00	31.25
Second	131.10	110.94	112.70	98.24	112.30	98.24	111.52
Third	276.80	261.13	284.77	281.45	290.23	—	269.92
Fourth	534.80	—	—	—	—	—	—

Table 6.7 Theoretical and Experimental Modal Frequencies of the Model Bridge Deck

Mode Type	Theory	After loaded up to						
		0 kN	60 kN	70 kN	86 kN	98 kN	115 kN	140 kN
1B	35.06	35.25	34.75	34.00	33.75	33.75	33.75	32.50
1B, 1T	41.75	41.25	39.75	40.50	39.50	39.50	40.00	36.50
2B	113.30	116.50	—	—	113.00	117.00	115.50	—
1B, 2T	137.30	139.25	136.00	136.00	135.00	135.00	—	—
2B, 2T	202.10	—	—	—	182.81	182.03	175.78	161.72

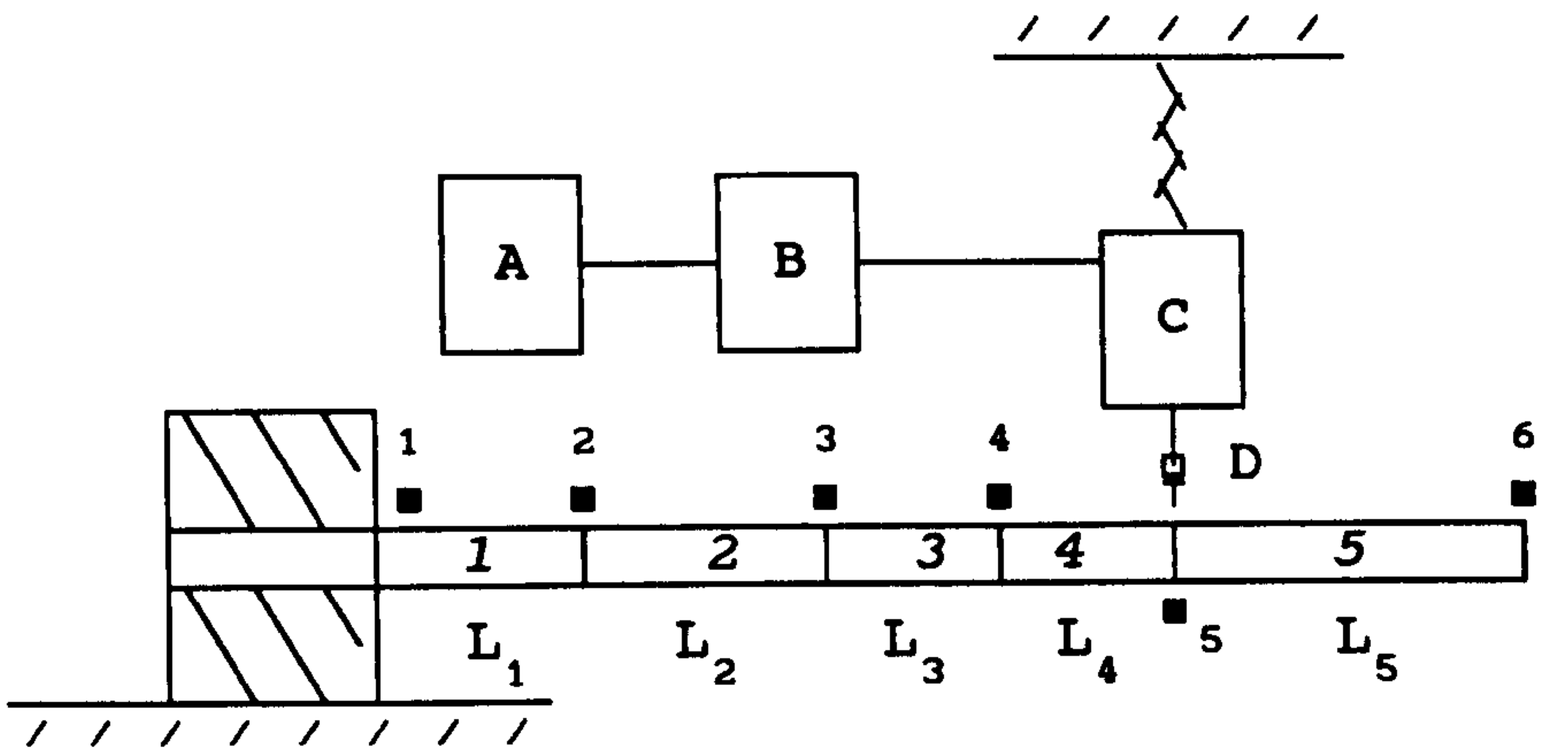

L_1= 250 L_2= 300 L_3= 200 L_4= 150 L_5= 300

Cross-section 38.04 H x 25.35 W

$E = 2.1 \times 10^5$ N/mm^2

A B&K 1027 signal generator
B Ling PO 300 amplifier
C Ling V409 exciter
D Force Transducer
1 ■ B&K 4370 accelerometer
1 Beam finite element number

FIG.6.1-Test Arrangement of Cantilever Beam

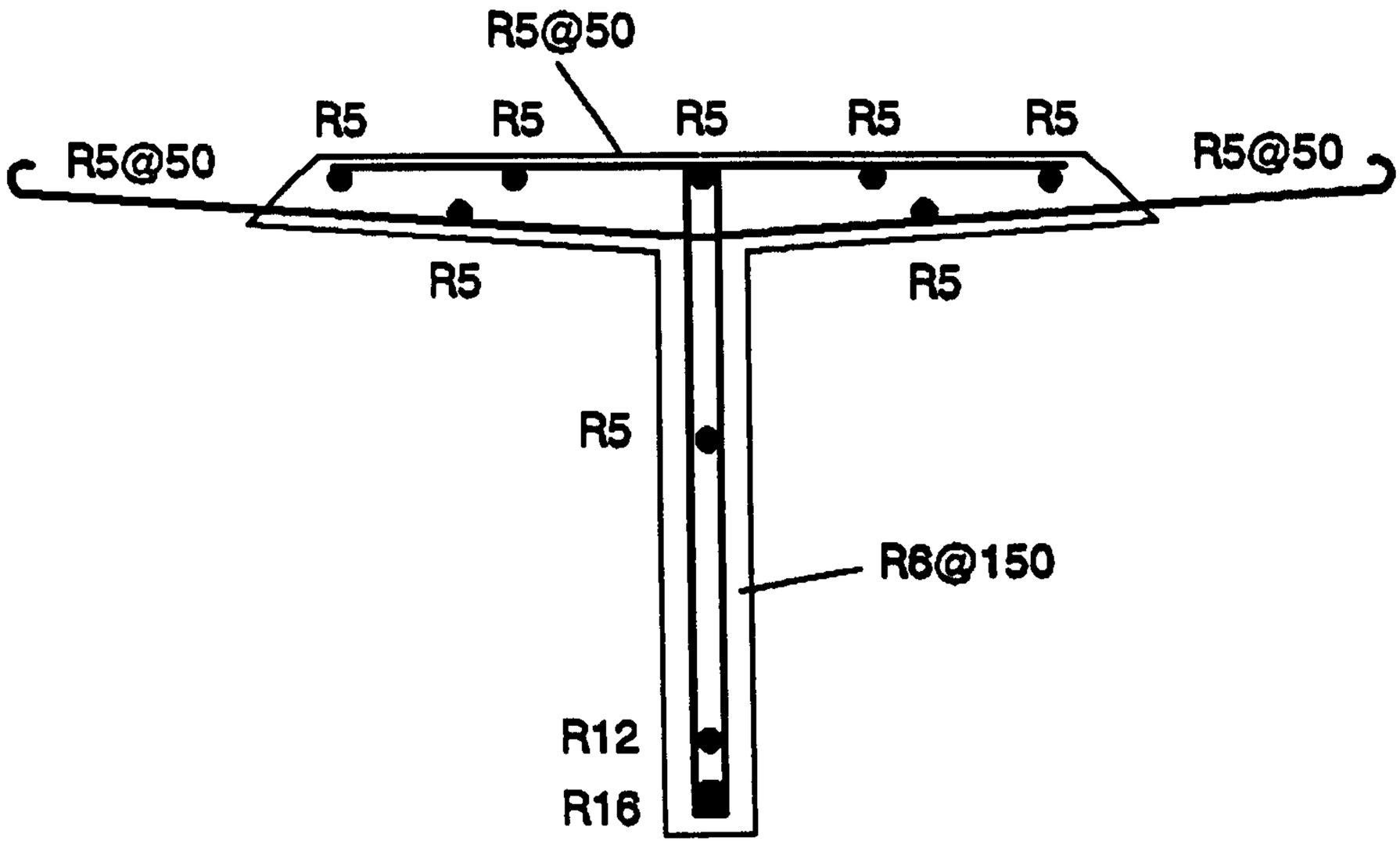

FIG.6.2-Reinforcement Details of Main Beam in the Model Bridge Deck

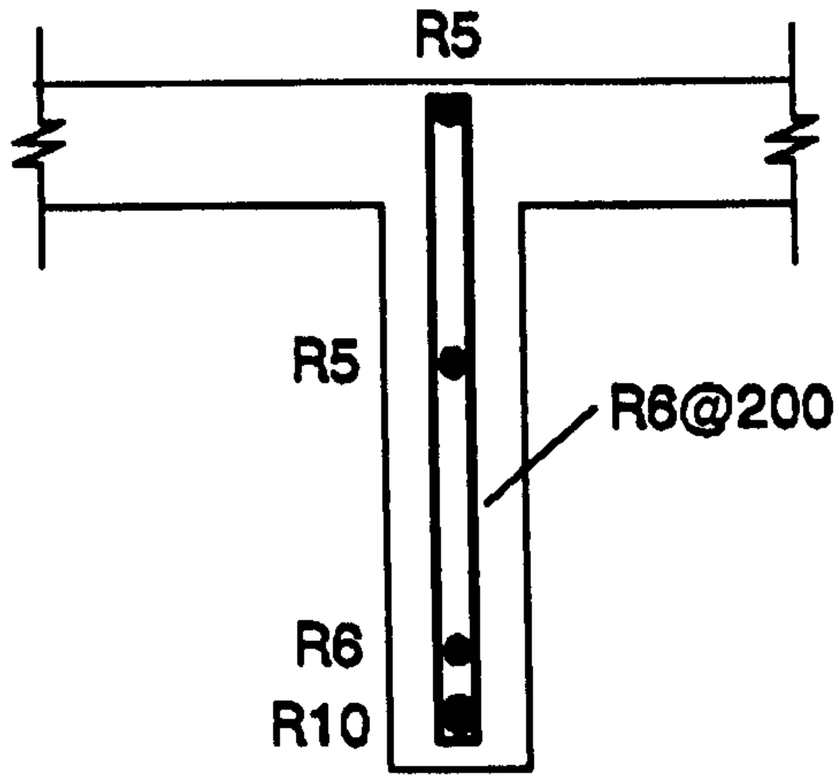

FIG.6.3-Reinforcement Details of Diaphragm in the Model Bridge Deck

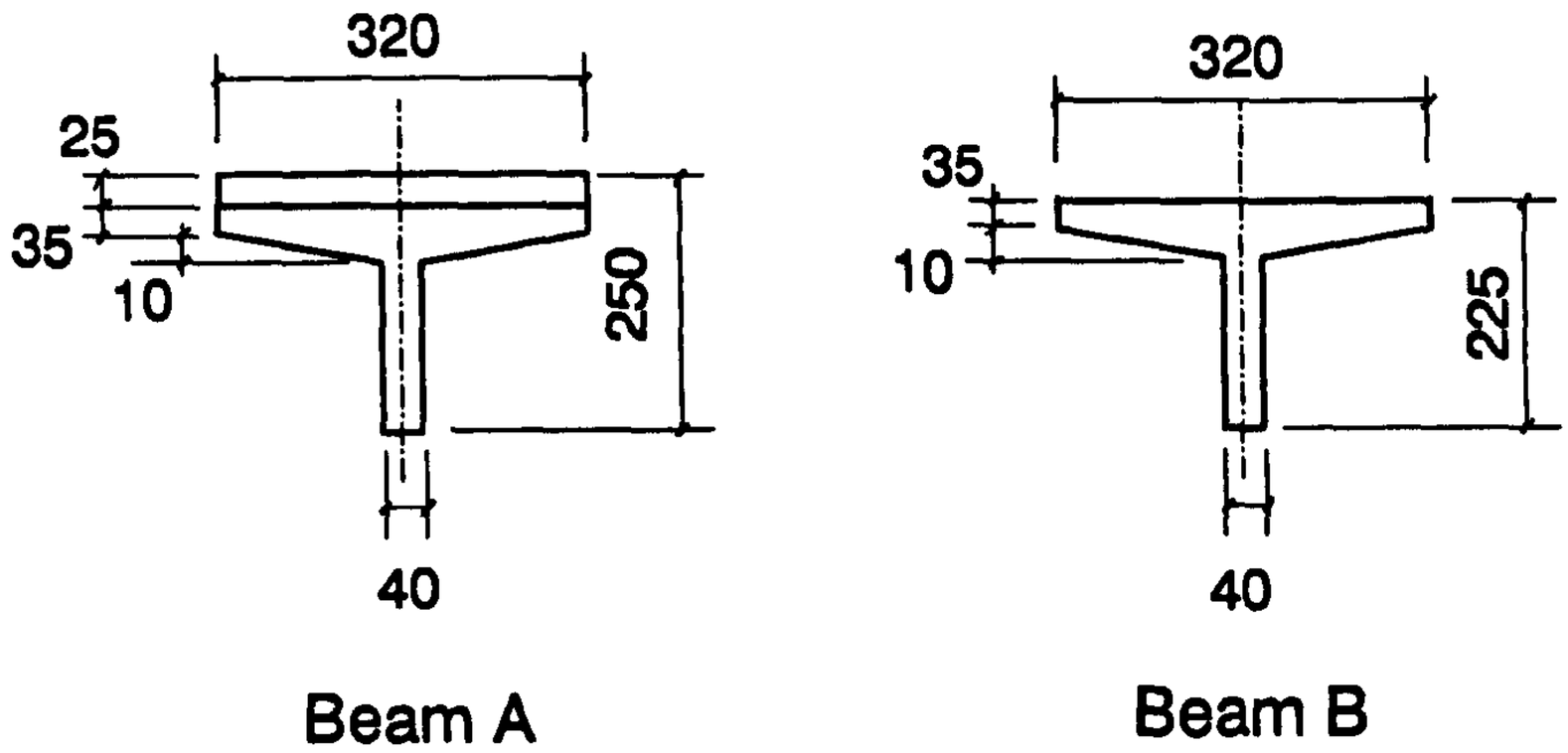

Beam A Beam B

FIG.6.4-Cross-section of Beams A and B

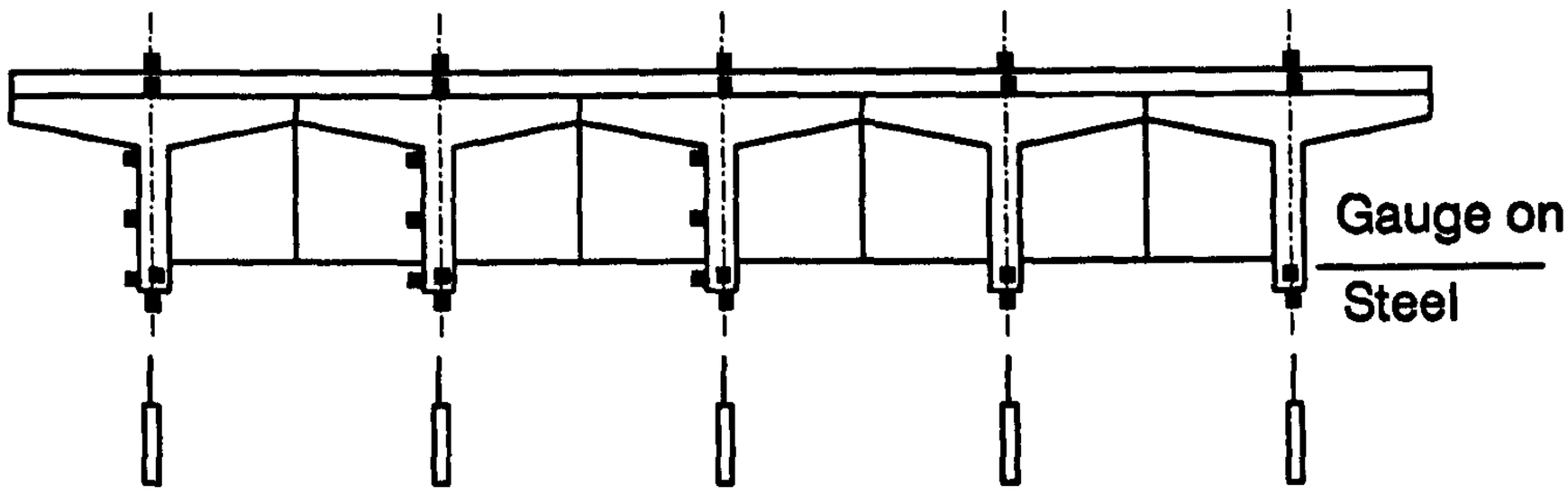

FIG.6.5-Arrangement of Strain Gauges and Transducers at Midspan of Model Bridge Deck

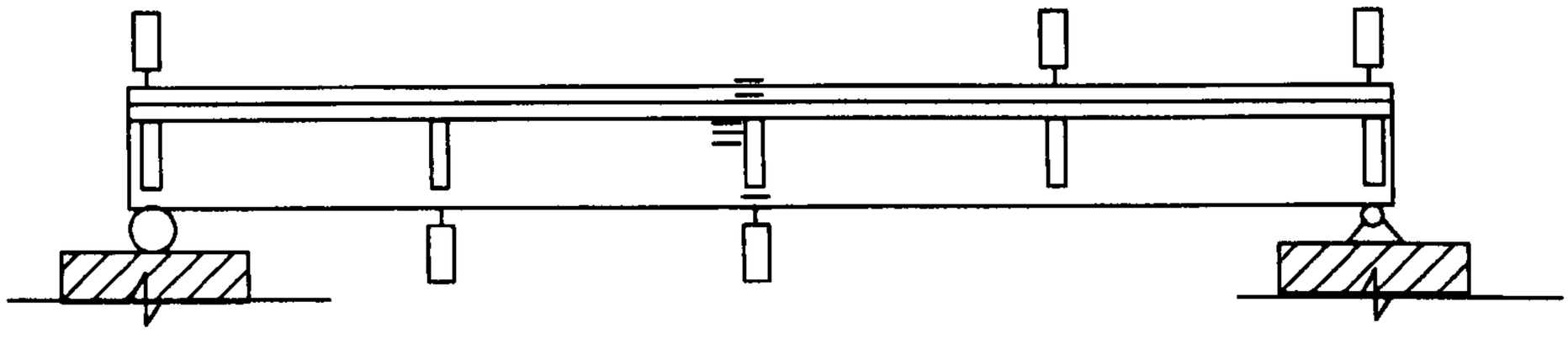

(a) Beam A

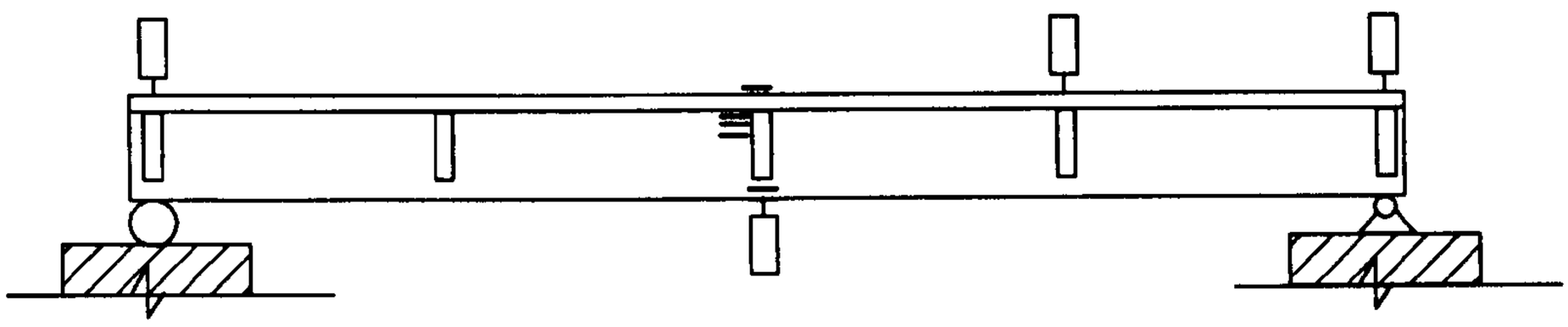

(b) Beam B

— Strain Gauge

⊏⊐ Displacement Transducer

FIG.6.6-Arrangement of Strain Gauges and Transducers in Beams A and B

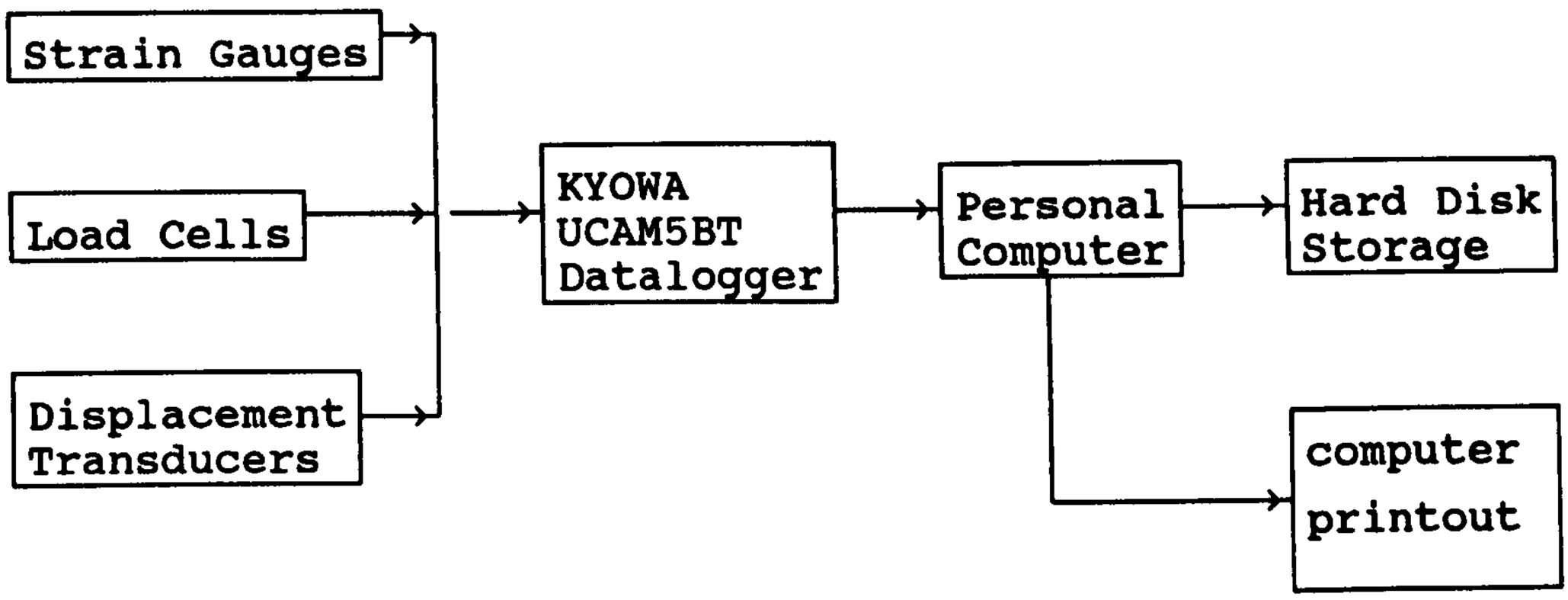

FIG.6.7-Arrangement of Instruments for Static Data Acquisition

Note: Numerical values are in Tonnes

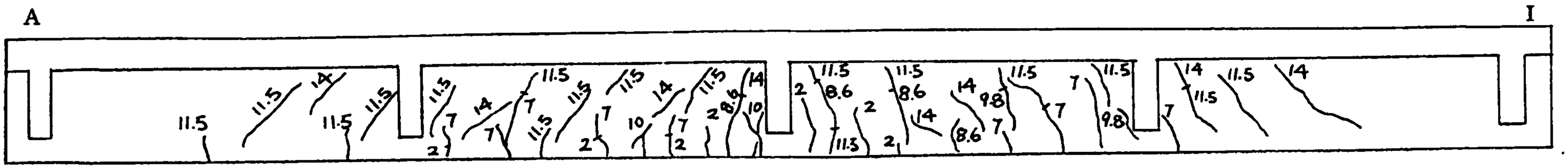

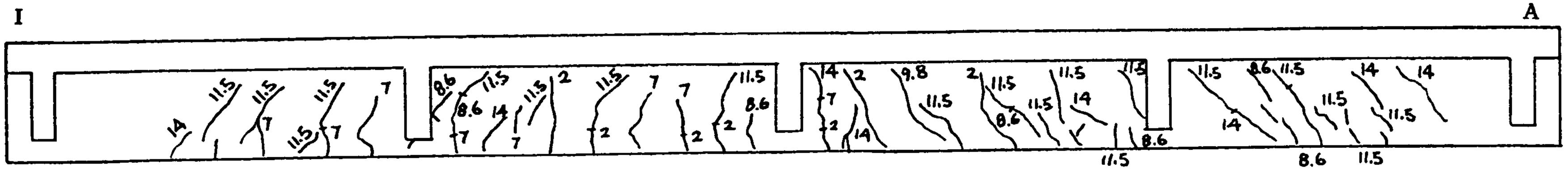

FIG.6.8(a)-Crack Pattern on the Sides of Beam #1 of the Model Bridge Deck

Note: Numerical values are in Tonnes

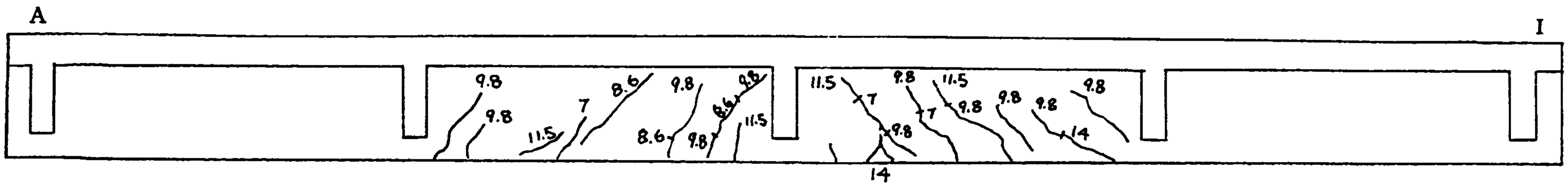

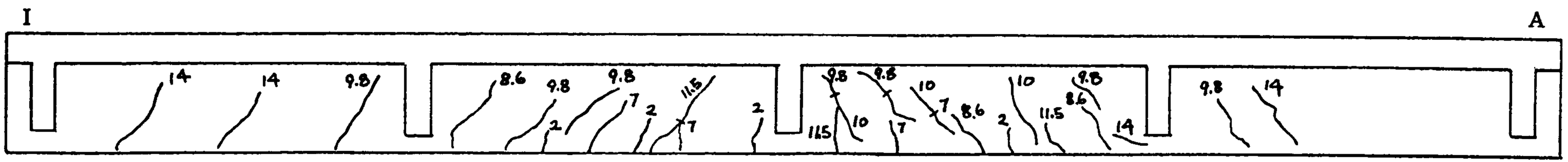

FIG.6.8(b)-Crack Pattern on the Sides of Beam #2 of the Model Bridge Deck

Note: Numerical values are in Tonnes

FIG.6.8(c)-Crack Pattern on the Sides of Beam #3 of the Model Bridge Deck

Note: Numerical values are in Tonnes

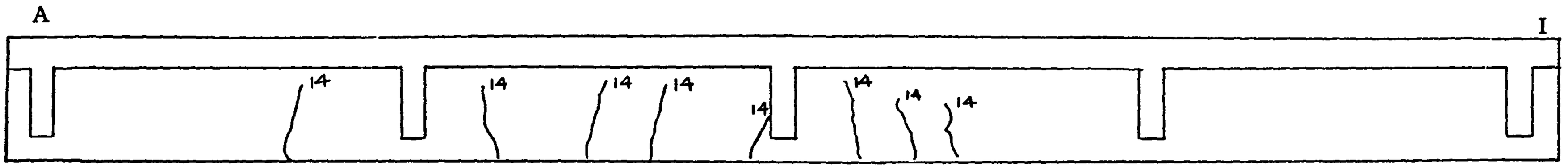

FIG.6.8(d)-Crack Pattern on the Sides of Beam #4 of the Model Bridge Deck

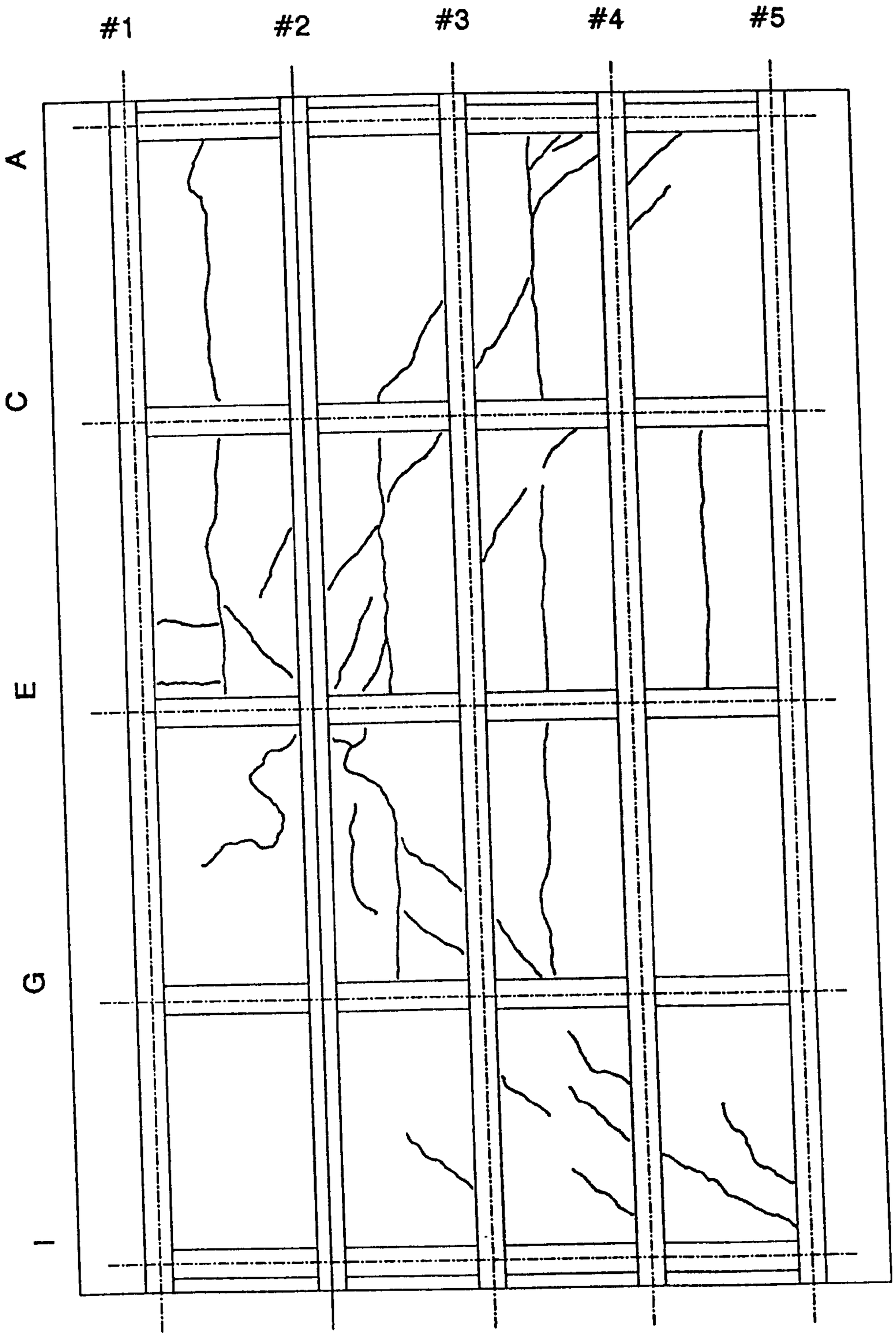

FIG.6.9-Underside View of Crack Pattern of Model Bridge Deck after Testing

Note: Numerical values are in Tonnes

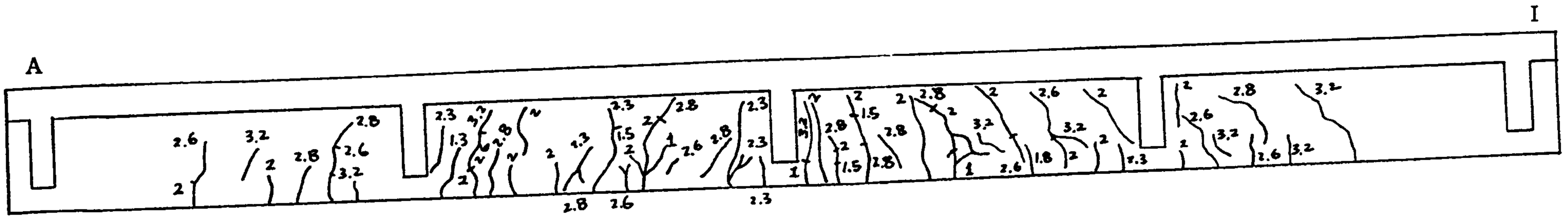

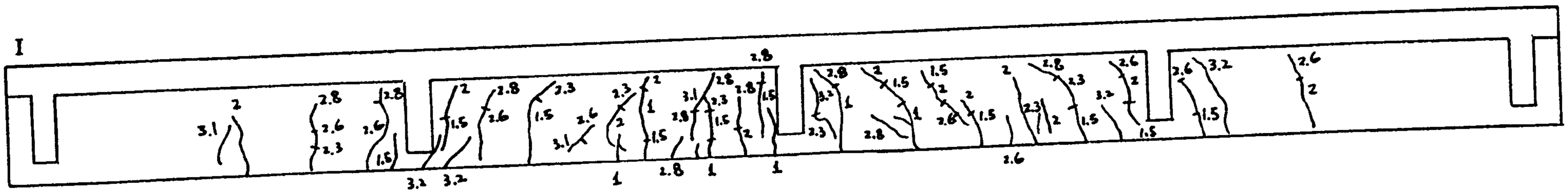

FIG.6.10(a)-Crack Pattern on the Sides of Individual Beam A

Note: Numerical values are in Tonnes

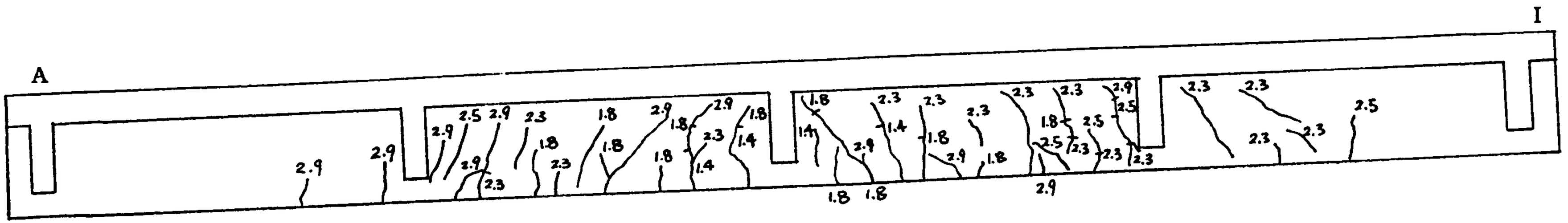

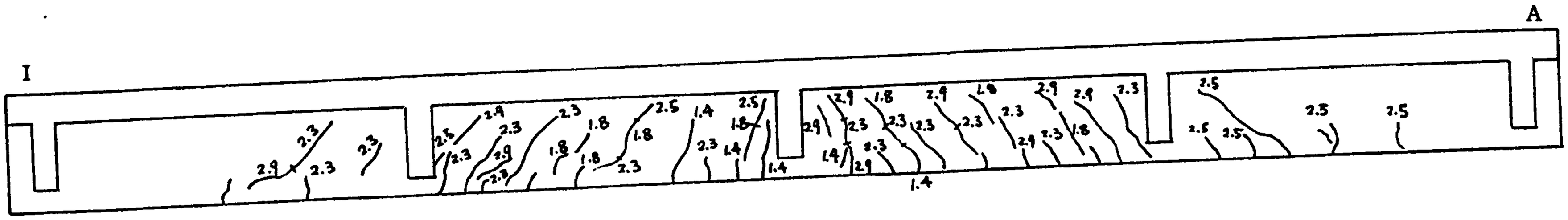

FIG.6.10(b)-Crack Pattern on the Sides of Individual Beam B

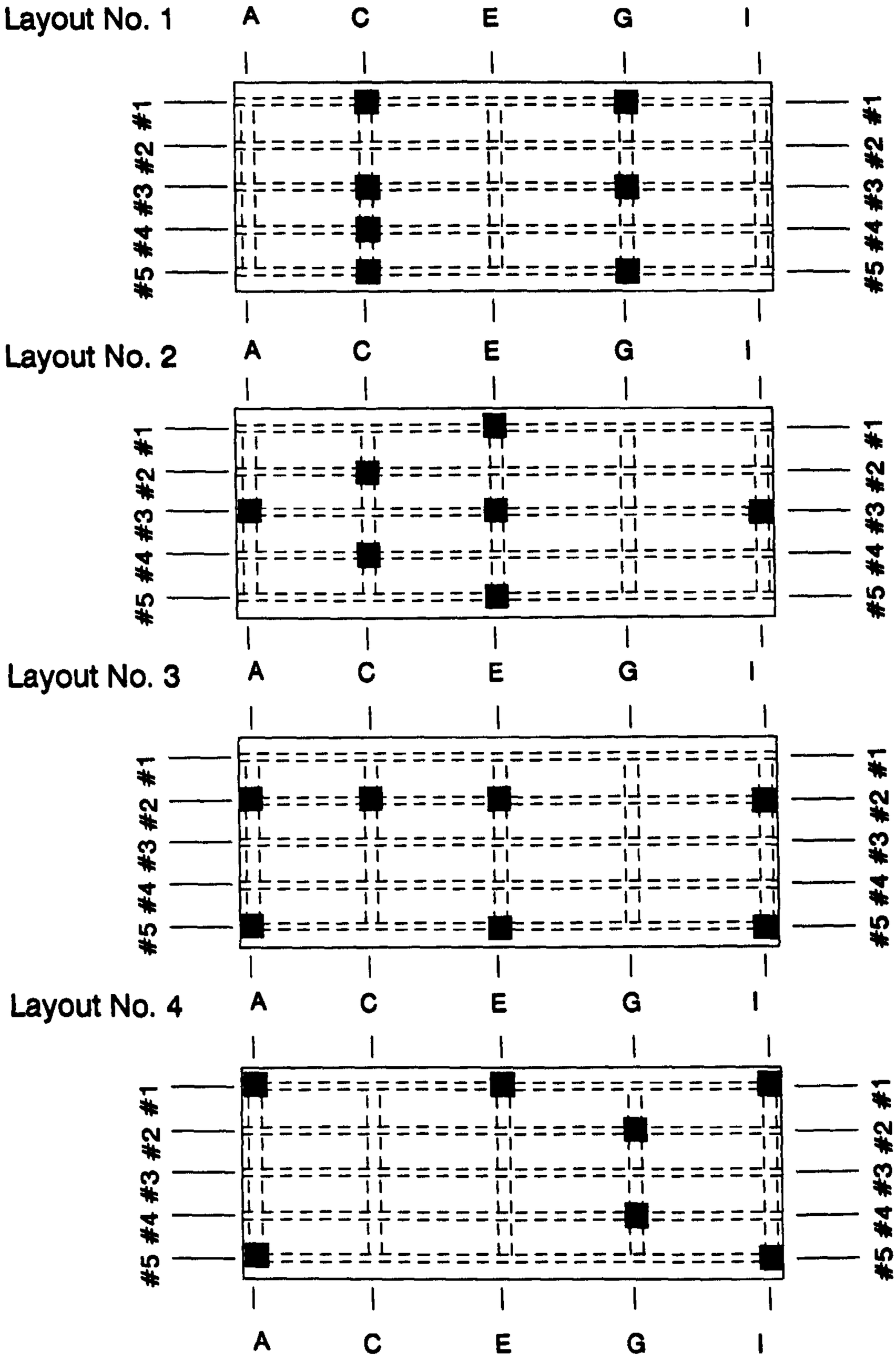

FIG.6.11-Arrangement of Accelerometers in the Dynamic Test of the Model Bridge Deck

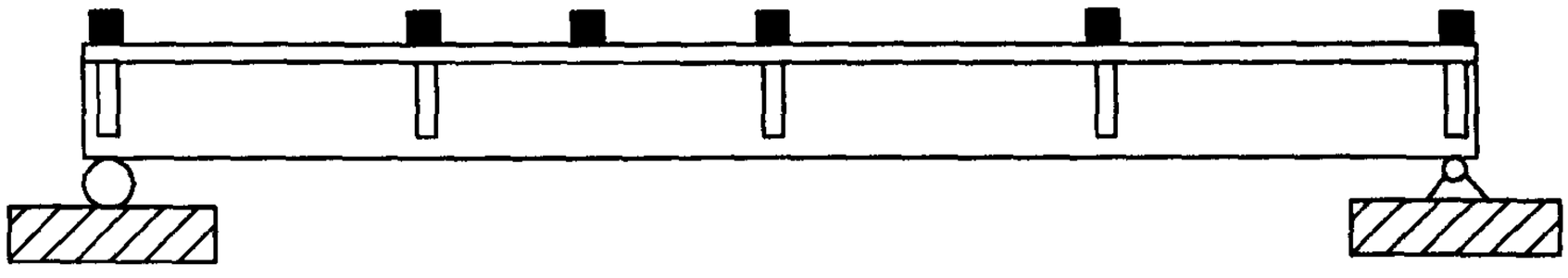

■ Accelerometer

FIG.6.12-Arrangement of Accelerometers in Dynamic Tests of Beams A and B

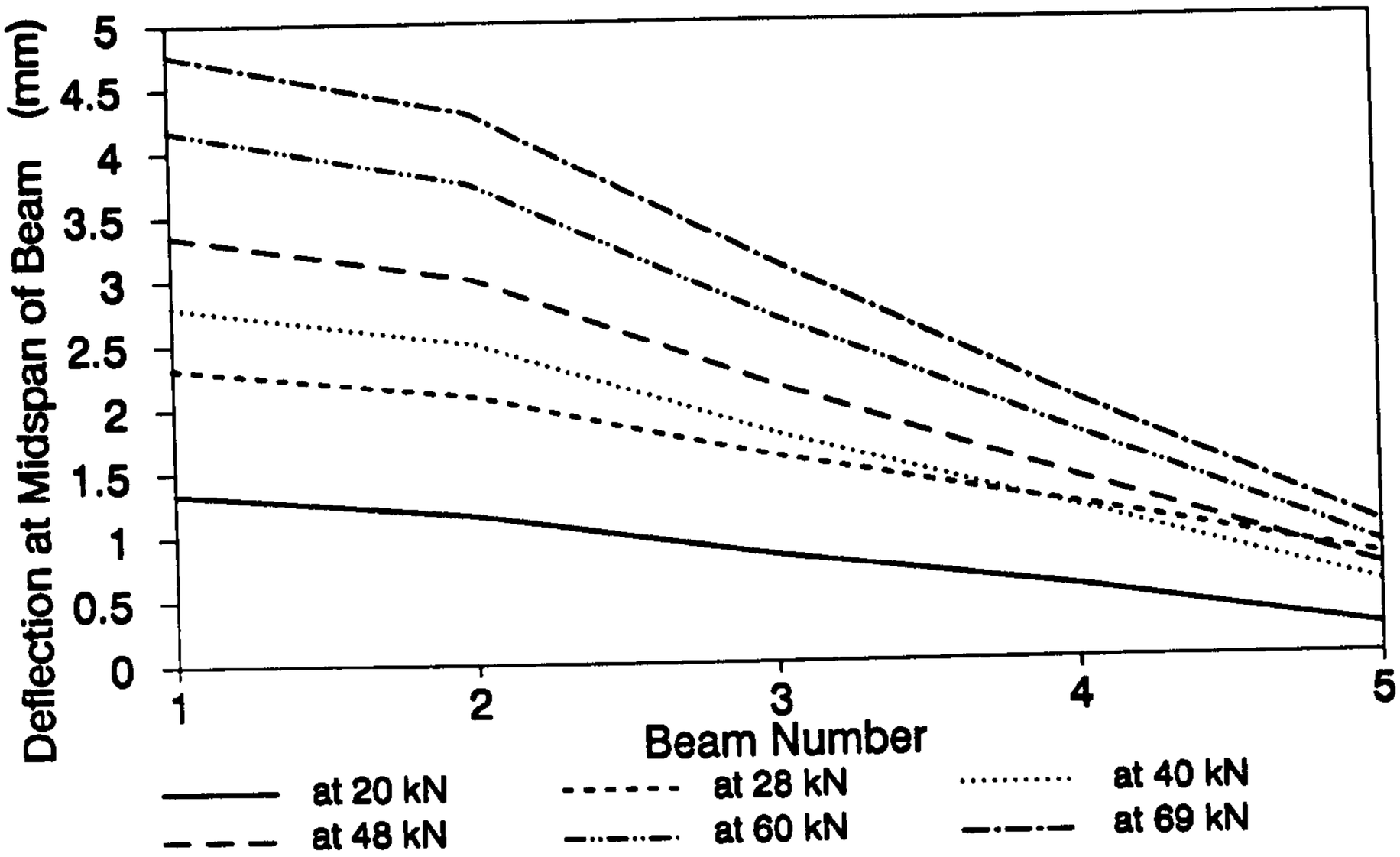

FIG.6.13(a)-Distribution of Deflection at Midspan in the 115 kN Loading Cycle

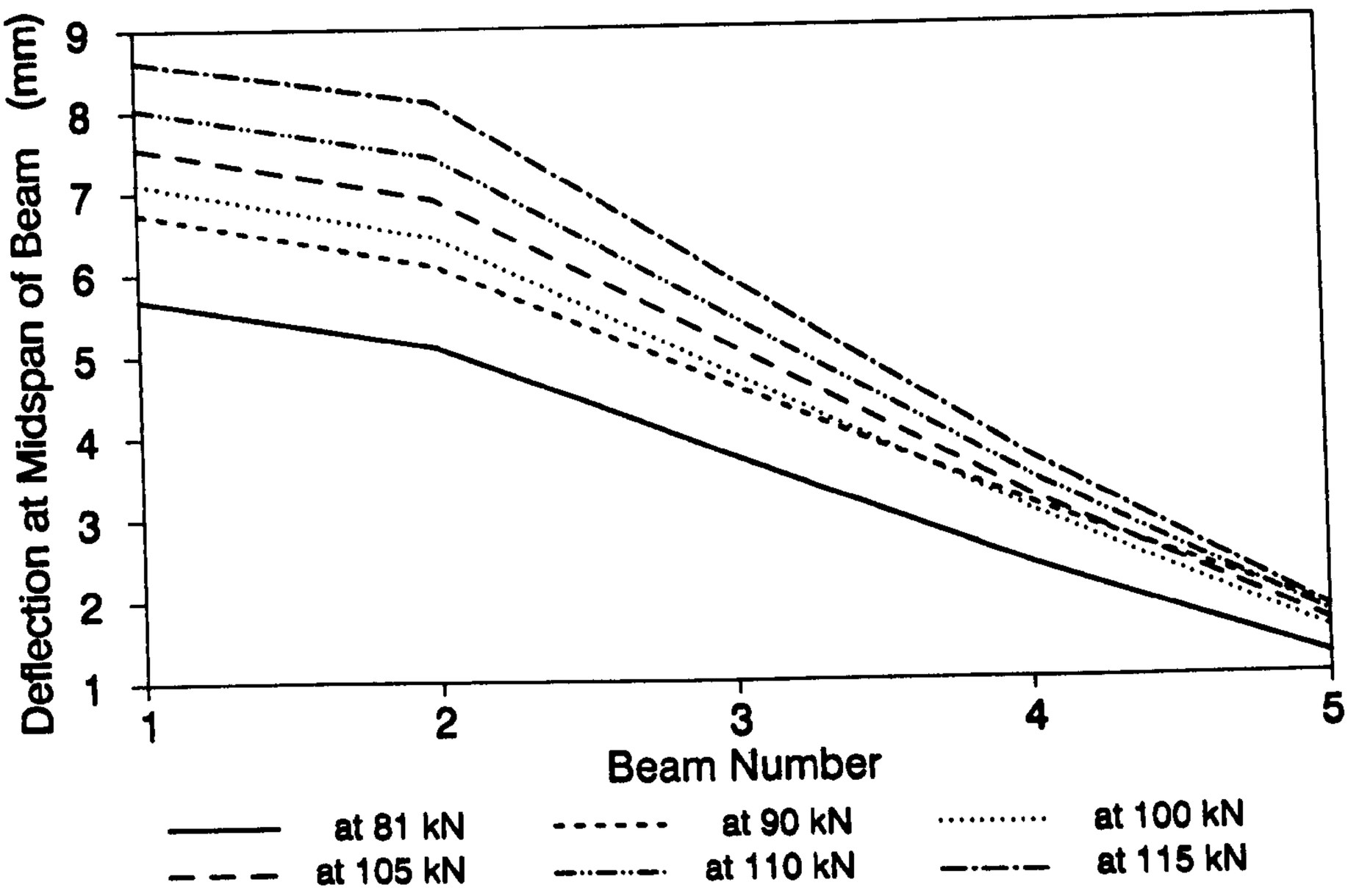

FIG.6.13(b)-Distribution of Deflection at Midspan in the 115 kN Loading Cycle

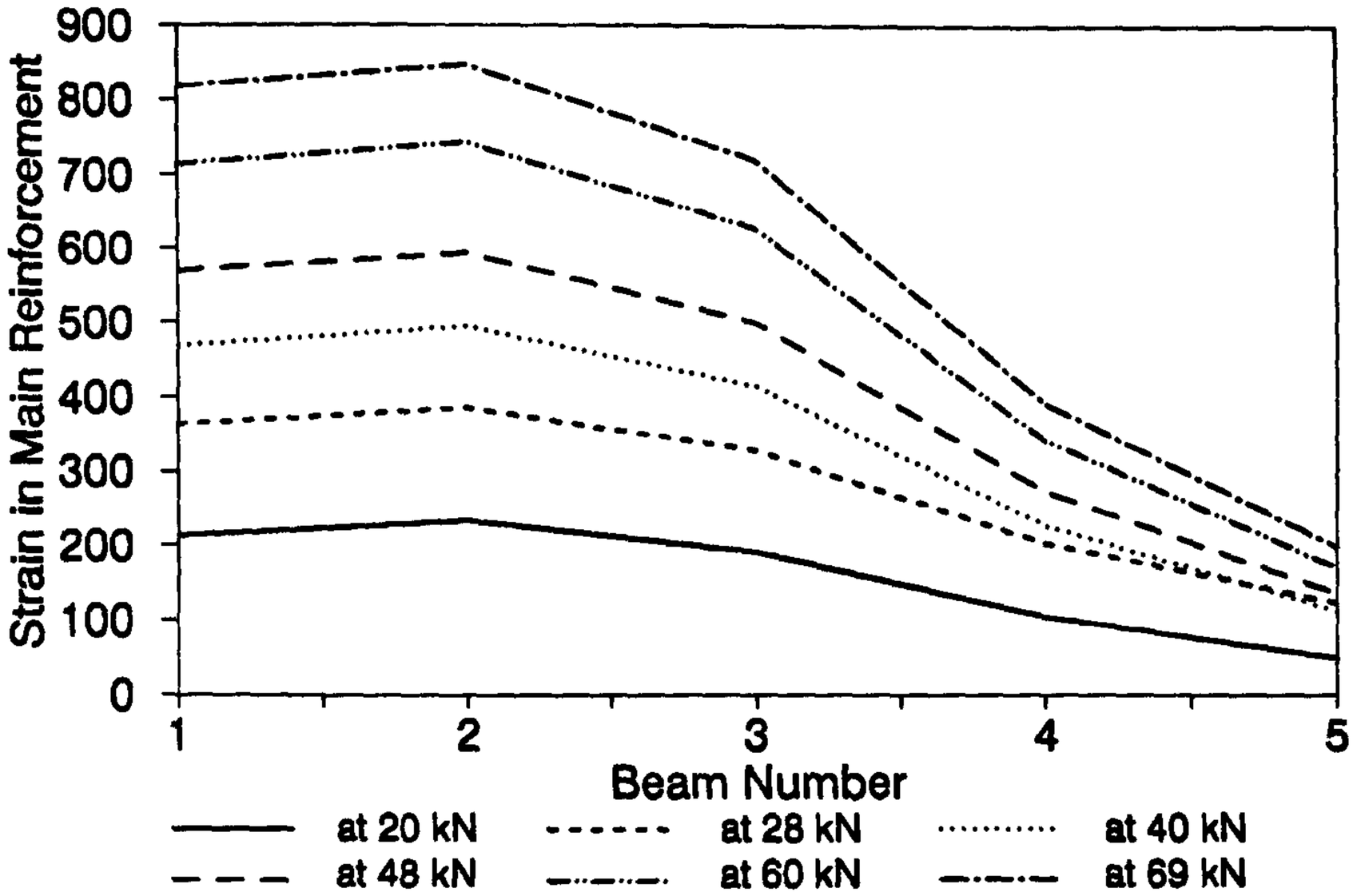

FIG.6.14(a)-Distribution of Strain in Reinforcement at Midspan in the 115kN Loading Cycle

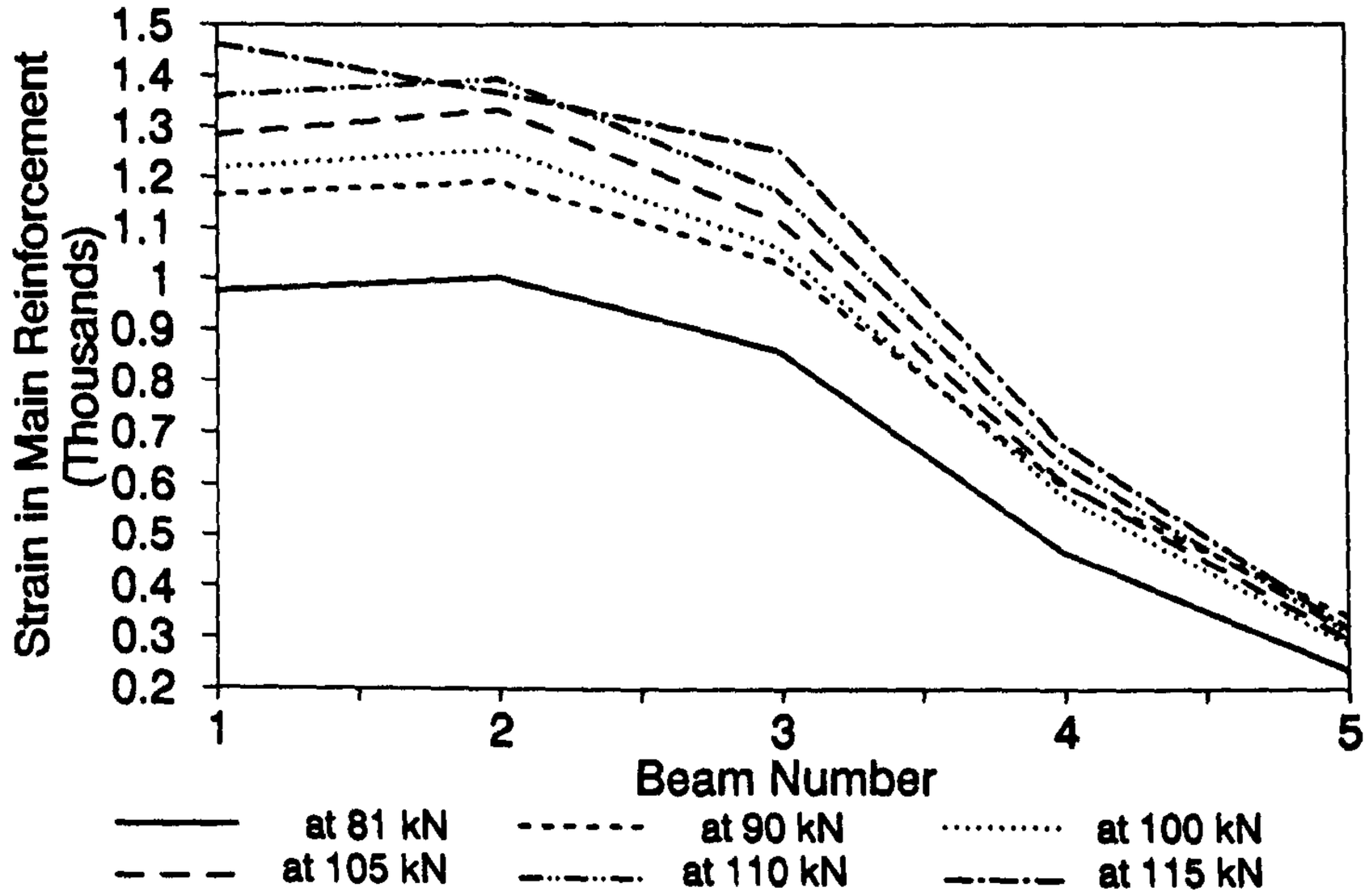

FIG.6.14(b)-Distribution of Strain in Reinforcement at Midspan in the 115 kN Loading Cycle

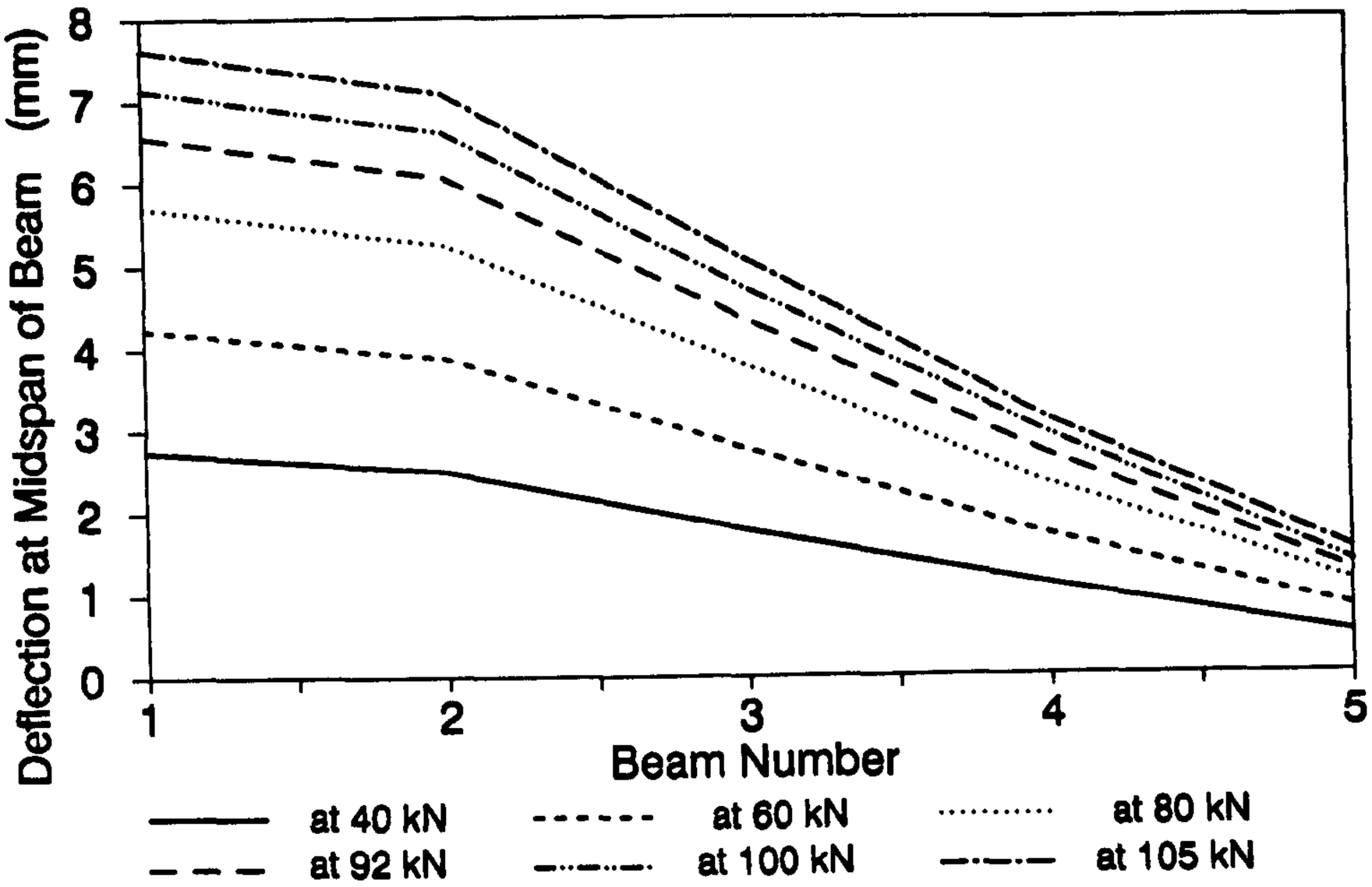

FIG.6.15(a)-Distribution of Deflection at Midspan in the 140kN Loading Cycle

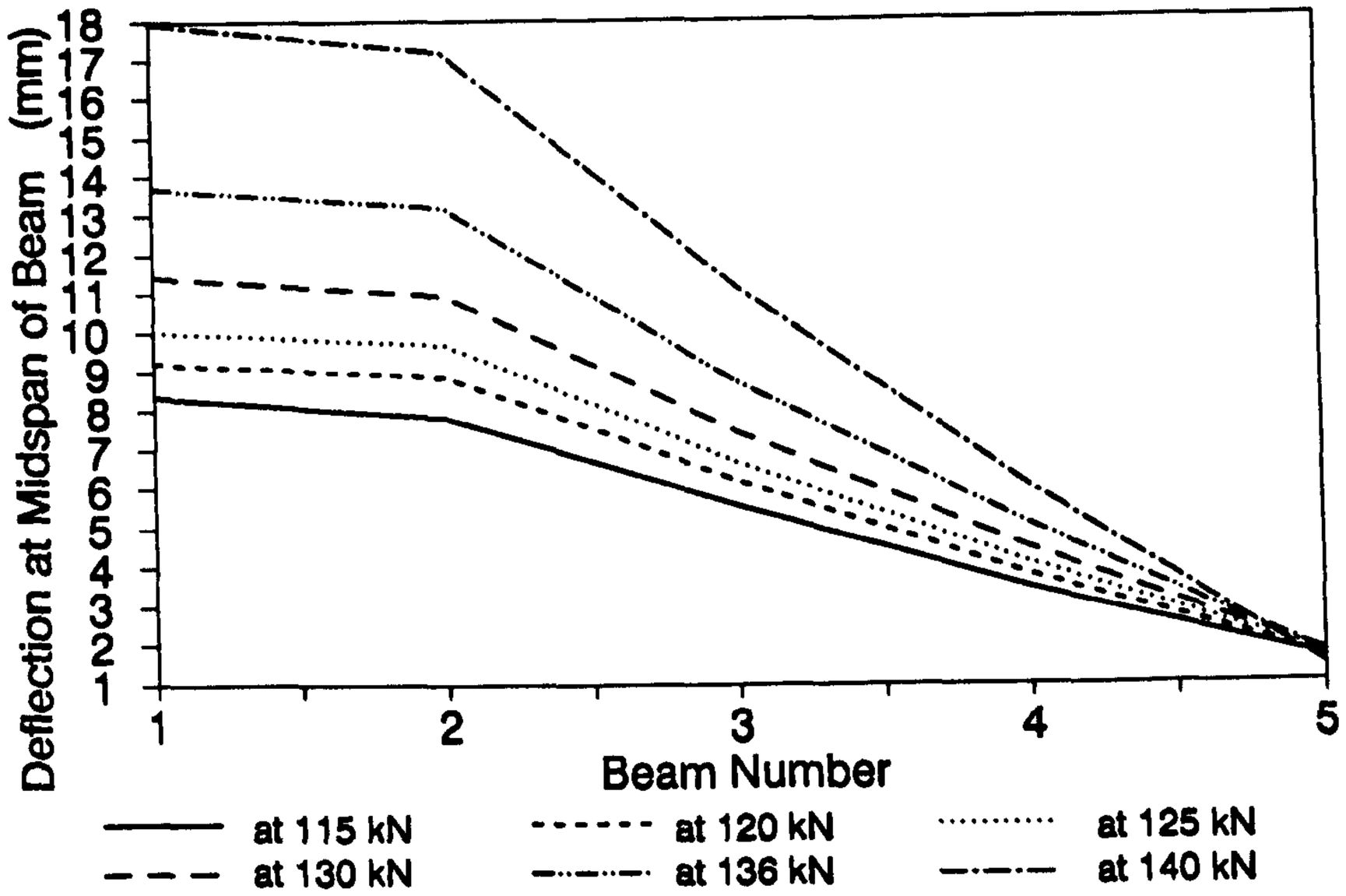

FIG.6.15(b)-Distribution of Deflection at Midspan in the 140kN Loading Cycle

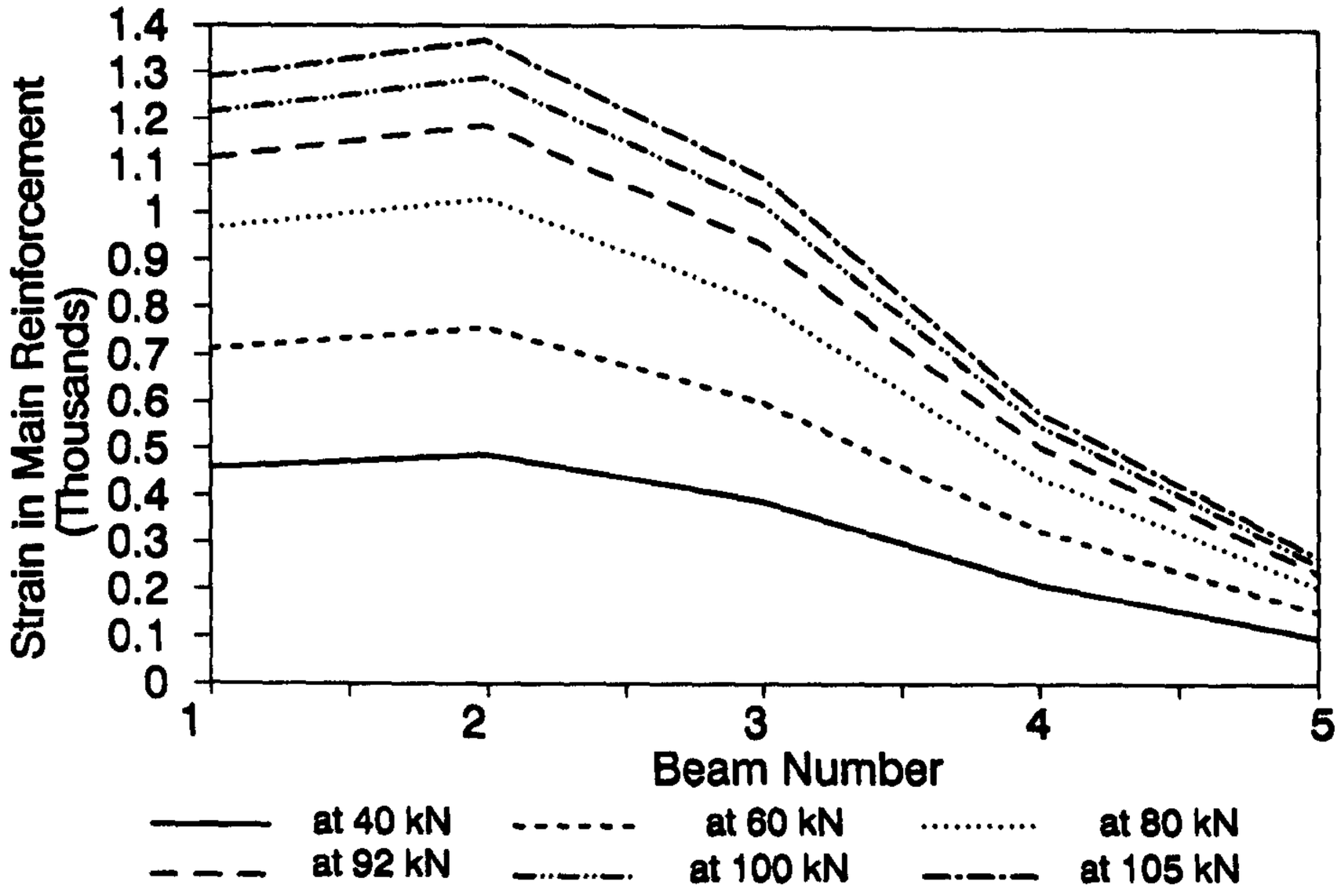

FIG.6.16(a)-Distribution of Strain in Reinforcement at Midspan in the 140kN Loading Cycle

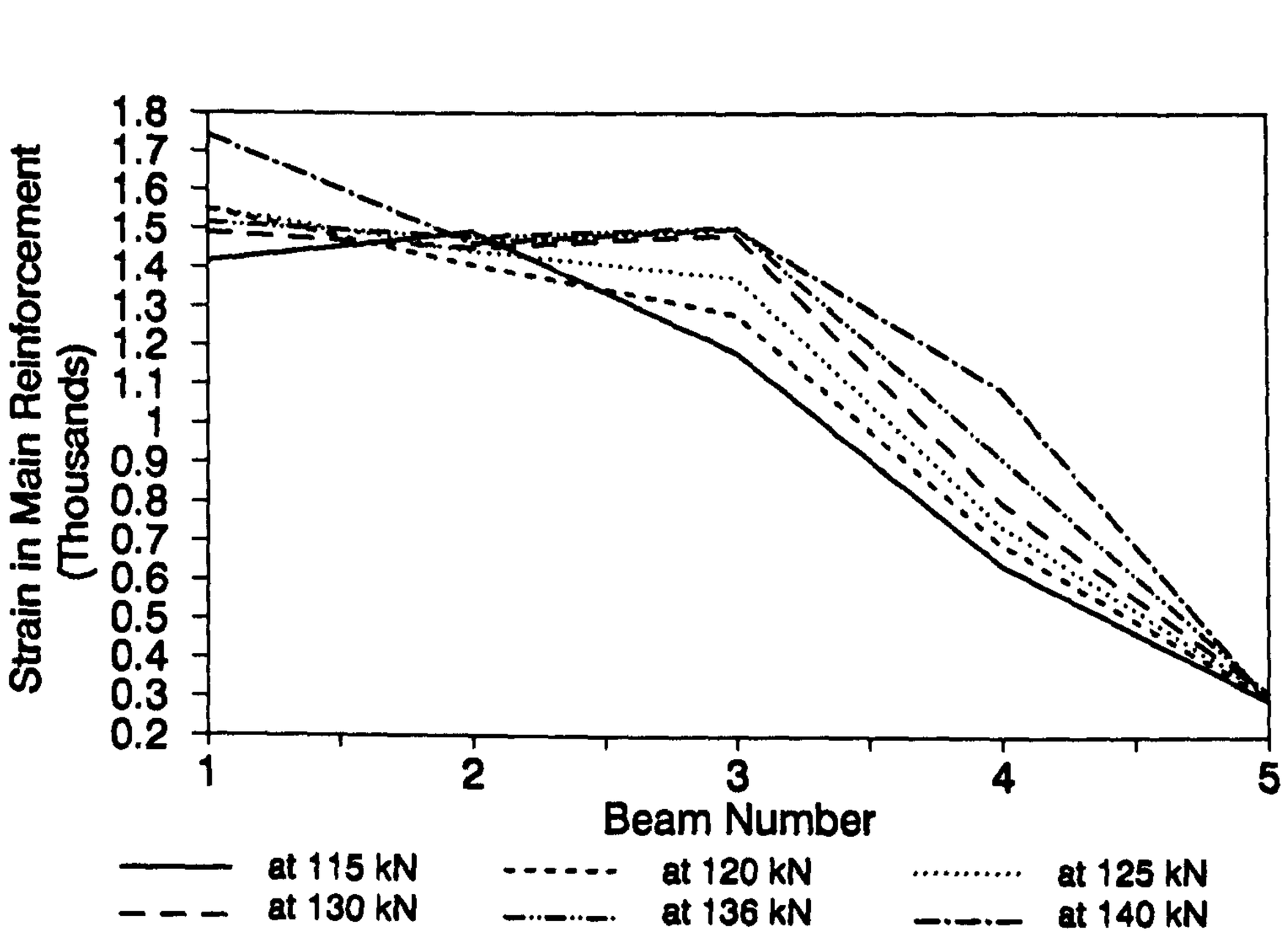

FIG.6.16(b)-Distribution of Strain in Reinforcement at Midspan in the 140kN Loading Cycle

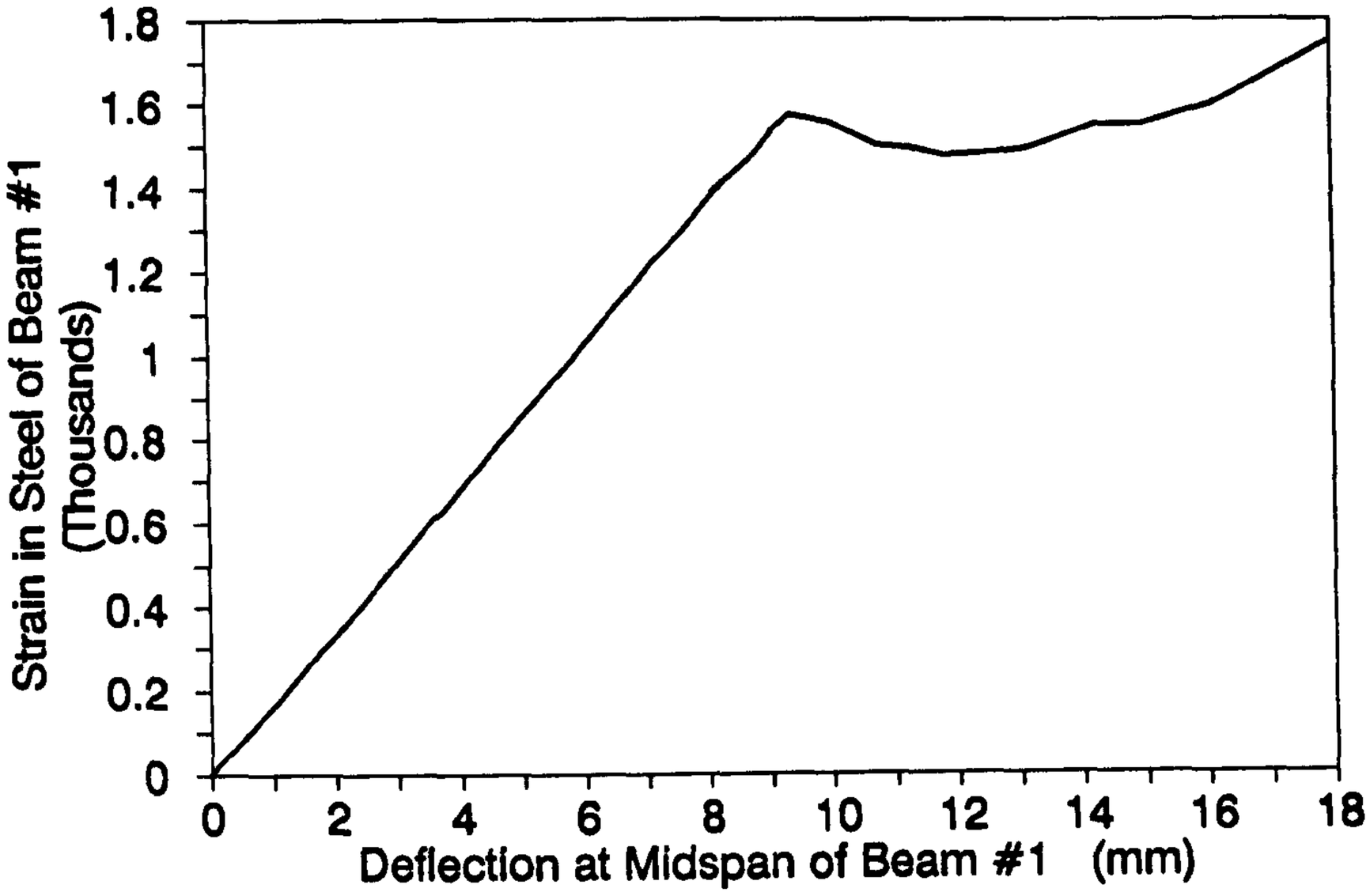

FIG.6.17-Deflection versus Steel Strain at Midspan in Beam #1 in the 140kN Loading Cycle

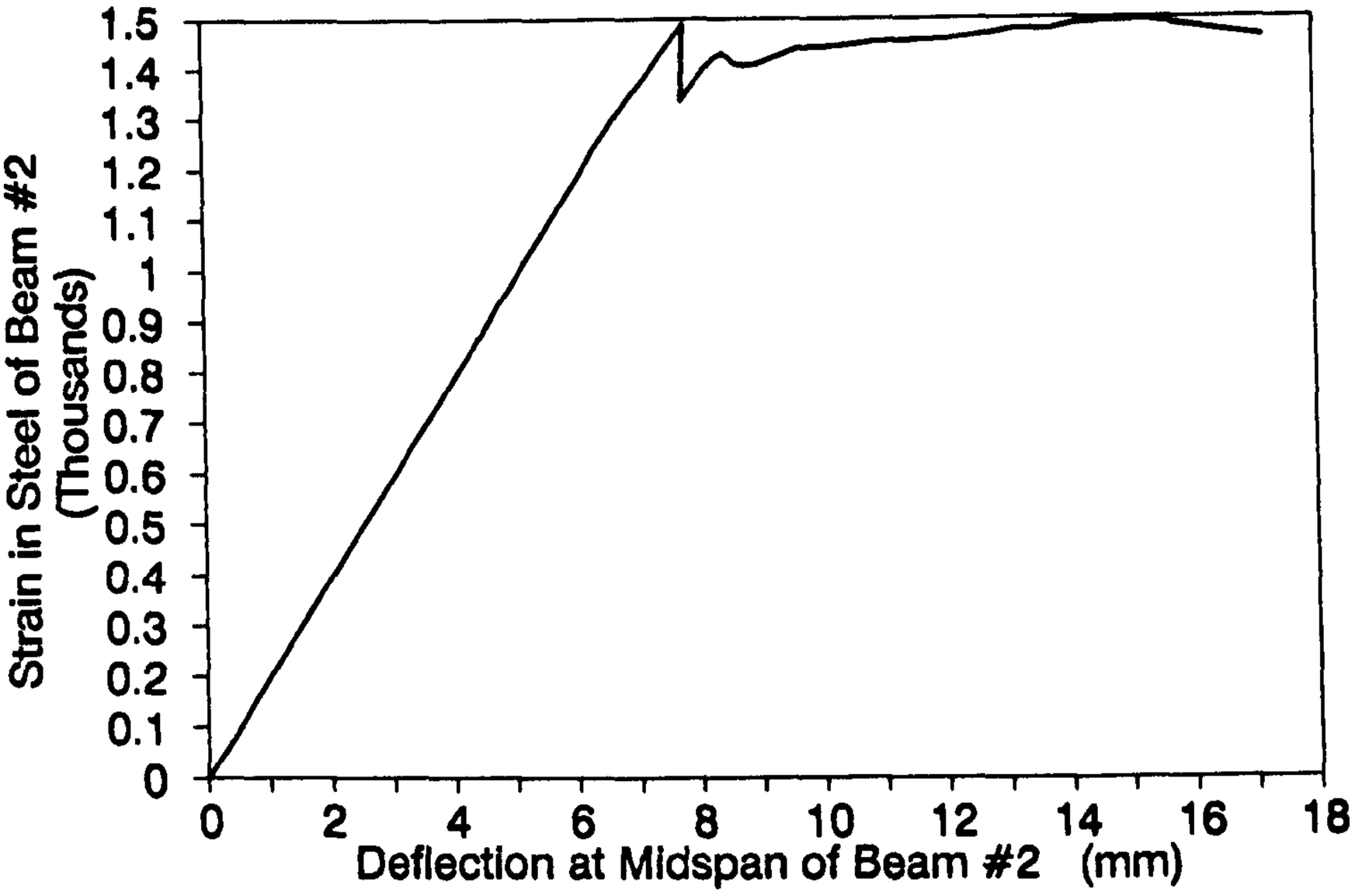

FIG.6.18-Deflection versus Steel Strain at Midspan in Beam #2 in the 140 kN Loading Cycle

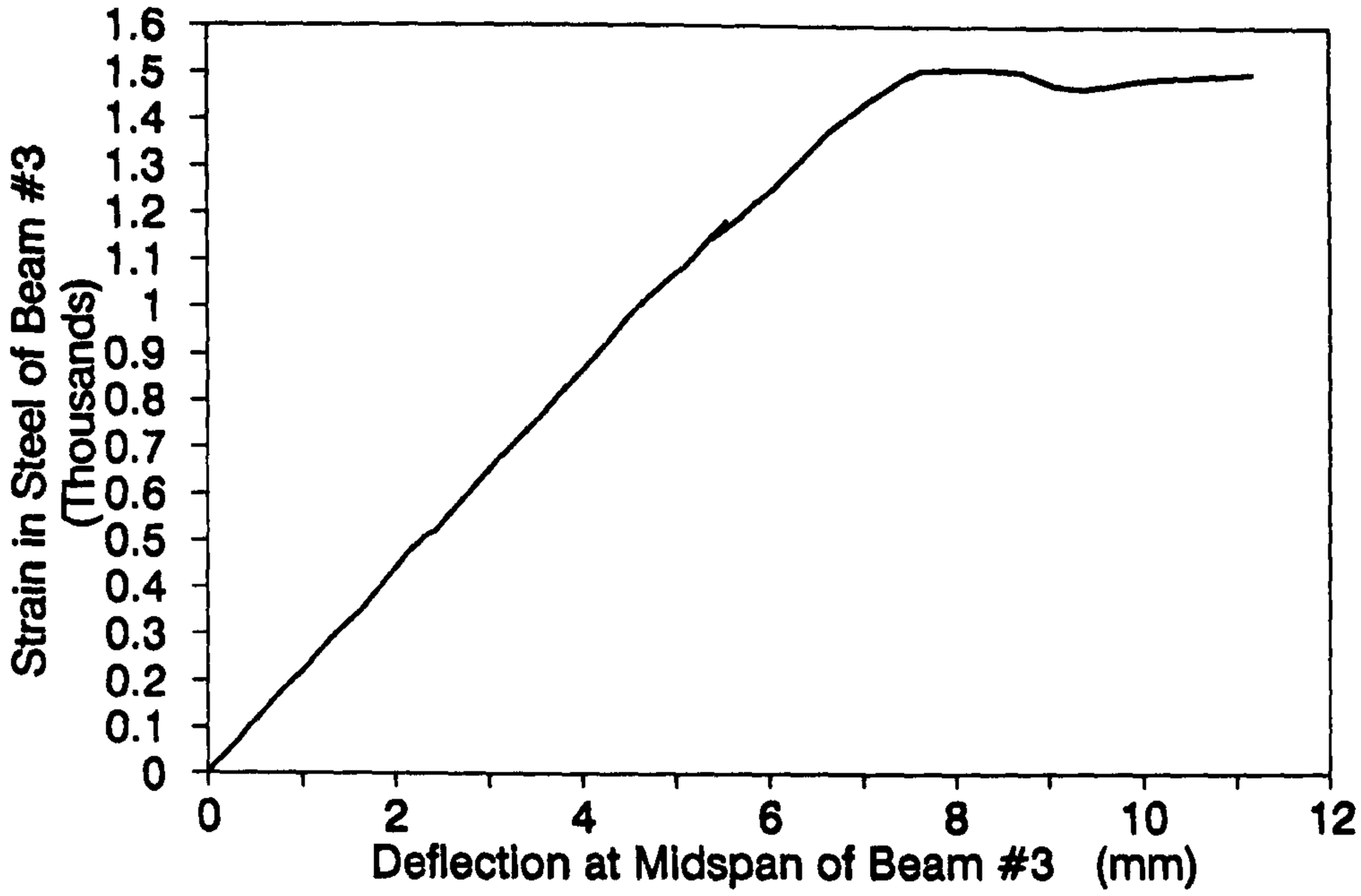

FIG.6.19-Deflection versus Steel Strain at Midspan in Beam #3 in the 140kN Loading Cycle

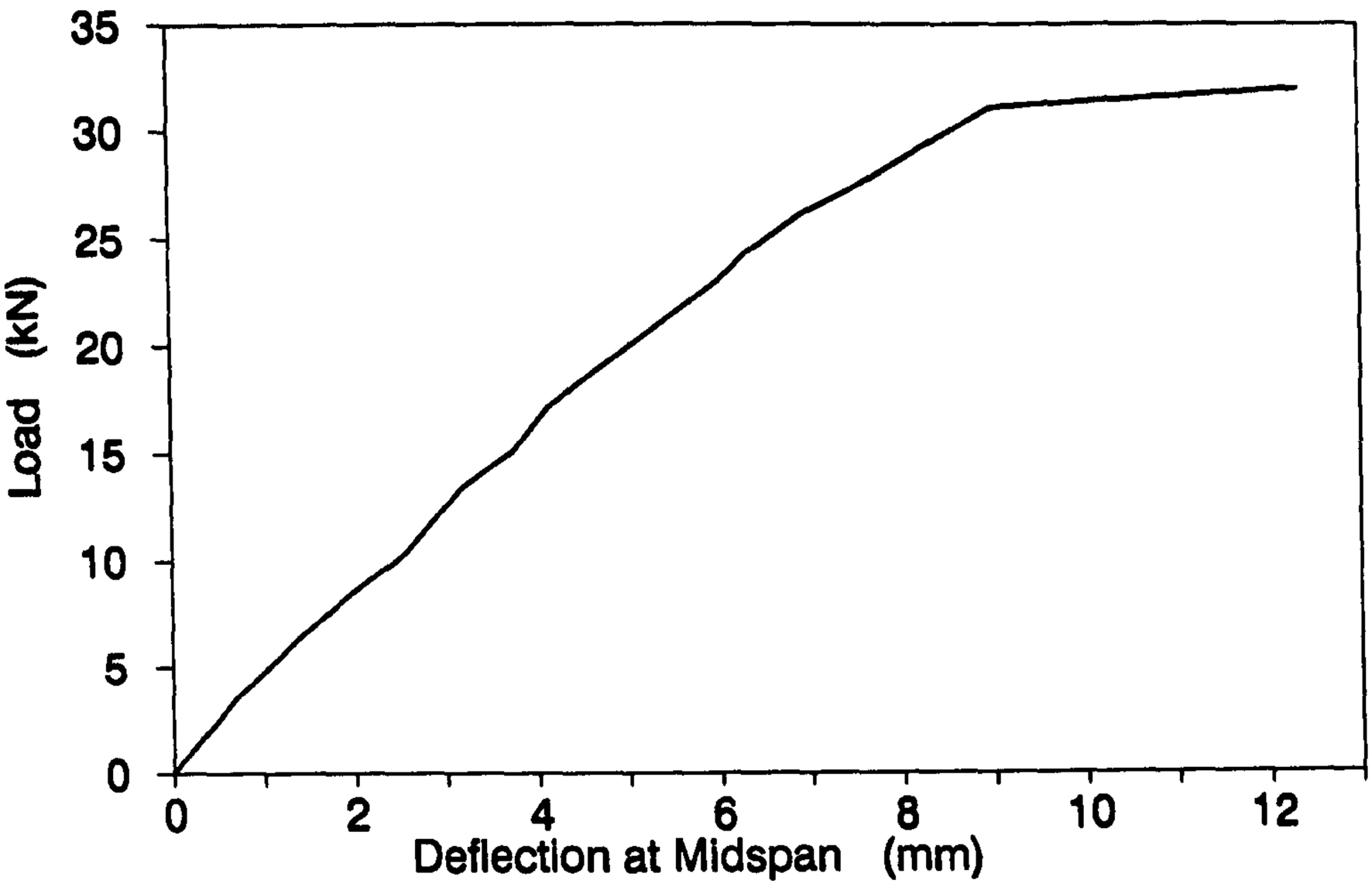

FIG.6.20-Load-Deflection History of Beam A

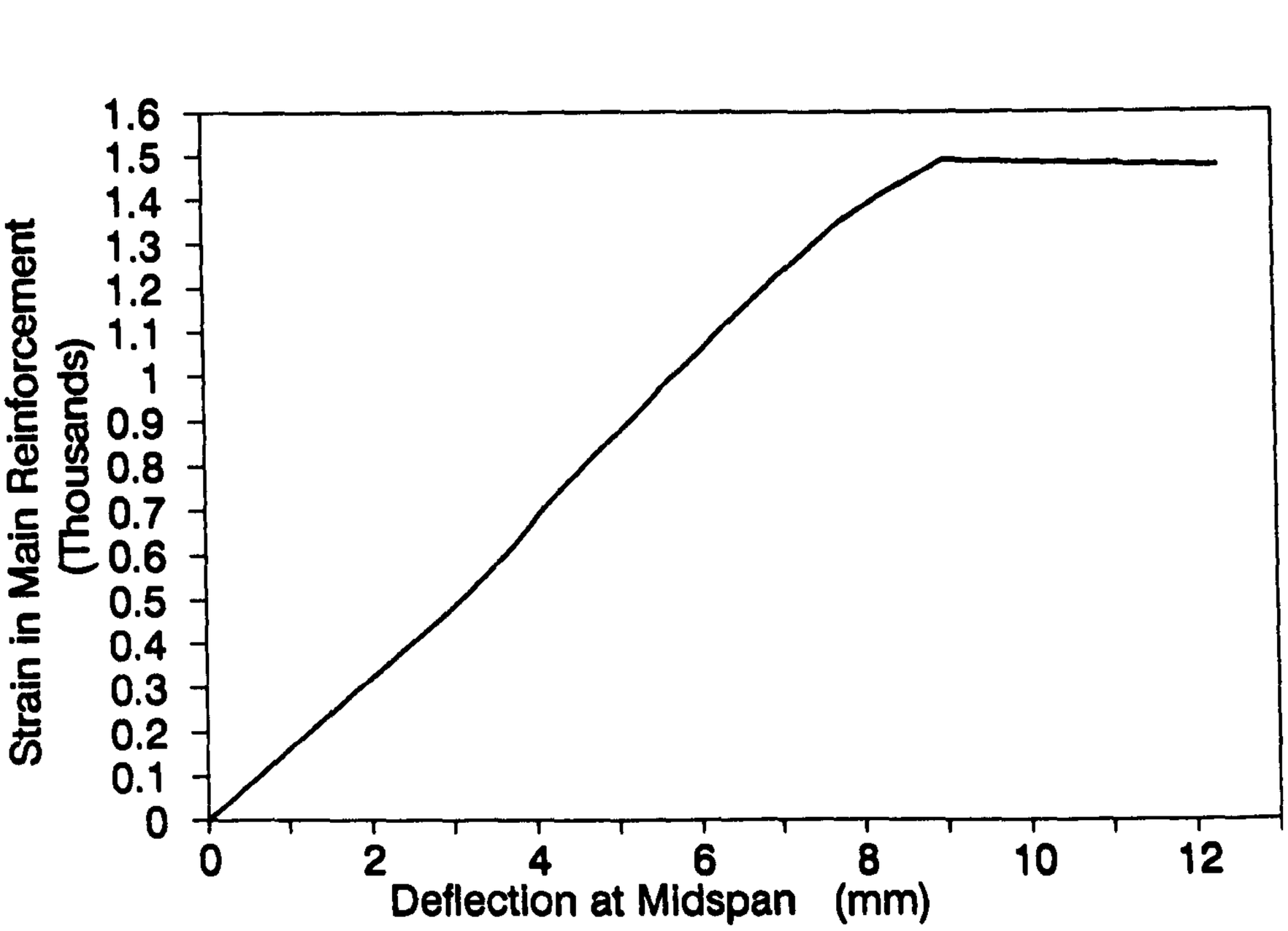

FIG.6.21-Deflection versus Steel Strain at Midspan of Beam A

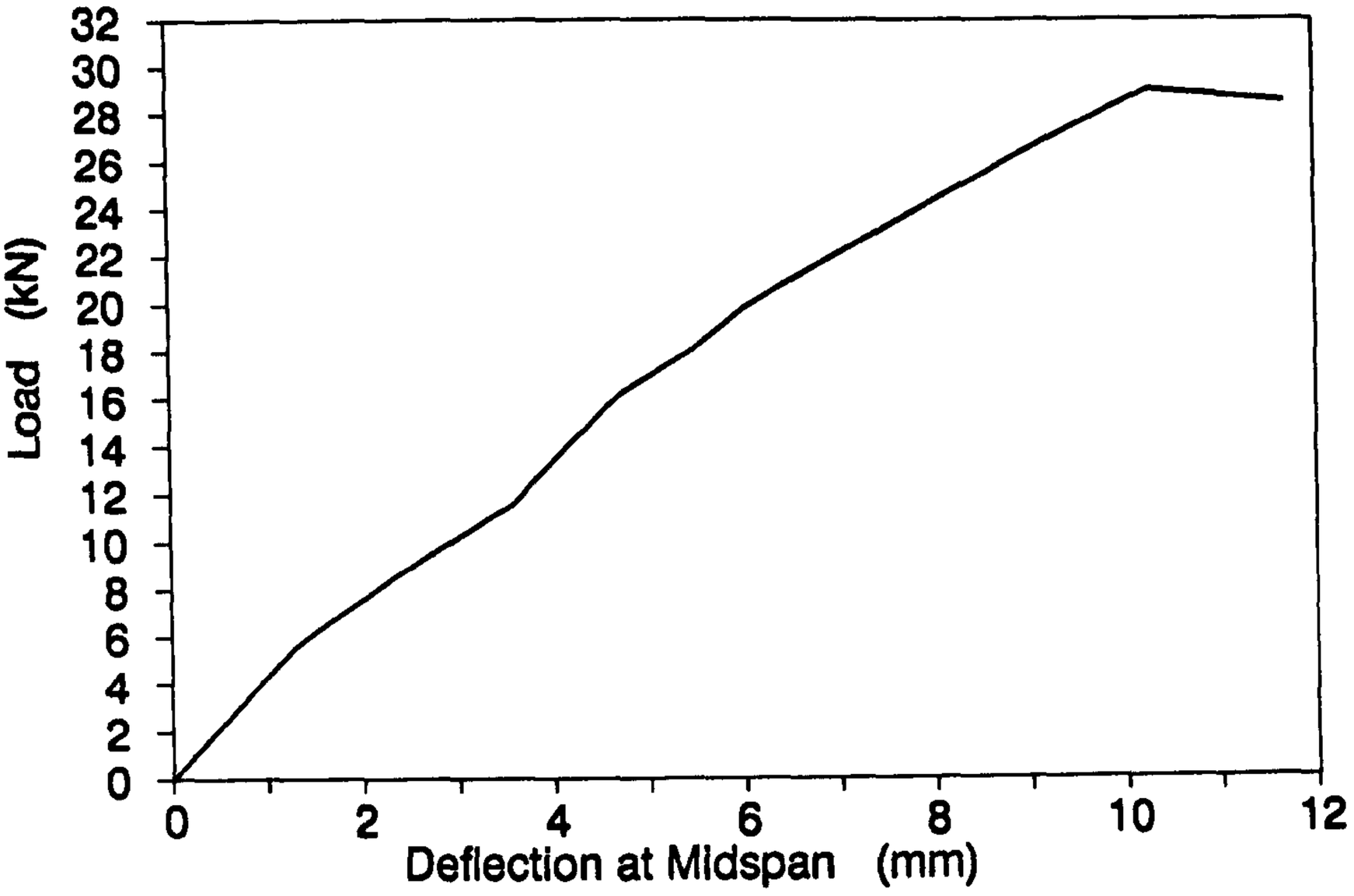

FIG.6.22-Load-Deflection History of Beam B

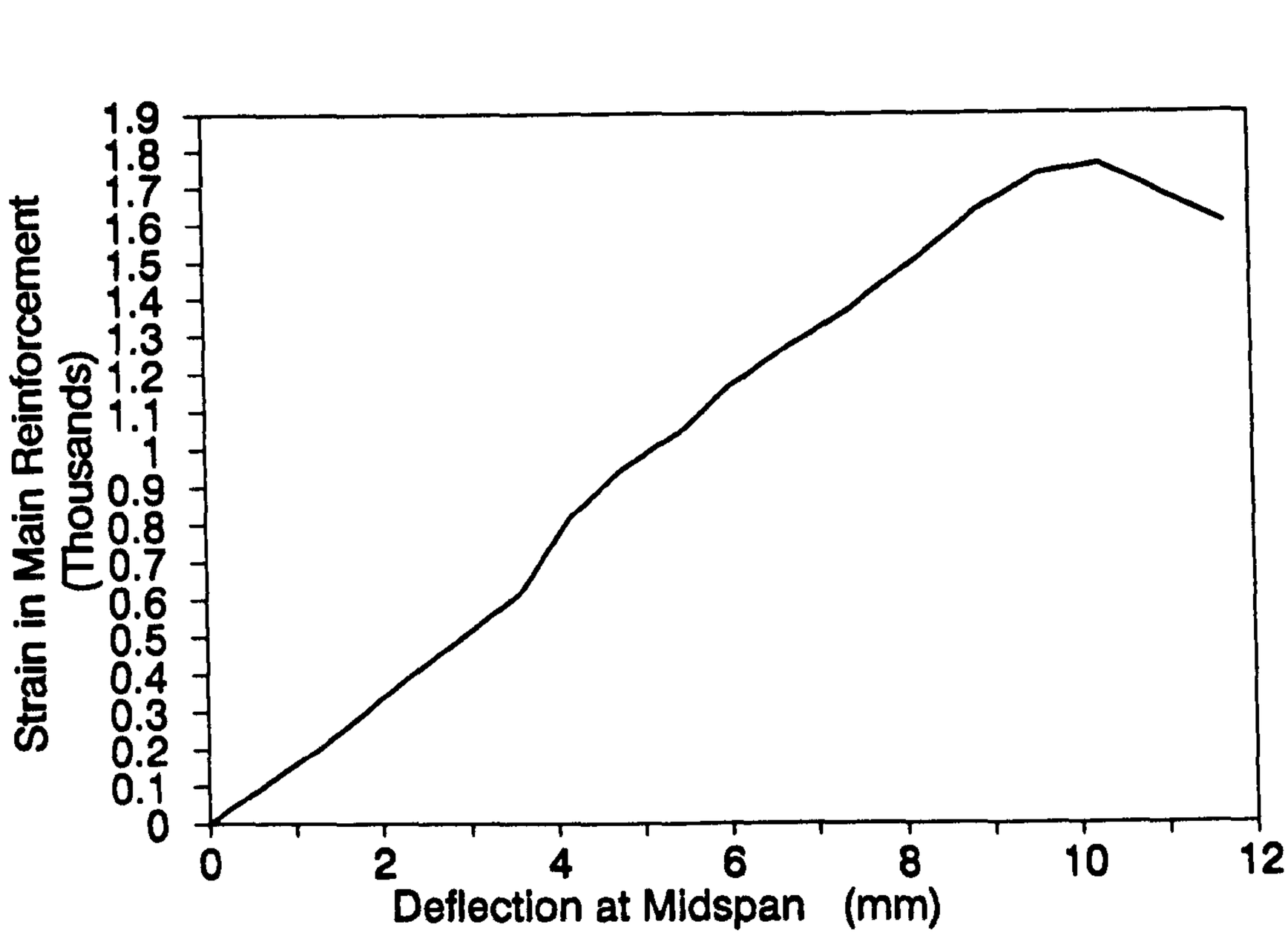

FIG.6.23-Deflection versus Steel Strain at Midspan of Beam B

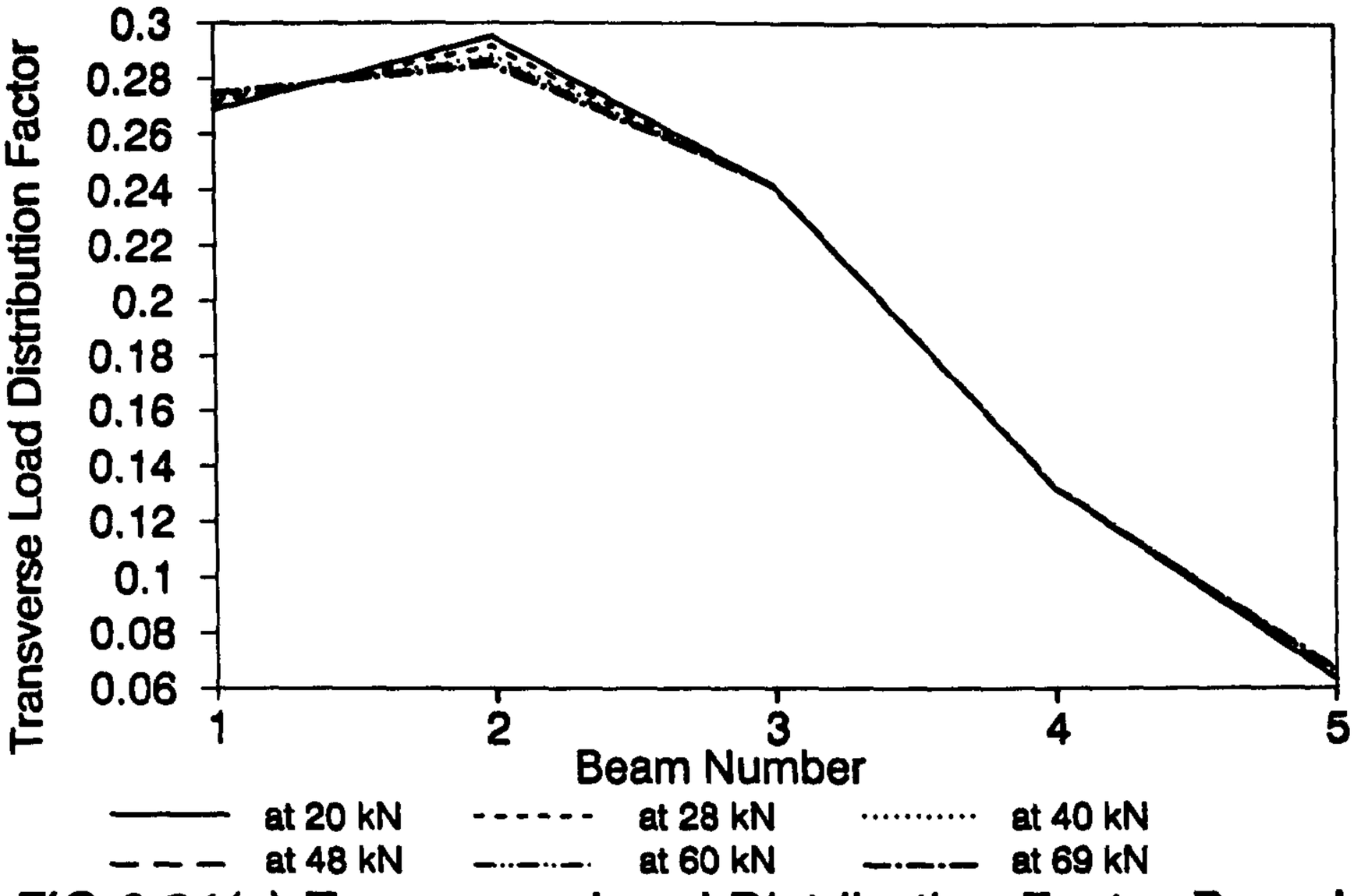

FIG.6.24(a)-Transverse Load Distribution Factor Based on Steel strain in the 115kN Loading Cycle

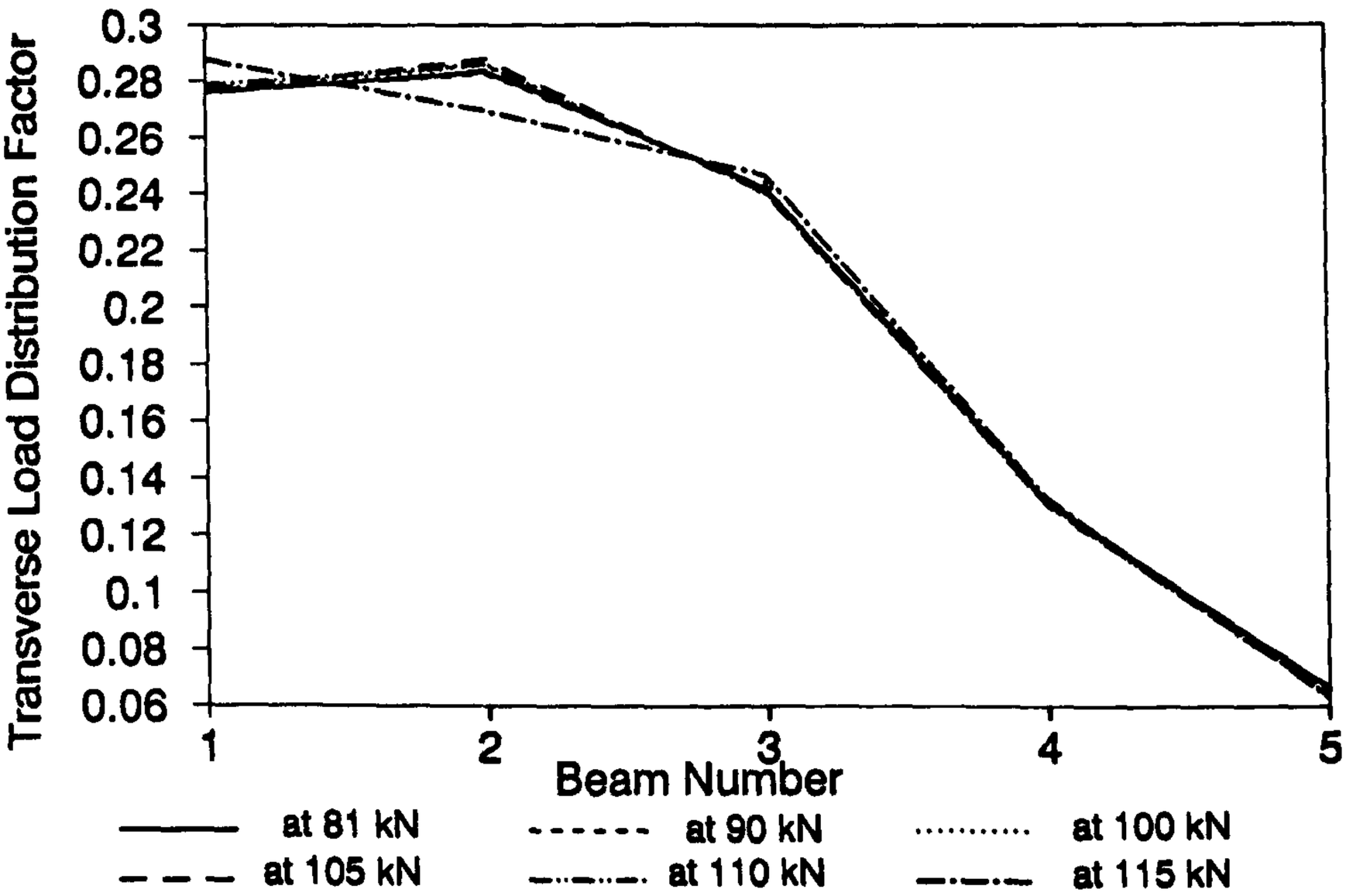

FIG.6.24(b)-Transverse Load Distribution Factor Based on Steel Strain in the 115kN Loading Cycle

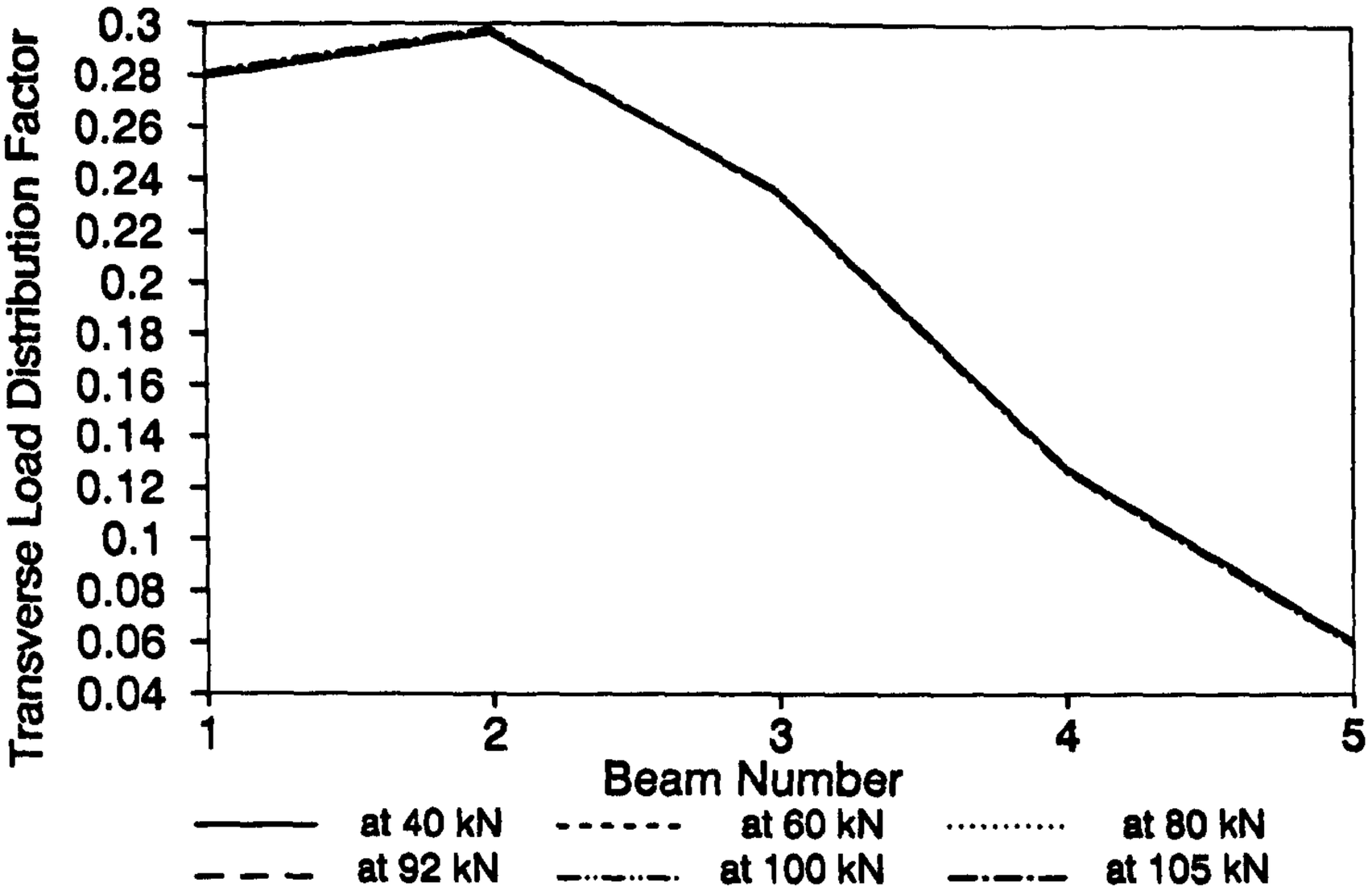

FIG.6.25(a)-Transverse Load Distribution Factor Based on Steel Strain in the 140kN Loading Cycle

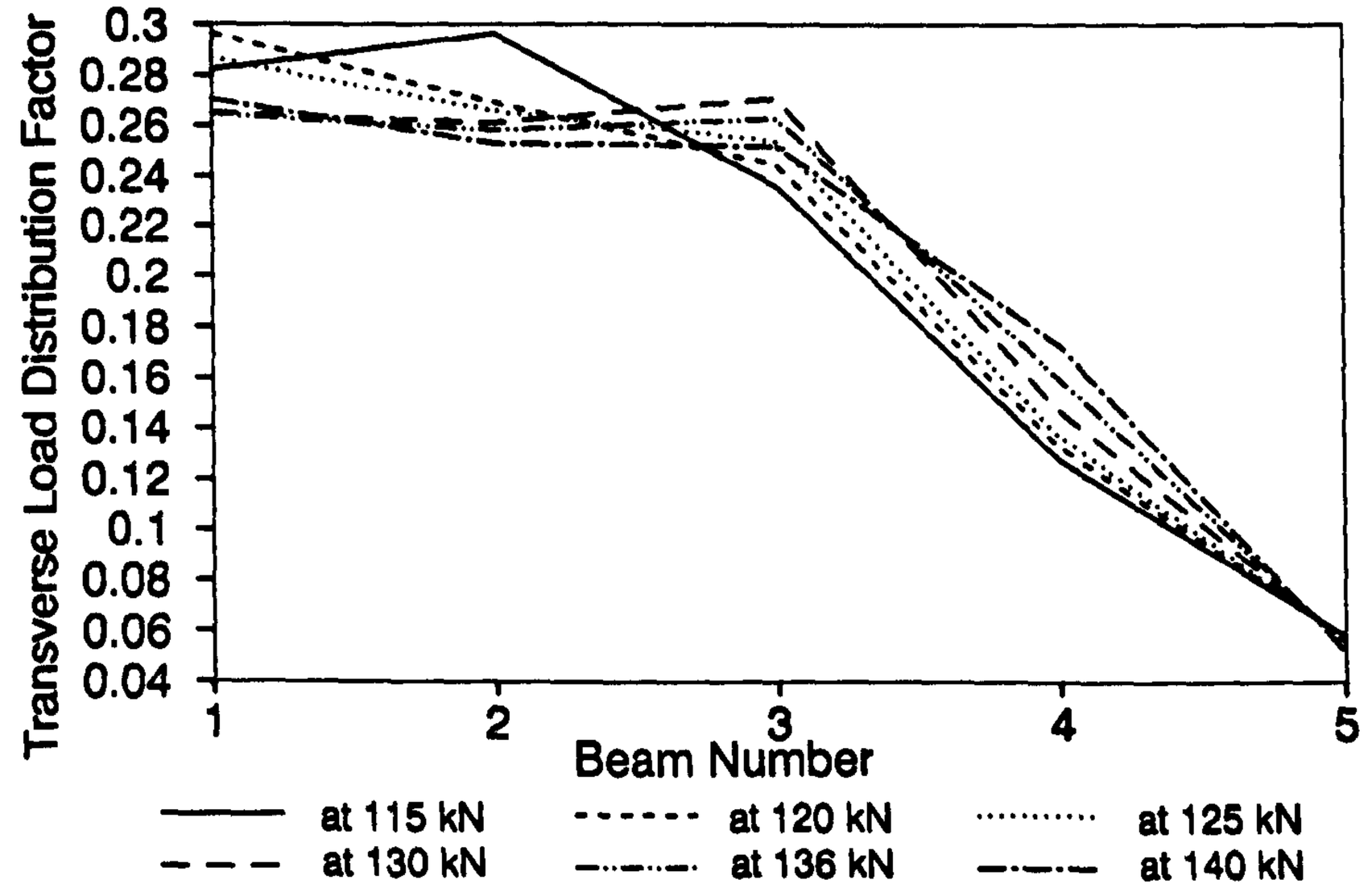

FIG.6.25(b)-Transverse Load Distribution Factor Based on Steel Strain in the 140kN Loading Cycle

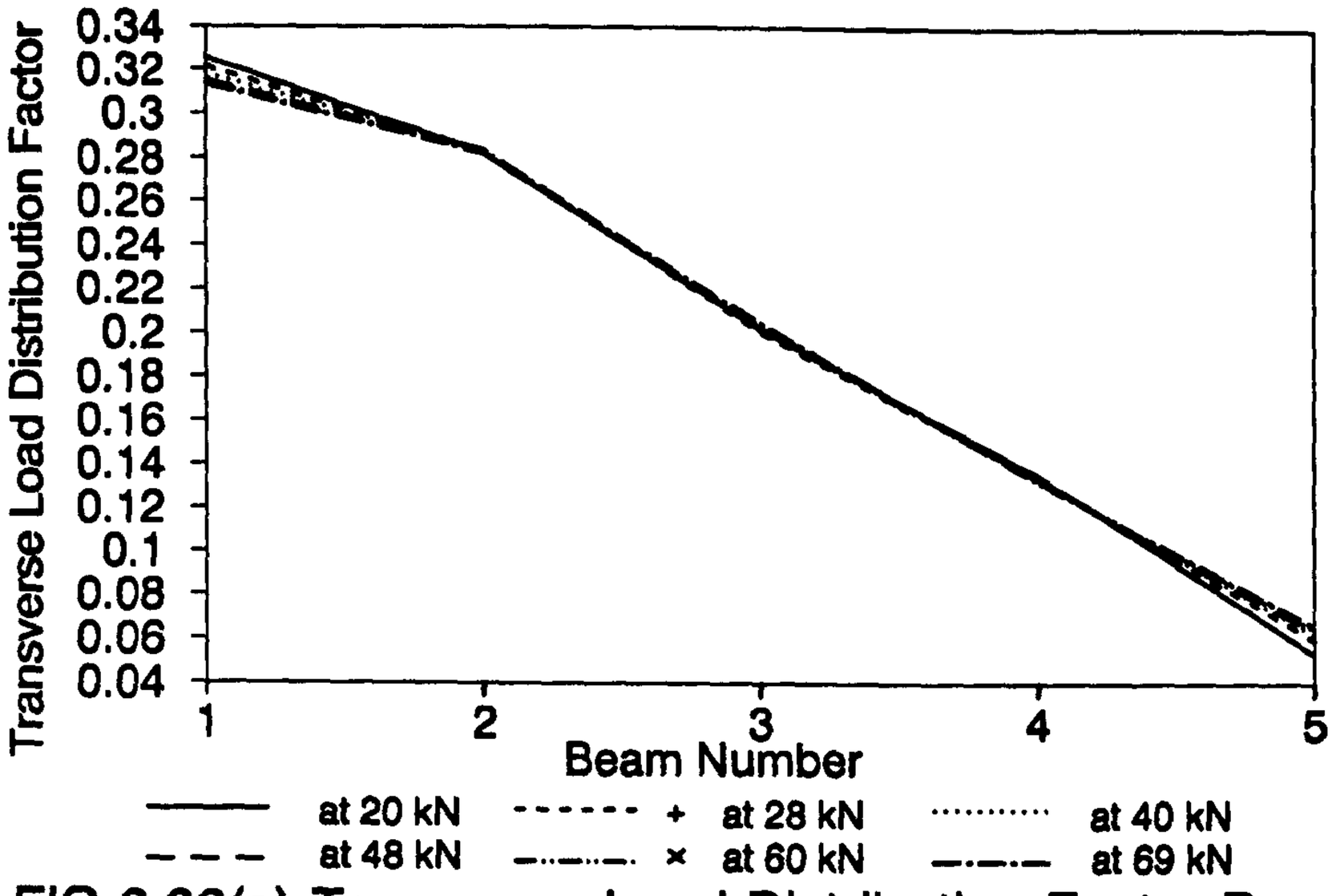

FIG.6.26(a)-Transverse Load Distribution Factor Based on Deflection in the 115kN Loading Cycle

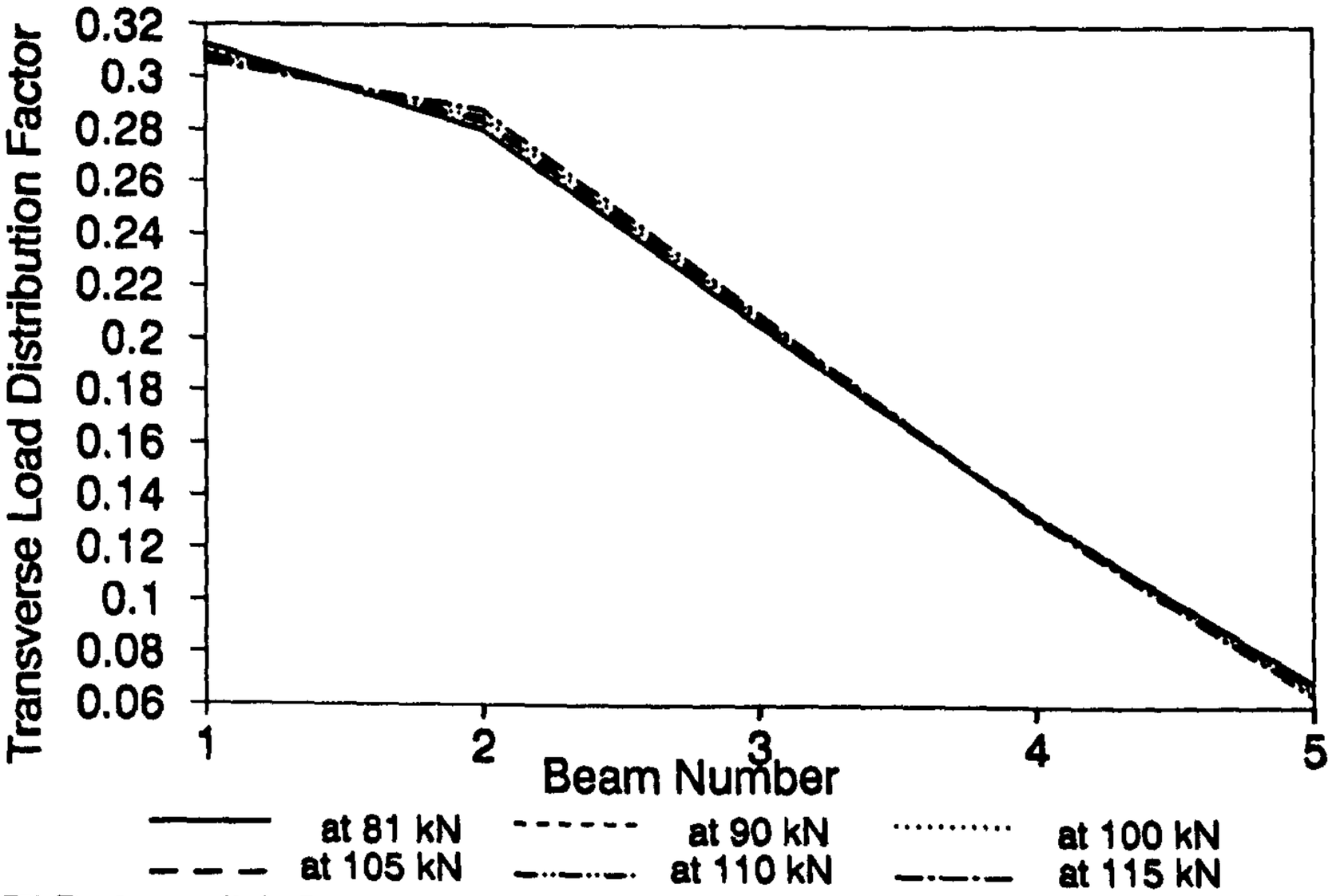

FIG.6.26(b)-Transverse Load Distribution Factor Based on Deflection in the 115kN Loading Cycle

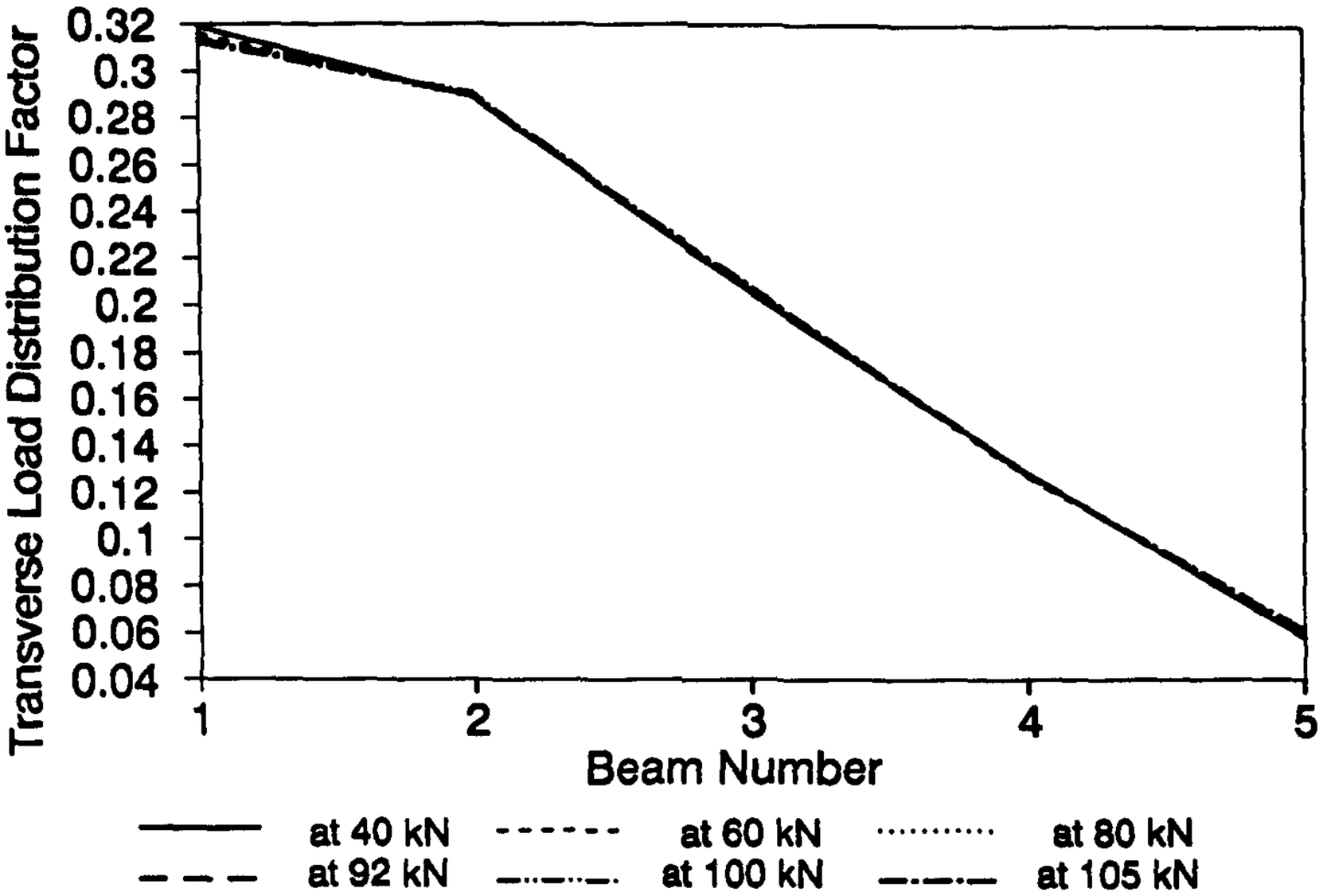

FIG.6.27(a)-Transverse Load Distribution Factor Based on Deflection in the 140kN Loading Cycle

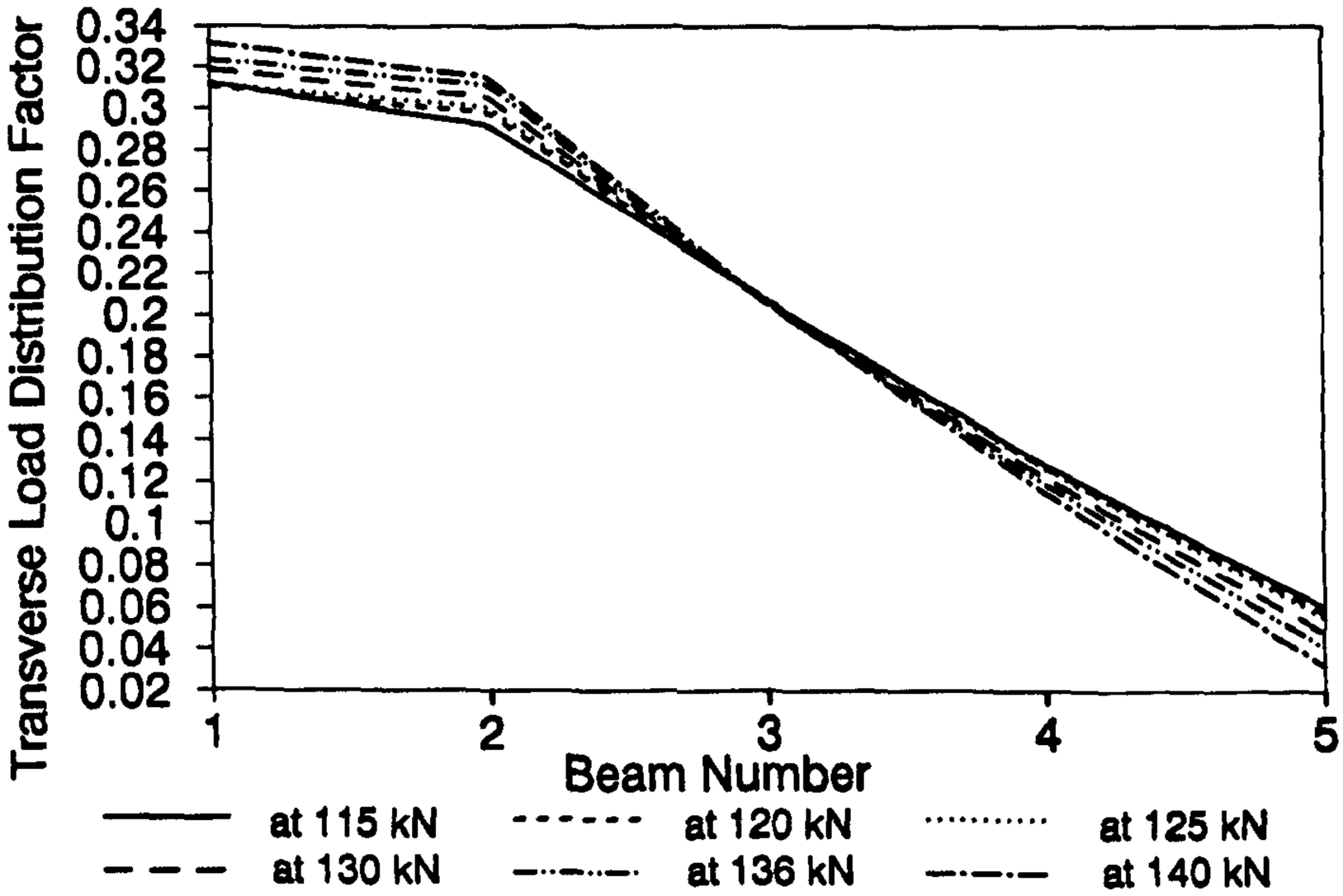

FIG.6.27(b)-Transverse Load Distribution Factor Based on Deflection in the 140kN Loading Cycle

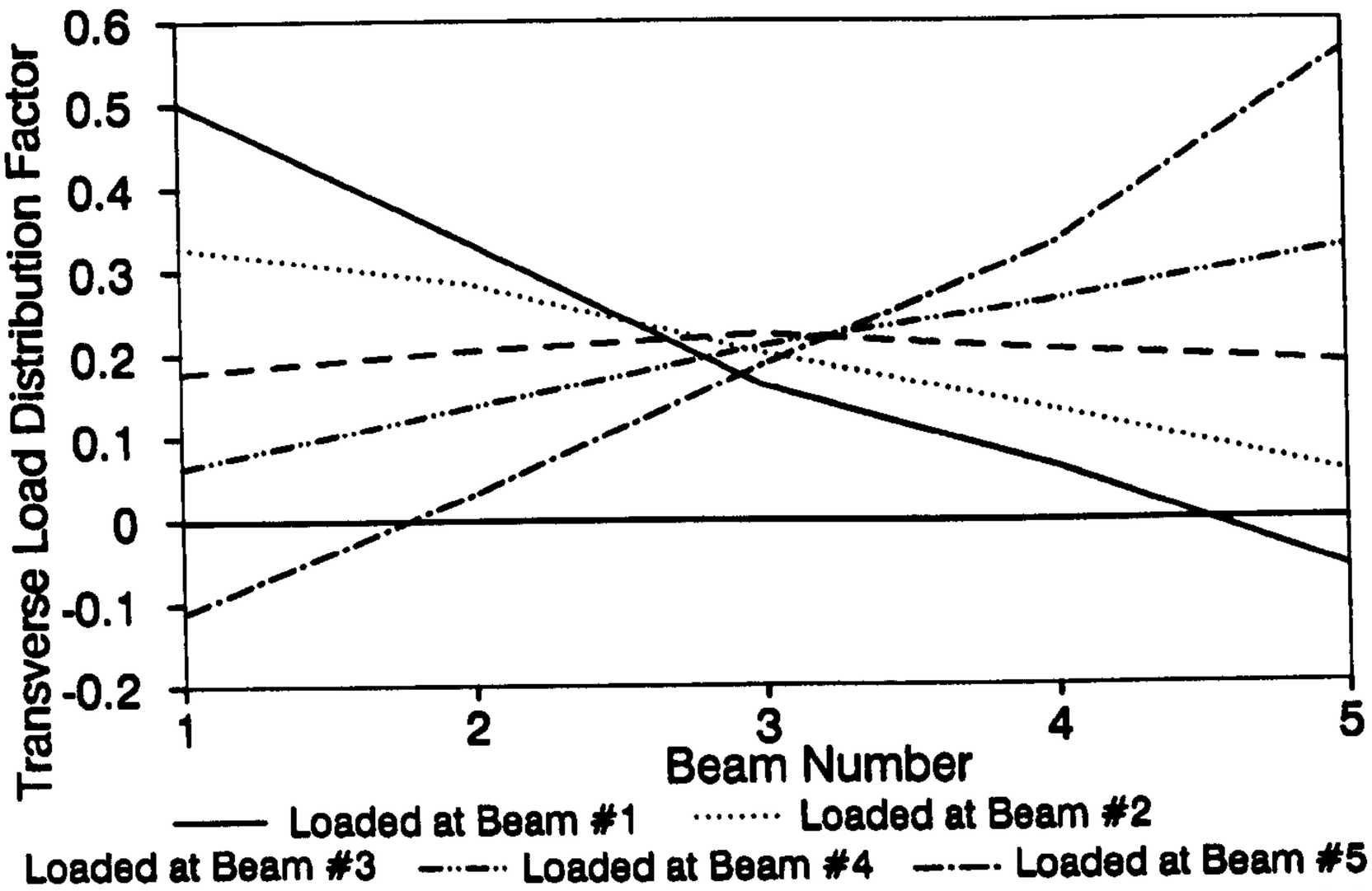

FIG.6.28-Transverse Load Distribution Factor at 12 kN with Load on each Beam in Turn after 70kN Loading Cycle

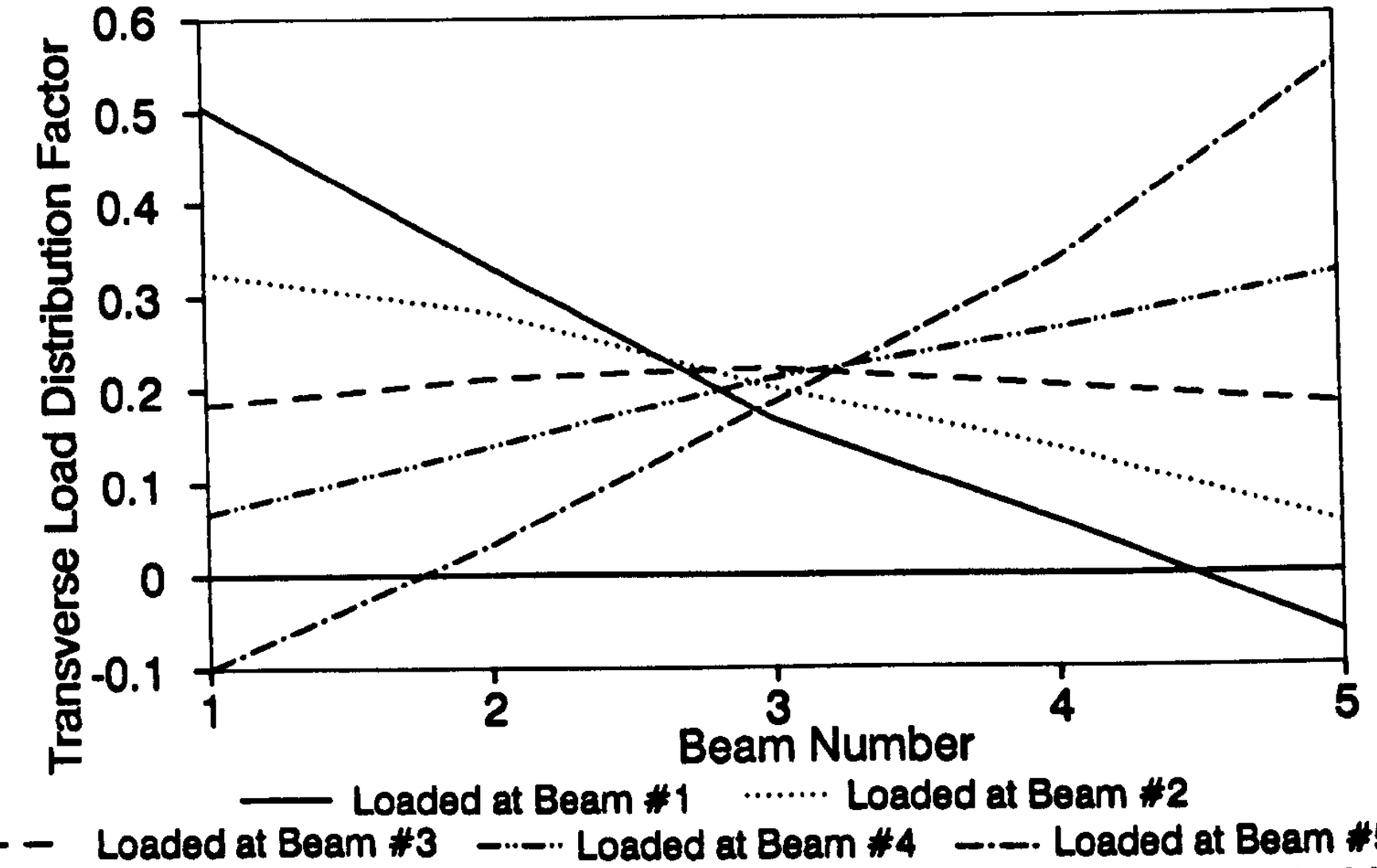

FIG.6.29-Transverse Load Distribution Factor at 20kN with Load on each Beam in Turn after 70 kN Loading Cycle

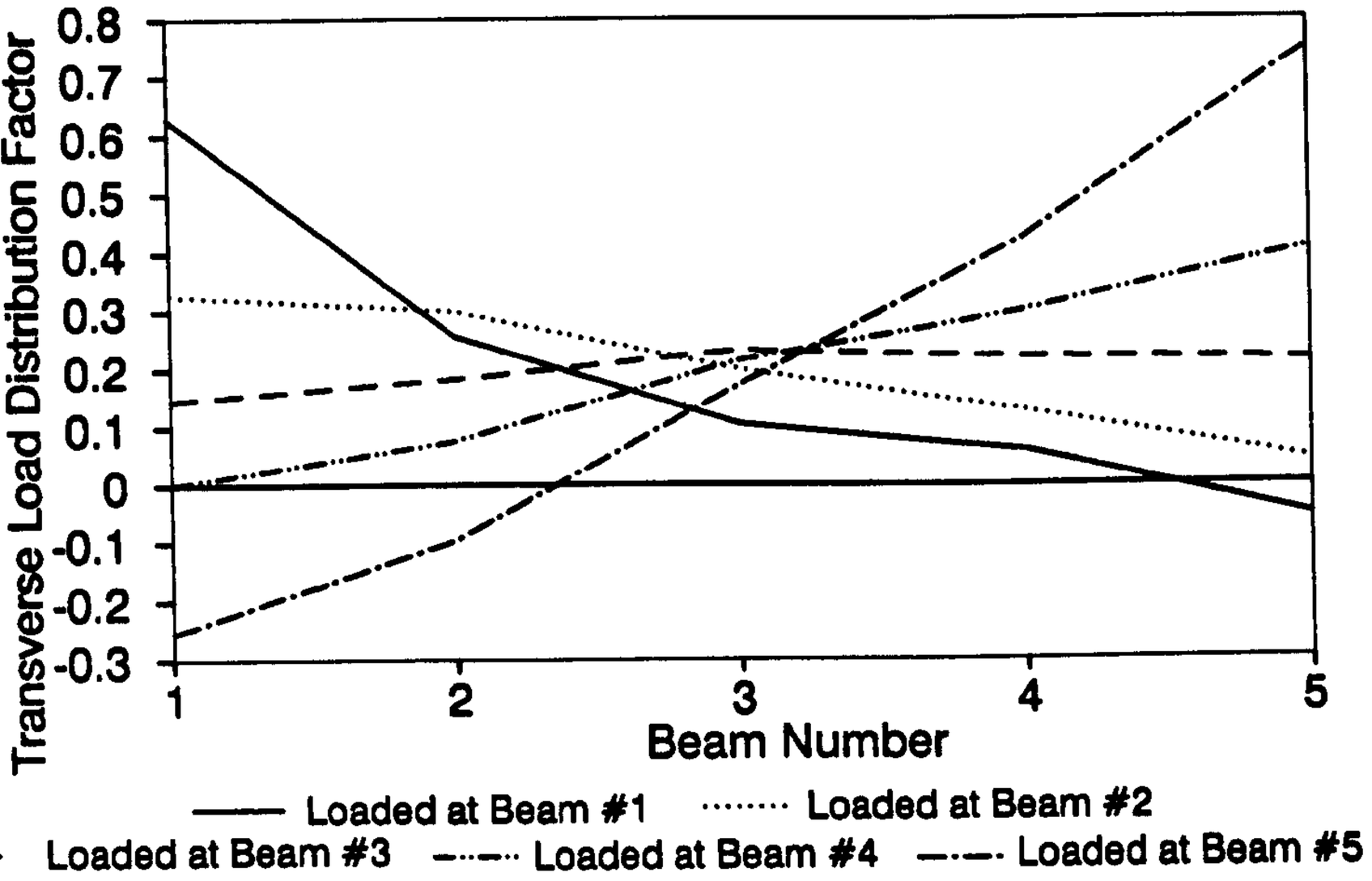

FIG.6.30-Transverse Load Distribution Factor at 10 kN with Load on Each Beam in Turn After Failure of the Bridge Deck

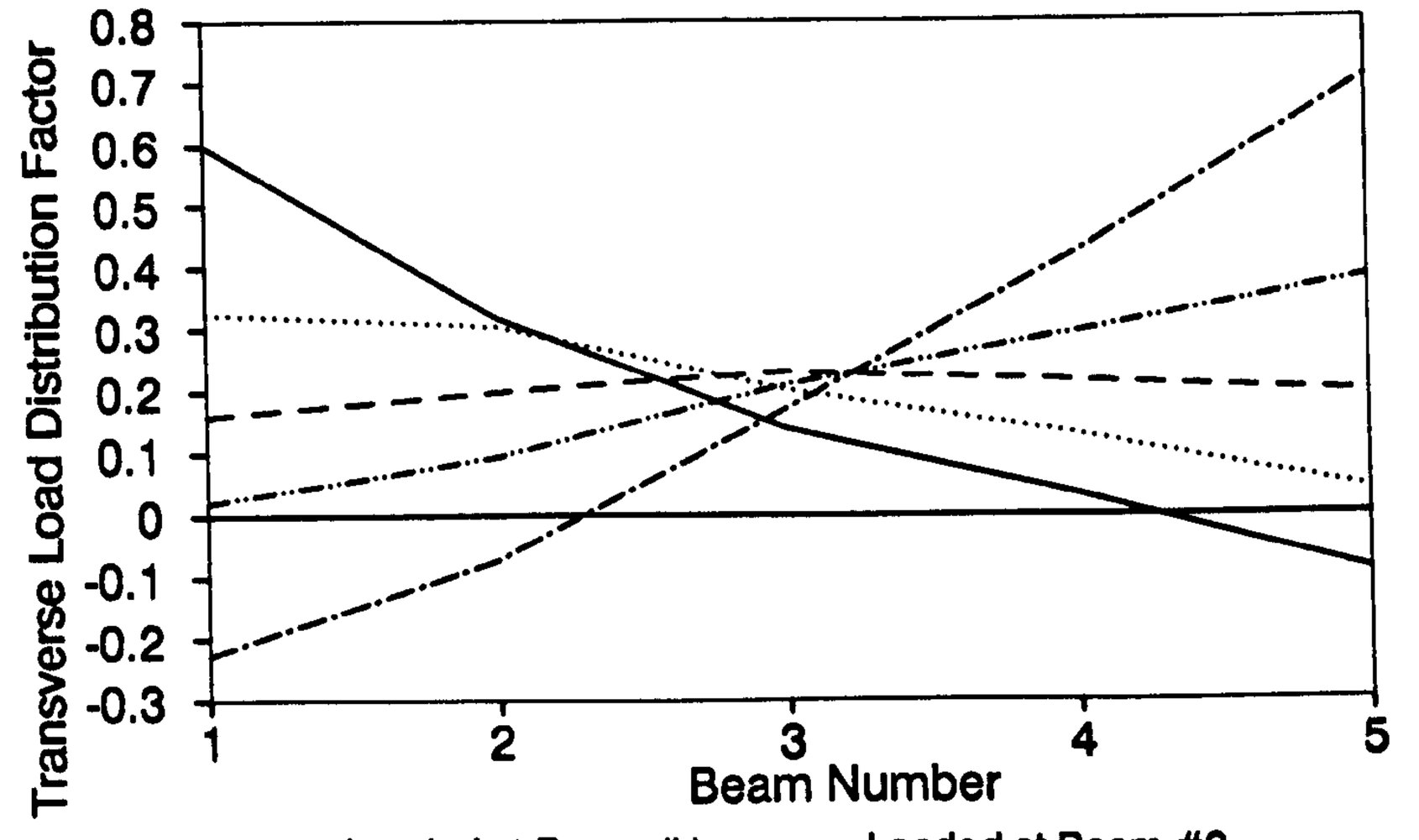

FIG.6.31-Transverse Load Distribution Factor at 20 kN with Load on each Beam in Turn After Failure of the Bridge Deck

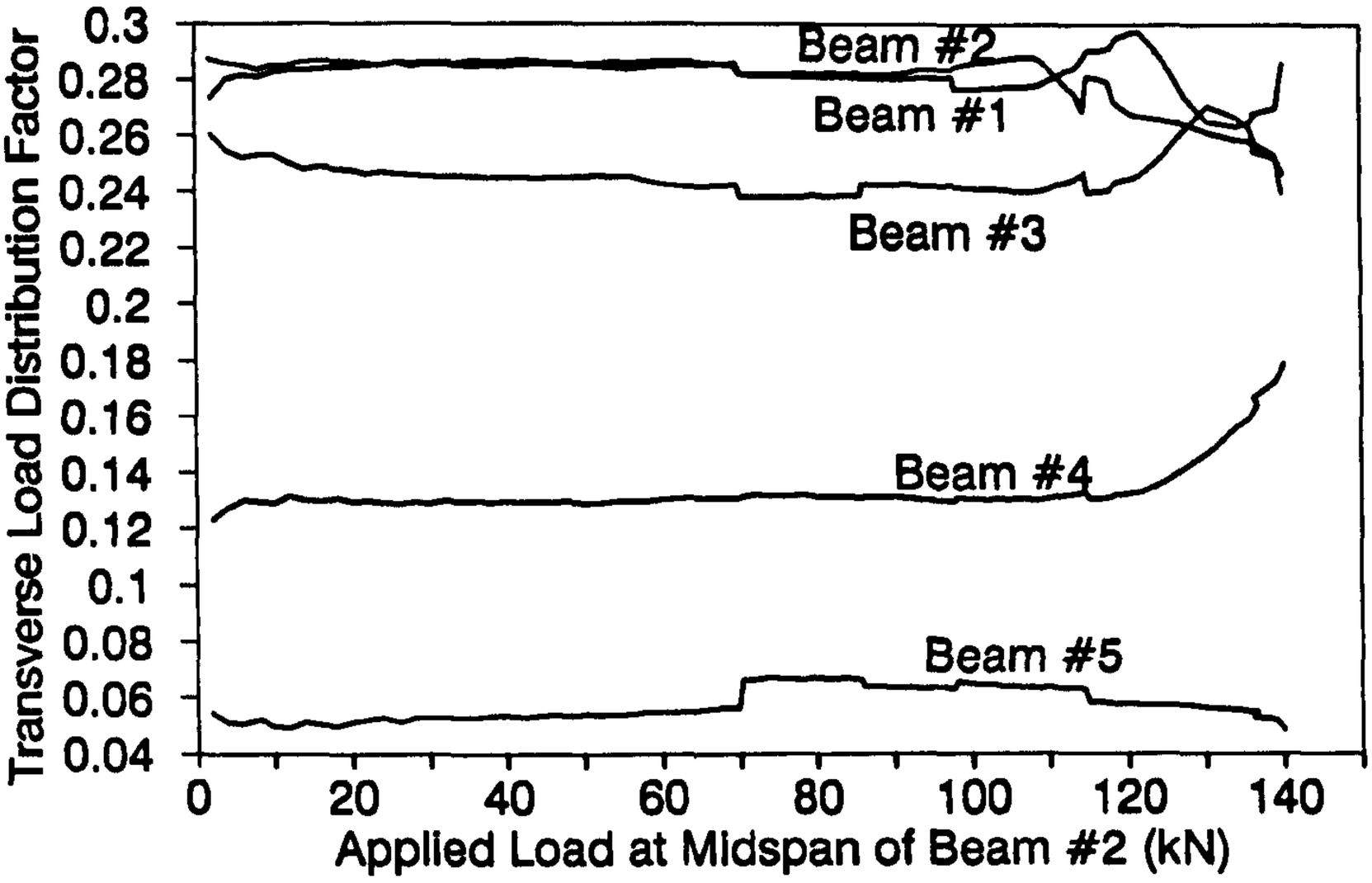

FIG.6.32-Transverse Load Distribution Factor for Each Beam Based on Steel Strain at Midspan Throughout the Loading Range

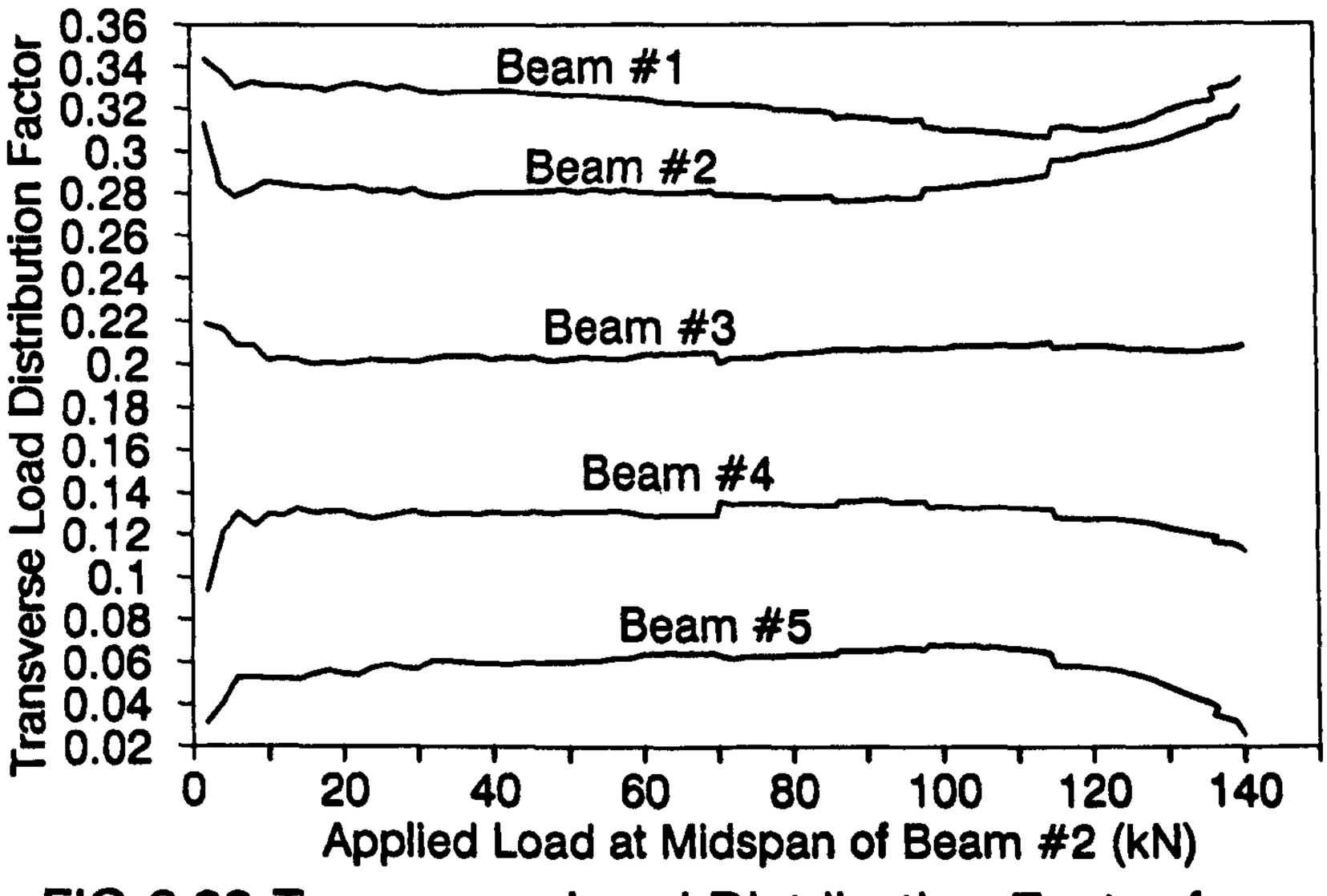

FIG.6.33-Transverse Load Distribution Factor for Each Beam Based on Deflection at Midspan Throughout the Loading Range

CHAPTER SEVEN

DEVELOPMENT OF THE PROPOSED TECHNIQUE AND STRATEGY FROM LABORATORY TESTS

7.1 DAMAGE DETECTION TECHNIQUE FROM MODAL TESTING

7.1.1 The Modified form of Frequency Response Function used in the Experiment

The equations for damage detection using phase angle as the measurable parameter have been drived in Chapter 4 basing on the frequency response function which is defined as the ratio of response at a point to a force input at another point. In the practical case of structure under ambient excitation coming from the points of support, it is not possible to measure the frequency response function at all the points. An alternative form of frequency response function is proposed by the author which relates to the true frequency response function as:

$$\bar{H}(\omega) = H(\omega) \cdot [R] \qquad (7.1)$$

where $\bar{H}(\omega)$ is the measured frequency response function matrix with its elements defined as the ratio of the response at one point to the response at the other point;

$H(\omega)$ is the true frequency response function with its elements defined at the ratio of the response at one point to the force input at the other point;

and $[R]$ is a diagonal matrix with the diagonal elements equal to the inverse of the corresponding diagonal elements of $H(\omega)$, i.e.

$$[R] = \begin{bmatrix} \ddots & & 0 \\ & \frac{1}{H_{11}} & \\ 0 & & \ddots \end{bmatrix} \tag{7.2}$$

An attempt is made in the following Sections to use the modified frequency response function as an approximation to the true FRF to avoid the practical difficulties in measuring the force in an ambient excitation problem. The error involved in this approximation has not been calculated in these pioneer tests. Eqn.(7.1) becomes

$$\bar{H}(\omega) \simeq H(\omega) \tag{7.3}$$

7.1.2 The Steel Cantilever Beam

The following gives a description of the data analysis and development of the technique based on the experimental results.

7.1.2.1 Signal Analysis

The recorded signals were played back from the tape recorder, and the frequency response functions were obtained from a dual channel analysis programme in a microcomputer using 8192 FFT length and 1024Hz sampling rate. The modified frequency response functions were calculated by taking response at one point as the input and that at the other point at the output. The phase value of the frequency response function H_{26}, i.e. θ_{26}, was selected as the measured parameter to identify the damage.

The second column and sixth row of the modified FRF matrix were calculated for the undamaged beam. Points of the frequency response function around the first three modal frequencies were selected. Only 128 points around the third modal frequency were chosen after editing out any corrupted data. The vector {B} in Eqn.(4.40) is formed from the

measured $\Delta\theta_{26}$. The sensitivity matrix [A] is calculated from the measured FRF of the undamaged beam according to Eqn.(4.39).

Hence Eqn.(4.40) becomes a set of simultaneous equations with the unknown vector $\{\Delta b_i\}$. The cantilever beam is divided into five finite elements as shown in Fig.6.1, and $\{\Delta b_i\}$ consists of five components each representing the small change in stiffness in one of the five finite elements forming the beam.

7.1.2.2 Stiffness of a Beam Element With a Slot

A beam element with a finite slot as shown in Fig.7.1 is represented by four nodes a, b, c and d and three elements 1, 2, and 3. The degree of freedom at nodes 2 and 3 can be removed by the static condensation method. According to the principle of Guyan reduction, Guyan (1965), the system stiffness matrix is written in partitioned matrix form,

$$[K] = \begin{pmatrix} [K_{aa}] & [K_{ab}] \\ [K_{ba}] & [K_{bb}] \end{pmatrix} \tag{7.4}$$

where the subscripts a and b refer to the end and internal coordinates respectively. The internal coordinates can be reduced by

$$[\bar{K}] = [K_{aa}] - [K_{ab}][K_{bb}]^{-1}[K_{ba}]^{T} \tag{7.5}$$

where $[\bar{K}]$ is a reduced stiffness matrix for the end coordinates only.

The reduction in stiffness in the beam element due to a slot is calculated as the difference between the stiffness matrix of a good element a-b and the reduced matrix $[\bar{K}]$ of the same element. The average reduction in the diagonal elements of the matrix is adopted in this study, and the reduction in

stiffness in element 1 of the cantilever beam in Fig.6.1 is calculated as 1.311%.

7.1.2.3 Damage Identification Results

Eqn.(4.40) was solved by the iterative least-squares method. The results of damage identification are shown in Fig.7.2. Results obtained using H_{26} and $|H_{26}|$ as the measured parameters are shown in Figs.7.3 and 7.4 for comparison. The percentage reduction in stiffness is listed in Table 7.1. The relative errors are related to the calculated value of 1.311%. Both the results obtained from using H_{26} and θ_{26} attain a stable value after 40 iterations while that obtained from using $|H_{26}|$ is not very stable attaining a value of -0.71% eventually. Only 64 good samples around the positive sensitive region of the modulus of FRF are used in the latter identification. Results of identification show that those from H_{26} and θ_{26} are close to the calculated value. This means that the phase difference, if not better, is as good as the frequency response function as a tool in structural damage diagnosis.

7.1.3 The Small Scale Reinforced Concrete Bridge Deck

7.1.3.1 Summary of Static Tests Results

The main reinforcement in Beam #2 of the bridge deck yielded at 115 kN. Further static loading up to 120 kN and 130 kN caused yielding of the reinforcement in Beams #1 and #3 respectively. Extensive cracks developed in both the main beams and diaphragms during the loading process. The crack pattern of the slab shown in Fig.6.9 shows that the diaphragms were very effective in transmitting the loads between beams. First cracking in Beam #2 was observed at midspan after 60 kN and the cracks extended rapidly up to the underside of the flanges after 70 kN. Further cracks appeared under subsequent loading, and a major crack

extended more than half-depth of the diaphragm between station 2E and 3E at the 86 kN load.

The transverse load distribution factors based on the deflection at midspan of the beams are shown in Table 6.2. The factors were calculated for each of the load levels and were almost the same before yielding of the reinforcement at 115 kN load.

7.1.3.2 Modelling of the Structure for Damage Detection

The bridge deck was modelled as a set of grillage beams with an effective width of the flange included in the calculation of the moment of inertia. The theoretical cracked moment of inertia of the diaphragm is plotted for different neutral axis depths in Fig.7.5. It shows that a reinforced concrete Tee-beam section has a cracked moment of inertia close to a relatively stable value throughout most of its working range as shown in Section 7.2.1.2. The central diaphragm was modelled as consisting of four elements between the grid points 1E, 2E, 3E, 4E and 5E as shown in Fig.7.6. The reduction in stiffness in the diaphragm due to cracking was expressed as a percentage of the uncracked flexural stiffness of 2.194E+6 N-m^2.

7.1.3.3 Signal Analysis

Accelerometers were placed at grid points 2C, 4C, 1E, 2E, 3E, 4E and 5E as shown on Fig.5.1, and the vertical response of the bridge deck was monitored in the form of acceleration recorded on tape recorder. Excitation to the structure was limited to ambient excitation transmitted through the supports.

The changes in the modified frequency response function, its modulus and the phase angle between response at grid points 2C and 4C were used to identify the changes in stiffness in

the central diaphragm.

For each of the loading cycles up to 70kN, 98kN, 115kN and 140kN, 450 sets of the modified frequency response function around the first modal frequency were calculated using a 8192 FFT length and a 255.1Hz sampling rate over a period of 10 minutes. Only 22 averages were taken due to the short length of record. The resulting FRF points that carried large noise were eliminated and the iterative least-squares method was used to identify the damage parameters $\{\Delta b_1\}$. Vector $\{\Delta b_1\}$ consisted of four elements each representing the small change in stiffness in one of the four finite elements shown in Fig.7.6.

The results of damage identification are shown in Fig.7.7 to 7.18. The percentage reduction in stiffness is listed in Table 7.2.

7.1.3.4 Damage Identification Results

The damage identification results using the FRF and its modulus as measured parameter converge rapidly after about a hundred iterations for analysis of signals at load levels below 115kN. Those results involving more heavily damaged elements above the 115kN load level are not stable and diverge.

The results using the phase difference as the measured parameter do not show a clear convergence and there is a large variation between the results of each iteration. This may be due to the large random error in the measured phase difference using only 22 averages in the FFT analysis.

All the results show a gradual deterioration of all the elements as observed from the static test. Both damage identification using FRF and its modulus show that element 2 between grid points 2E and 3E was suffering from larger

damage at all the load levels. Element 1 between grid points 1E and 2E suffered slightly less damage as the deformation between Beams #1 and #2 under static load were almost the same.

7.1.4 A "Search" Strategy for the Damage Identification Problem

The subscripts r and s in Eqn.(4.39) denote points in the measurement domain, and subscripts p and q denote points in the damage domain. A "search" strategy is therefore possible with the structure divided into a number of large finite elements, and the first identification would locate elements with possible problems. The structure is divided again into a number of smaller elements, and the second identification is confined to the elements identified in the first trial. The accuracy of this method therefore depends on the complexity of the finite element model considered in the formulation of the structural stiffness matrix.

7.1.5 Discussion

The sensitivity equations show that the change in phase difference is more sensitive to changes in stiffness than the FRF and its modulus especially at small values of phase angle. The effectiveness and accuracy of phase difference in detecting damage is demonstrated through a test on a steel cantilever beam.

It has also been demonstrated using a model reinforced concrete bridge deck, that ambient excitation would be a useful source of excitation for damage assessment using this method. As only a low level of excitation is used, minimum non-linearity of the structure is involved in this problem.

The error induced by omitting matrix [R] in Eqn.(7.1) in the calculation has not been studied further in these experiments. But the identification results seem promising

even with limited success in the case of ambient excitation test of the model bridge deck.

This method can be used for multiple damage detection, and a minimum of one single mode is required for identification.

7.2 DAMAGE CLASSIFICATION AND ASSESSMENT OF LOAD CARRYING CAPACITY FROM VIBRATIONAL RESPONSE

7.2.1 The Cracked Moment of Inertia of a Reinforced Concrete Beam Section

7.2.1.1 The Theoretical Values

Curves are plotted for neutral axis depth versus the theoretical cracked moment of inertia for Beams A, B and C in Fig.7.19. Concrete is assumed not to take any tensile stress, hence the neutral axis is at the level of the tip of the crack.

There are three stages in the variation of the cracked moment of inertia. When a bending moment is applied, cracks develop together with a decrease in the moment of inertia. The cracks grow very rapidly under a small load until the tensile stress in the main steel increases to form a balancing moment with the concrete in compression to resist the applied bending moment. The beam is 'weakened' since the moment of inertia is decreasing at this stage. The second stage has a relatively constant moment of inertia of about 71.0E-6 m^4 for Beams A and C and 53.0E-6 m^4 for Beam B. This relatively constant value of moment of inertia is considered to be a property of the beam. It is therefore called I_{nom} denoting a nominal cracked moment of inertia of the cracked section. The last stage is an unstable stage where the moment of inertia decreases rapidly with further reduction in the neutral axis depth until the beam section is fully cracked over its depth.

7.2.1.2 The Experimental Values

The variation in cracked moment of inertia can be seen in the load-deflection curves of the individual beams (Figs.6.20 and 6.22). There is a very short section with a relatively steep gradient at the start of loading followed by a longer second stage having a less steep gradient and a third stage of gentle gradient as the yield of the reinforcement is approached.

The variation of the neutral axis depths for Beams #1, #3 and #5 of the bridge deck throughout the loading cycles are studied here in detail. The depth of neutral axis is calculated using the strain of concrete at the top of precast beam and the strain of the main steel reinforcement. Only the values corresponding to the first attainment of load in each of the loading cycles have been selected. The changes are plotted in Fig.7.20 with all the residual strain included in the calculations. Similar plots for Beams A and B are shown in Fig.7.21. At 5 kN applied load, the neutral axis depth is 57 mm and 37 mm for Beams A and B respectively, and 56 mm, 44 mm and 50 mm for Beams #1, #3 and #5 respectively in the model bridge deck. Further loading causes only a small reduction in the neutral axis depth. The neutral axis depth changes throughout the loading range from 56 mm to 44 mm for Beam #1, 44 mm to 48 mm for Beam #3 and 50 mm to 59 mm for Beam #5. For the individual Beams A and B, the neutral axis depth changes from 51 mm to 60 mm and 31 mm to 40 mm respectively.

This phenomenon of small change in the neutral axis depth in the cracked states in all the beams indicates the cracked section is resisting bending moment with a relatively constant moment of inertia close to the nominal value I_{nom} of the section.

7.2.2 Moment Capacity of a Reinforced Concrete Beam Section

In an under-reinforced concrete beam section, the moment capacity is dependent on the amount of tensile reinforcement. The serviceability requirements of crack width and deflection in the Standard JTJ023-85 (1985) can also be expressed in terms of the steel percentage. Therefore, by expressing the moment capacity under the different limiting criteria as a function of the steel percentage, the theoretical moment capacity of Beams A and B have been plotted in Figs.7.22 and 7.23. The steel percentage is based on the global cross-sectional area of the Tee-beam section.

In both beams, the deflection criterion controls for most of the practical range of steel percentage up to 7.5%. Strength criterion takes over control only for more heavily reinforced sections. The moment capacity due to limiting crack width increases steadily, whereas that due to the strength requirement has significant variations in the curve around 4~5.5% of steel percentage. This is due to a shift of the neutral axis out of the flange of the beam.

It is concluded that if the percentage of reinforcement of a beam is known, the moment capacity of a bridge beam can be estimated from graphs similar to Figs.7.22 to 7.23. The load carrying capacity of a bridge deck can then be estimated from information on the transverse load distribution properties of the structure.

Details of the calculations on the moment resistance of a beam section in accordance with the different limiting criteria in the Chinese Bridge Design Standard JTJ023-85 (1985) are referred to in Appendix 6.1.

Similar limiting requirements from BS5400 Part 4 (1984) can also be expressed as a relationship between the percentage

of reinforcement and the moment of resistance of a beam section. The strength limit requirement, deflection limit requirement and the crack width limit requirement are defined by Cl. 5, Cl 6.3.2 and Cl.6.8.8.2 respectively.

7.2.3 The Static Moment of Inertia of The Individual Beams and Bridge Deck

By accepting the small error in assuming the same distribution of load across a cross-section along the length of each beam in the bridge deck, the flexural stiffness EI of each beam at each load increment can be estimated by the following formula:

$$\Delta\delta_i = \frac{\Delta P_i \, L^3}{48(EI)_i} \qquad i = 1,2,3,4,5 \qquad (7.3)$$

where $\Delta\delta_i$ is the incremental deflection at midspan of the beam;

ΔP_i is the fraction of incremental applied load acting on each beam calculated by multiplying the transverse load distribution factor by the incremental applied load;

L is the span length.

It should be noted here that only the value obtained for Beam #2 is likely to be accurate. The others must be considered to be approximate as the loads are transferred to the beams along their length as well as from the concentrated load applied at midspan.

Fig.7.24 shows a plot of the cracked moment of inertia of the bridge deck and each main beam separately at the first attainment of each load in the different loading cycles. The moments of inertia of all five beams are very similar to each other. There is a generally decreasing trend with increasing load. The curve for the whole bridge deck shows a

more marked decreasing trend. This corresponds to the second and third stages in the theoretical variation of the cracked moment of inertia of a beam section.

Variations of the static moment of inertia of Beams A, B and C under static load are shown in Fig.7.25. The experimental values obtained from static test varies from 80.0E-6 m^4 to 110.0E-6 m^4 for Beam A, 67.0E-6 m^4 to 100.0E-6 m^4 for Beam B and 69.0E-6 m^4 to 130.0E-6 m^4 for Beam C. These values are assumed to be uniform over the beam length in the calculation. They are all larger than the nominal value of the beams. This may possibly be due to the non-uniform distribution of flexural stiffness along the member length under a concentrated point load. This non-uniformity is reduced in Beam #2 of the bridge deck at higher load level where the static moment of inertia approaches the theoretical nominal value of the beam.

7.2.4 The Distribution of Cracked Moment of Inertia Along the Beam

Fig.7.19 shows the three stages of the variation of the cracked moment of inertia of the beam section with linear change in the neutral axis depth. If the variation of neutral axis depth along the beam is assumed to be linear from the support to midspan, a nearly uniform distribution of cracked moment of inertia is obtained by inverting the curve in Fig.7.19 and eliminating the portion of the curve at small neutral axis depths, as shown in Fig.7.26.

In a section containing a crack, the moment of inertia for a cracked section is appropriate. However in between cracks the bond between concrete and the reinforcement bar is not the same as in an uncracked section, and neither the moment of inertia for the uncracked section nor that for a cracked section is appropriate. BS8110 (1985) recommends that the properties associated with the partially cracked section should be used for the entire beam. The recommended values

of the moment of inertia are calculated in the same way as used in this research.

In prototype bridge decks, a portion of the tension reinforcement of the beam is bent up as shear reinforcement close to the supports thus reducing the cracked moment of inertia of the beam section. Furthermore, tension cracks have been observed to be uniformly distributed along the beams. Therefore it may be concluded that a uniform distribution of moment of inertia is appropriate for prototype bridge beams.

7.2.5 Summary of Conclusions Drawn From the Model Tests

1. The transverse load distribution properties of the bridge deck are relatively constant over the whole loading range before any yielding of reinforcement in the main beams occurs;
2. The neutral axis of a Tee-beam section goes near to the soffit of the beam section after cracking first appears. Under further loading, the variation is small.
3. A cracked Tee-beam section resists the applied bending moment with a nominal cracked moment of inertia I_{nom} throughout most of its working range of loading. A deep penetration of the crack into the flange thickness corresponds with a rapid reduction in the moment of inertia of the beam section;
4. All beams in a bridge deck have approximately the same value of cracked moment of inertia throughout the loading range, (Fig.7.24);
5. The load carrying capacity of an under-reinforced beam can be expressed as a function of the percentage of reinforcement in the member;
6. The load carrying capacity of an otherwise undamaged bridge deck can be estimated from the information on the percentage of reinforcement of the main beams and the transverse load distribution properties of the

bridge deck.

7.2.6 The Proposed Method for Damage Classification and Load Carrying Capacity Assessment

The modal frequencies of a bridge deck are dependent on the mechanical properties of the structure, in particular its flexural stiffness. Modal frequencies involving the first bending mode are more important in this study as their mode shapes mobilize more cracked elements near midspan than the other modes. For example, the second bending mode involves a node at midspan of the bridge deck in its mode shape and is not sensitive to cracks near midspan of the structure (Fig.5.2). The first bending mode with torsional mode shapes are dependent more on the transverse load distribution property of the bridge deck. Only the first bending mode is less affected by changes in the transverse load distribution properties of the bridge deck and is more sensitive to cracks near midspan of the structure. Therefore the first bending modal frequency is used in the estimation of the cracked moment of inertia of the bridge beams.

It is therefore possible to estimate the flexural stiffness, with an assumed longitudinal distribution in the major members of the bridge deck by developing the best match to the measured first modal frequency with a FEM.

A method is proposed based on the above considerations to estimate the percentage of reinforcement in the longitudinal members of the bridge deck and hence the load carrying capacity of the structure. The steps of the implementation are described below.

Step 1. Measure the fundamental modal frequency of the structure in free vibration.

Step 2. Select a finite element model (FEM) which best represents the bridge deck.

Step 3. The moment of inertia of the beams in the FEM is adjusted to have the best match in the fundamental modal frequency in free vibration. A uniform distribution of the cracked moment of inertia is assumed over the length of the main beams, and all the main beams have the same pattern of distribution in the FEM. The value of inertia that gives the closest fit of the measured first modal frequency is the best estimate of the moment of inertia of the beams, I_{est}.

Step 4. Modify the estimated moment of inertia I_{est} by dividing it by a Reference Factor β_{LS}, which is a statistical average of the Factor β, defined as the ratio of I_{est} over I_{nom} of many similar test samples. The result is an improved estimate of I_{nom}.

Step 5. Calculate I_{nom} of the bridge beam for different percentages of reinforcement.

Step 6. Plot the graph of I_{nom} of the cracked section versus percentage of reinforcement in the beam. Find the percentage of reinforcement in the beam from the graph using the estimated I_{nom} obtained from Step 4.

Step 7. Calculate a factor α defined as the ratio of I_{est} over I_{max} of the beam where I_{max} is the calculated moment of inertia of the uncracked composite beam section.

Step 8. Calculate the moment of resistance of the beam according to different limiting criteria, and plot the theoretical moment capacity of the beam against different steel percentages.

Step 9. Find the moment resistance of the beam from the graph plotted in Step 8 with the percentage of reinforcement obtained from Step 6.

Step 10. Obtain the transverse load distribution property of the bridge deck from test or from the literature. Calculate the load carrying capacity of the structure according to the required load configuration.

The Factor α is a measure of the condition of the beam defined as the measured I_{est} over I_{max} of the beam. When I_{est} equals I_{nom}, Factor α has the lowest value. (This is based on the assumption that when I_{est} is less than I_{nom}, the beam is too badly damaged to be in service). When a beam is uncracked with I_{est} equals I_{max}, Factor α has its maximum value of unity. This Factor α is therefore called the Structural Damage (SD) Factor.

Factor β is a measure of the deviation of I_{est} from the nominal value I_{nom} of the beam, and Reference Factor β_{LS} is a statistical average of β with which the percentage of reinforcement of the beam can be estimated from the measured I_{est}. Hence Factor β is called the Load Carrying Capacity (LCC) Factor.

As I_{est}, I_{nom} and I_{max} are functions of the steel percentage of the beam, Factors α and β can be assumed to be independent of the steel percentage. However since I_{est} is calculated from the FEM and an assumed uniform distribution of moment of inertia along the length of the beams, Factors α and β are therefore assumed to be dependent on the length dimension of the structure.

7.2.7 Application of The Proposed Method in The Assessment of The Small Scale Bridge Deck

The SAP IV software package was used in the modelling of the individual beams and the bridge deck. The bridge deck was modelled as a grillage of beams resting on rigid supports. An average value of 28 kN/mm^2 modulus of elasticity was used to cater for the different grades of concrete in Beam A and the model bridge deck. A value of 26.4 kN/mm^2 was used for Beam B. The density of the structure was obtained from the actual weight of the test samples.

The I_{est} from dynamic measurements are plotted in Fig.7.25 and shown in Tables 7 and 8. All the experimental values are of a global nature and are larger than the theoretical values for a cross-section. The dynamic curves are more gentle and smoother than the static curves and are in the same range as the static values. The structure is vibrating at a small amplitude with the cracks and damages unloaded, while the static values are obtained with the structure stressed under load at a large amplitude of deformation. This loaded condition gives rise to the gradual reduction of static moment of inertia close to failure. The large difference between the theoretical and dynamic values is again explained by a possible non-uniform distribution of moment of inertia along the beam.

The results of the estimation of steel percentage are shown in Tables 7.3 and 7.4. The actual steel percentage of Beam A, Beam B and Beam C are respectively 1.114%, 1.555% and 1.065%. The steel percentages are calculated based on the gross area of the concrete section. The graphs of I_{nom} versus steel percentage calculated theoretically are plotted in Fig.7.27 for Beams A, B and C. The cracked moment of inertia of the beams obtained by matching the measured fundamental modal frequency are shown under the column of I_{est}.

A set of Structural Damage (SD) Factors α is calculated for each of the cracked moments of inertia of the beam. This Structural Damage Factor α varies from 0.664 in the bridge deck after first cracking to 0.552 in the failed bridge Beam A. The magnitude of Factor α indicates the degree of cracking in the different states of damage of the beams. The Load Carrying Capacity (LCC) Factor β is also calculated, and it varies from 1.467 in the bridge deck after first cracking to 1.213 in the failed bridge Beam A. The magnitude of β indicates the appropriateness of assuming I_{nom} for the beams in the FEM. The larger β is the less appropriate the assumption. However, the small range of β indicates that it might have a potential use as an invariant factor in the different cracked states of the structure.

Reference factor β_{LS} is taken to be 1.31 for illustration of the method, and the I_{est} is modified by dividing with β_{LS} to get an estimate of I_{nom}. Estimates of the percentage of reinforcement based on these estimated I_{nom} are obtained from Fig.7.27, and they are shown in the next column of the tables. Inspection of the percentage error in the estimate of reinforcement in the beam shows that the individual beams and the bridge deck exhibit a variation of between -6.29% to +15.73% with the larger value for the bridge deck after first cracking and the smaller value for Beam A close to failure. This suggests that the error in the estimate is little affected by the width of the deck and the steel percentage in the structure.

7.2.7.1 Discussion

1. The results shown here are for beams with a constant percentage of reinforcement throughout their length.

2. The SD Factor α varies from 0.664 to 0.565 over the whole working range of the individual beams and beams in the model bridge deck. If Beam A is taken as

example, here is a 5% reduction in the SD Factor α at first cracking of the beam under load. Then it remains at a relatively stable value until the beam fails in tension with a another drop of 2.3% in the factor.

3. The LCC Factor β varies from 1.467 to 1.243 over the whole working range of the individual beams and beams in the bridge deck. The range of Factor β is narrow and it is therefore possible to assume a Reference Factor β_{LS} within the working range such that the percentage error in the estimate of the reinforcement in all the cracked states are minimized.

7.2.8 Potential Sources of Errors

The Structural Damage Factor α and the Load Carrying Capacity Factor β are calculated by matching the measured first modal frequency of the structure from a FEM. Its accuracy depends on that of the measured modal frequency and that of the finite element model. Effects of different boundary restraints on the bridge structure have been studied in Chapter Five and the more important ones are listed below. The errors due to finite element modelling are minimized by reasonable formulation of the model and allocation of nodal restraints, while the material properties can be obtained from design documents or from field measurement.

7.2.8.1 The Effect of Compression Reinforcement on the Cracked Moment of Inertia of the Beam

In the precast flange of each model bridge beam, there are five 5 mm diameter reinforcement. When they are included in the estimation of the cracked moment of inertia I_{nom}, their effect is shown in Fig.7.28 for Beam A. This effect is small for all the practical steel arrangements.

7.2.8.2 The Effect of the Rubber Bearing Pad Underneath Each Beam on The First Modal Frequency

The model bridge deck is modelled again as a grillage of beams on spring supports using software DDJ-W. The stiffnesses of the springs are the same as that usually found in practice which is 840.0E+3 kN/m in the vertical direction. The moment of inertia I_{est} of the beams is estimated and the difference from that obtained using the rigid support assumption is calculated and shown in Table 7.5. The difference is very small and the effect of support flexibility can be neglected.

7.2.8.3 Effect of Modulus of Elasticity on the First Modal Frequency

As elastic flexural stiffness is defined as the product of elastic modulus and the moment of inertia, a reduction in the value of elastic modulus used in the FEM would give a proportional increase in the estimate of I_{est}. Therefore an accurate assessment of the elastic modulus is essential which can be obtained from the literature, a design document or from site measurements. However the LCC Factor β in Tables 7.3 and 7.4 are all greater than unity. This may possibly be due to the non-uniformity of cracks along the beam and the inappropriateness of the FEM in modelling the behaviour of a cracked reinforced concrete member. If the modulus of elasticity of the structure is multiplied by a factor of 1.35 to take account of these effects, the estimated dynamic moment of inertia would be close to I_{nom} to within +8.7% and -8.0% in all the cracked working states.

7.2.8.4 Effect of Rotational Restraint at Beam Ends on the First Modal Frequency

The parametric study in Chapter Five shows that for the usual rubber and steel bearings used in practice, the restraint is very small and has little influence on the

first modal frequency.

7.2.8.5 The Effect of Local Damage in the Diaphragm on the First Modal Frequency

In order to examine this effect, the bridge deck was modelled as a grillage of beams but with the stiffness in one element of the diaphragms reduced. Three cases were studied. The first case was with the stiffness of the diaphragm at quarter span between Beams #1 and #2 reduced by 25 %. The second case was with the stiffness of the diaphragm at midspan between Beams #1 and #2 reduced by 75 %. The third case was with the global stiffness of the diaphragm at midspan reduced by 25 %. There was no change in the first modal frequency in all three cases.

It can be concluded that local damage or global damage in one or more diaphragms does not affect the first modal frequency of the bridge deck.

7.2.8.6 The Effect of Different Stiffnesses in the Main Beams on the First Modal Frequency

The bridge deck was analysed with the flexural stiffness in Beam #2 reduced by 20% and that in Beam #4 increased by 20%. There was no change in the first modal frequency of the structure.

7.2.9 Conclusions

1. The Load Carrying Capacity Factor β is independent of the percentage of reinforcement in the main beams and width of the bridge deck. A study in Section 5.3.6 on the effect of width/span ratio of the bridge deck on the first modal frequency supports this conclusion.

2. A Reference Factor β_{LS} can be chosen for the different cracked states of the structure with a minimum

least-square error in the estimate of steel percentage of the beam.

3. The Load Carrying Capacity Factor β which varies within a very narrow range throughout the working range of the beams and bridge deck, can be used to assess the percentage of reinforcement in the main beam of the structure.

4. The Structural Damage Factor α varies from a higher value for the uncracked state to a lower value for a more cracked state. It can be used as an indicator of the cracked condition of the beam. It has a maximum value of unity and minimum value defined by I_{nom} / I_{max}.

5. A correction factor of 1.35 on the modulus of elasticity is suggested to account for the errors due to an assumed uniform distribution of the cracked moment of inertia along the member and errors of the linear FEM in modelling a cracked reinforced concrete structure. The resulting estimated dynamic moment of inertia of the main beam would be within +8.7% and -8.0% of its I_{nom} in all the cracked working states of the structure.

The proposed strategy provides a method of estimating the steel percentage and hence the load carrying capacity of a bridge deck from the first modal frequency. A Reference Factor β_{LS} of 1.31 has been adopted to modify the measured moment of inertia I_{est} to an estimate of the nominal cracked moment of inertia I_{nom} of the beam section. The percentage error in the estimation of steel percentage in the beams is relatively small (+15.73%). Further evaluation of the method using measured data from prototype bridge structures is presented in Chapter Nine.

Table 7.1 Reduction in Stiffness in Element 1 of Cantilever Beam

Damage Parameter	H	|H|	θ
Percentage Reduction in Stiffness	1.06	0.71	1.09
Relative Error (%)	19.1%	45.8%	16.9%

Table 7.2 Damage Identification Results of Central Diaphragm of Model Bridge Deck

	Percentage Reduction After Loaded up to							
	70 kN		98 kN		115 kN		140 kN	
	H_{rs}	$\|H_{rs}\|$	H_{rs}	$\|H_{rs}\|$	H_{rs}	$\|H_{rs}\|$	H_{rs}	$\|H_{rs}\|$
Element 1	11.4	13.2	10.4	13.0	*	22.8	*	*
Element 2	13.2	17.3	13.7	18.1	22.2	28.2	22.4	30.0
Element 3	11.4	12.5	10.4	12.0	*	21.0	*	*
Element 4	10.3	11.2	9.3	10.8	14.4	18.0	14.1	18.4

Note: Results not converged.

Table 7.3 Estimate of Percentage of Reinforcement in Beams A and B from the First Modal Frequency

After Loaded up to (kN)	Beam A I_{est} (10^{-6} m^4)	Beam B I_{est} (10^{-6} m^4)	$\alpha=\frac{I_{est}}{I_{max}}$	$\beta=\frac{I_{est}}{I_{nom}}$	Steel Percentage Estimate (%)	Percen. Error in Estimate (%)
0	99.876		0.633	1.392	1.200	+ 7.79
		80.606	0.712	1.491	1.697	+ 9.15
10	94.779		0.601	1.321	1.126	+ 1.10
14		73.129	0.645	1.350	1.503	- 3.31
15	94.090		0.597	1.311	1.116	+ 0.20
18		73.730	0.650	1.362	1.518	- 2.35
20	91.200		0.578	1.271	1.073	- 3.60
23	93.400		0.592	1.302	1.106	- 0.71
		74.242	0.654	1.371	1.531	- 1.53
25		76.629	0.676	1.415	1.590	+ 2.28
26	89.795		0.570	1.251	1.053	- 5.44
28	89.150		0.565	1.243	1.043	- 6.29
29		68.717	0.606	1.268	1.394	-10.33
32	87.053		0.552	1.213	1.013	- 9.04

Note: Actual steel area of Beam A = 1.114%

Actual steel area of Beam B = 1.555%

Table 7.4 Estimate of Percentage of Reinforcement in the Main Beam C of the Model Bridge Deck from the First Modal Frequency

After Loaded up to (kN)	Beam C I_{est} (10^{-6} m^4)	$\alpha = \frac{I_{est}}{I_{max}}$	$\beta = \frac{I_{est}}{I_{nom}}$	Estimated Steel Percentage (%)	Percen. Error in Estimate (%)
0	109.61	0.683	1.509	1.275	+19.76
60	106.58	0.664	1.467	1.232	+15.73
70	101.99	0.636	1.404	1.168	+ 9.72
86	100.48	0.626	1.383	1.147	+ 7.77
98	100.48	0.626	1.383	1.147	+ 7.77
115	100.48	0.626	1.383	1.147	+ 7.77
140	93.46	0.582	1.286	1.051	- 1.29

Note: Actual steel area of Beam C = 1.065%

Table 7.5 Effect of Supporting Rubber Pad on the I_{est} of Beam C in the Bridge Deck

After Loaded Up to (kN)	0	60	70	86	98	115	140
Percentage Increase in I_{est} (%)	0.006	0.003	0.005	0.007	0.003	0.004	0.006

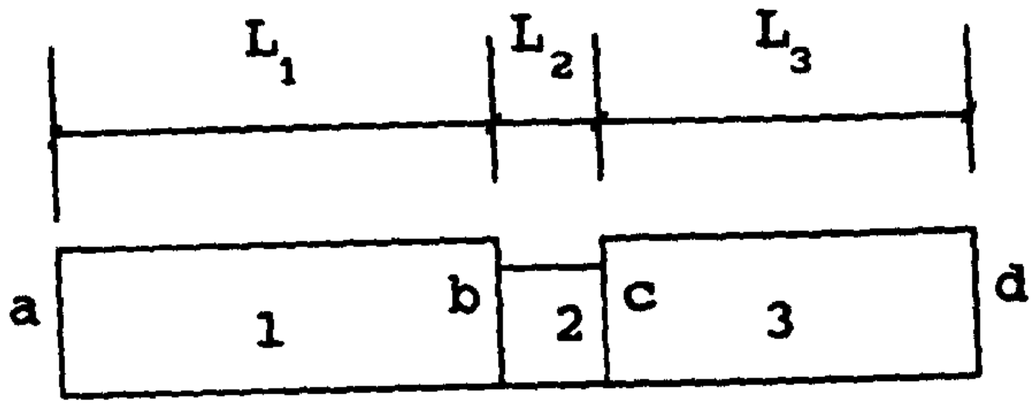

FIG.7.1-Beam Element with a Finite Slot

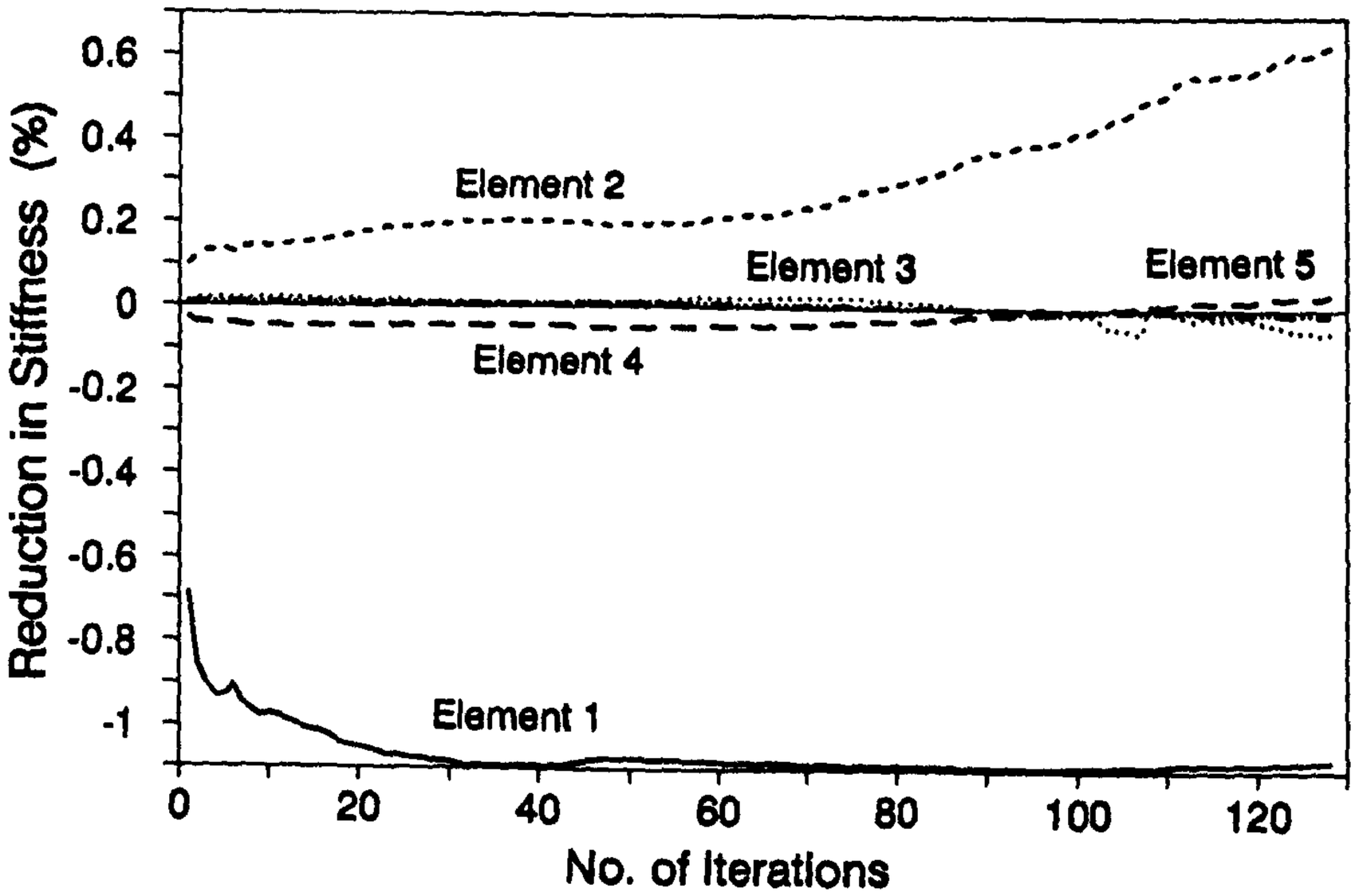

FIG.7.2-Damage Identification from the Phase Angle of the Frequency Response Function

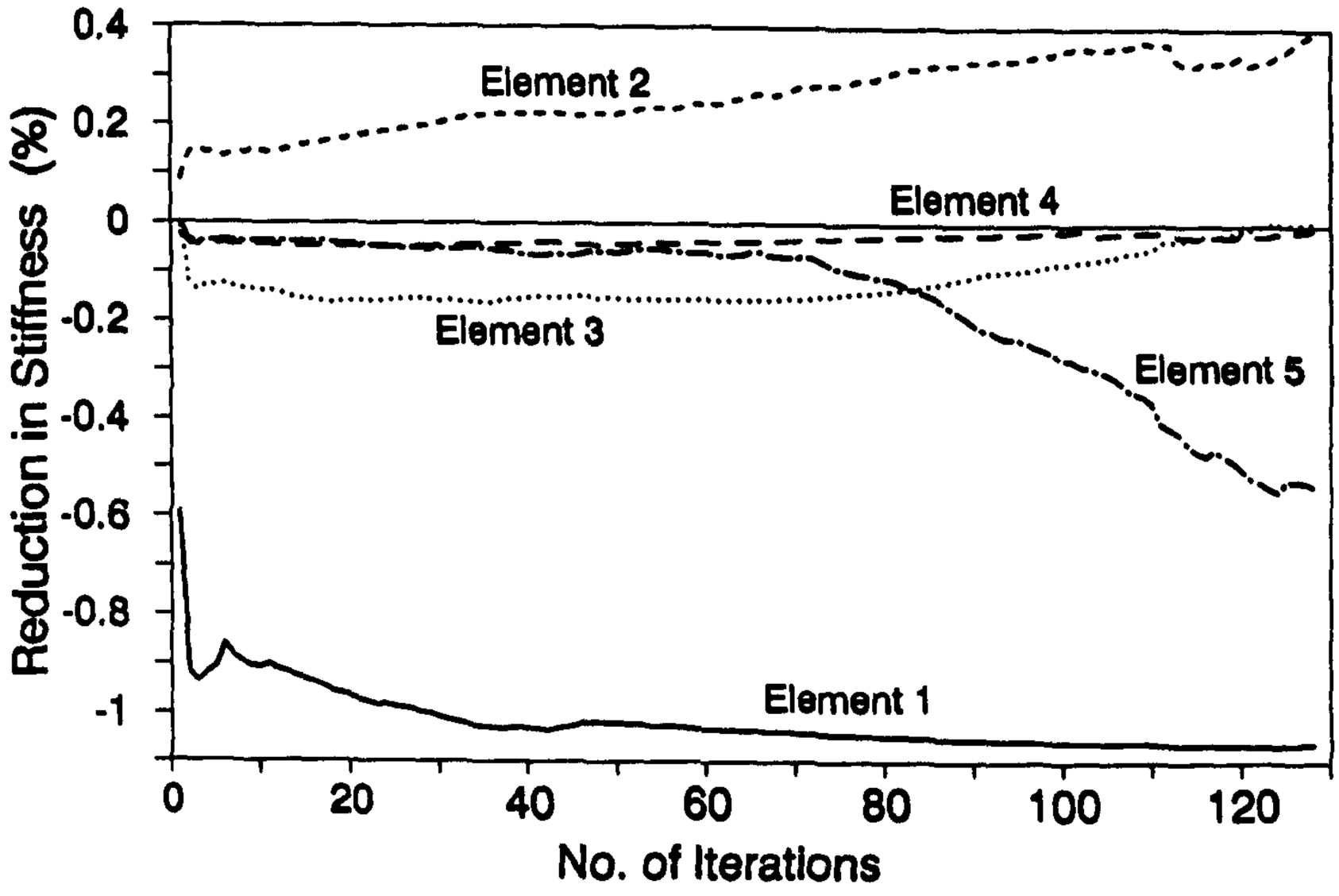

FIG.7.3-Damage Identification from the Frequency Response Function

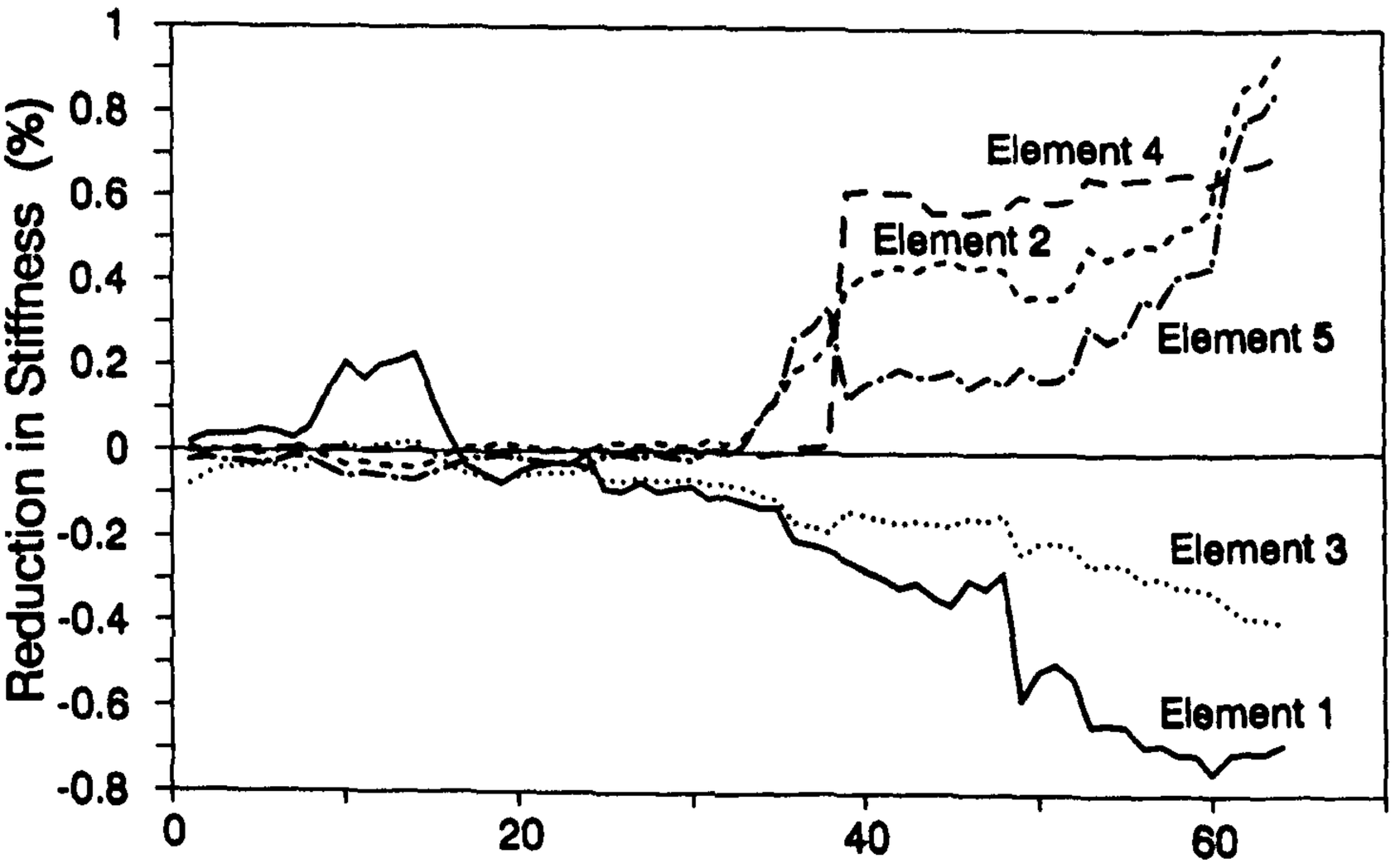

FIG.7.4-Damage Identification from the Modulus of the Frequency Response Function

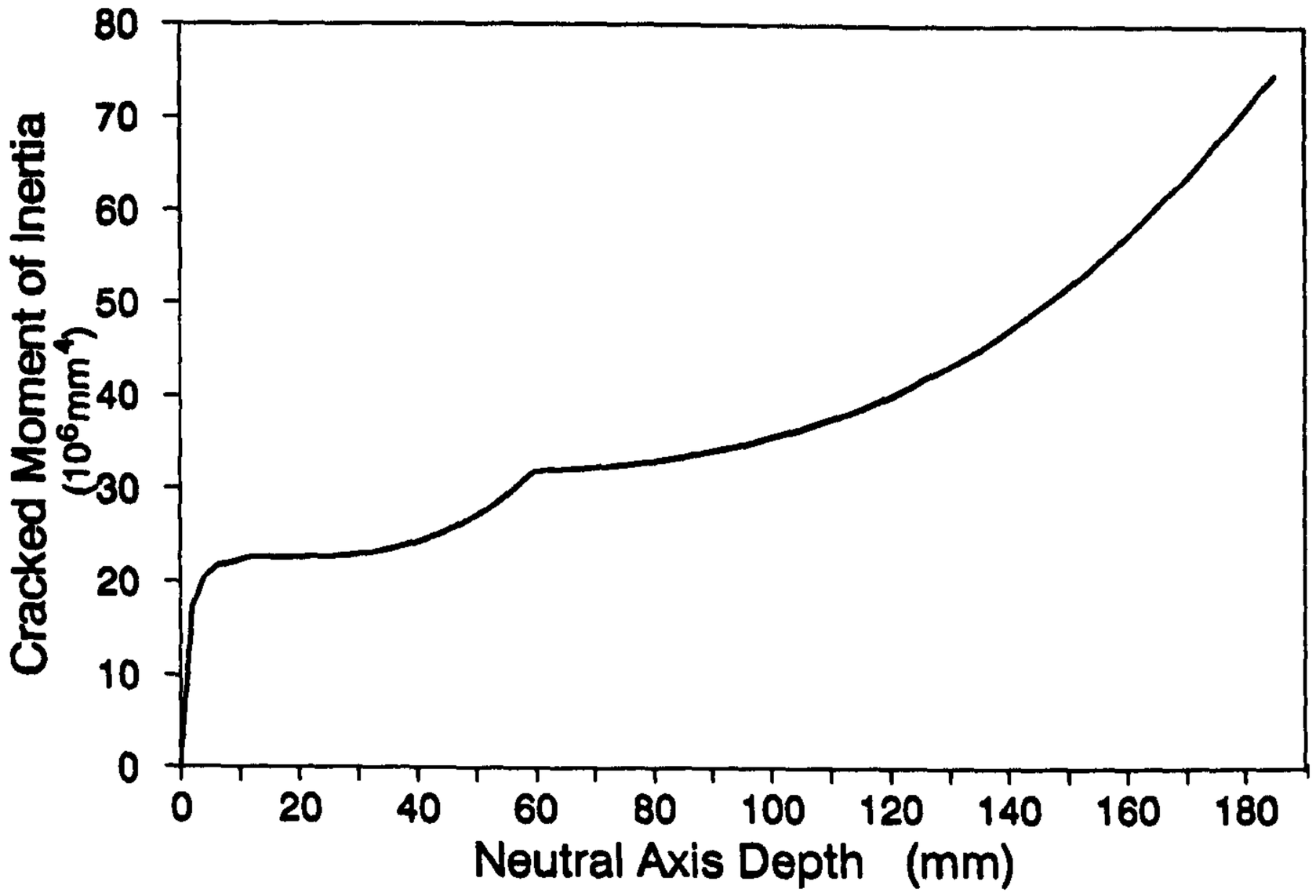

FIG.7.5-Theoretical Cracked Moment of Inertia of Diaphragm

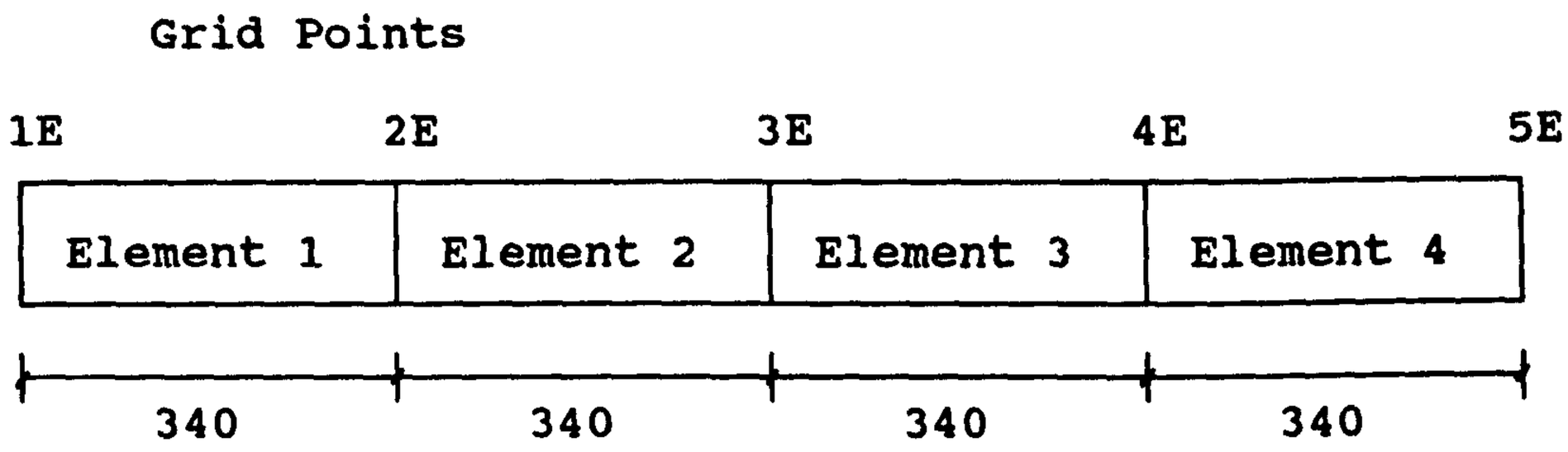

$E = 26.4\ kN/mm^2$

FIG.7.6-Finite Elements in the Central Diaphragm

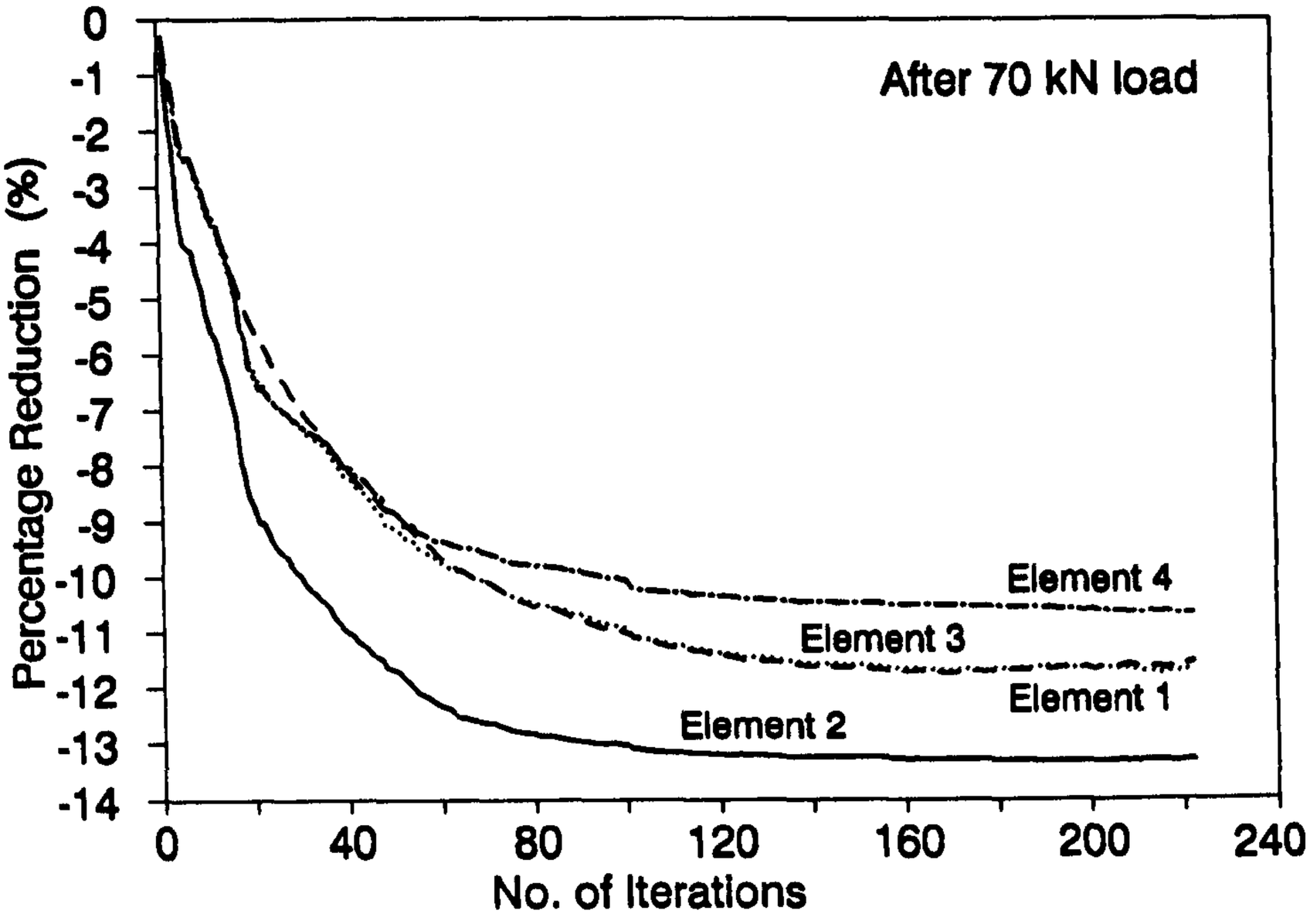

FIG.7.7-Damage Identification Results from FRF After 70 kN load

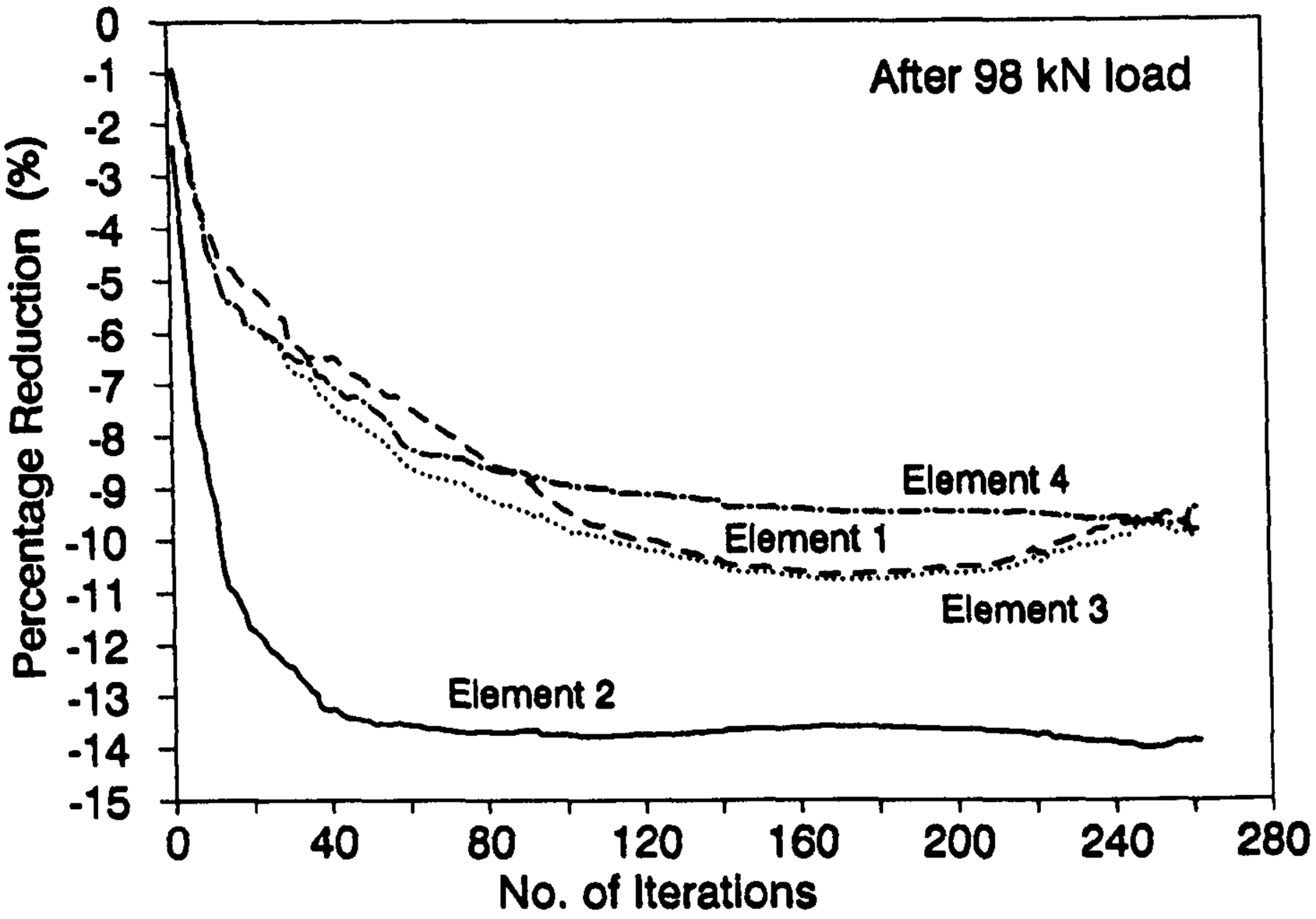

FIG.7.8-Damage Identification Results from FRF After 98 kN load

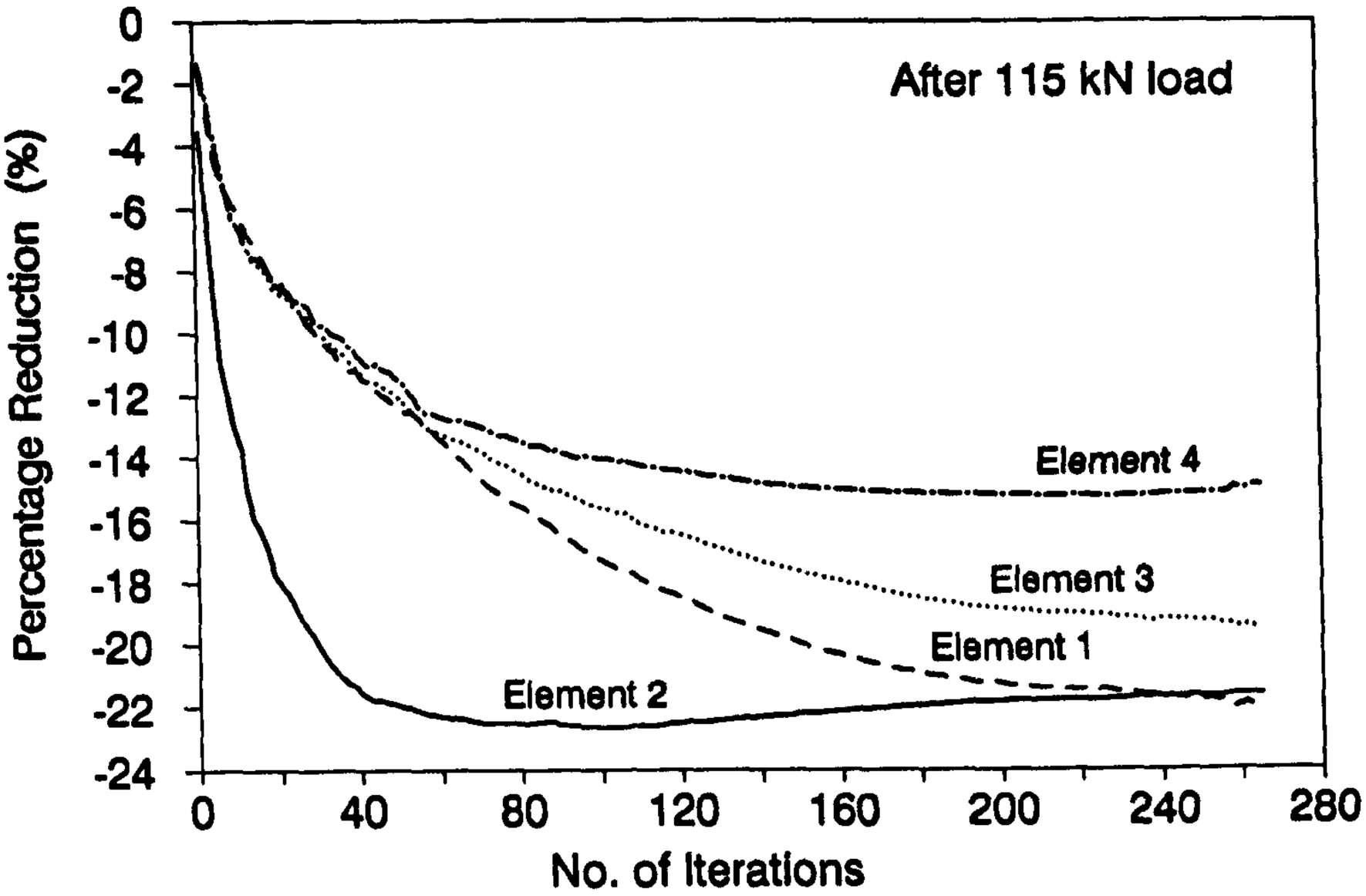

FIG.7.9-Damage Identification Results from FRF After 115 kN load

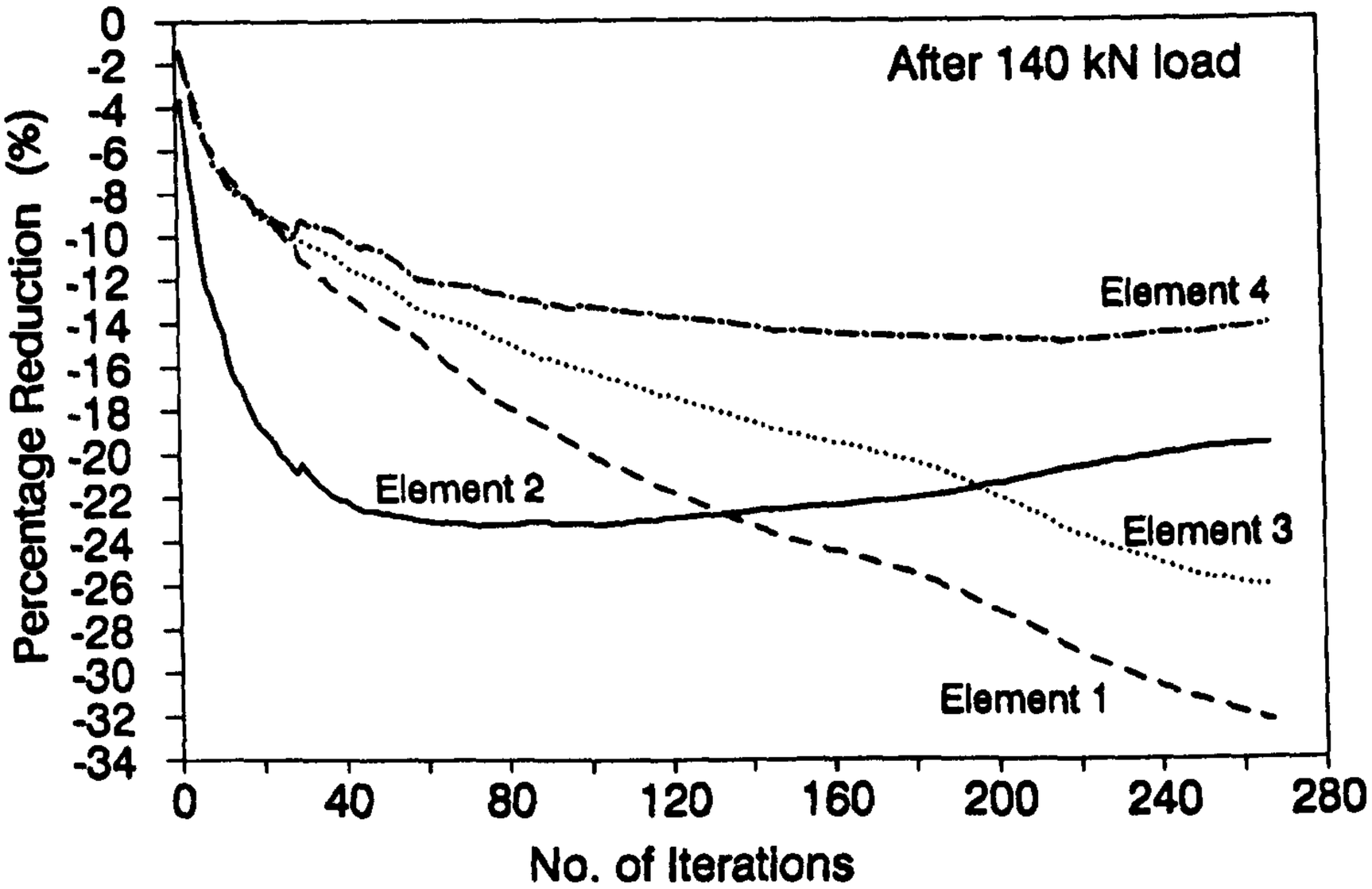

FIG.7.10-Damage Identification Results from FRF After 140 kN load

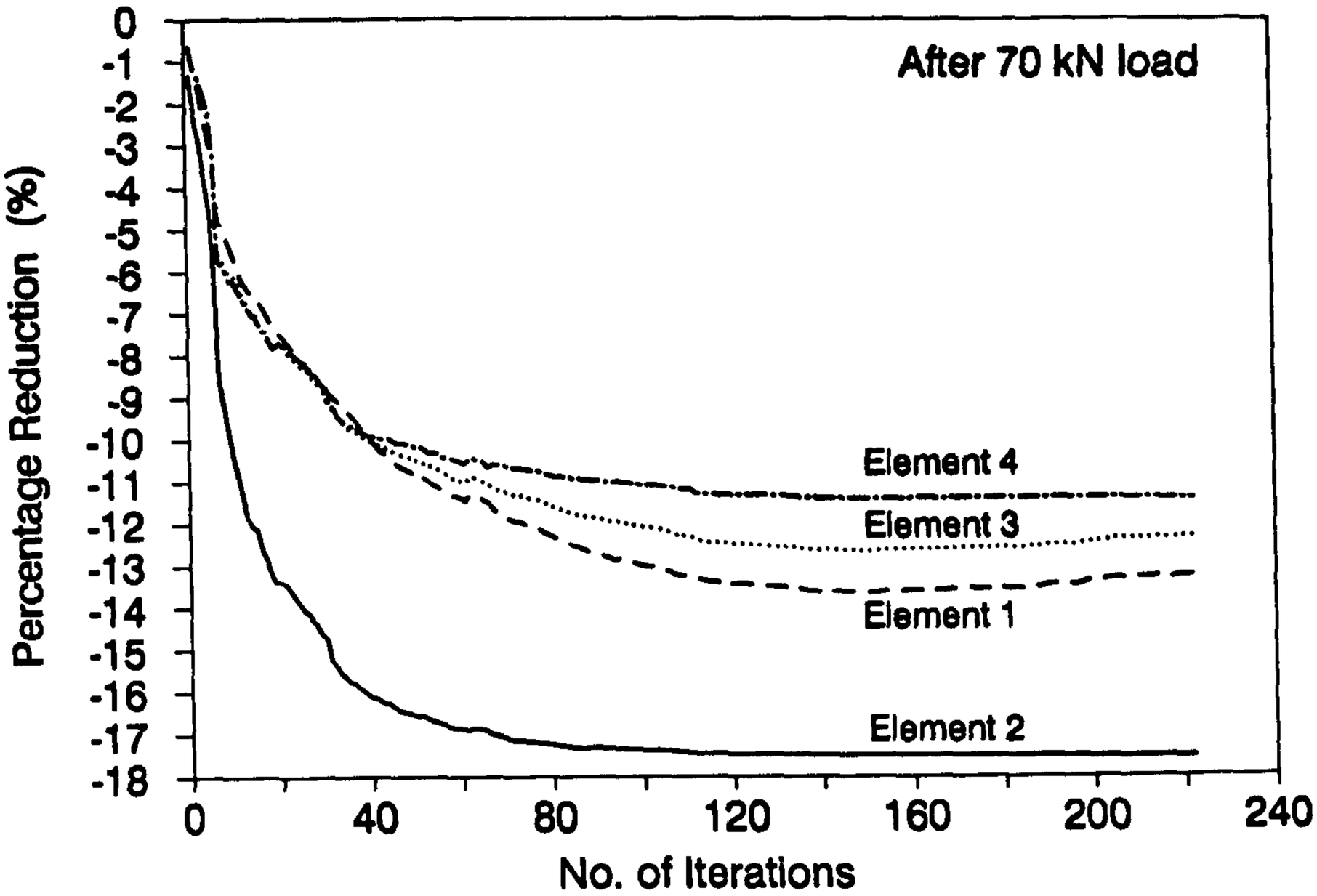

FIG.7.11-Damage Identification Results from the Modulus of FRF After 70 kN load

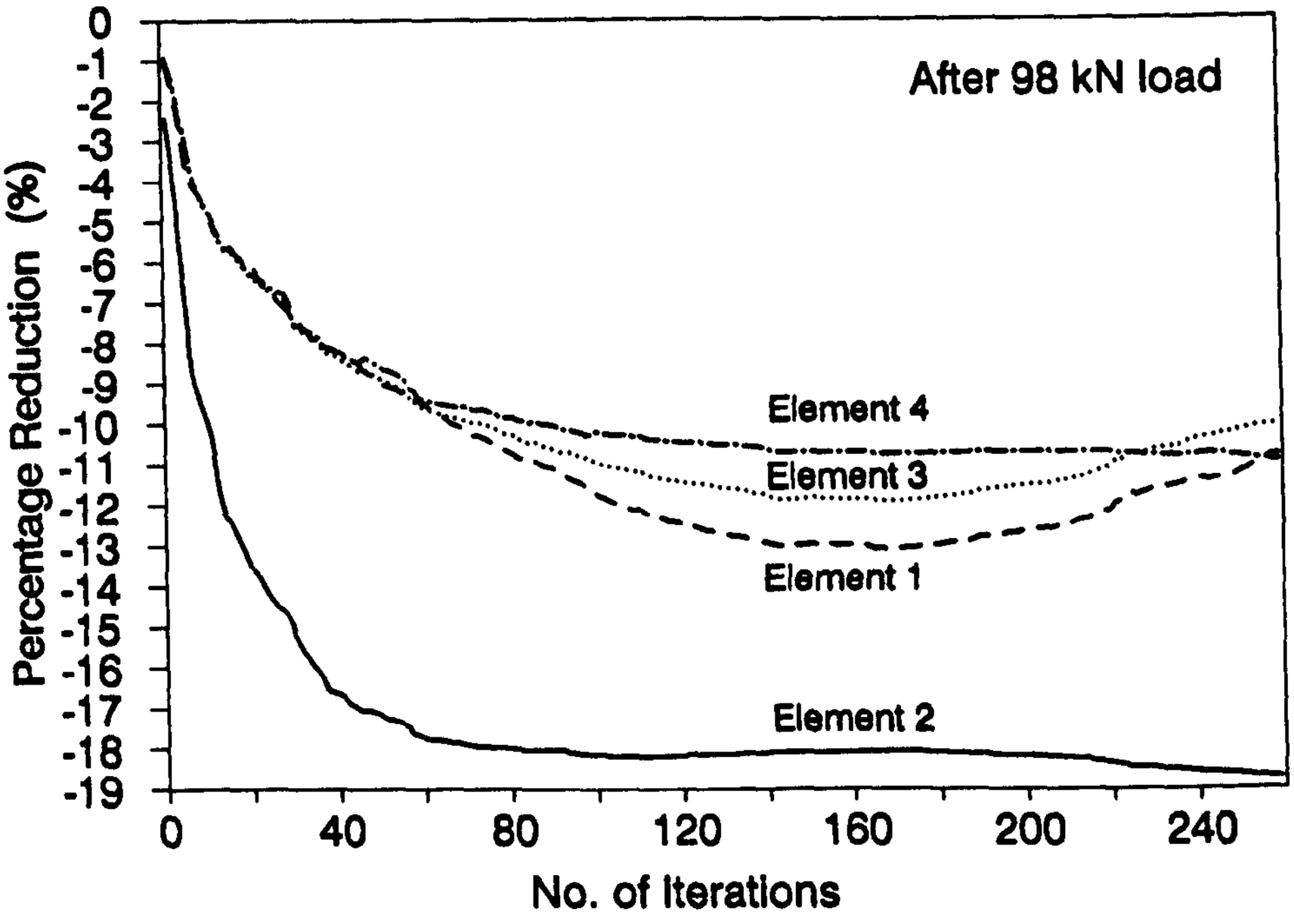

FIG.7.12-Damage Identification Results from the Modulus of FRF After 98 kN load

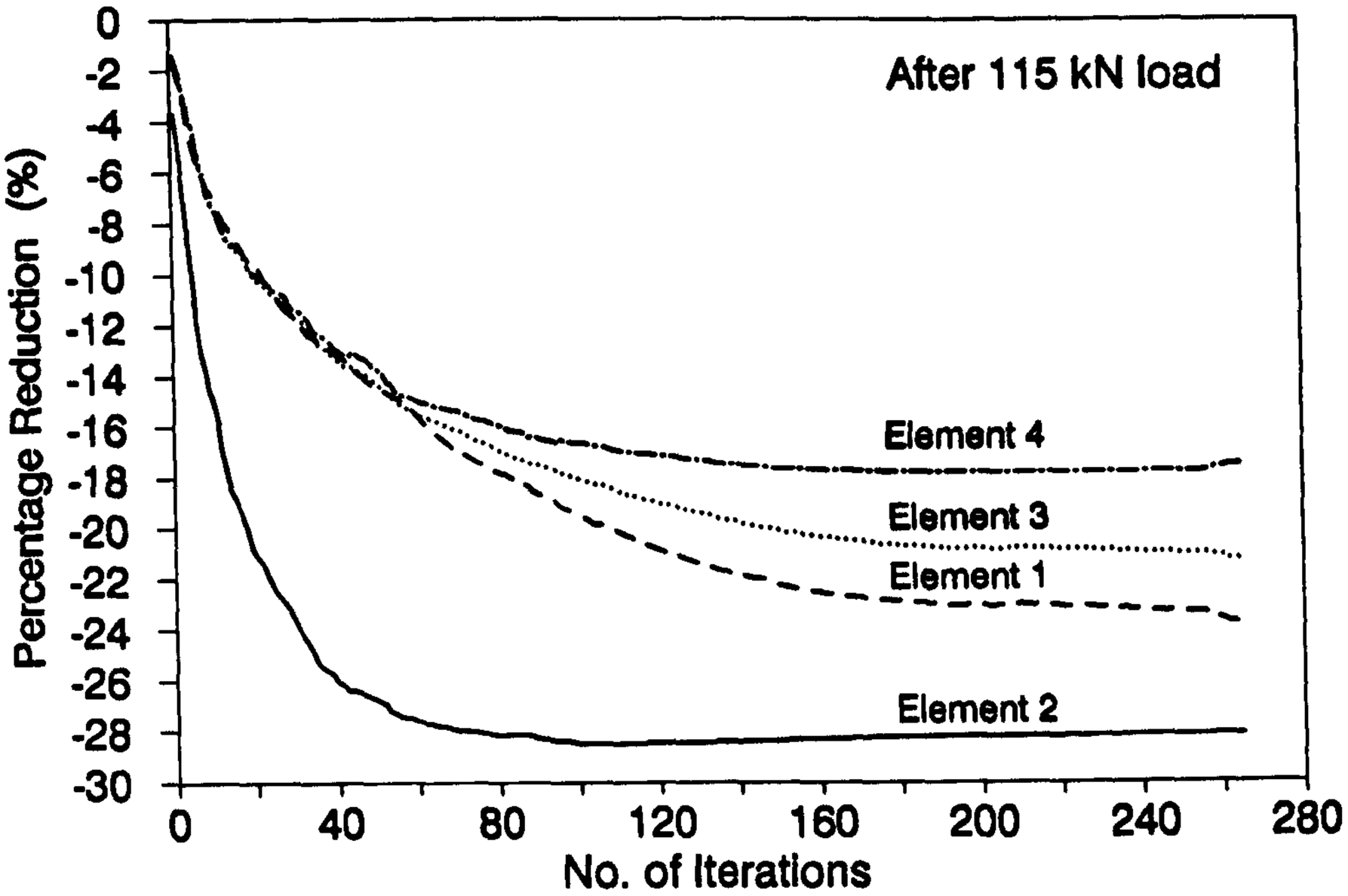

FIG.7.13-Damage Identification Results from the Modulus of FRF After 115 kN load

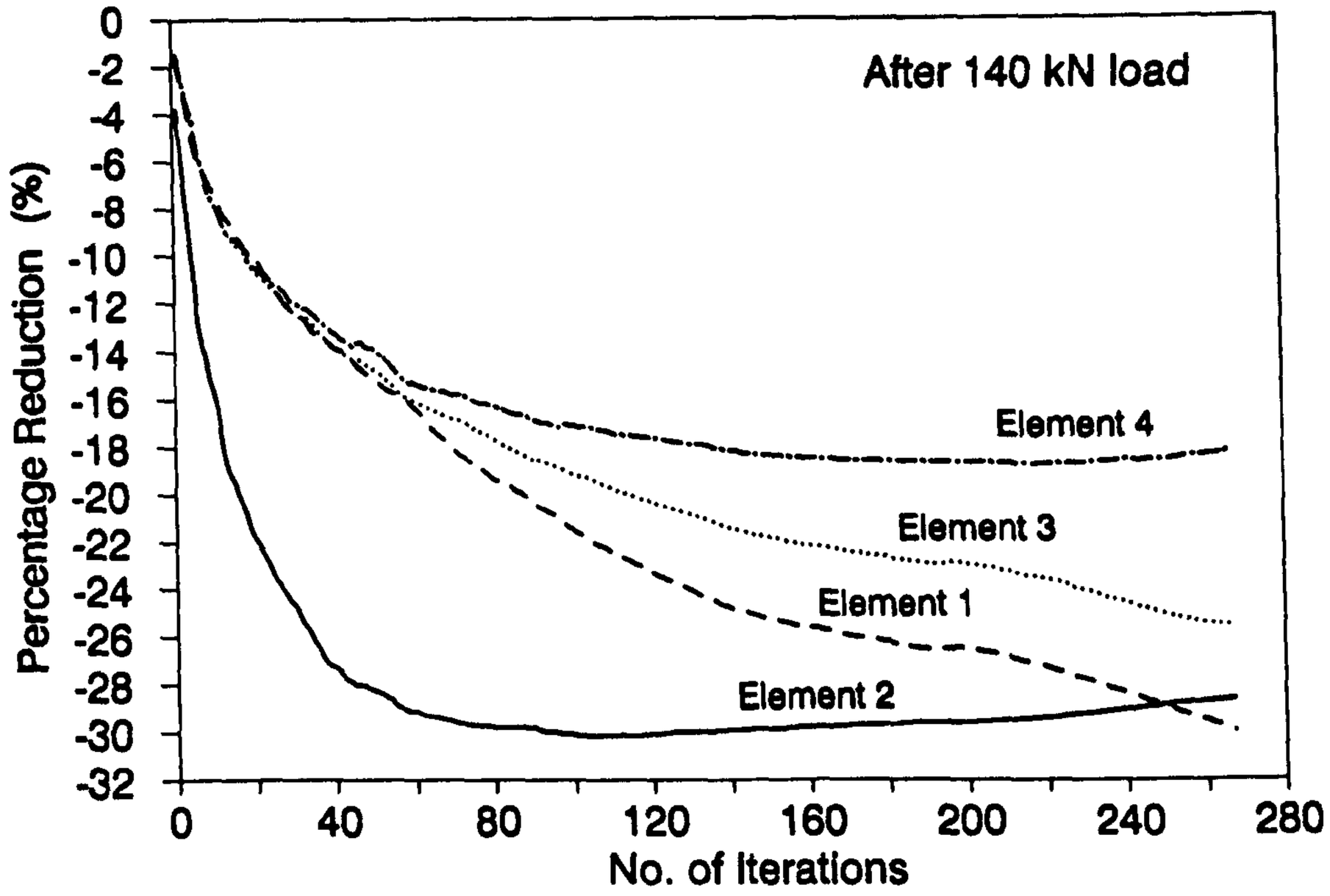

FIG.7.14-Damage Identification Results from the Modulus of FRF After 140 kN load

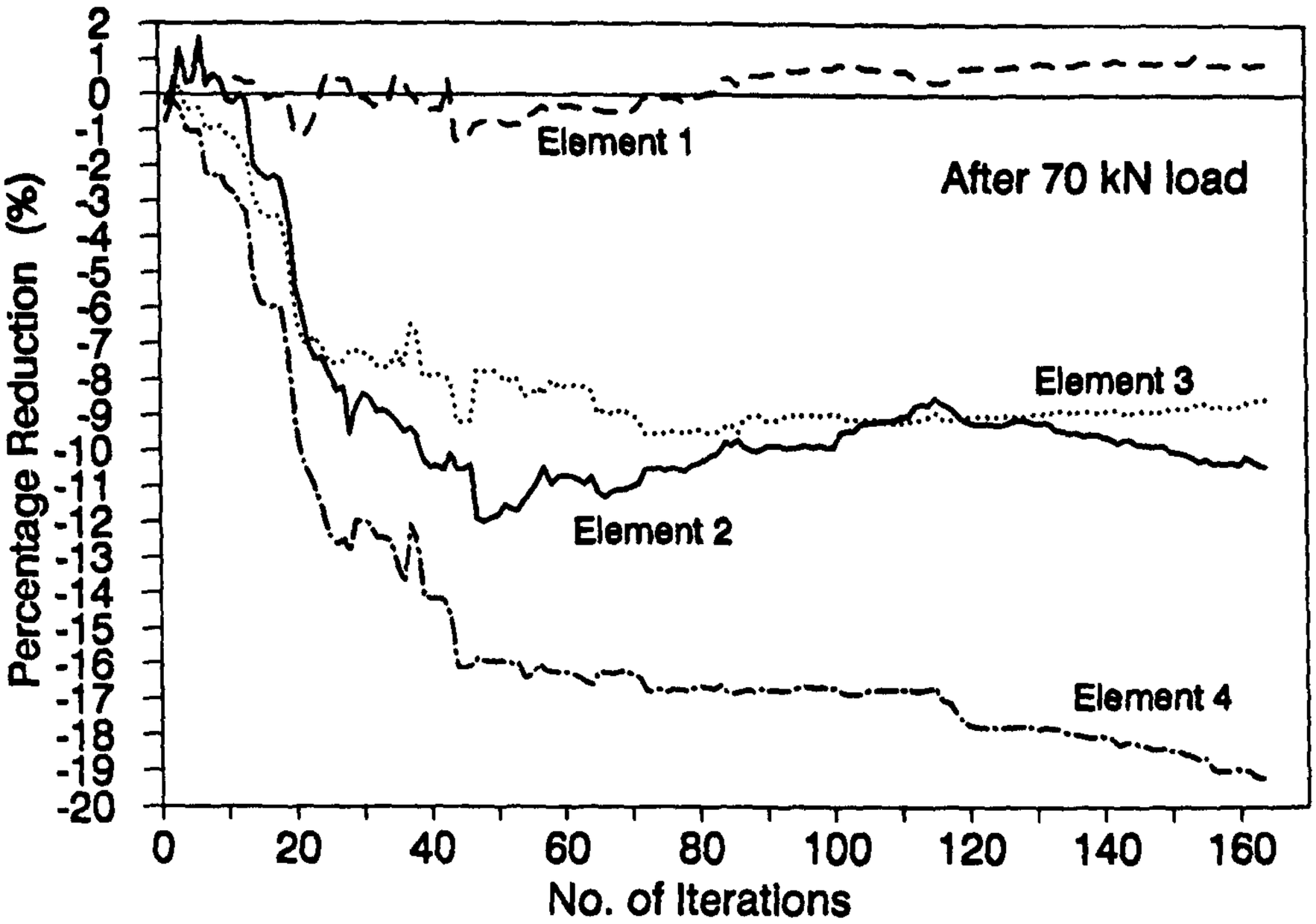

FIG.7.15-Damage Identification Results from the Phase Angle of FRF After 70 kN load

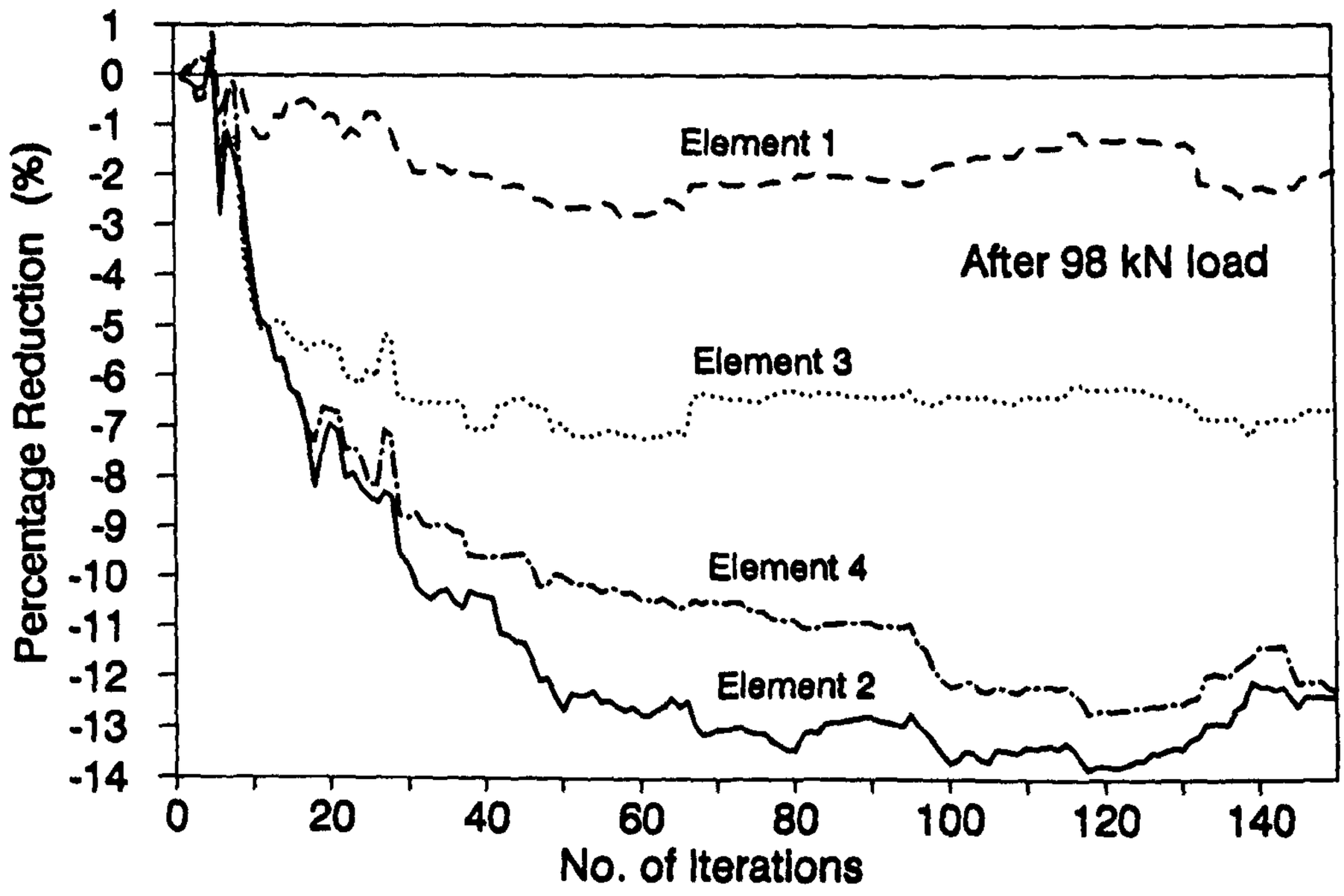

FIG.7.16-Damage Identification Results from the Phase Angle of FRF After 98 kN load

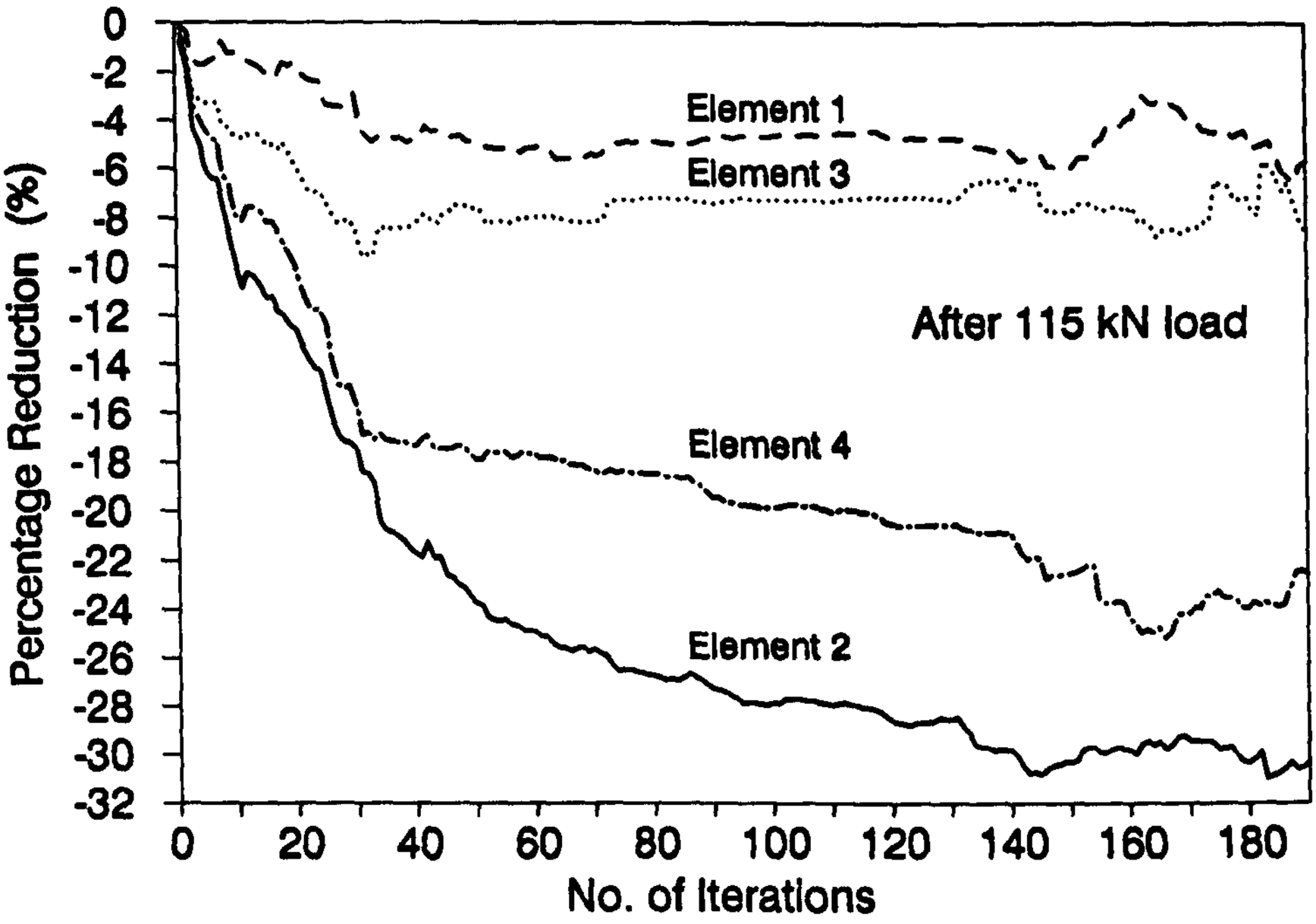

FIG.7.17-Damage Identification Results from the Phase Angle of FRF After 115 kN load

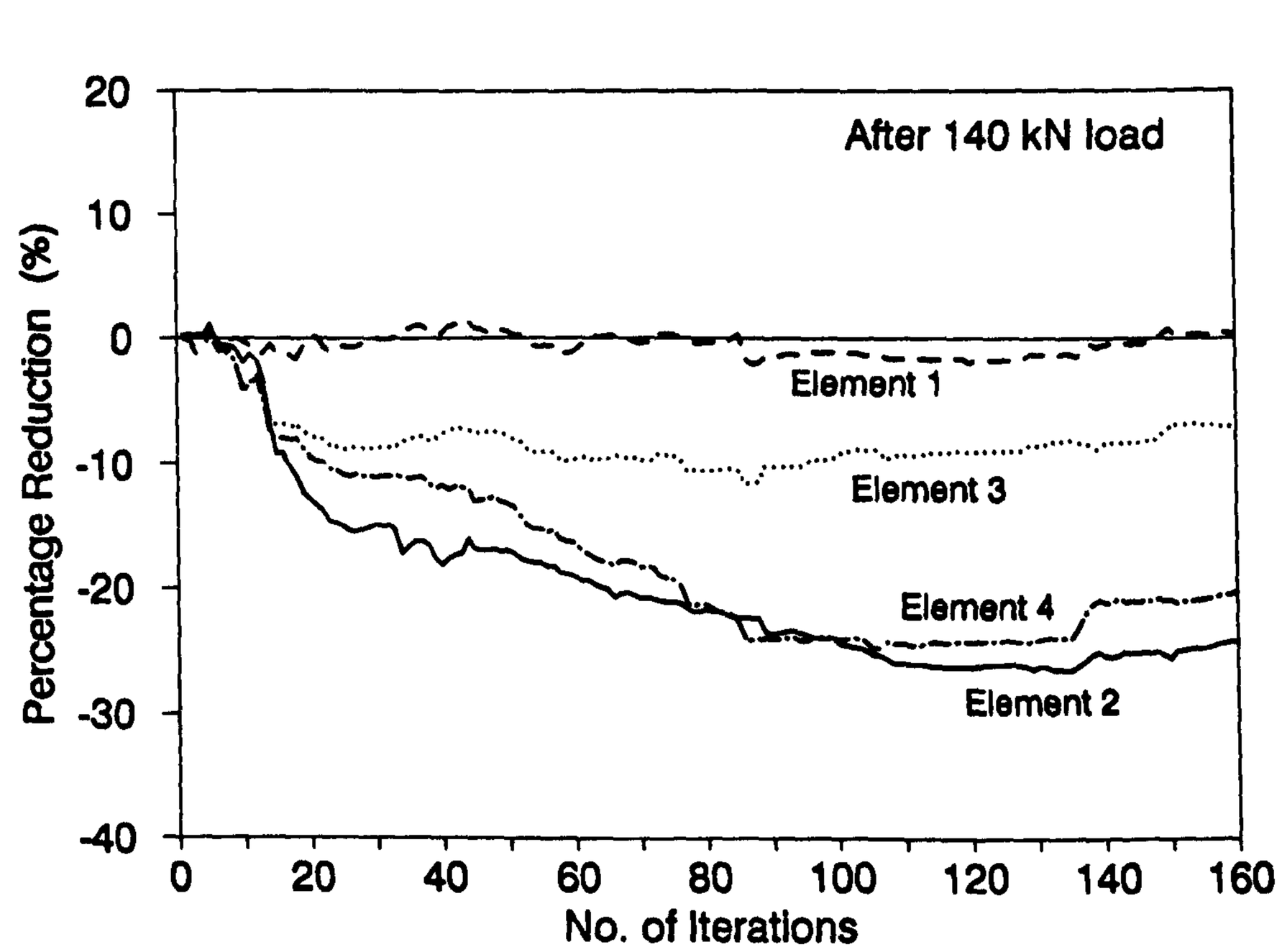

FIG.7.18-Damage Identification Results from the Phase Angle of FRF After 140 kN load

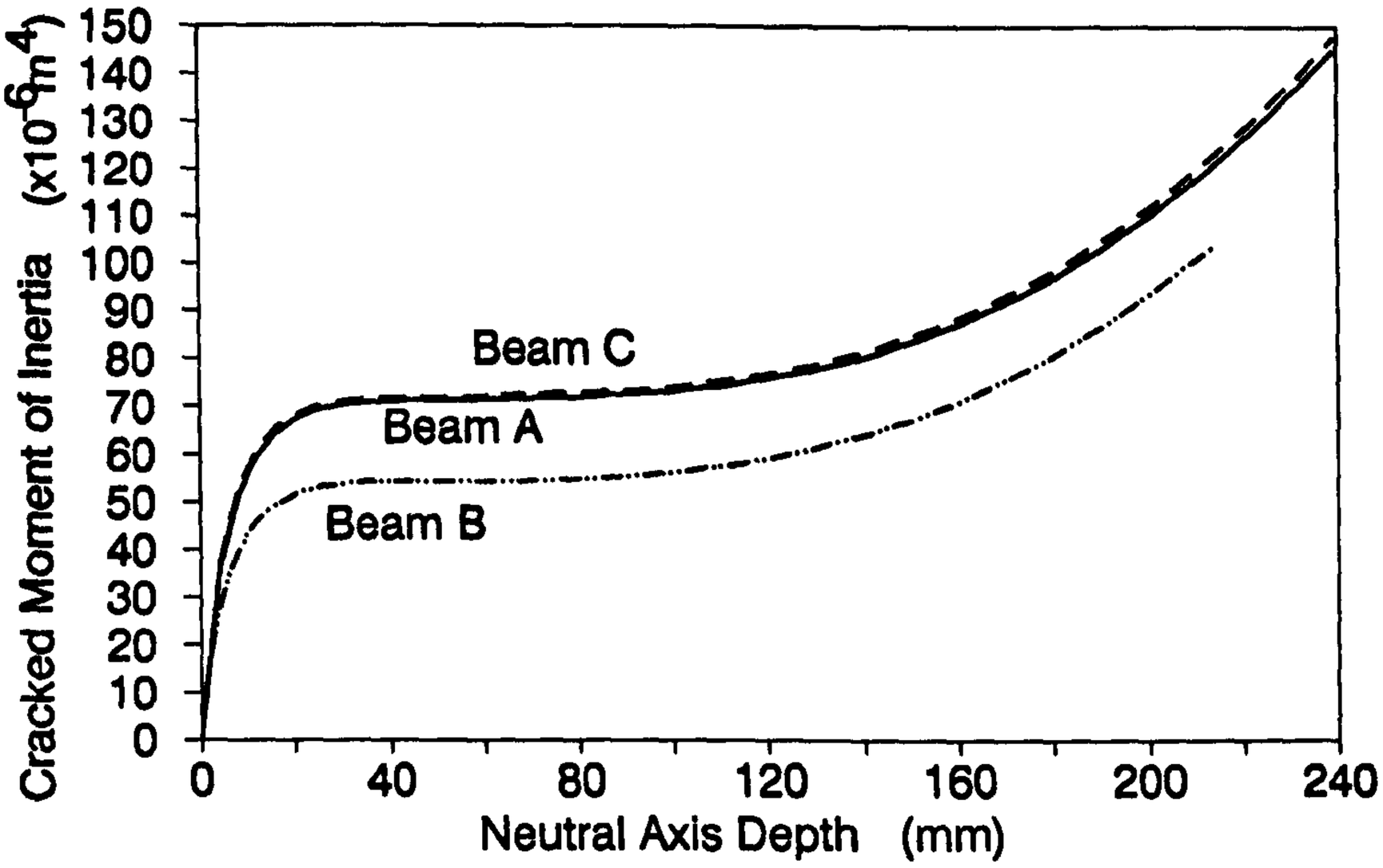

FIG.7.19-Theoretical Cracked Moment of Inertia of Beams A, B and C

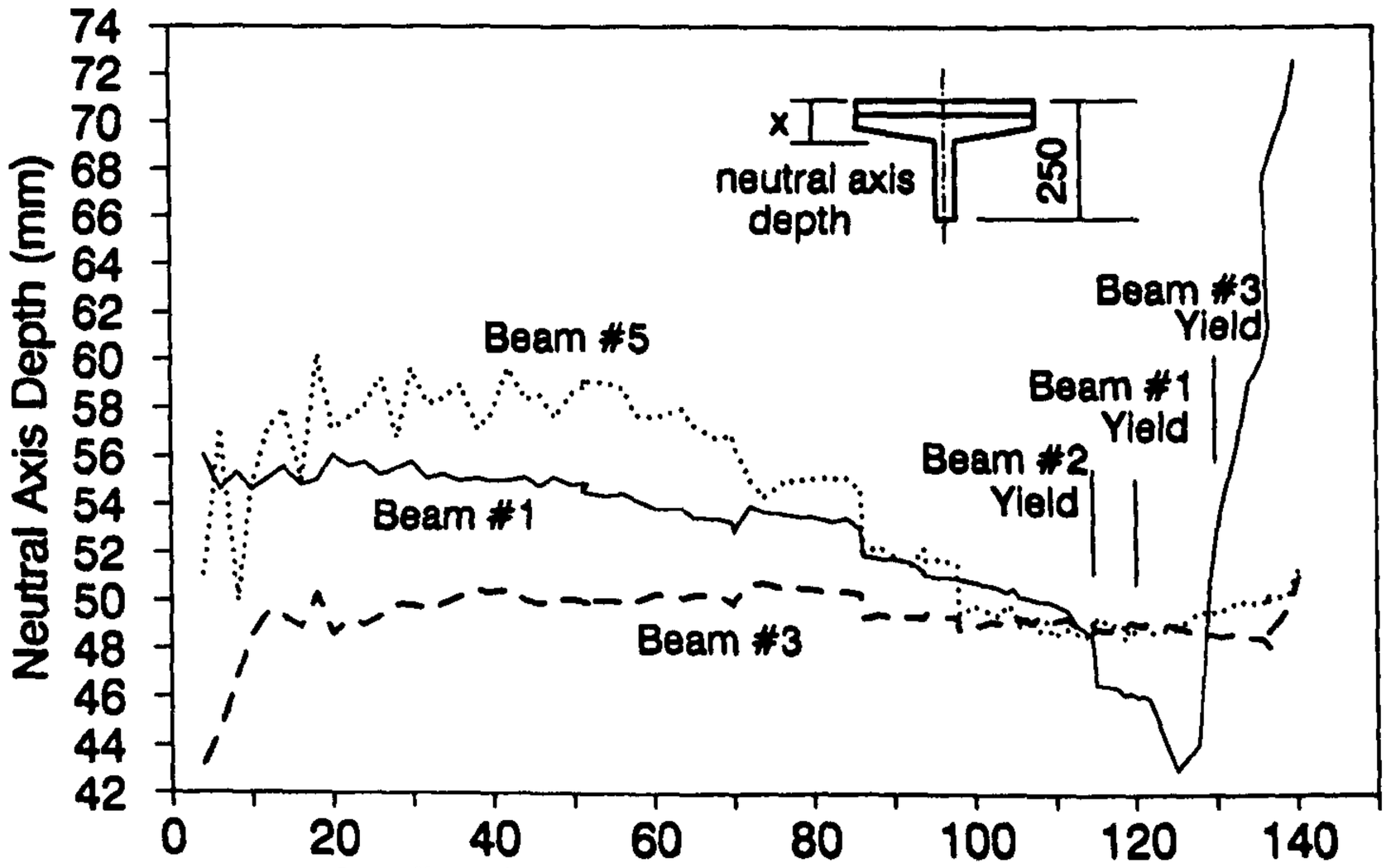

FIG.7.20-Variation of Neutral Axis Depth in Beams of Model Bridge Deck under Static Load

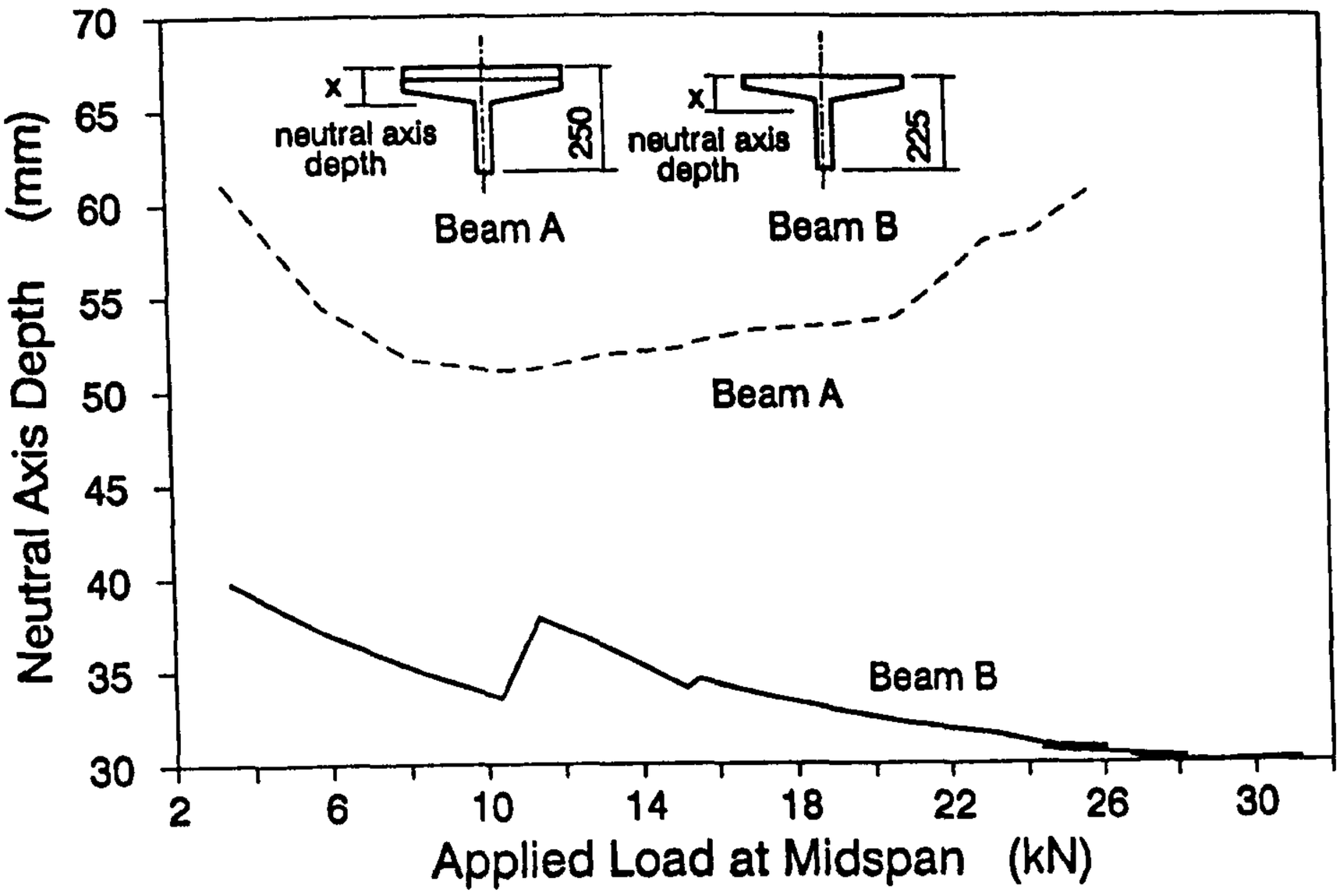

FIG.7.21-Variation of Neutral Axis Depth of Beams A and B under Static Load

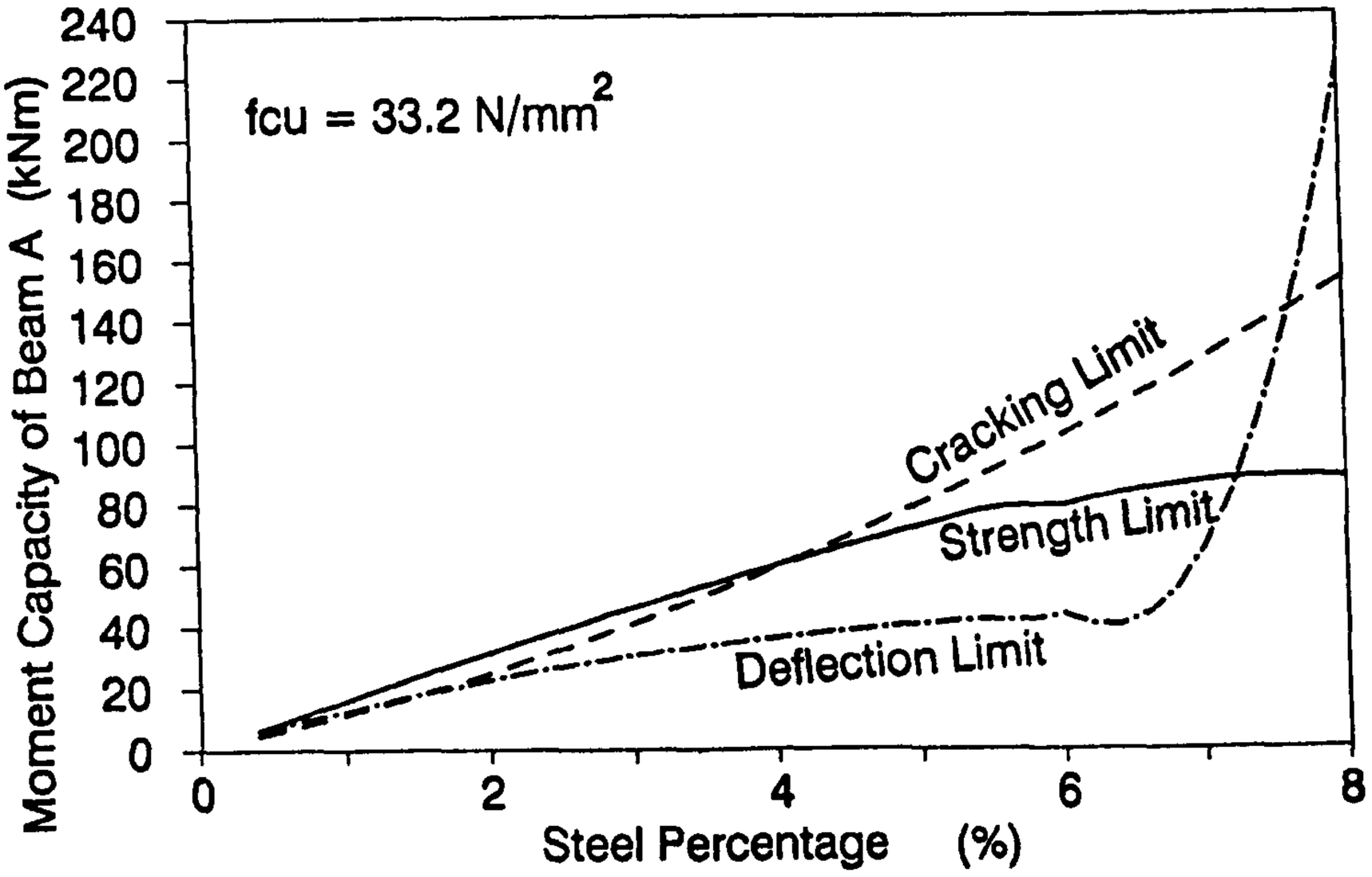

FIG.7.22-Moment Capacity of Beam A According to Different Design Limiting Criteria

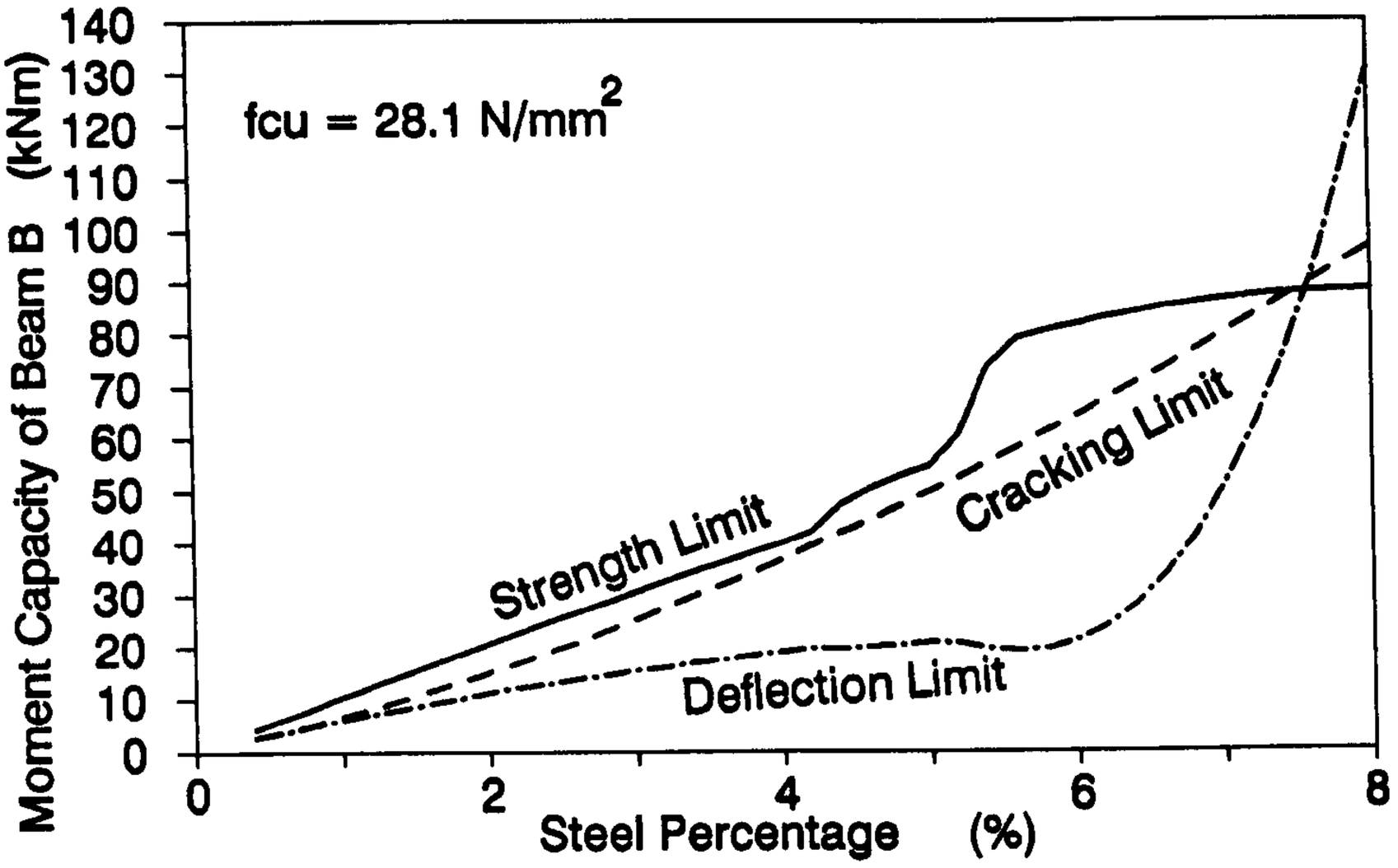

FIG.7.23-Moment Capacity of Beam B According to Different Design Limiting Criteria

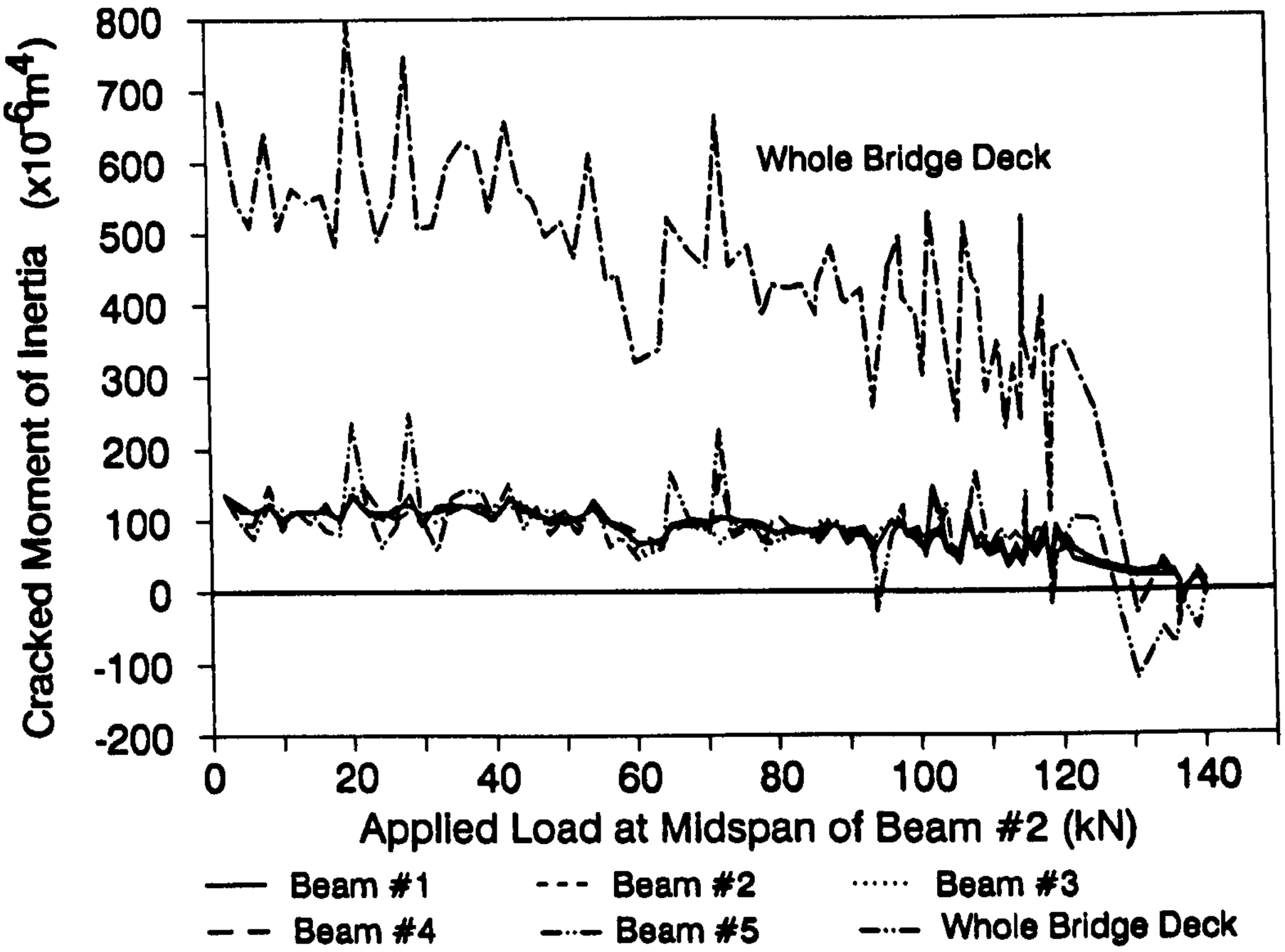

FIG.7.24-Moment of Inertia of Beams in the Model Bridge Deck

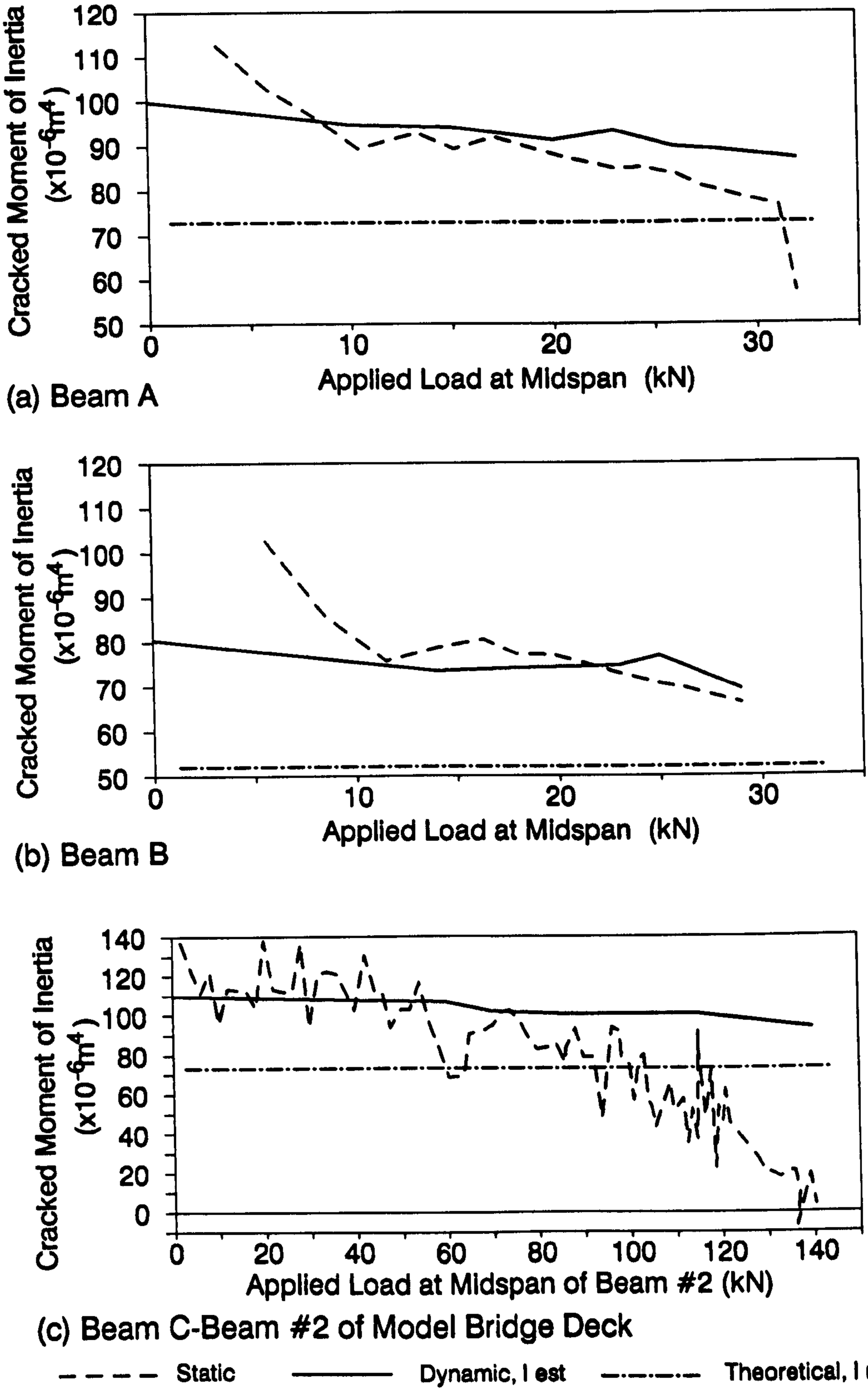

FIG.7.25-Moment of Inertia of Beams A, B and C

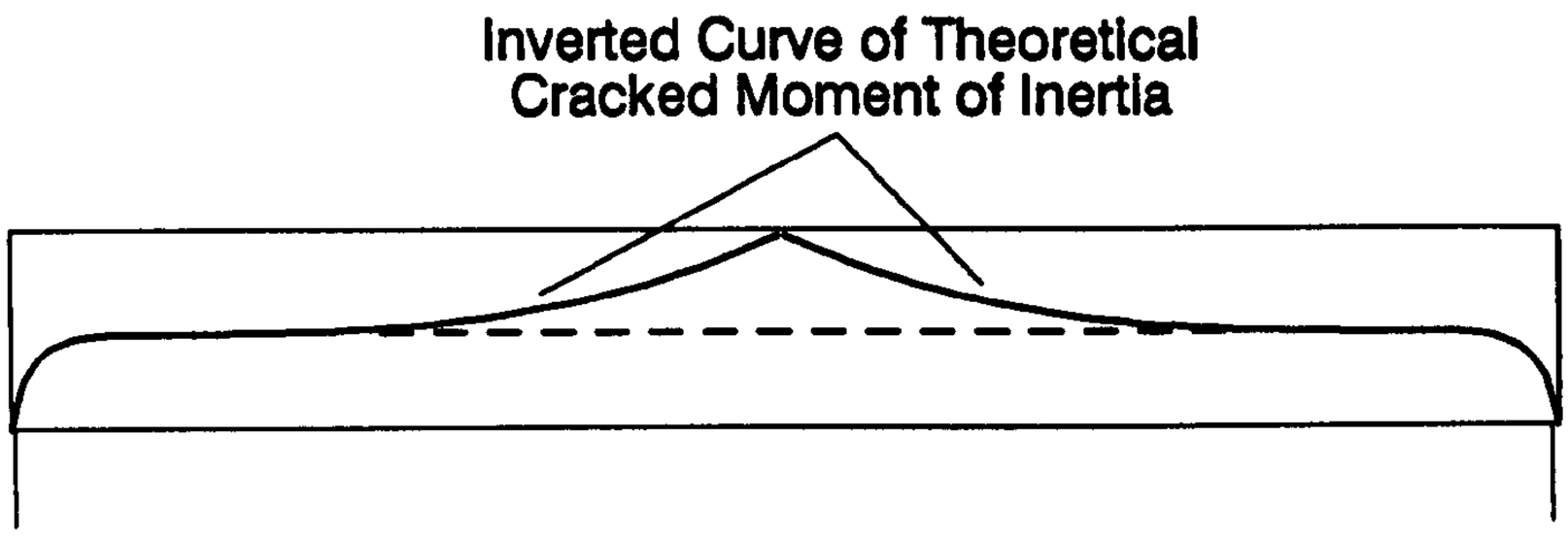

FIG.7.26-Theoretical Distribution of Cracked Moment of Inertia along a Beam

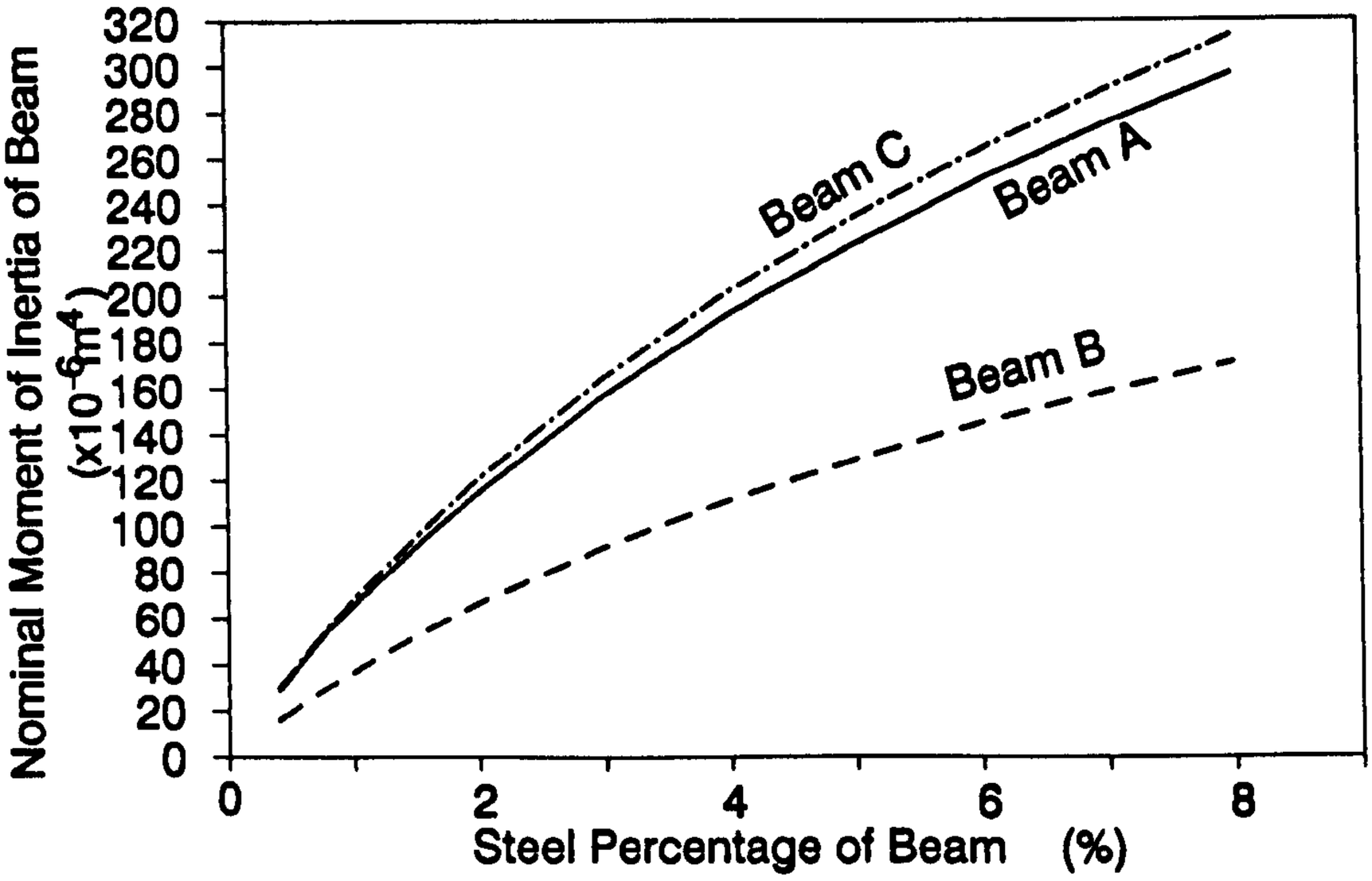

FIG.7.27-Theoretical I_{nom} of Model Bridge Beams

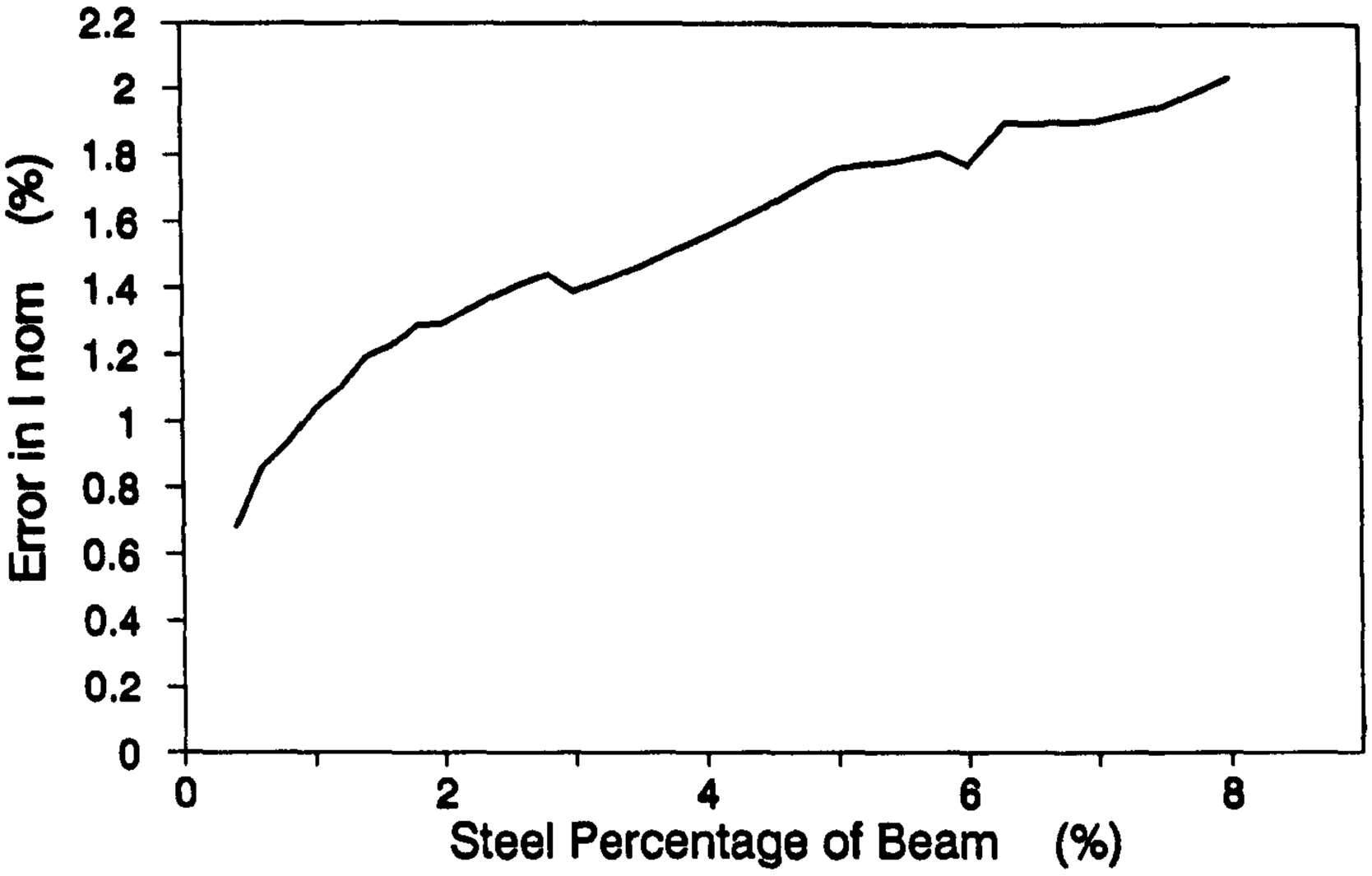

FIG.7.28-Effect of Compression Steel on Cracked Moment of Inertia of Model Beam C

CHAPTER EIGHT

DYNAMIC TESTING
OF PROTOTYPE REINFORCED CONCRETE BRIDGE DECKS

8.1 OBJECTIVE OF THE TESTS

The proposed method has been developed under the controlled environment of the laboratory and there is a need to evaluate the method using full-scale on site measurements. This Chapter gives a description of the dynamic testing of a set of prototype bridge decks, the results of which form a database for the evaluation. A detailed example of dynamic testing is illustrated with a case study of Yuan Dun Bridge where an attempt is made to relate the damage in the bridge deck to the shift of modal frequencies of the structure.

8.2 GENERAL DESCRIPTION OF THE BRIDGES

A total of seventeen full-scale reinforced concrete Tee-beam and slab bridge decks have been measured for their dynamic response to traffic-generated vibration in the People's Republic of China from 1984 to 1987. A detailed study on their dynamic responses has been reported by Law et al (1990c). Most of them are single span simply supported bridge decks whereas five of them are of multi-span construction. Altogether twenty-two measurements were made. This type of bridge deck consists of precast Tee-beams at approximately 1.6 m spacing with a layer of in-situ concrete cast on top and were designed according to Standard JT/GQB011-73 (1973). There are diaphragms equally spaced along the bridge deck which is of the same general type of construction as the one tested in the laboratory.

Principal details of the bridge decks are given in Table

8.1. Details of fencing and kerbs arrangements are those given in Standard JT/GQB011-73 (1973).

8.3 PARTICULARS ABOUT THE BRIDGES

Chi Ling Bridge was tested in 1984. A traffic accident occurred later where part of the fencing on one side together with a small part of the deck slab was torn off. It was again tested in 1985.

In Sha Wan Bridge and Dan Zhu Tou Bridge, the new bridge was built just adjacent and parallel to the old bridge as widening of the existing carriageway. The horizontal joint between the bridge decks was filled with bituminous material.

The first, third and fifth span of Yuan Dun Bridge were tested before and after rehabilitation works.

Yuan Dun Bridge consists of 7 spans. The central three spans are 30 metre long and the two spans at either ends are 22 metre long. It was classified as dangerous in 1986 and required repair. The visual damage was widespread cracking in the ribs of the beams, corrosion of exposed reinforcement on the vertical sides and soffits of the beams, corrosion of the steel bearings which were hinges at one end and guided sliding bearing at the other end, serious cracks in the top slab forming the carriageway and excessive deflection of the bridge deck. The first and third span were static load tested by the Highway Management Office of Guangdong Province of China before the rehabilitation programme, and the strain in the main reinforcement under load was very large compared to the theoretically obtained value. The transverse load distribution was not linear within the range of the test loads as reported in Project Report (1986). The first set of dynamic measurements was made in November 1986 one month after the static load test. The bridge was then

reinforced by attaching additional steel bars to the bottoms of the beams anchored at both ends to original reinforcement by welding. The bars and surfaces of the ribs were later covered with sprayed concrete, Hui and Zhong (1987). Another set of measurements was made after the rehabilitation work in April 1987.

8.4 THE FIELD MEASUREMENT AND DYNAMIC TESTING

8.4.1 The As-Constructed Information

The following items were checked and recorded on site before the dynamic measurement:

1. Dimensions and geometry of the bridge deck.
2. Type and condition of the supporting material.
3. Type and condition of the pier and abutment.
4. Visual damage like deflection in the structural components, cracks and spalls and stains from exposed and corroded reinforcement.
5. Condition of the pedestrian fencing and kerbstones.

However, due to practical limitations, the underside of some of the bridge decks were inaccessible and some of this important information could not be collected. Also, the design drawings and as-constructed drawings of some of the bridges could not be traced.

8.4.2 The Dynamic Testing

The simplest test procedure consisted of applying a controlled sinusoidal force, the single frequency of which could be varied to give the steady-state response at each of a number of test frequencies. In this case there is a maximum amplification of the effect of the force at the natural frequencies of vibration in the structure; this is the resonance condition. The technique has been used by

Leonard (1974) on highway bridges, but it has disadvantages, mainly due to the physical size of the the equipment limiting access to the bridge during testing.

Another well established approach for dynamic testing of structures is based upon the use of ambient excitation. The use of low level ambient excitation in the modal identification of large structures was investigated by Schiff (1972). Mazurek and DeWolf (1990) considered vibration generated by light vehicles as a convenient and suitable means of excitation for bridge structures. Oehler (1957); McLamore et al (1971); Abdel-Ghaffar and Housner (1978); Douglas (1979); Ward (1984) and Ward et al (1987) have made use of ambient excitation in measuring dynamic properties of bridge superstructures with good results.

All the bridges measured were open to traffic and they were excited by passing vehicles of various weights. The accelerometers were placed along the edge of the bridge deck so as not to interfere with the normal traffic operation. The measuring stations were at midspan, quarter-points and at the ends of the deck. The responses at midspan and quarter-points were for the determination of modal frequencies. It was not possible to determine completely the shape of each resonant mode, and the result of computer modelling was used as a supplementary source of information to determine the correct modal frequency. A typical arrangement of the sensors is shown in Fig.8.1.

The acceleration responses of the bridge deck to traffic-generated excitation were recorded onto magnetic tape via a data tape recorder. As most of the bridge decks have their fundamental frequencies above 10 Hz, a record length of 20 minutes was adopted. This record length gave a maximum bias error and random error of 10% in the subsequent spectral analysis as discussed in Chapter Three. In some cases, the record length was extended to cover a lower

fundamental frequency of interest.

The level of response from traffic-generated vibration varies when the vehicle passes over the bridge. Since there were only five to six accelerometers available, it was not possible to record each signal with two accelerometers one at a lower gain and one at a higher gain, to cover the complete range of the signal. Only one accelerometer was used at each station with ±1.0 Volt input limits.

In the second measurement of Yuan Dun Bridge in 1987, the vibration velocity was recorded instead of acceleration by mistake.

8.4.3 Instrumentation

The instruments used for field measurement were for data acquisition only and they were easily packed inside the back of a van. A list of them is given below. All the instruments ran on a power supply of 12 Volts, and this made them very suitable for field work.

1. Accelerometer Model B&K 8306
2. Accelerometer Model 6153
3. Charge Amplifier Model B&K 2635
4. RMS Voltmeter Model DATRON-1030
5. Dual Trace Oscilloscope Model Deltax DX-5015S
6. Data Tape Recorder Model KYOWA-RTP-800A
7. Data Tape Recorder Model TEAC R-81

8.5 THE EXPERIMENTAL MODAL FREQUENCIES AND DAMPING

The recorded signal was assumed to be random, and a Hanning window was used before the Fourier transformation. Overlap segments of data were used in the analysis.

In the response of an actual bridge deck, the influence of

each crack or a combination of a set of damaged area on the spectrum would be represented by a cluster of spectral peaks close to the true modal frequencies. The true modal frequency is thus defined as the one which corresponds to a state of damage in the structure, which when given an excitation would generate the largest response. In other words, the structure will be vibrating with the smallest stiffness to the vibration mode shape corresponding to the true modal frequency. In the case of wide-band white noise excitation, it is the frequency corresponding to the largest amplitude in the frequency spectrum.

Considering the superstructure of a bridge as a vibrating body, overall damping can be separated into internal or structural damping and external or system damping. The structural damping is due to energy dissipation during all kinds of vibrations of the superstructure, and system damping is due to energy dissipation during relative movements between super and sub-structures and during all kind of vibration of the sub-structure element. As only small elastomeric bearing were used to support the concrete bridges, material damping was not considered. When cracks occur over the length of the bridge beams, energy dissipation in the cracks during the flexural mode of vibration causes an increase in the structural damping of the structure.

The modal frequencies of the bridge decks are obtained from an inspection of the autopower spectrum, phase and coherence values. The damping ratios are obtained from the half-power bandwidth method. The modal frequencies are not distinguishably different from those peaks arising from noise, and there is always a cluster of peaks around the modal frequency. These make the identification of damping difficult and in most cases impossible. Examples of the autopower spectrum are shown in Fig.8.8. The experimental modal frequencies are listed in Table 8.2 and the damping

ratios are given in Table 8.3.

8.6 THE COMPUTER MODEL AND THEORETICAL MODAL FREQUENCIES

The theoretical modal frequencies are calculated by treating the bridge deck as consisting of three dimensional beam elements, triangular plate bending elements and non-harmonic plane stress elements resting on rigid supports. The static modulus of elasticity from design documents is adopted in the modelling. The masses of the fencing and bituminous road surfacing have been taken into account. However, the stiffness of fencing, kerbstones and road surfacing have not been considered. The modal frequencies, calculated using the DDJ-W software package developed by Dalian Institute of Technology of the People's Republic of China, are given in Table 8.4.

8.7 COMPARISON OF RESULTS

The measured modal frequencies are generally higher than the theoretical values except those from Ni Zi Bridge.

The Chi Ling and Er Tou Tang Bridges have measured modal frequencies much higher than the theoretical values. These two bridges have bituminous material as road surfacing and the bridge joints were sealed up to full depth of the deck slab by this material. Large end rotational restraint existed in these structures and they behaved quite differently from a simply supported structure.

Inspection of the results of the Ni Zi Bridge and Chi Ling Bridge shows that after the bridges were in service for one year, the fundamental modal frequency decreased by 2% and 7% respectively. This may be due to the development of cracks in the beams and a reduction in the contribution of stiffness provided by the fencing and kerbstones sub-system.

Monitoring of Yuan Dun Bridge before and after rehabilitation showed that the modal frequencies increased after improvement. Only the longitudinal flexural stiffness of the bridge beams was improved in the rehabilitation exercise and the transverse load distribution properties were not changed. As a result, the increase in the First Bending frequency was greater than that for the First Bending First Torsional Modal frequency. The First Bending Second Torsional modal frequency could not be identified from the autospectra because of the small amplitude of vibration. This means the structure has a relatively poor transverse load distribution properties.

No theoretical values are presented for the Old Sha Wan Bridge because of lack of design information. The theoretical value of the First Bending Second Torsional modal frequency of New Dan Zhu Tou Bridge is missing because such a mode is not calculated by the software programme.

No comment is possible on the damping values because of the small number of data.

8.8 THE CASE STUDY OF YUAN DUN BRIDGE

Yuan Dun Bridge has a total length of 180.4 metres, with 2 spans of 22 metres at each end and 3 central spans of 30 metres. It was constructed in 1959 based on an early Russian bridge design, with a 7 metre wide carriageway and a 1.0 metre wide edge strip. It was designed for a Load Class of 13 Tonnes, Standard JTJ023-85 (1985). The superstructure consists of six precast Tee-beams at 1.4 metres centres supporting a cast-in-situ deck slab. There are 9 transverse diaphragms in the 22 metres spans and 12 diaphragms in those of 30 metres. The diaphragms are precast together with the Tee-beams, and the connections are made by welding together the steel reinforcement projecting from the top and bottom of adjacent diaphragms. The beam supports are steel roller

bearings and steel guiding plates. Substructures are gravity type piers and abutments. The plan and elevation of a 22 metre span bridge deck is shown in Fig.8.2.

The major visual damage report from Chen et al (1990) include: excessive deflection at midspan, ranging from 30 to 60 mm; depth of carbonation of concrete in the main beams ranging from 10 to 35 mm; extensive cracking, with 60 to 100 cracks in each beam spaced 200 to 300 mm apart with depths from 400 to 800 mm and maximum crack widths from 1.5 to 2.0 mm; serious corrosion in the exposed main tensile steel and shear steel; and all the construction joints of the in-situ slab were broken. Some of the deck slab was also extensively cracked.

Since the bridge is on a major highway, carrying more than 8000 vehicles every day majority of which are freight trucks, a programme was carried out to assess its safety and and to strengthen the bridge decks to a higher load carrying capacity.

8.8.1 The Load Test and Rehabilitation

The first and third spans were tested statically with the loading configurations as required by Report YC4-4/1978 (1982) which are shown in Fig.8.3. Three Load Classes of 15, 20 and 24.3 Tonnes were selected. The deflection of the beams at midspan are plotted in Fig.8.4, and strain of the main tensile reinforcement and concrete in compression on top of slab are plotted in Fig.8.5, Project Report (1986). The deflection and strain values are small and their changes are proportional to the load. However, the transverse load distribution property was not linear within the range of the test loads.

Each main beam in all seven spans was strengthened by external prestressing as reported by Hui and Zhong (1987)

with 6 number of 28 mm diameter cold drawn steel bars. The bars were machined to have a screw-threaded at one end and the other end was welded to the main tensile reinforcement near the end of each beam. The screw-thread end from two half length bars were screwed into a coupler at midspan thus allowing for the post-tensioning of the steel bars. The ribs of all the main beams were roughened and the exposed post-tensioned reinforcement and the ribs of the beams were then covered with a minimum of 25 mm thick sprayed concrete. Typical details at midspan are shown in Fig.8.6.

After the strengthening, the deflection of the bridge deck under dead load was found to be acceptable according to the Bridge Design Standard JTJ023-85 (1985). There was an average improvement of 22.4 mm in the deflection measured after three months of service. The crack widths at selected points were found to be less than 0.2 mm.

A second load test on Spans #1 and #3 was carried out using again the same three Load Classes. The deflection, crack width and strain measurements showed that the bridge decks were satisfactory, and calculations showed that the structure could carry a service load of 20 Tonnes with a sufficient safety margin.

8.8.2 The Computer Modelling

A finite element analysis of the bridge deck was undertaken using the finite element package DDJ-W developed by Dalian Institute of Technology. The deck slab was modelled with triangular plate bending elements and non-harmonic plane stress elements. The main beams and diaphragms were modelled as three dimensional grids on rigid supports. Results from the Schmidt Hammer Test on the beams and slab from Chen et al (1990) gave a correlated modulus of elasticity of 26.0 kN/mm^2 from the Design Standard JTJ023-85 (1985). Poisson's ratio was taken to be 0.1667 and density of reinforced

concrete was taken as 23.5 kN/m^3. The dead weight of the concrete fencing was distributed over the edge nodes of the bridge deck. Six degrees of freedom were allowed in all of the nodes except those at the supports. The computed modal frequencies are shown in Table 8.4.

8.8.3 The Dynamic Measurements

Two sets of measurements were made, one before and one after the rehabilitation in November 1986 and in April 1987 respectively. Spans #1, #3, #5 and #6 were measured in the first set, and Spans #1, #3, #5, and #7 were measured in the second set. The tests were conducted on days with only light traffic during a measurement period of 30 minutes. The total number of vehicles counted for each measurement period was less than 50.

Four to seven accelerometers were used for the measurements. The sensors were placed on top of the edge strip furthest away from the passing vehicles. Fig.8.7 shows the arrangement of the sensors in the measurements. The vertical vibrational response in the form of acceleration was then amplified and filtered (low-pass cut off at 1 kHz) and recorded on a tape recorder. (Velocity responses were recorded in the second set of measurements). The vibrational signal was then analysed using a spectrum analyzer. The major equipment used included accelerometers B&K 8306, charge amplifiers B&K 2635, data tape recorders KYOWA-RTP-800A and TEAC R-81, and spectrum analyzer HP-5420B.

8.8.4 Experimental Results

The autospectra of the responses from the midspan of the bridge decks are shown in Fig.8.8, and the modal frequencies and damping ratios are tabulated in Tables 8.2 and 8.3 respectively. The following observations have been drawn:

- The fundamental modal frequency of Spans #1 and #6 differs by 0.6 Hz, despite the fact that they are of the same construction and span length. It has not been possible to identify the actual reason for this difference although there are many possible explanations, such as a variation in the concrete quality or different levels of structural damage.

- The experimental modal frequencies are generally higher than the theoretical values, especially in the lower group of frequencies. This suggests that the assumed value of the modulus of elasticity might be too low. In actual fact, if it is assumed that the modulus of elasticity is increased by 46% for Span #5, the difference between the experimental and theoretical frequencies gets close to -5%. Given this close correlation, it would seem reasonable to say that before rehabilitation, Span #1 was in good condition, Spans #6 was about 22% less stiff than Span #1, and Span #3 was about 6% less stiff than Span #5.

- It is interesting to note that the damping of Span #3 is significantly lower than that for the other measured spans, and this is a factor which bears closer examination.

- Vibration of one span appeared to be transmitted to other spans, presumably through some or all of the expansion joints, bearings and piers, as seen in the results of Spans #3 and #5.

- The mode shapes cannot be identified uniquely from the limited number of measurement stations, and the matching of different modes to the identified modal frequencies makes reference to the theoretical values.

- The damping ratios were obtained from the autospectrum by the half-power bandwidth method. Only a few of the autospectra were smooth enough to obtain the damping estimates.

- The autospectrum for Span #7 shows double peaks close to the fundamental frequency. This is due to the large gain set in the amplifier during the recording. The large response from vehicles produced 'clipping' of the recorded signals and so affected the spectral analysis estimates. In effect this introduces the harmonics associated with a square wave.

- The modal frequencies and damping estimates obtained from different stations were slightly different. Generally, in the results quoted here, close values for frequencies obtained from different sensors have been taken as being the same frequency.

- With the exception of the fundamental bending mode, there is a clear pattern of correlation between the experimental and theoretical frequencies of modes 1B,1T and 2B1T after rehabilitation. If the changes in the fundamental frequency are used as a measure of the effect of the rehabilitation process this would suggest that Span #1 was stiffened by at least 12% whereas Spans #3 and #5 were stiffened by about 20%. These increases would be slightly larger because the calculations have not included the associated increase of mass.

8.8.5 Sources of Error in The Field Measurement

The 30 minutes of random response measurement of the structure could be responsible for the introduction of a large bias error in the spectral estimates. For instance a 3.8 Hz frequency requires at least 44 minutes of random

response signal to achieve a minimum of 10% bias error in the spectral estimates.

Another possible source of error is the small number of vehicles crossing the bridge. This would allow each vehicle to set the bridge in vibration for a relatively long period of time. This would then differ from the assumed approximation of the vibrations to a random pattern.

8.9 DISCUSSIONS

Richardson and Douglas (1987) have reported that the measured modal frequencies of a reinforced concrete bridge deck change during the course of a day's testing. This was suspected to be due to the diurnal changes of temperature. But in the present field study, the only references to temperature are the prevailing weather conditions and the time and date of measurement. This may pose possible difficulties in direct comparison of modal frequencies with those from later periodic tests.

Since changes in the condition of bearings, road fencing, mass of surface material, etc. affect the modal frequencies, it is essential that dynamic measurement should be part of an overall programme of inspection and monitoring. Any physical changes which have taken place between tests must be taken into account in assessing the results from dynamic measurements.

8.10 CONCLUSIONS

The vibrational response from traffic-generated excitation of seventeen simply supported reinforced concrete bridge decks were measured and analyzed. It would appear from the results that a comparison between the measured and theoretical frequencies of a bridge structure could present a viable method for assessing the changes that are occurring

in the integrity of the structure. Further work is needed to see if this approach could be used to determine the absolute value of structural stiffness rather than its relative value. More study is required to assess the influence of structural integrity on structural damping.

Bridge	Year of Construction	No. of Span in Bridge	Type of Foundation		Support Material	Overall Span(m)	Design Span(m)	Overall deck Width(m)	Type of Construction	No. of Diaphragm	Remarks
Chi Ling	1981	1	Abutment on caisson		bituminous felt	10.0	9.70	10.50	6-Tee beam & slab	3	
She Gang	1981	1	Abutment on footing		200x150x21 rubber pad	10.0	9.80	10.60	7-Tee beam & slab	3	
Old Sha Wan (1st span)	1965	2	Abutment on footing	Pier on footing	200x150x21 rubber pad	14.13	13.80	5.70	cast-in-situ 3-Tee beam & slab	4	
Er Tou Tang (2nd span)	1981	4	Pier on footing		steel bearing	16.0	15.50	10.00	6-Tee beam & slab	5	
Er Tou Tang (1st span)	1981	4	Abutment on footing	Pier on footing	steel bearing	16.0	15.50	10.00	6-Tee beam & slab	5	
Ni Zi (1st span)	1981	6	Abutment on caisson	Pier on caisson	200x150x21 rubber pad	16.0	15.50	12.40	7-Tee beam & slab	5	
Ni Zi (2nd span)	1981	6	Pier on Caisson		200x150x21 rubber pad	16.0	15.50	12.40	7-Tee beam & slab	5	
Zhong Tang Yin Qiao (8th span)	1981	10	Pier on caisson		200x150x21 rubber pad	16.0	15.50	12.40	7-Tee beam & slab	5	
Zhong Tang Yin Qiao (1st span)	1981	10	Pier on caisson	Abutment on caisson	200x150x21 rubber pad	16.0	15.50	12.40	7-Tee beam & slab	5	
Old Dan Zhu Tou	1965	1	Abutment on footing		200x150x21 rubber pad	16.76	16.24	5.2	3-Tee beam & slab	5	
New Dan Zhu Tou	1984	1	Abutment on footing		200x180x28 rubber pad	16.76	16.24	4.5	3-Tee beem & slab	5	
New Sha Wan	1985	1	Abutment on caisson		300x200x42 rubber pad	28.16	27.46	13.65	8-Tee beam & slab	7	

Table 8.1 Major Information on the Prototype Bridges

Bridge	Year of Construction	No. of Span in Bridge	Type of Foundation		Support Material	Overall Span(m)	Design Span(m)	Overall deck Width(m)	Type of Construction	No. of Diaphragm	Remarks
Yuan Dun (1st span) 1986	1959	7	Abutment on footing	Gravity type pier	Steel bearing	22.16	21.16	8.98	6-Tee beam & slab	9	Excessive deflection and vibration
Yuan Dun (3rd span) 1986	1959	7	Gravity type pier		Steel bearing	30.2	29.60	8.98	6-Tee beam & slab	12	Excessive deflection and vibration
Yuan Dun (5th span) 1986	1959	7	Gravity type pier		Steel bearing	30.2	29.60	8.98	6-Tee beam & slab	12	Excessive deflection and vibration
Yuan Dun (6rd span) 1986	1959	7	Gravity type pier		Steel bearing	22.16	21.16	8.98	6-Tee beam & slab	9	Excessive deflection and vibration
Yuan Dun (1st span) 1987	1959	7	Abutment on footing	Gravity type pier	Steel bearing	22.16	21.16	8.98	6-Tee beam & slab	9	After rehabilitation work
Yuan Dun (3rd span) 1987	1959	7	Gravity type pier		Steel bearing	30.2	29.60	8.98	6-Tee beam & slab	12	After rehabilitation work
Yuan Dun (5th span) 1987	1959	7	Gravity type pier		Steel bearing	30.2	29.60	8.98	6-Tee beam & slab	12	After rehabilitation work
Yuan Dun (7th span) 1987	1959	7	Abutment on footing	Gravity type pier	Steel bearing	22.16	21.16	8.98	6-Tee beam & slab	9	After rehabilitation work

Table 8.1 Major Information on the Prototype Bridges (cont.)

Table 8.2 Experimental Modal Frequencies of Bridge Decks

Bridge Deck	Span (m)	Modal Frequencies				
		1B	1B,1T	1B,2T	2B	2B,1T
She Gang	9.8	18.555	29.492	-	51.172	-
Chi Ling (84)	9.7	23.828	41.019	55.469	51.953	-
Chi Ling (85)	9.7	23.437	36.328	-	51.953	-
Ni Zi (84) (1st span)	15.5	7.8125	15.234	-	27.25	25.00
Ni Zi (85) (1st span)	15.5	7.25	13.625	-	-	-
Ni Zi (2nd span)	15.5	7.031	14.258	-	22.461	-
Zhong Tang Yin Qiao (8th span)	15.5	8.125	15.25	-	-	-
Zhong Tang Yin Qiao (1st span)	15.5	8.0	15.0	-	23.625	-
Er Tou Tang (1st span)	15.5	13.125	23.125	44.625	39.062	54.75
Er Tou Tang (2nd span)	15.5	13.0	21.25	43.555	38.281	53.125
New Sha Wan	27.5	5.469	9.57	19.531	17.578	23.437
Yuen Dun (86) (1st span)	21.5	5.469	6.445	22.852	18.812	27.539
Yuen Dun (86) (6th span)	21.5	4.875	5.625	-	17.773	25.293
Yuen Dun (87) (1st span)	21.5	5.813	6.375	-	-	20.063
Yuen Dun (87) (7th span)	21.5	5.625	6.25	-	-	19.5625
Old Sha Wan	14.0	12.305	17.187	23.633	35.352	-
Yuen Dun (86) (3rd span)	29.0	3.8125	4.563	-	14.375	11.375
Yuen Dun (86) (5th span)	29.0	3.939	4.688	-	13.625	14.25
Yuen Dun (87) (3rd span)	29.0	4.188	4.75	22.31	16.0	14.375
Yuen Dun (87) (5th span)	29.0	4.313	4.875	-	16.375	15.0
Old Dan Zhu Tou	16.2	7.5	9.375	12.5	30.625	-
New Dan Zhu Tou	16.2	7.563	9.438	12.312	23.437	30.273

Table 8.3 Experimental Damping Ratio of Bridge Decks

Bridge Deck	Span (m)	Damping Ratio at Different Freq.				
		1B	1B,1T	1B,2T	2B	2B,1T
She Gang	9.8	-	-	-	-	-
Chi Ling (84)	9.7	-	-	-	-	-
Chi Ling (85)	9.7	-	-	-	-	-
Ni Zi (84) (1st span)	15.5	-	-	-	-	-
Ni Zi (85) (1st span)	15.5	-	-	-	-	-
Ni Zi (2nd span)	15.5	3.18%	-	-	-	-
Zhong Tang Yin Qiao (8th span)	15.5	2.41%	2.59%	-	-	-
Zhong Tang Yin Qiao (1st span)	15.5	-	2.90%	-	-	-
Er Tou Tang (1st span)	15.5	1.26%	-	-	-	-
Er Tou Tang (2nd span)	15.5	-	1.38%	-	-	-
New Sha Wan	27.5	-	-	-	-	-
Yuen Dun (86) (1st span)	21.5	-	3.40%	-	-	-
Yuen Dun (86) (6th span)	21.5	3.56%	-	-	2.10%	-
Yuen Dun (87) (1st span)	21.5	-	-	-	-	-
Yuen Dun (87) (7th span)	21.5	-	-	-	-	-
Old Sha Wan	14.0	-	-	-	-	-
Yuen Dun (86) (3rd span)	29.0	2.47%	-	-	-	-
Yuen Dun (86) (5th span)	29.0	3.72%	-	-	-	-
Yuen Dun (87) (3rd span)	29.0	-	-	-	-	-
Yuen Dun (87) (5th span)	29.0	-	-	-	-	-
Old Dan Zhu Tou	16.2	-	-	-	-	-
New Dan Zhu Tou	16.2	2.35%	-	-	-	-

Table 8.4 Theoretical Modal Frequencies of Bridge Decks

Bridge Deck	Span (m)	Modal Frequencies				
		1B	1B,1T	1B,2T	2B	2B,1T
She Gang	9.8	19.724	21.459	27.330	52.854	56.786
Chi Ling (84)	9.7	16.706	17.544	22.732	55.525	57.438
Chi Ling (85)	9.7	16.706	17.544	22.732	55.525	57.438
Ni Zi (84) (1st span)	15.5	7.836	10.603	19.469	39.184	30.718
Ni Zi (85) (1st span)	15.5	7.836	10.603	19.469	39.184	30.718
Ni Zi (2nd span)	15.5	7.836	10.603	19.469	39.184	30.718
Zhong Tang Yin Qiao (8th span)	15.5	7.836	10.603	19.469	39.184	30.718
Zhong Tang Yin Qiao (1st span)	15.5	7.836	10.603	19.469	39.184	30.718
Er Tou Tang (1st span)	15.5	9.586	10.358	22.989	26.546	28.944
Er Tou Tang (2nd span)	15.5	9.586	10.358	22.989	26.546	28.944
New Sha Wan	27.5	4.454	7.268	25.292	14.926	29.354
Yuen Dun (86) (1st span)	21.5	3.887	4.996	20.153	14.817	16.028
Yuen Dun (86) (6th span)	21.5	3.887	4.996	20.153	14.817	16.028
Yuen Dun (87) (1st span)	21.5	4.485	6.14	22.941	16.926	18.769
Yuen Dun (87) (7th span)	21.5	4.485	6.14	22.941	16.926	18.769
Old Sha Wan	14.0	-	-	-	-	-
Yuen Dun (86) (3rd span)	29.0	3.065	4.12	32.468	11.567	12.268
Yuen Dun (86) (5th span)	29.0	3.065	4.12	32.468	11.567	12.268
Yuen Dun (87) (3rd span)	29.0	3.419	4.857	30.969	12.882	12.724
Yuen Dun (87) (5th span)	29.0	3.419	4.857	30.969	12.882	12.724
Old Dan Zhu Tou	16.2	11.647	15.969	64.809	35.236	41.102
New Dan Zhu Tou	16.2	9.375	12.356	-	32.552	33.289

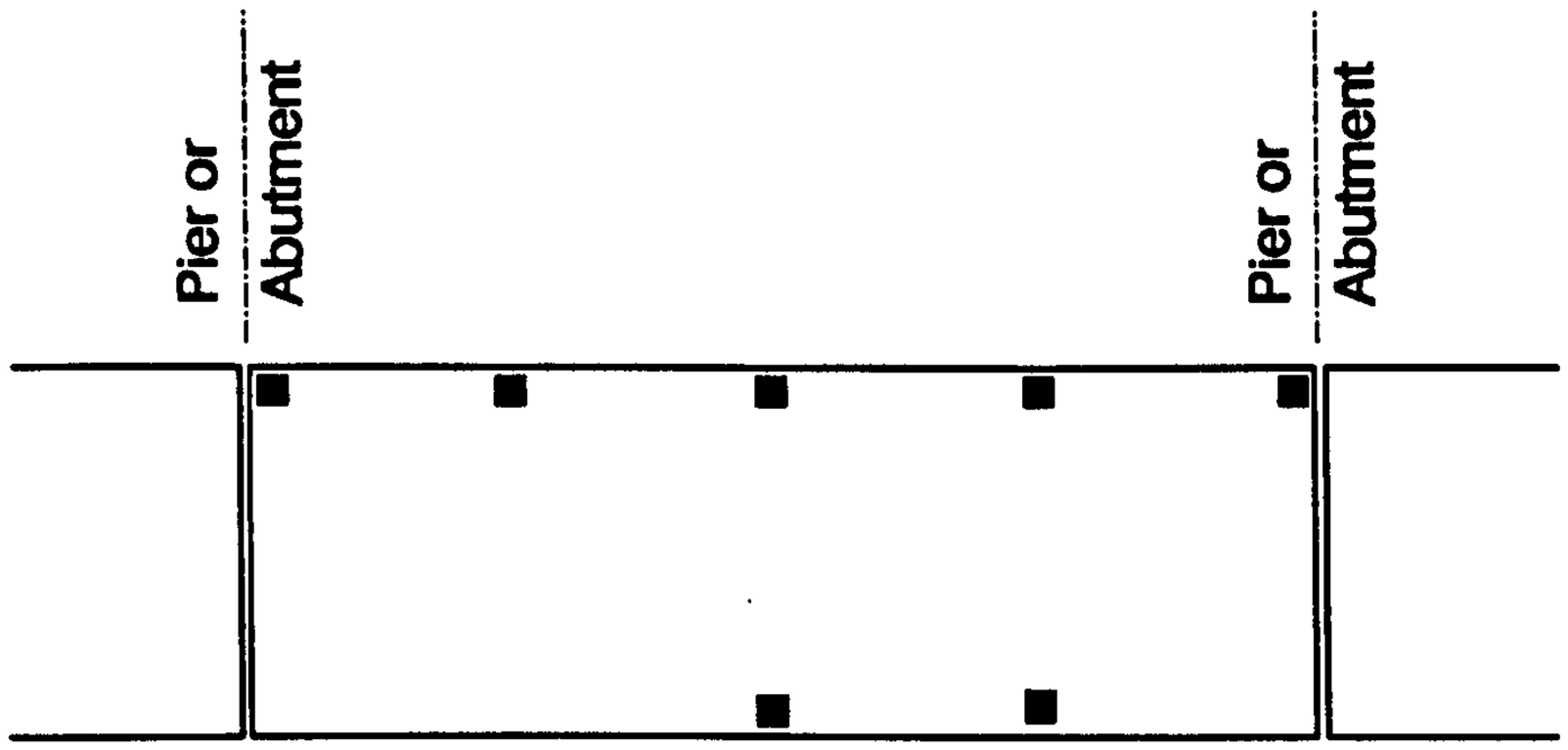

FIG.8.1-General Layout of Accelerometers on a Bridge Deck

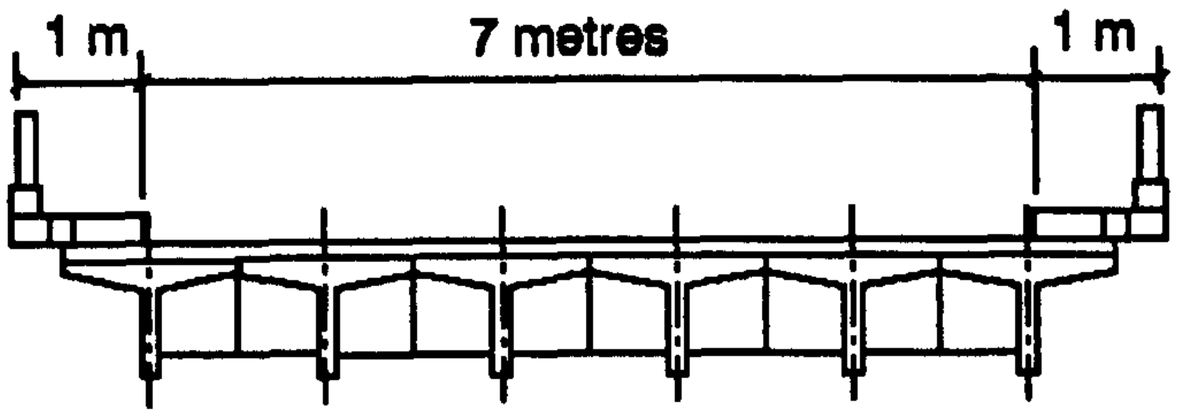

SECTION 1-1

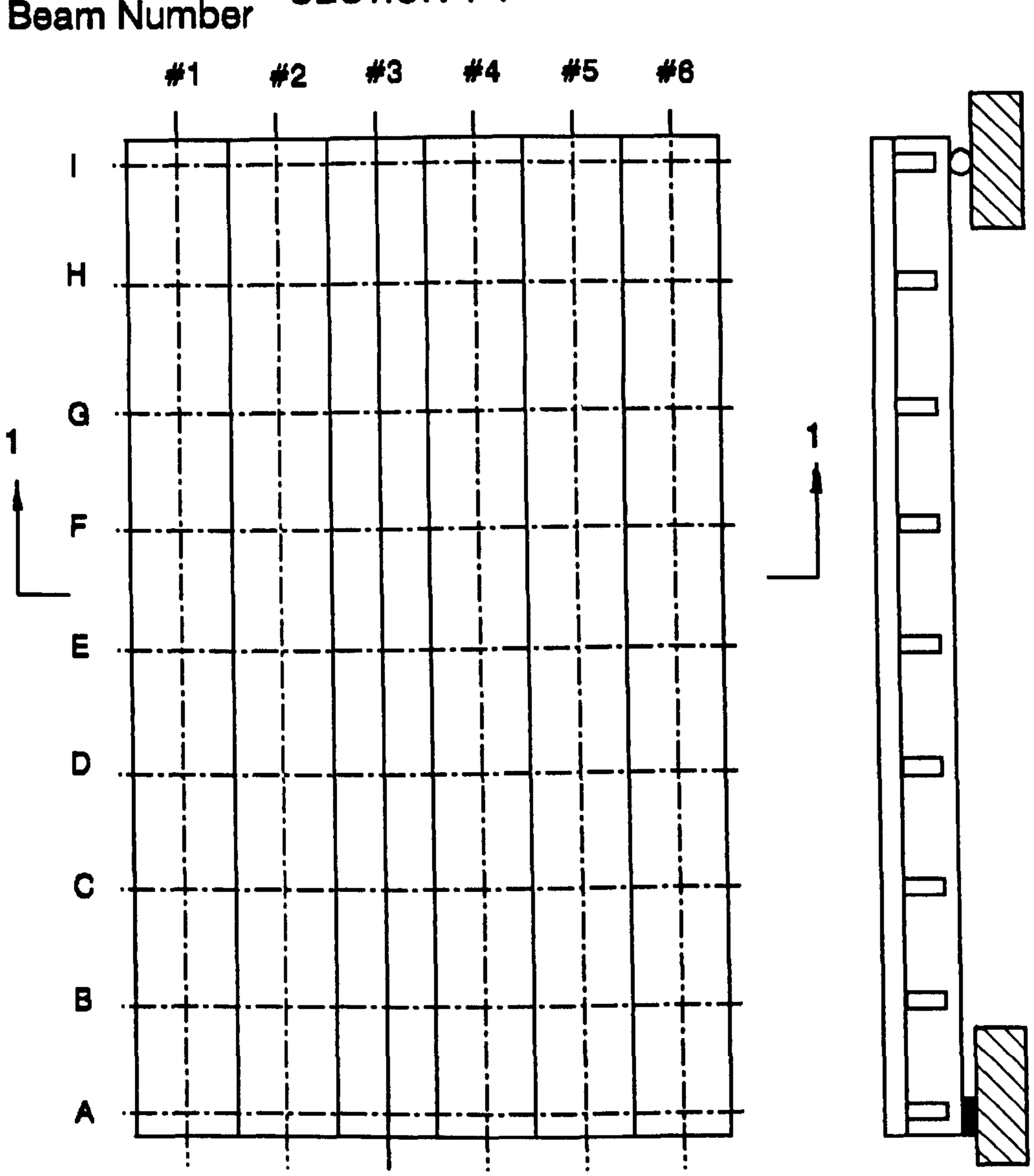

PLAN

FIG.8.2-Plan, Elevation and Section of 22m Span
Yuan Dun Bridge Deck

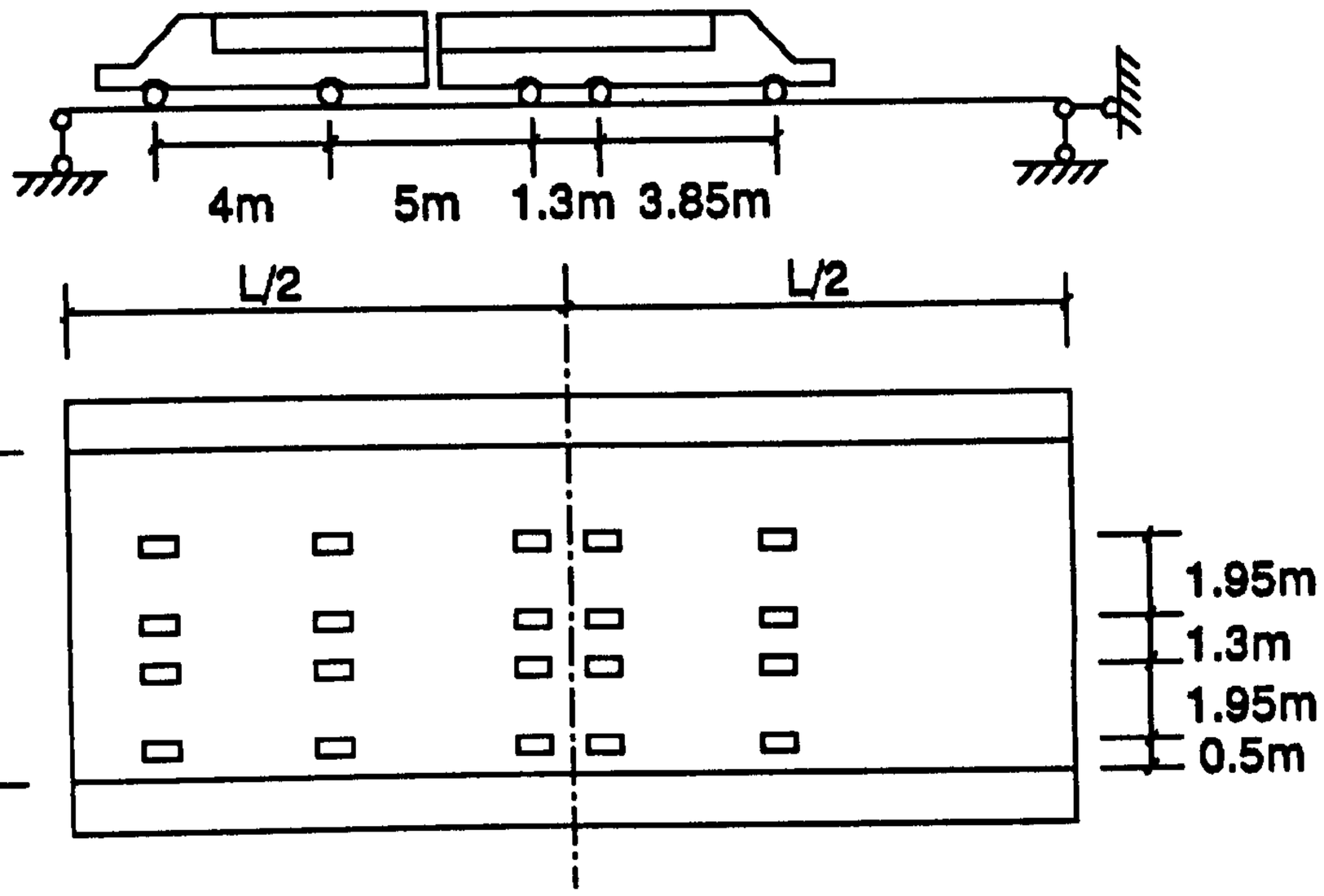

(a) 15 and 20 Tonne Load

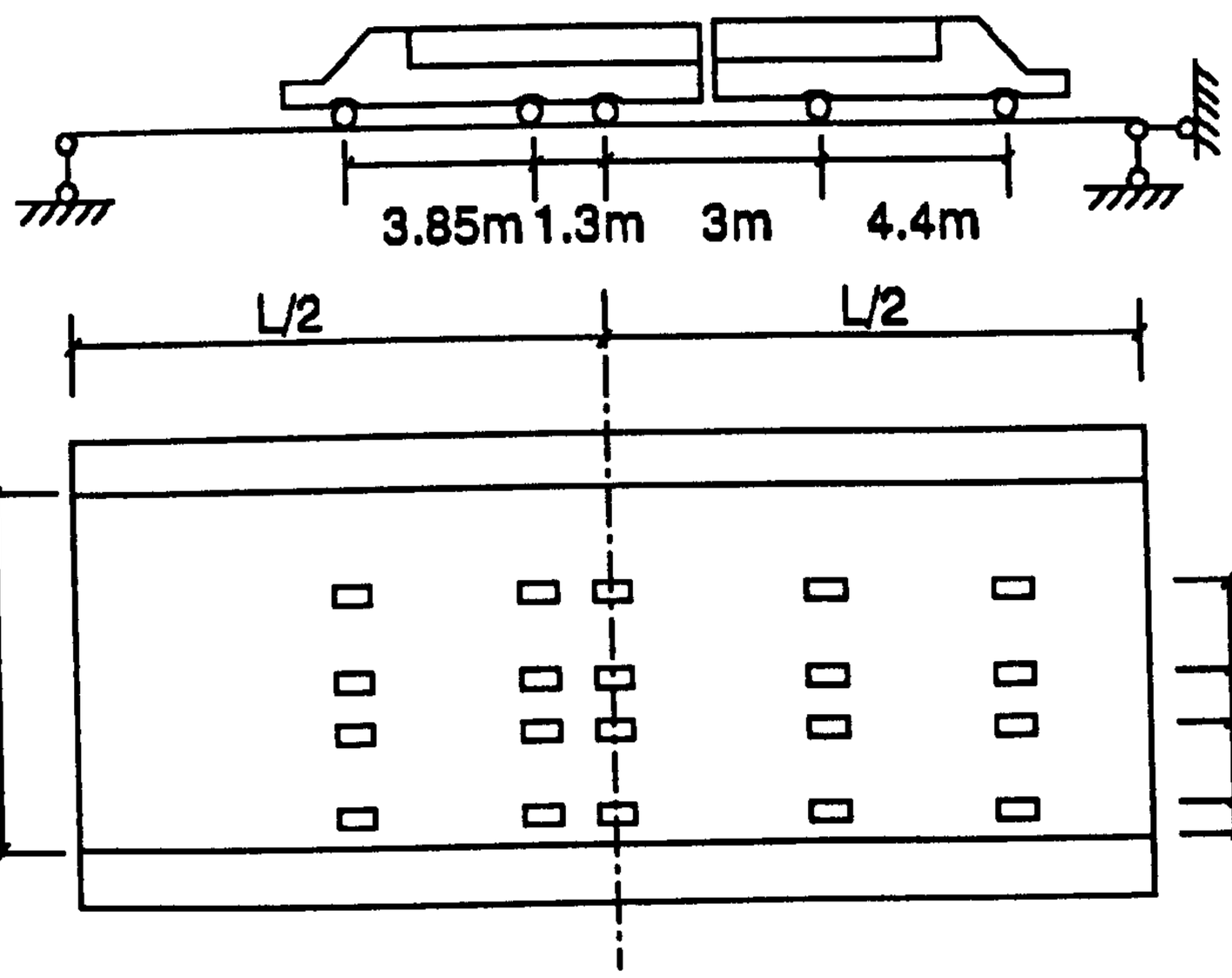

(b) 24.3 Tonne Load

FIG.8.3-Load Configuration in the Proof Load Test of Yuan Dun Bridge

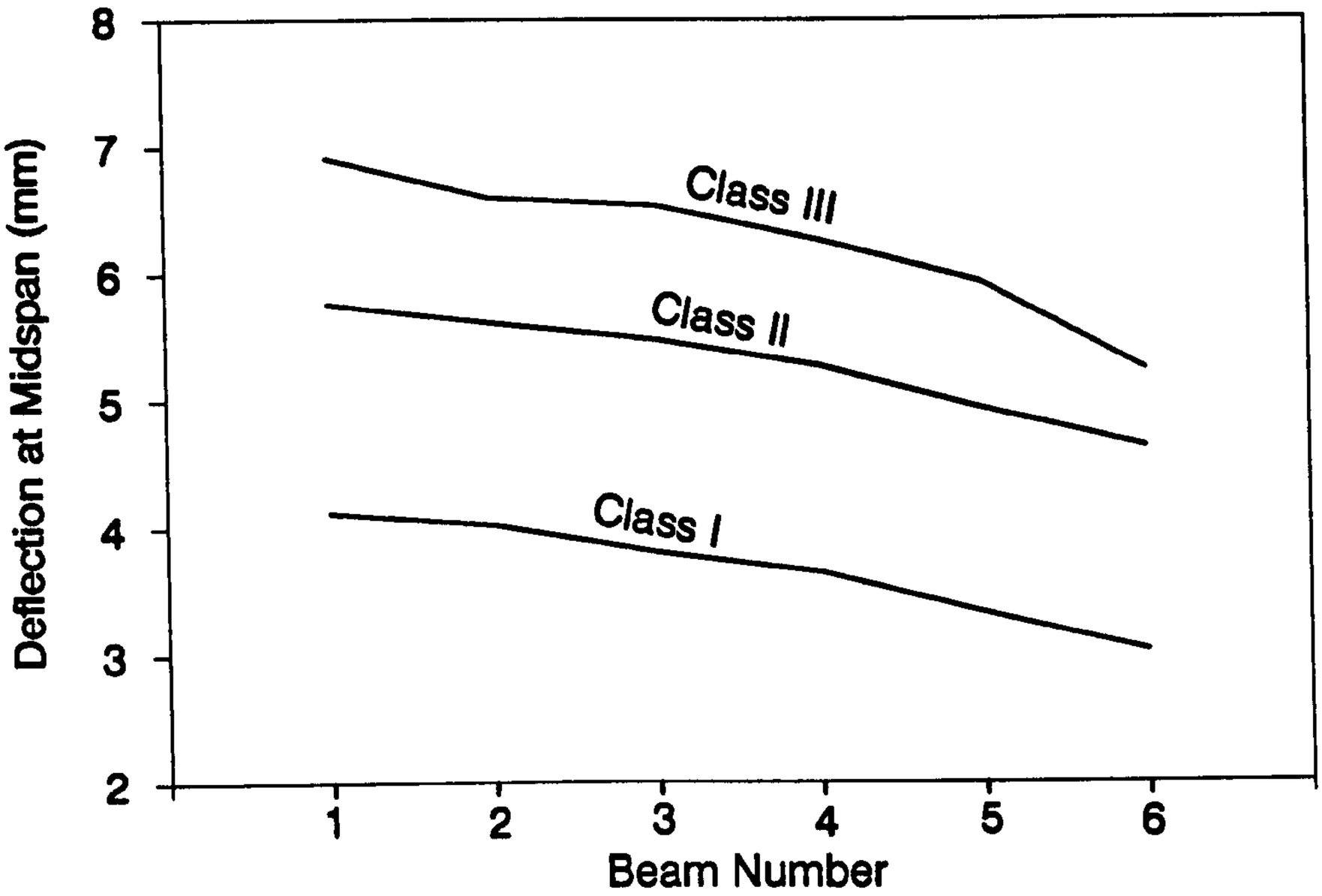

FIG.8.4(a)-Deflection at Midspan of Span #1 of Yuan Dun Bridge Before Rehabilitation

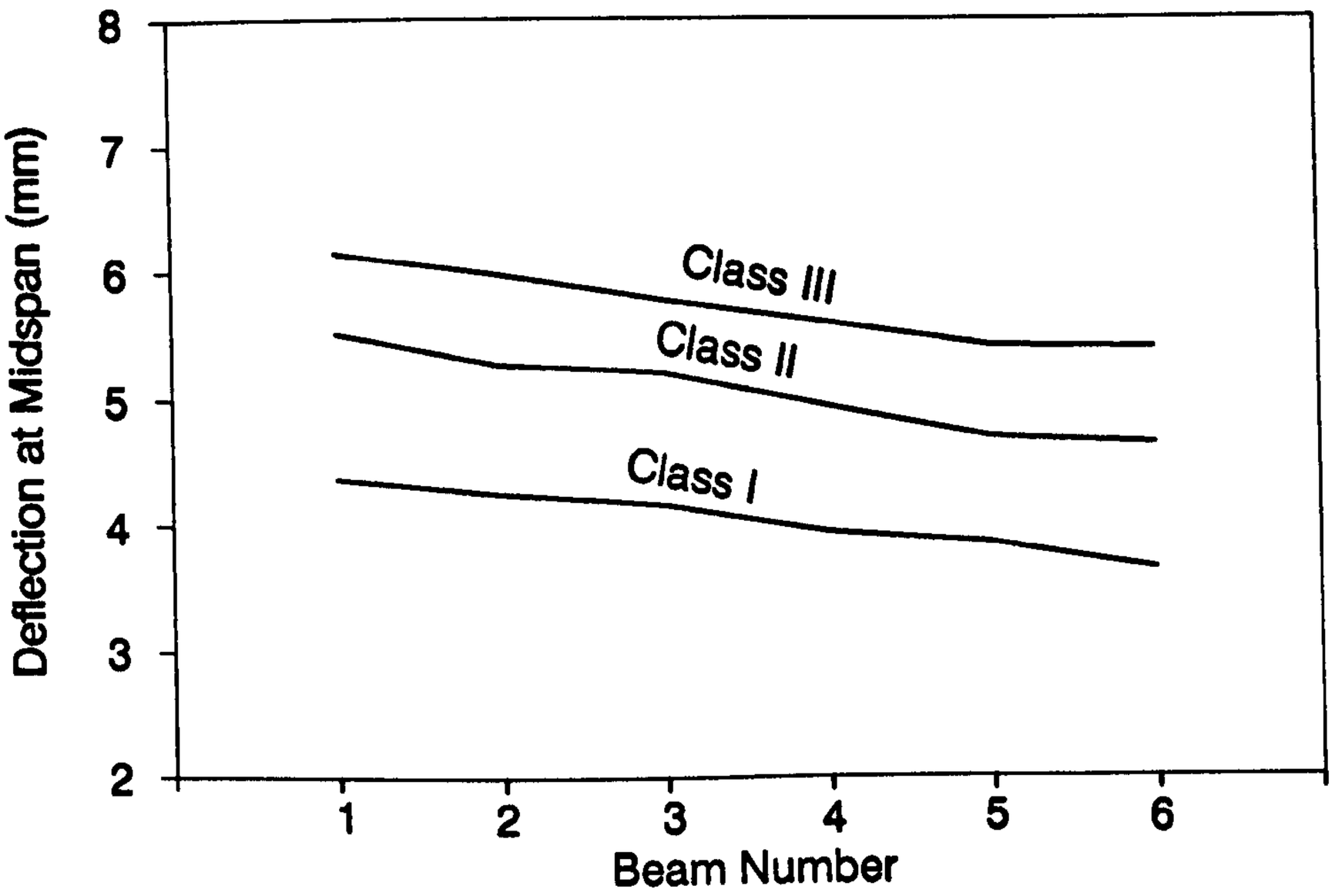

FIG.8.4(b)-Deflection at Midspan of Span #3 of Yuan Dun Bridge Before Rehabilitation

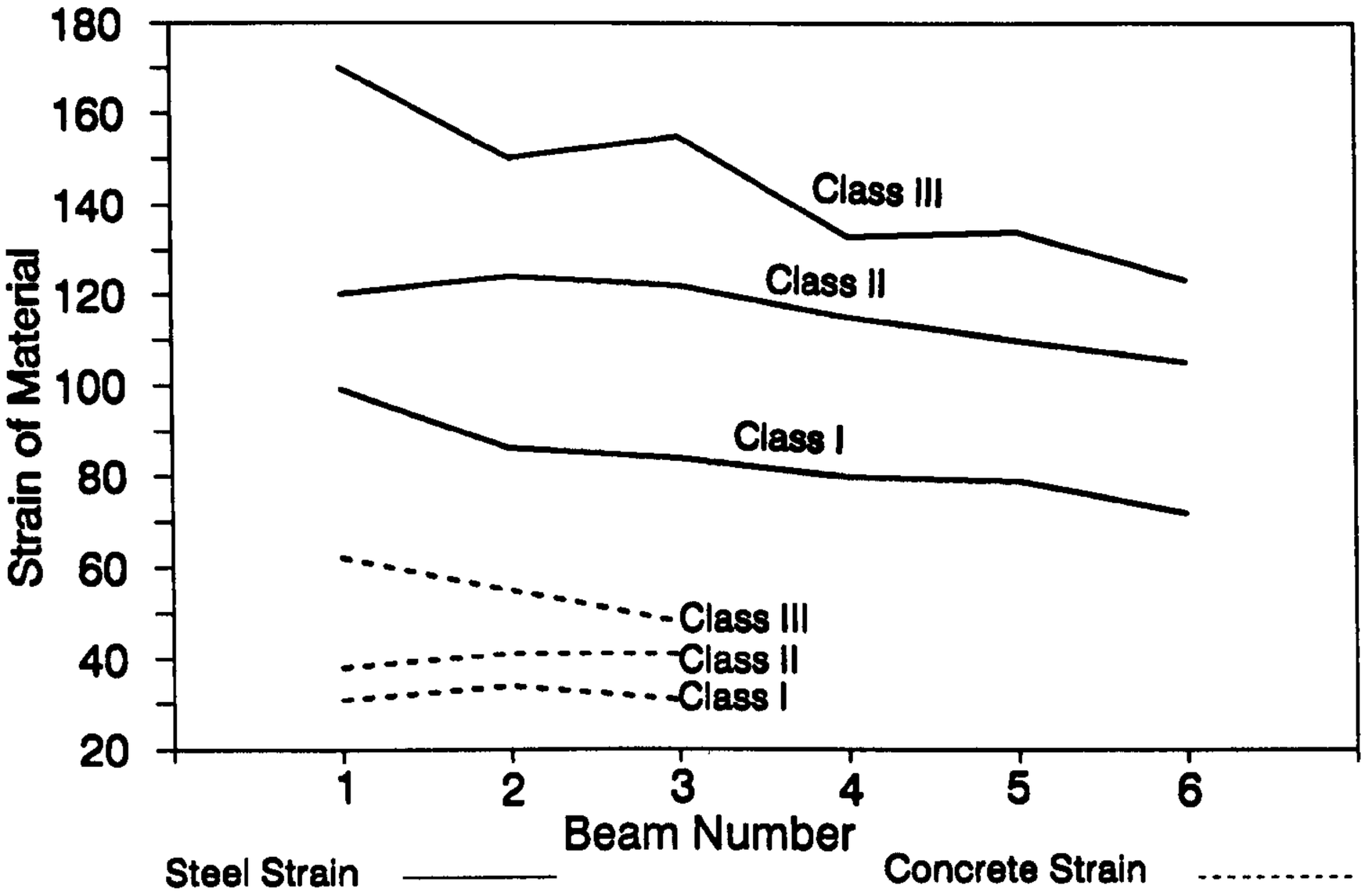

FIG.8.5(a)-Steel and Concrete Strain at Midspan of Span #1 of Yuan Dun Bridge Before Rehabilitation

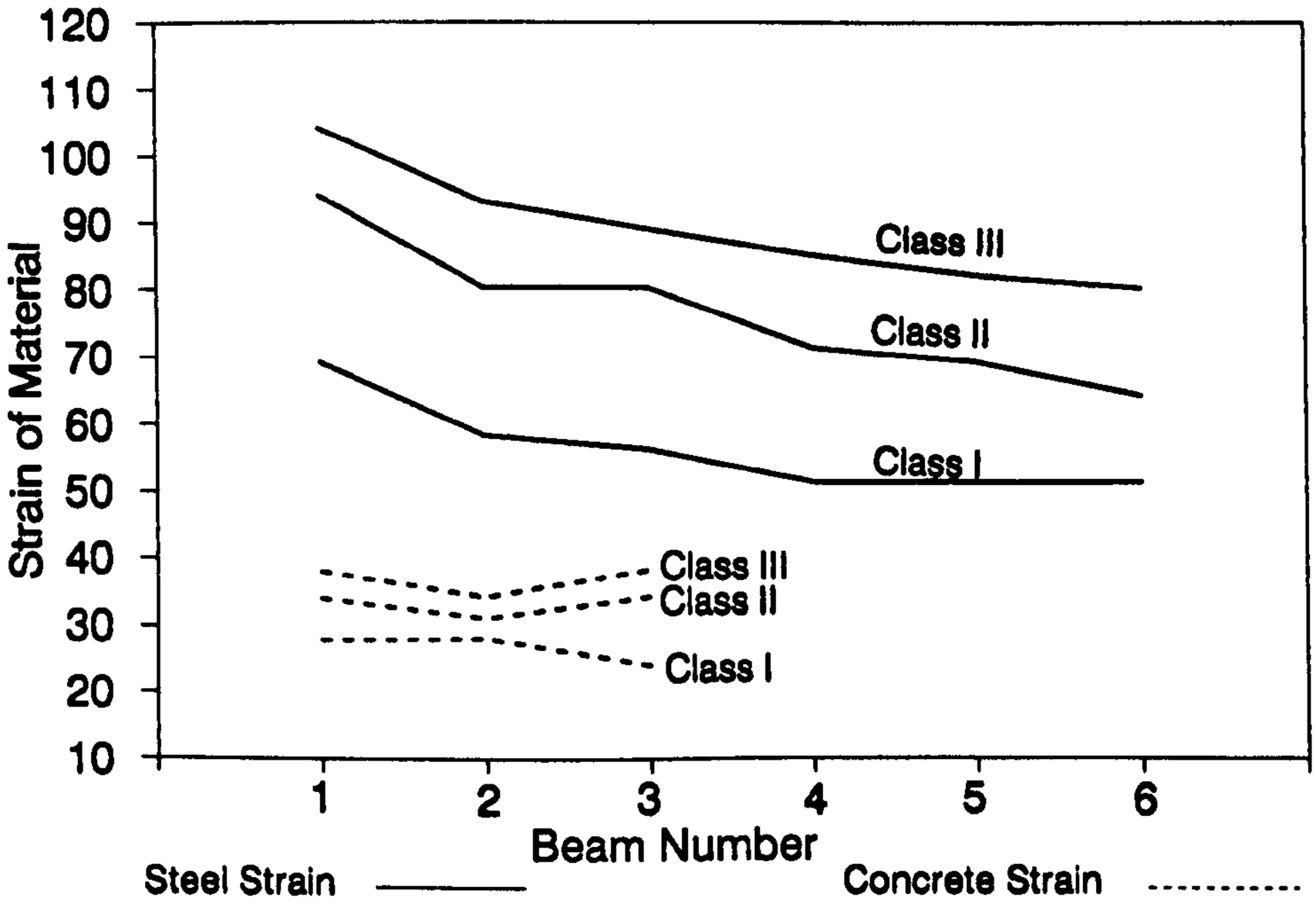

FIG.8.5(b)-Steel and Concrete Strain at Midspan of Span #3 of Yuan Dun Bridge Before Rehabilitation

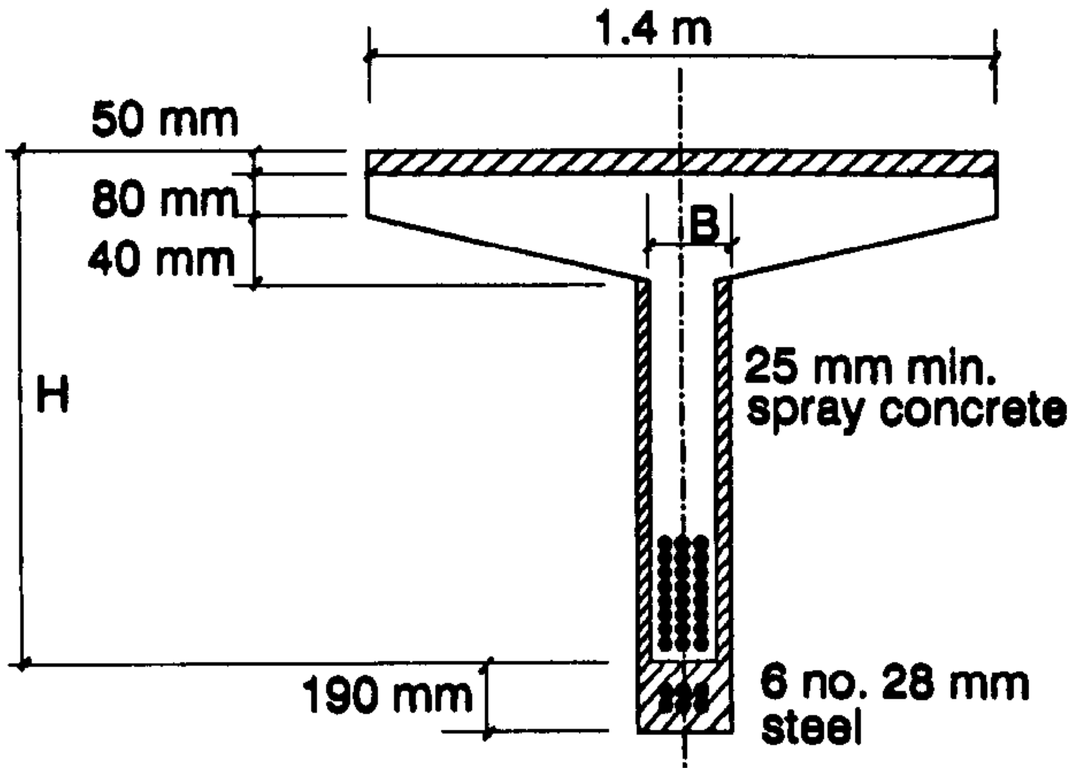

	22m Span	30m Span
B	180 mm	220 mm
H	1300 mm	1850 mm

FIG.8.6-Details of Rehabilitation at Midspan of Yuan Dun Bridge Beams

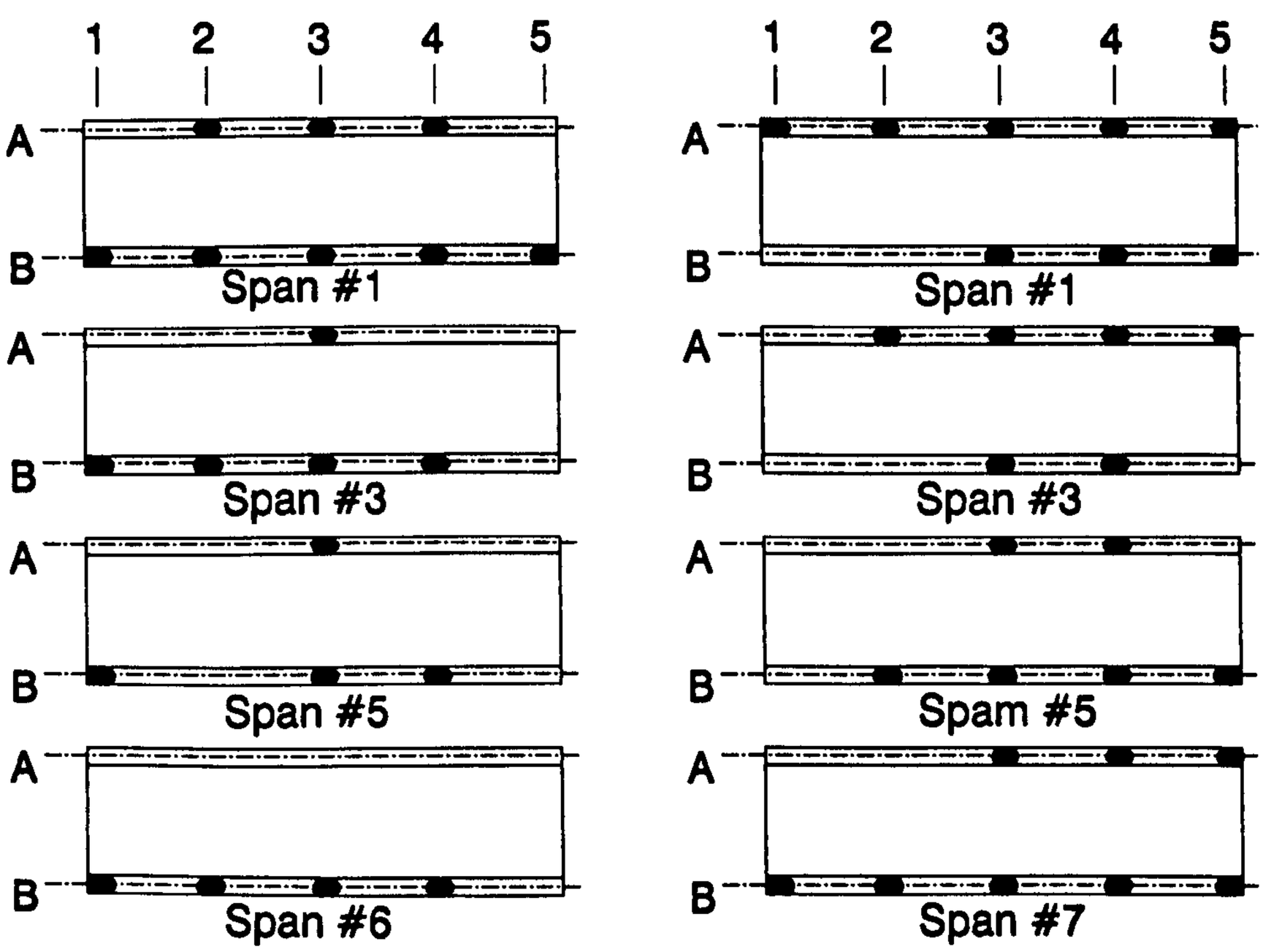

FIG.8.7-Arrangement of Accelerometers in the Dynamic Test of Yuan Dun Bridge Decks

Before Rehabilitation

After Rehabilitation

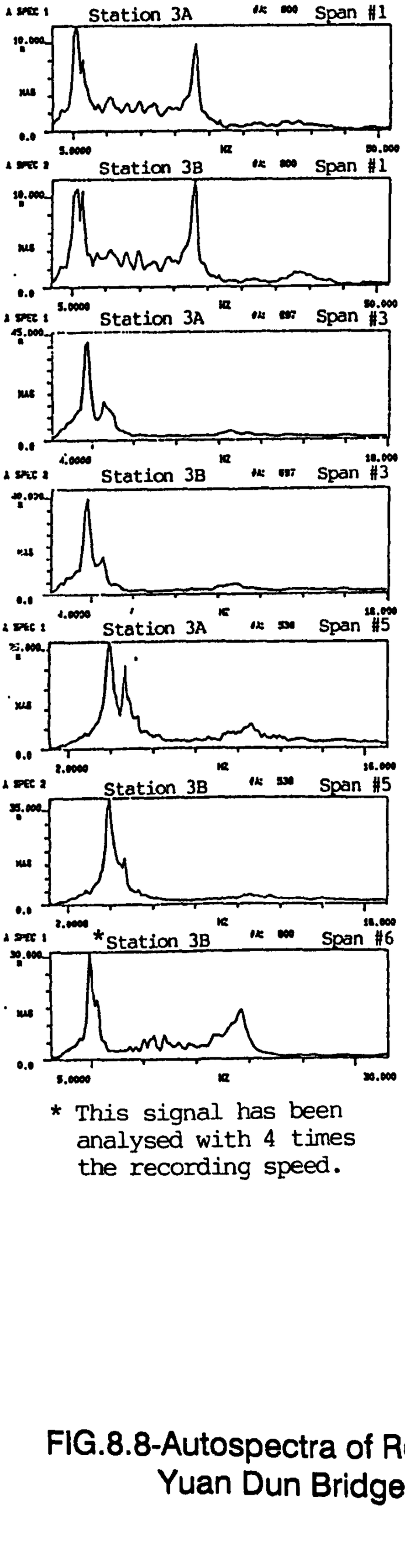

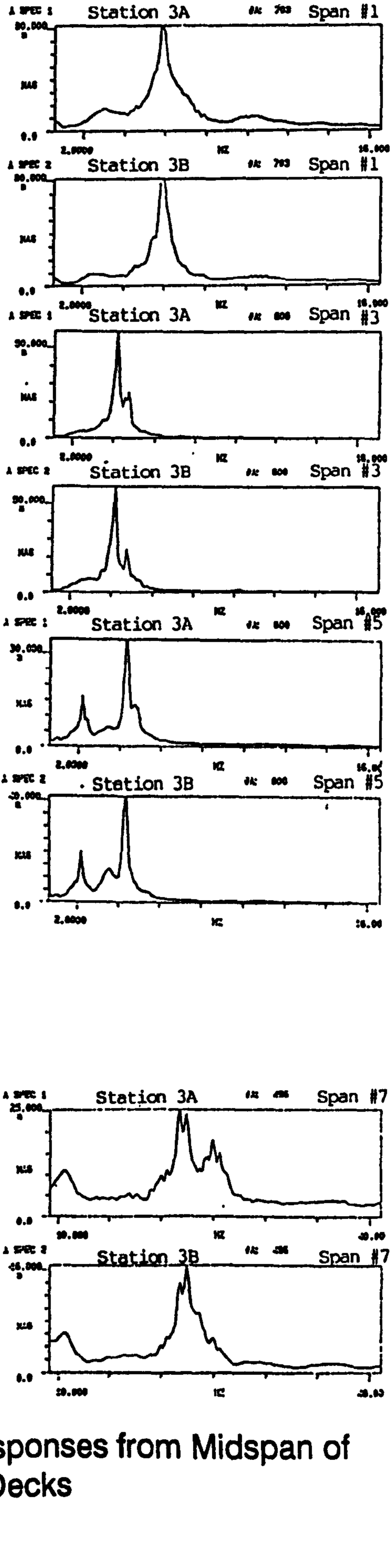

* This signal has been analysed with 4 times the recording speed.

FIG.8.8-Autospectra of Responses from Midspan of Yuan Dun Bridge Decks

CHAPTER NINE

EVALUATION OF THE PROPOSED METHOD AGAINST DATA FROM THE PROTOTYPE BRIDGE TESTS

9.1 FINITE ELEMENT MODELLING CONSIDERATIONS

Dynamic results of thirteen prototype beam-slab type bridge decks with spans of 16 metres, 22 metres and 30 metres have been used to evaluate the proposed method. Details of the bridges can be found in Table 9.1. The other bridge decks are not suitable because of insufficient information or unclear boundary conditions.

Ni Zi, Zhong Tang Yin Qiao and New Dan Zhu Tau Bridges are of 16 metres span. When they were tested, they had been in service for at least one year. Ni Zi and Zhong Tang Yin Qiao bridges do not have bituminous pavement on top, and Standard JT/GQB011-73 (1973) requires 70 mm minimum of concrete pavement to be used in construction. For a seven beam bridge deck as in Ni Zi and Zhong Tong Yin Qiao, with 0.015% cross-fall in the finished pavement, an average thickness of 100 mm in-situ concrete pavement on top of the precast beams was assumed. The modulus of elasticity of concrete was taken to be 28.5 kN/mm^3 as stated in the Standard JTJ023-85 (1985). Density of reinforced concrete was taken to be 23.5 kN/m^3. Stiffness arising from fencing and pedestrian pavements on the edges was not considered in the finite element modelling, but the masses of these elements were added on to the nodes along the edge beams in the finite element model. The main beams are on stiff rubber bearings which were modelled as rigid supports. The bridge deck was modelled as an orthogonal grid, and the dynamic analysis was carried out using the SAP IV finite element software package.

The New Dan Zhu Tau bridge is an extension to the existing bridge deck, parallel but separate from the old bridge. The whole bridge deck surface is on a horizontal bend, and the required superelevation is provided by a sloping layer of in-situ concrete deck, with the thicker side on the new bridge. An average 100 mm thick concrete deck was assumed in the finite element modelling. Other features and considerations were the same as for the Ni Zi Bridge described in Chapter Eight and in the previous paragraph.

In Yuan Dun Bridge, the 50 mm thick in-situ deck slab was included in the finite element modelling. The rehabilitation work involved attaching additional reinforcement to the bottom of the main beams protected by spray concrete such that the depth and width of the rib section were increased. The modulus of elasticity was taken to be 26.0 kN/mm^2 correlated from Schmidt Hammer Tests results, Chen et al (1990). Other features and considerations were the same as for the Ni Zi bridge.

The actual reinforcement detail along the beam, (i.e. part of the tensile reinforcement being bent up near the ends as shear reinforcement and the position of the centroid of tension reinforcement) were not taken into account in calculating the stiffness of each beam element in the finite element model.

Experience from the assessment of the model bridge deck and beams shows that a correction factor of 1.35 is required to apply to the modulus of elasticity of structure to account for the effect of non-uniformity of moment of inertia along the member and the inaccuracy of the FEM in modelling a cracked reinforced concrete structure. This factor is used in this FEM.

9.2 EVALUATION OF THE CRACKED CONDITION OF THE BRIDGE DECK

The Structural Damage Factor α calculated for each bridge deck are listed in the third column of Table 9.2.

The Structural Damage Factor α for the first span of Yuan Dun Bridge did not increase after rehabilitation. This is because the increase in I_{max} offset the effect of additional stiffness due to strengthening. In the third and fifth span, the effect of strengthening was larger than the increase in I_{max} resulting in a net increase of 7% in the Structural Damage Factor α.

There are cases where the SD Factor α was greater than unity which is due to the additional stiffness from fencing and other non-structural components of the bridge deck. This effect is more significant in newly constructed structures as is shown in the group of 16m long bridge decks. New Dan Zhu Tau Bridge is relatively new and it has a SD Factor α equal to 1.293. As a further example, the first span of Ni Zi Bridge possesses a SD Factor α of 1.011 in the first test carried out in 1984 (not on Table 9.2). This factor dropped to 0.869 in a later test carried out in 1985. This may be due to the loosening of connection in the fencing or between the fencing and the structural deck. All these examples indicate that this effect due to non-structural components is greatly reduced after a few years of service.

A Reference Factor α_m was calculated for each group of bridge decks of a particular span length. This factor is the mean value of the Structural Damage Factor α in each of the groups. The Reference Factors α_m for 16 m, 22 m and 30 m span bridge decks are 0.999, 0.997 and 0.707 respectively. They are plotted against span length in Fig.9.1 with an upper limit of unity. When a bridge deck with design information available on its steel arrangement, geometry and material properties is suspected of having structural

deficiencies, I_{est} is estimated from the measured first modal frequency, and hence the Structural Damage Factor α is calculated. If α falls far below the value of α_m, the structure may be assumed to be in a badly damaged state. If it is close to the curve of α_m, it is in good condition. If a sufficient number of SD Factors α for bridges of different damage states are available, bands of Reference Factor α_m may be allocated to denote bridge decks of different damage states as shown in Fig.9.1.

9.3 ESTIMATION OF THE LOAD CARRYING CAPACITY OF THE BRIDGE DECK

The steel percentages in the main beams in the different bridge decks were estimated by the proposed method. The cracked moments of inertia of the bridge beams are plotted versus the neutral axis depth in Figs.9.2 and 9.3. There is a nominal value of I_{nom} in every bridge beam. Curves plotting the I_{nom} value versus steel percentage of the different bridge beams are shown in Figs.9.4 to 9.6. The LCC Factors β are calculated and are listed in Table 9.2. Reference Factor β_{LS} is obtained for bridges of the same span length with minimum least-squares error on the estimated steel percentages of the bridge beams. The errors on the estimates of the percentage of reinforcement are shown in the last column of Table 9.2.

The maximum error in the estimates of percentage of reinforcement in the 16 m span group is only -12.33 % whereas that in the 22 m and 30 m group is +16.17% and -14.74% respectively. It is noted that the first group of 16m long bridge decks consists of relatively new structures whereas the last two groups are combinations of good and damaged bridge decks.

It is also noted that if the Reference Factor β_{LS} used in the calculation is obtained from a set of undamaged structures, assessment in a badly damaged structure gives a

negative error which is on the safe side.

The accuracy on the estimate of steel percentage in the bridge beams is not sensitive to the amount of non-structural stiffness contribution in each bridge deck as seen from Table 9.2. This is probably due to the reduction of the random error in the estimate by including the Reference Factor β_{LS} in the calculation.

Reference Factor β_{LS} varies with the span length of the structure as shown in Table 9.2. This is as expected as the LCC Factor β is calculated based on an uniform distribution of moment of inertia along the beam. In fact, less tensile reinforcement towards the ends of the beams in practice would give a smaller moment of inertia of the beam section. This actual distribution of moment of inertia along the beam length deviates from a straight line assumption. This phenomenon increases with the span length of the structure. However, if all the bridge decks are constructed to the same steel detailing practice, the Reference Factor β_{LS} obtained should be relatively constant for a particular span length.

9.4 THE SOLUTION PATH TO THE PROPOSED METHOD

The solution path to the proposed method is shown diagrammatically in Fig.9.7. The major element of the proposed method is to have a good estimate of I_{est} for the major members of the structure. If the general condition of the bridge deck is required for a structure with known design information, the Structural Damage Factor α is compared to the Reference Factor α_m from the database for a quick assessment. If the LCC of an old bridge deck with no design information is required, The LCC Factor β and the Reference Factor β_{LS} are used to estimate the steel percentage in the major members.

Table 9.1 Details of Prototype Bridge Decks in the Evaluation

	Ni Zi	Zhong Tong Yin Qiao	New Dan Zhu Tau	Yuan Dun 1st, 6th, 7th span	Yuan Dun 3rd, 5th span
Year of construction	1981	1981	1984	1959	1959
Type of foundation	Abutment/pier on caisson				
Support material	rubber bearings			steel bearings	
Overall span (m)	16.0	16.0	16.76	22.16	30.2
Design Span (m)	15.5	15.5	16.24	21.16	29.6
Overall deck width (m)	12.4	12.4	4.5	8.98	8.98
Type of Construction	7T-beams		3T-beam	6T-beams	
Steel Percentage	0.958%	1.175%	1.408%	2.188% (2.576%)	2.585% (2.631%)
No. of diaphragm	5	5	5	9	12
Overall Depth of Beam (mm) (Average)	1200		1200	1250	1800
Width of Beam (mm)	1600	1600	1400	1400	
Width of Rib (mm)	180	180	180~230	220 ~ 270	

Note: Values in bracket indicate the steel percentage after rehabilitation work.

Table 9.2 Steel Percentage Estimate and Factors α, β and β_{LS} of Bridge Decks

Span (m)	Bridge Deck	SD Factor α	LCC Factor β	Reference Factor β_{Ls}	Steel Percentage Estimate	Percentage Error in Estimate
16	Ni Zi (1985) (1st span)	0.869	2.082	2.034	0.984 %	+ 2.73 %
	Ni Zi (2nd span)	0.817	1.960		0.919 %	- 4.08 %
	Zhong Tang Yin Qiao (1st span)	1.012	2.198		1.286 %	+ 9.53 %
	Zhong Tang Yin Qiao (8th span)	1.006	2.131		1.241 %	+ 5.67 %
	New Dan Zhu Tau	1.293	1.818		1.234 %	-12.33 %
22	Yuan Dun (1st span) (before rehab.)	1.115	1.782	1.593	2.541 %	+16.17 %
	Yuan Dun (6th span) (before rehab.)	0.886	1.416		1.883 %	-13.94 %
	Yuan Dun (1st span) (after rehab.)	1.025	1.609		2.614 %	+ 1.45 %
	Yuan Dun (7th span) (after rehab.)	0.960	1.506		2.382 %	- 7.54 %
30	Yuan Dun (3rd span) (before rehab.)	0.661	0.977	1.097	2.204 %	-14.74 %
	Yuan Dun (5th span) (before rehab.)	0.707	1.045		2.416 %	- 6.53 %
	Yuan Dun (3rd span) (after rehab.)	0.709	1.118		2.707 %	+ 2.86 %
	Yuan Dun (5th span) (after rehab.)	0.752	1.186		2.954 %	+12.26 %

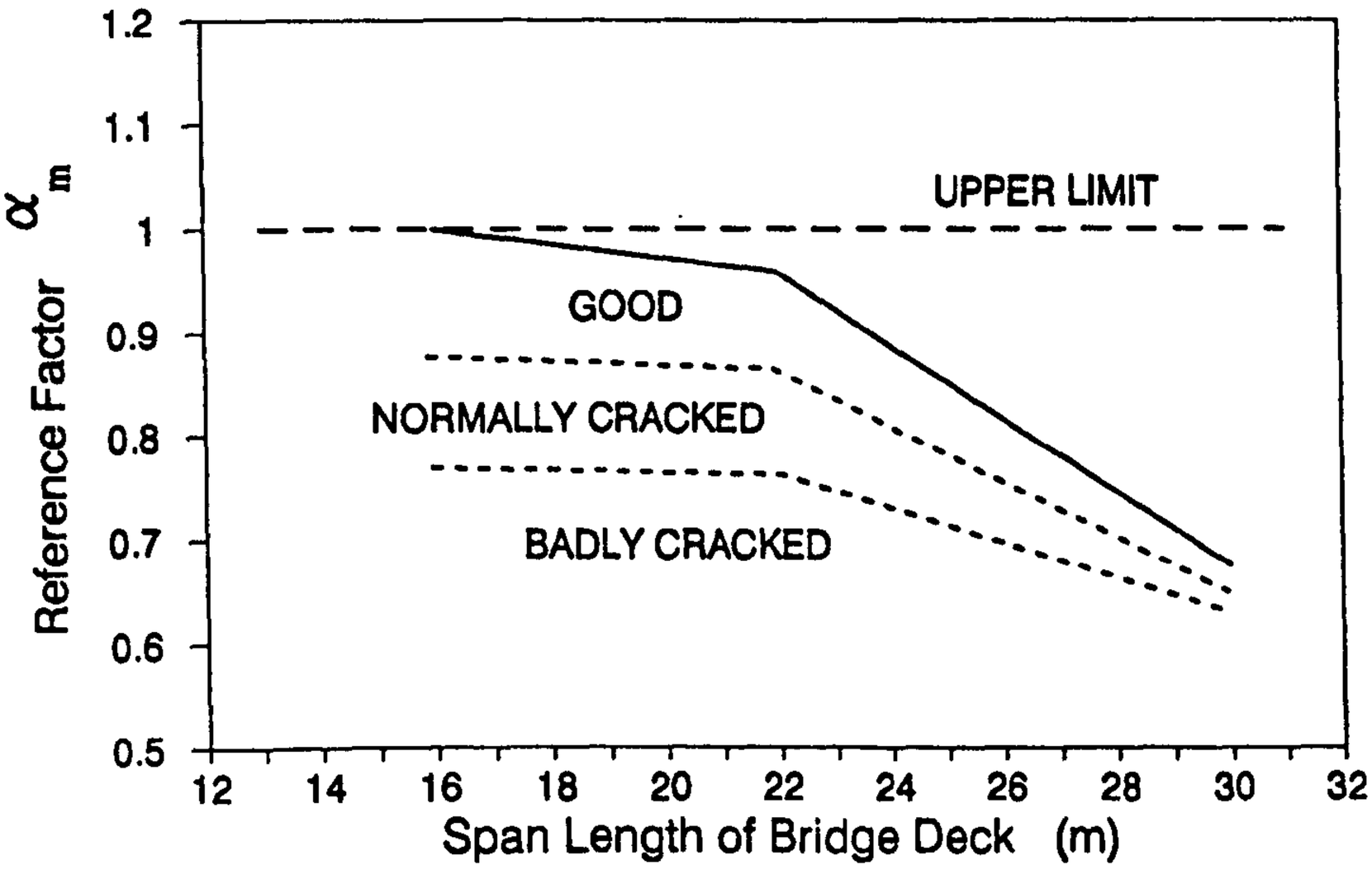

FIG.9.1-Reference Factor α_m for Different Span Length of Beams

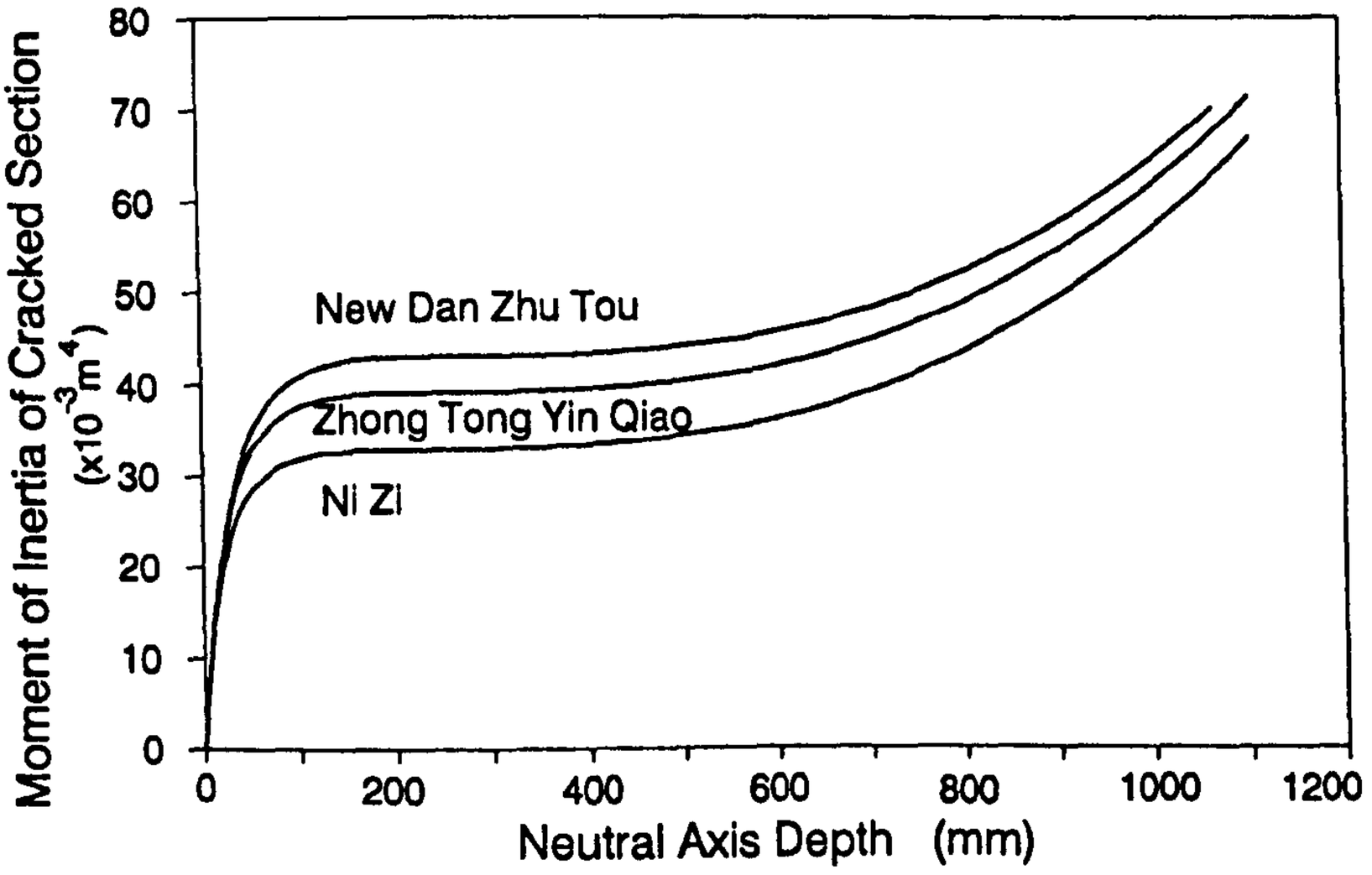

FIG.9.2-Theoretical Cracked Moment of Inertia of Bridge Beam 16m Long

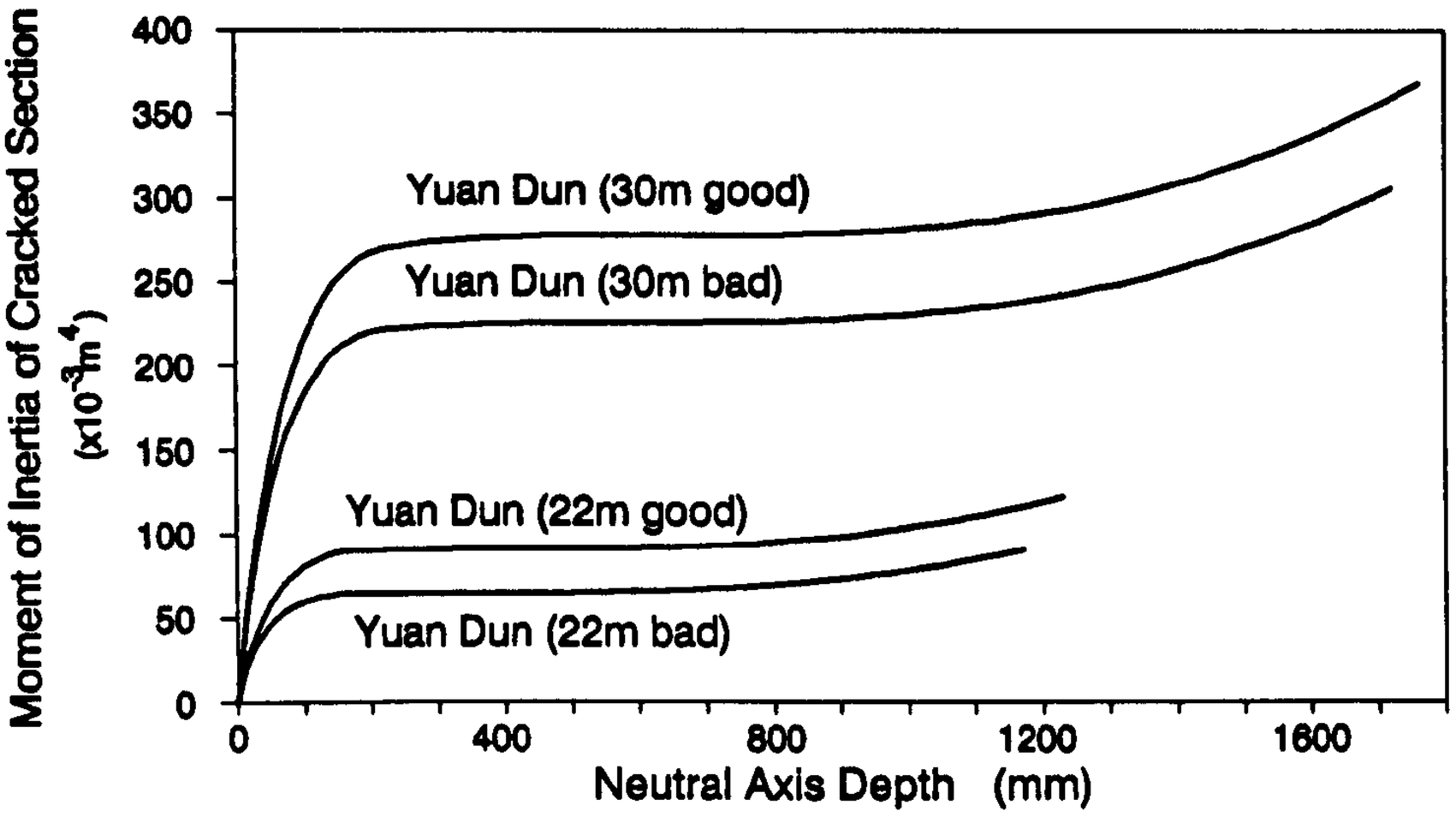

FIG.9.3-Theoretical Cracked Moment of Inertia of Bridge Beam Above 16m Long

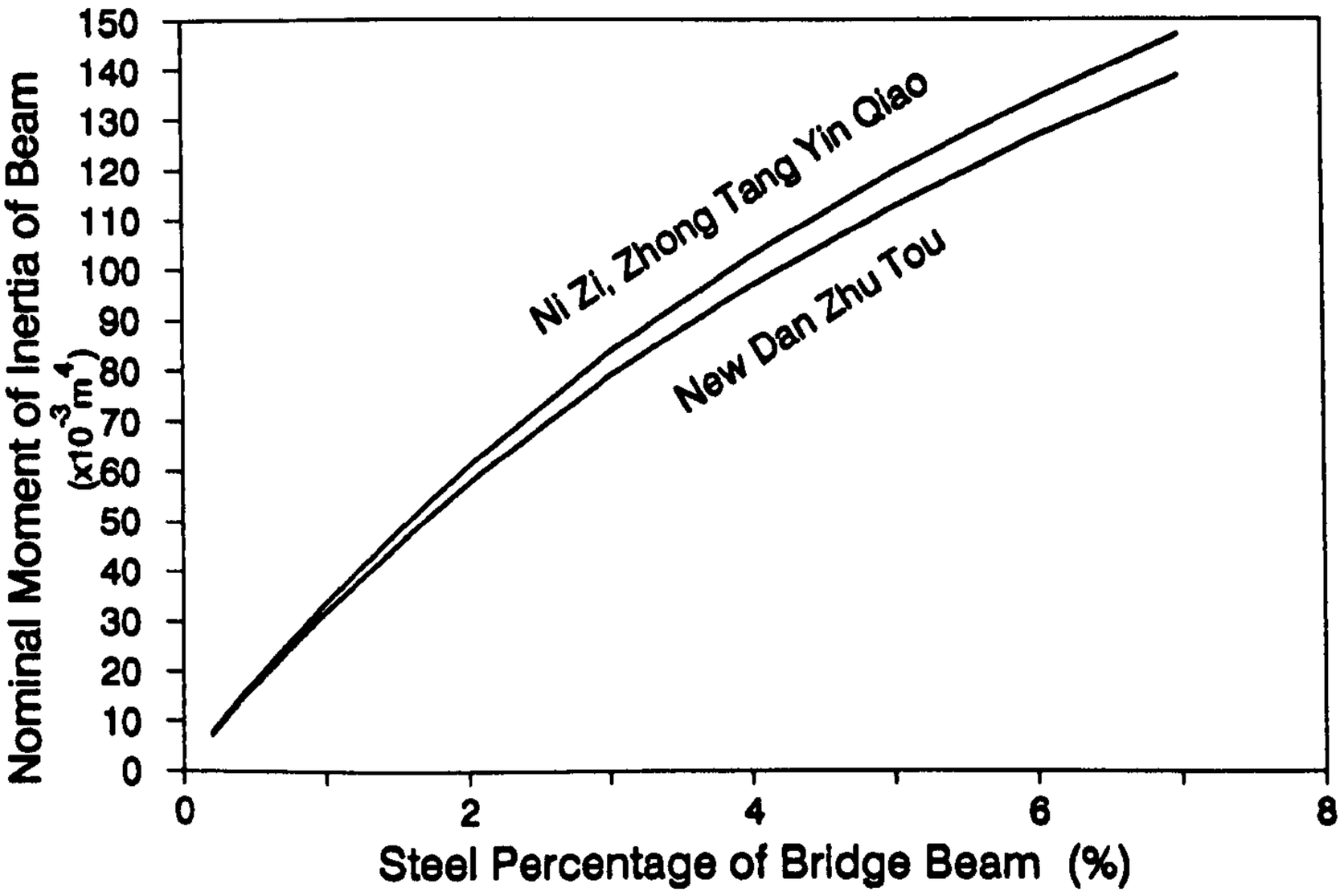

FIG.9.4-Theoretical I_{nom} of 16m Bridge Beams

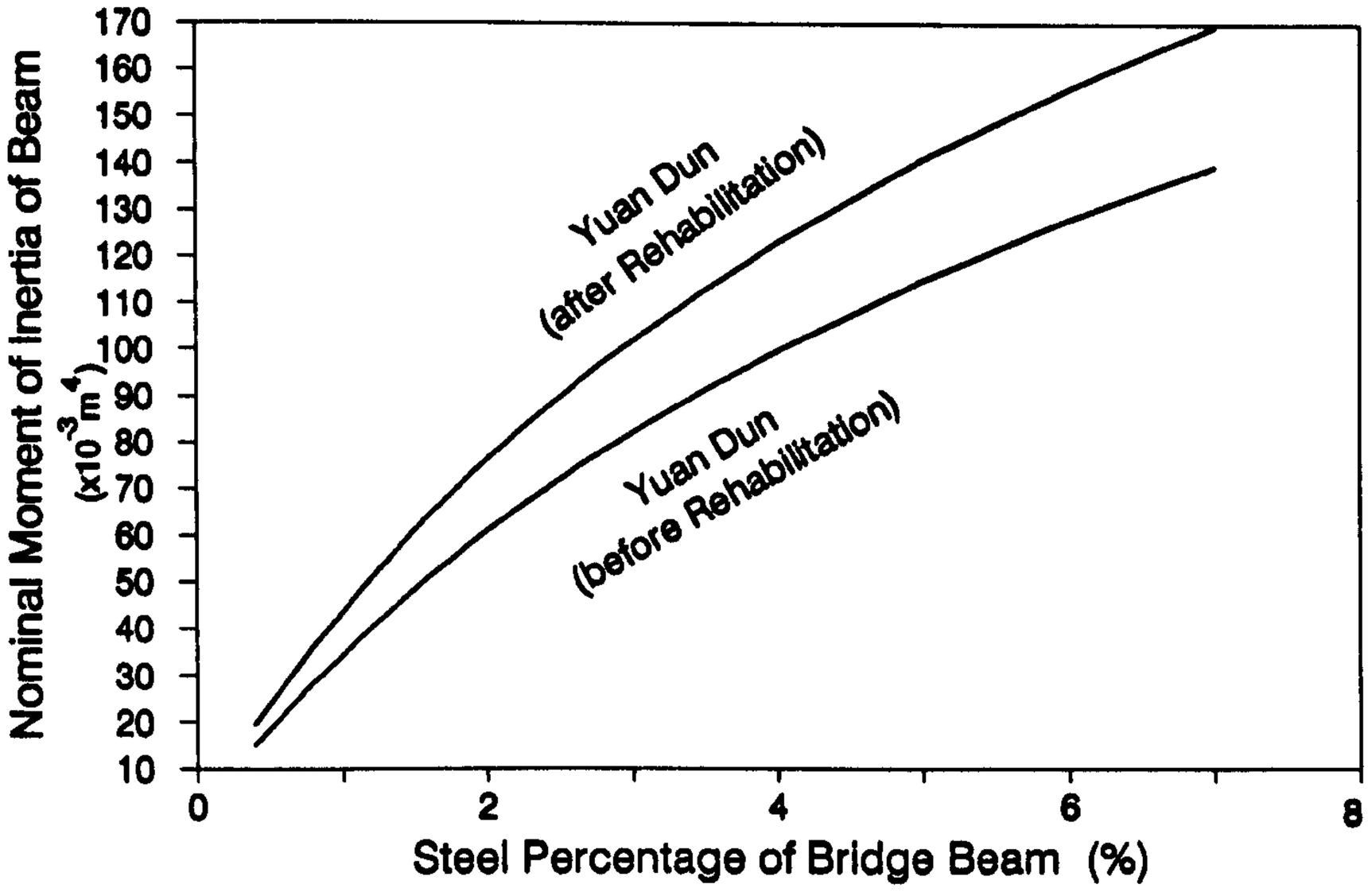

FIG.9.5-Theoretical I_{nom} of 22m Bridge Beams

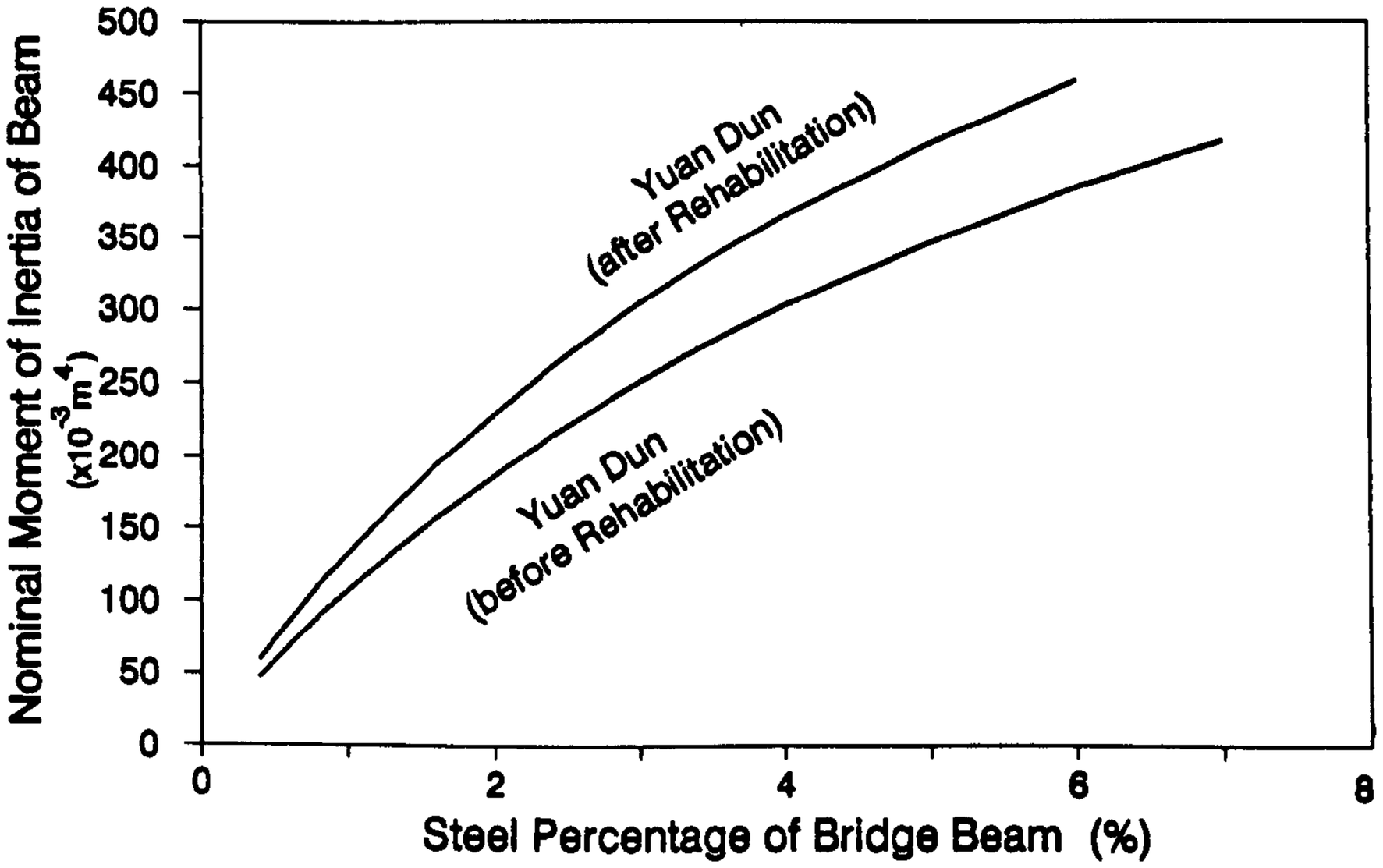

FIG.9.6-Theoretical I_{nom} of 30m Bridge Beams

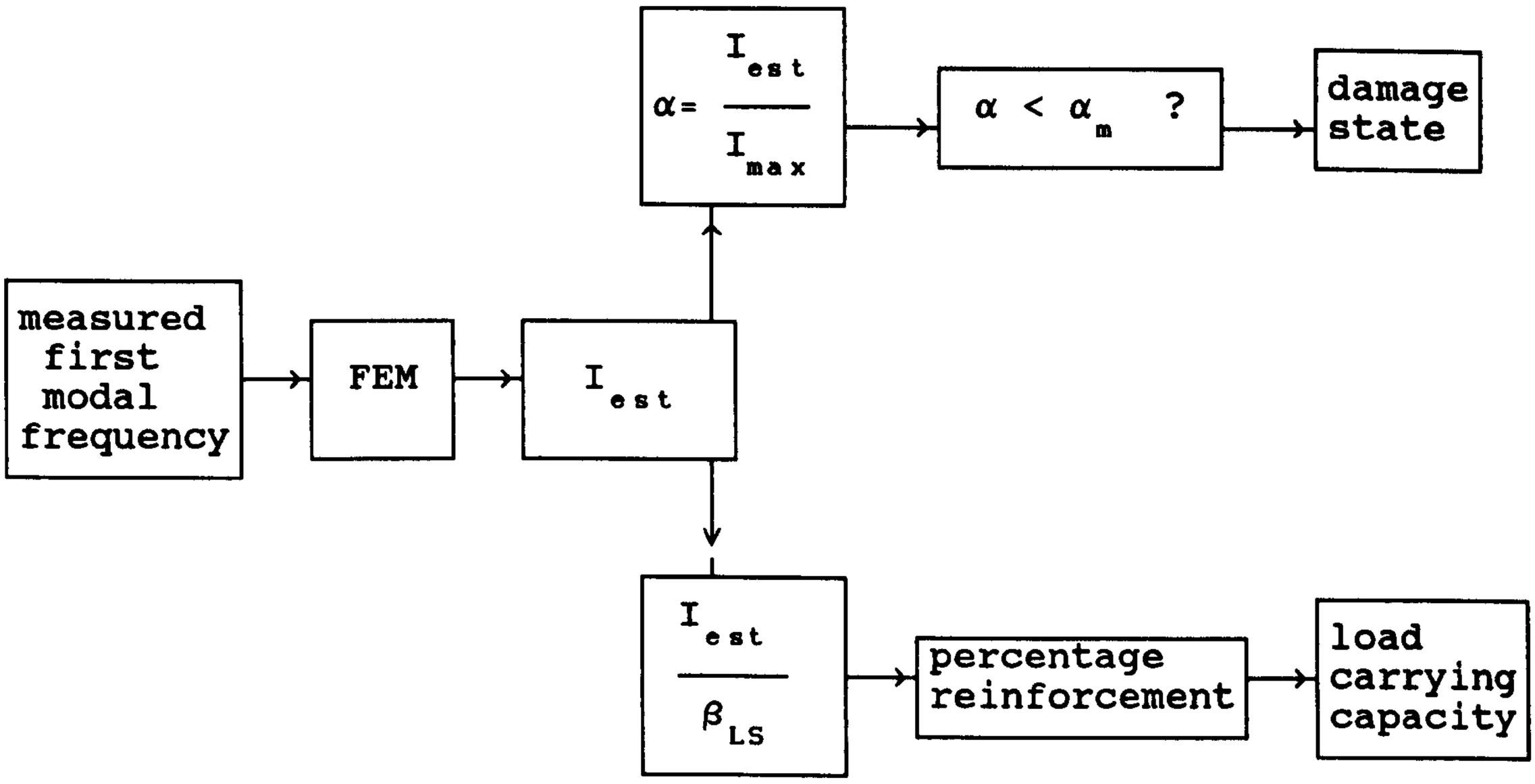

FIG.9.7-Solution Path of the Proposed Strategy

CHAPTER TEN

CONCLUSIONS AND RECOMMENDATIONS

Although simply supported Tee-beam and slab reinforced concrete bridge decks have been selected for this study of damage assessment, the results are applicable to other forms of beam-slab structure.

A 3.2 metre long small scale reinforced concrete bridge deck was tested incrementally to destruction, and the modal frequencies at different stages of damage were obtained. The change in modal frequencies due to cracking in the main beams and diaphragms was found to be small. Further study showed that the moments of inertia of the main beams were fairly constant and were close to the "nominal" value throughout most of the loading range. The transverse load distribution properties of the bridge deck also remained relatively constant throughout the loading range up to yield of the tensile reinforcement in the main beam.

Seventeen full-scale reinforced concrete Tee-beam and slab bridge decks, in which four were classified as dangerous, have been measured for their vibrational response from traffic-generated excitation, and their modal frequencies have been studied.

An optimal finite element model of grillage beams representing the bridge deck has been developed, and the calculation on the effective width of the beam has been studied.

A parametric study on the effects of boundary conditions on the modal frequencies shows that only the stiffness from the non-structural components of fencing and kerbstones has a

large effect on the modal frequencies. However, this effect is greatly reduced after a few years of service. In general their effect can be accounted for by detailed site inspection and careful modelling of details of the components.

10.1 THE DAMAGE DETECTION TECHNIQUE

A damage detection technique based on the measurement of phase angle difference θ_{rs} between the response at two points r and s of a structure has been derived and implemented in the laboratory testing of a steel cantilever beam and a small scale model bridge deck. The accuracy of detecting single area of damage has been established. Narrow-band excitation gives good results in the steel cantilever beam but this is not the case using ambient excitation in the more complicated bridge deck. This may be due to the small signal to noise ratio.

This technique has the limitation of identifying only small changes in stiffness as noted in the damage identification results for the bridge deck with large damage. This is because the formulation of Eqn.(4.32) is based on the first order term of Taylor's series. Inclusion of higher order terms would improve its accuracy. The disadvantage of this technique is the large effort required in calculating the FRF using FFT especially if the identification domain of damage elements is large. Error has been introduced with the omission of the matrix [R] in Eqn.(7.1) but its effect has not been studied further in this work.

The following areas of further research is suggested to prove its general applicability to bridge structures:

1. Conduct further ambient excitation tests;
2. Work on multi-damage detection;
3. Work on a more rational formulation of stiffness of a

damaged structural element;

4. Extend damage detection to other structural elements like membrane element or bending plates element;
5. Work on detection of multi-damage in a single element;
6. The damage is assumed to be invariant with respect to frequency in the original assumption of the technique. This may not be true in the real case, and an adaptive identification algorithm has to be developed to solve Eqn.(4.33);
7. Work on detection of damage which involves both changes in the stiffness and damping of the system.
8. Study on the effect of error due to the omission of matrix [R] in Eqn.(7.1) on the accuracy of this technique.

It is noted that damage identification using FRF, its modulus or the phase difference fails in one or other case. Hence, this technique using phase difference as the observable parameter should be used as part of a programme using different measured parameters.

10.2 METHOD OF CLASSIFICATION OF BRIDGE DECK

When a bridge deck with design information on its steel arrangement, geometry and material properties is suspected of being structural deficient, a Structural Damage (SD) Factor α may be calculated from simulating the measured first modal frequency with a FEM. The relative difference of the SD Factor α and the Reference Factor α_n from the database serve as a good indicator for the condition monitoring of the bridge deck.

A set of Structural Damage (SD) Factors α is calculated for the model bridge deck which shows its effectiveness in quantifying the general condition of the structure at different stages of deterioration, especially between normally cracked and badly cracked states after yielding of

the main reinforcement. The set of SD Factors for the prototype bridge deck also shows fairly consistent values for structures of the same span length.

However, the contribution of non-structural stiffness from fencing and kerbstones has a significant effect on this SD Factor. This effect has to be separated from the structural contribution such that the SD Factor can be used to quantify the cracking condition of the bridge deck. A database containing information of this effect is required.

The SD Factor α has the disadvantage of having a small range for a particular span length of structure. Also it cannot be used to quantify the reduction in stiffness in the transverse diaphragms since such damage has little influence on the first modal frequency of the structure.

10.3 METHOD OF ASSESSMENT OF LOAD CARRYING CAPACITY OF BRIDGE DECKS HAVING NO DESIGN INFORMATION

The proposed method relates the nominal cracked moment of inertia of the reinforced concrete beam to its load carrying capacity. In the case of assessing the load carrying capacity of a bridge deck with no drawings and design information, the nominal moment of inertia of the main beams may be simulated from the measured first modal frequency with a FEM. A LCC Factor β may then be calculated from which the percentage of reinforcement in the main beams is obtained. The load carrying capacity of the bridge deck may then be obtained with further information on the transverse load distribution properties of the bridge deck.

This LCC Factor, unlike the SD Factor, is not sensitive to the effect of non-structural stiffness on the modal frequency. This is advantageous in the identification of the steel percentage of the reinforced concrete beam.

The proposed method has been evaluated against the test

results of the model reinforced concrete bridge deck and a database of seventeen prototype reinforced concrete bridge decks. Good results were obtained with a maximum error in the estimate of steel percentage of -16.2%.

Since any reinforced concrete cross-section exhibits a similar nominal cracked moment of inertia under static load, this method is also applicable to other bridge decks of different beam-slab configurations.

Further research recommended for the improvement of this method would be:

1. Consider other beam-slab type bridge decks;
2. Set up a relationship between the nominal cracked moment of inertia and the LCC of a beam based on the British Bridge Design Code BS5400 (1982);
3. Collect more experimental evidence on the distribution of cracked moment of inertia along a reinforced concrete beam in different stages of cracking.

In fact, a full-scale bridge deck has already been tested to destruction by the author for the study of its dynamic and static behaviour, Law et al (1991a). Vibration signals were recorded at different stages of damage. The tests results are being used for further evaluation of the proposed method.

10.4 CONCLUSION

All the developments presented in this Thesis demonstrate the applicability of the proposed technique and method for the assessment of bridge decks. It would be advisable for these developments to be used as tools in the routine maintenance operation such that they can be improved and developed with more field measurement results.

REFERENCES

Abdel-Ghaffar A M and Housner G W (1978)
"Ambient Vibration Tests of Suspension Bridges", J of Engg Mech, ASCE, EM5, Oct., 1978.

Adams R D, Cawley P, Pye C J and Stone B J (1978)
"A Vibration Technique for Non-Destructively Assessing the Integrity of Structures", J of Mechanical Engg Science, Vol.20, No.2, 1978, pp93-100

Afolabi D (1987)
"An Anti-Resonance Technique for Detecting Structural Damage", Proc of the Fifth Int Modal Analysis Conf, Vol.1, London, England, 1987, pp491-495

Agbabian M S, Masri S F, Traina M I and Waqfi O (1990)
"Detection of Structural Changes in a Bridge Model", Proc of the NATO Advanced Research Workshop on Bridge Evaluation, Repair and Rehabilitation, April, 1990, pp133-143

Agbabian M S, Masri S F, Miller R K and Caughey T K (1991)
"System Identification Approach to Detection of Structural Changes", J of Engg Mech, ASCE, February 1991, pp370-390

Akgun M, Ju F D and Paez T L (1985)
"Transmissibility as a Means to Diagnose Damage in Structures", Proc of the Third Int Modal Analysis Conf, Vol.2, Orlando, Florida 1985, pp701-707

Akgun M and Ju F D (1987a)
"Diagnosis of Multiple Cracks on a Beam Structure", Int J of Analytical and Experimental Modal Analysis, Vol.2, No. 4, October 1987, pp149-154

Akgun M and Ju F D (1987b)
"Diagnosis of Fracture Damage in Frame Structures (A Π-Circuit Analogy)", Int J of Analytical and Experimental Modal Analysis, Vol.2, No. 4, October 1987, pp155-162

Baker G and Edwards A D (1985)
"Numerical Assessment of Existing Concrete Structures", Proc of the Second Int Conf on Civil and Structural Engg Computing, London, 5 Dec. 1985.

Bakht B and Csagoly P F (1981)
"Load Carrying Capacity of Highway Bridges", Third Int Conf on Structural Safety and Reliability, The Norwegian Institute of Technology, Trondheim, Norway June 23-25, 1981

Bakht B and Jaeger L G (1990)
"Bridge Testing - A Surprise Every Time", J of Structural Engg, ASCE, Vol.116, May 1990

Bakht B and Moses F (1990)
"Lateral Distribution Factors for Highway Bridges", J of Structural Engg, ASCE, Vol.114, No. 8, 1990

Bao Z W (1981)
"Random Vibration of Structures", (in Chinese), Chinese J Earthquake Engg and Engg Vibration, September 1981

Beauchamp K and Yuen C K (1979)
"Digital Methods for Signal Analysis", George Allen and Unwin, London, 1979

Beauchamp J C , Chan M Y T and Pion R H (1984)
"Repair and Evaluation of a Damaged Truss Bridge-Lewes, Yukon River", Canadian J of Civil Engg, Vol.1, September 1984

Bendat J S and Piersol A G (1986)
"Random Data Analysis and Measurement Procedures", (Second Edition), John Wiley & Sons, USA, 1986

Billing J R (1984)
"Dynamic Loading and Testing of Bridges in Ontario", Canadian J of Civil Engg, Vol.1, December 1984

Biswas M, Pandey A K and Samman M M (1990a)
"Diagnostic Experimental Spectral/Modal Analysis of a Highway Bridge", The Int J of Analytical and Experimental Modal Analysis, Vol.5, No. 1, January 1990

Biswas M, Pandey A K and Samman M M (1990b)
"Modal Technology for Damage Detection of Bridges", Proc of the NATO Advanced Research Workshop on Bridge Evaluation, Repair and Rehabilitation, April, 1990, pp161-174

Brandon J A (1987)
"Eliminating Indirect Analysis - The Potential for Receptance Sensitivities", Int J of Analytical and Experimental Modal Analysis Vol.2, No. 2, April 1987, pp73-75

BRITISH STANDARDS INSTITUTION (1972)
"Code of practice for the structural use of concrete. CP110: Part 1:1972", November 1972, (withdrawn)

BRITISH STANDARDS INSTITUTION (1982)
"Code of practice for the design of steel bridges. BS5400: Part 3:1982"

BRITISH STANDARDS INSTITUTION (1982)
"Code of practice for the structural use of steelwork in buildings, BS5950 Part 4, 1982"

BRITISH STANDARDS INSTITUTION (1983)
"Method for the Determination of Compressive Strength of Concrete Cubes, BS1881:Part 116:1983"

BRITISH STANDARDS INSTITUTION (1984)
"Code of practice for the design of concrete bridges. BS5400:Part 4: 1984"

BRITISH STANDARDS INSTITUTION (1985)
"Code of practice for the structural use of concrete. BS8110: Parts 1-3, 1985"

BRITISH STANDARDS INSTITUTION (1985)
"Code of practice for the structural use of steelwork in buildings, BS5950 Parts 1 and 2, 1985"

Brown D L, Allemang R J, Zimmerman R and Mergeay M (1976)
"Parameter Estimation Techniques for Modal Analysis", SAE Paper Number 790221, SAE Transactions, Vol.88, 1976, pp828-846

Brownjohn J M W, Dumanoglu A A, Severn R T and Taylor C A (1987)
"Ambient Vibration Measurements of the Humber Suspension Bridge and Comparison with Calculated characteristics", Proc of the Inst of Civil Engineers, Part 2, 1987, Vol.83, Sept., pp561-600

Buckle I G , Dickson A R and Phillips M H (1985)
"Ultimate Strength of Three Reinforced Concrete Highway Bridges", Canadian J of Civil Engg, Vol.12, 1985, pp63-72

Cabrera J (1988)
"Towards a Performance Index for Concrete Bridges", Seminar on Assessment of Reinforced & Prestressed Concrete Bridges, Inst of Structural Engineers, 1988

Cawley P and Adams R D (1979)
"The Location of Defects in Structures from Measurements of Natural Frequencies", J of Strain Analysis, Vol.14, No.2, 1979, pp49-57

Chen J C and Garba J A (1988a)
"Structural Damage Assessment Using a System Identification Technique", Structural Safety Evaluation Based on System Identification Approaches, Vieweg, Braunschweig, FRG, 1988, pp474-492

Chen J C and Garba J A (1988b)
"On-Orbit Damage Assessment for Large Space Structures", AIAA Journal, Vol.26, No. 9, September 1988, pp1119-1126

Chen R Z, Shi G B, Law S S and Ward H S (1990)
"Dynamic Testing of Yuan Dun Bridge Before and After Rehabilitation", (in Chinese), Research Report, Hong Kong Polytechnic, April 1990

Chondros T G and Dimarogonas A D (1989)
"Dynamic Sensitivity of Structures to Cracks", J of Vib, Acoustics, Stress, and Relibility in Design, Vol.111, July 1989, pp251-256

Cole H A Jr (1973)
"On-Line Failure Detection and Damping Measurement of Aerospace Structures by Random Decrement Signature", NASA Cr. 2205, 1973

Coppolino R N (1981)
"A Simultaneous Frequency Domain Technique for Estimation of Modal Parameters from Measured Data", Paper No. 811046, SAE Aerospace Congress and Exposition, October 1981

Deblauwe F, Brown D L and Allemang R J (1987)
"The Polyreference Time Domain Technique", Proc of the Fifth Int Modal Analysis Conf, Vol.2, London, 1987, pp832-845

Dharaneepathy M V (1984)
"Phase Sensitivity to Structural Damages", J of Structural Engg, ASCE, Vol.11, No. 1, April 1984, pp23-32

Douglas B M (1979)
"Experimental Dynamic Response Investigations of Existing Highway Bridges", Proc of a Workshop on Earthquake Resistance of Highway Bridges, January 29-31, 1979, Applied Technology Council.

Fox R L and Kappor M R (1968)
"Rates of Change of Eigenvalues and Eigenvectors", AIAA Journal, Vol.6, No.12, December 1968, pp2426-2429

Flint A R, Smith B W, Baker M J and Manners W (1981)
"The Derivation of Safety Factors for the Design of Highway Bridges", The design of Steel Bridges, Granada, 1981

Grace N F and Kennedy J B (1988)
"Dynamic Response of Two-Span Continuous Composite Bridges", Canadian J of Civil Engineers, Vol.15, No. 4, August 1988

Gu S N, Zhang J L, Jiang J S and He C A (1989)
"A Vibration Diagnosis Approach to Structural Fault", J of Vibration, Acoustics, Stress, and Reliability in Design, Transactions, ASME, Vol.111, January 1989, pp88-93

Guyan R J (1965)
"Reduction of Stiffness and Mass Matrices", AIAA Journal Vol.3, No. 2, February 1965

Hajela P and Soeiro F J (1990a)
"Recent Developments in Damage Detection Based on System Identification Methods", Structural Optimization, 2, No. 1, 1990, pp1-10

Hajela P and Soeiro F J (1990b)
"Structural Damage Detection Based on Static and Modal Analysis", AIAA Journal, 28, No. 6, June 1990, pp1110-1115

Han J B and Yang J Y (1987)
"Identification of Physical Parameters with A Combined Algorithm of Least-Squares Stochastic Approximation", Proc of the Fifth Int Modal Analysis Conf, Vol.1, London, England, 1987

He G Y (1987)
"System Identification", (in Chinese) Beijing University of Aeronautics and Astronautics Press, 1987

He J and Ewins D.J (1986)
"Analytical Stiffness Matrix Correction Using Measured Vibration Modes", Int J Analytical and Experimental Modal Analysis, 1 (3), 9-14, July 1986

Hearn G and Testa R B (1991)
"Modal Analysis for Damage Detection in Structures", J of Structural Engg, ASCE, Vol.117(10) 1991, pp3042-3063

Hudson D E (1977)
"Dynamic Tests of Full-scale Structures", J of the Engg Mech Division, ASCE, Vol.103, No. EM6, December 1977.

Hui G P and Zhong J Y (1987)
"External Prestressing in the Strengthening of Yuan Dun Bridge", (in Chinese), Highway Management Office of Guangdong Province of China, The People's Republic of China, July 1987

Ibrahim S R and Mikulcik E C (1973)
"A Time Domain Modal Vibration Test Technique", The Shock and Vibration Bulletin, Bulletin 43, June 1973, pp21-37

Ibrahim S R and Mikulcik E C (1976)
"The Experimental Determination of Vibration Parameters from Time Responses", The Shock and Vibration Bulletin, Bulletin 46, August 1976, pp187-196

Ibrahim S R (1977)
"Random Decrement Technique for Modal Identification of Structures", J of Spacecraft and Rockets, (AIAA), Vol.14, No.11, 1977, pp696-700

Ibrahim S R and Mikulcik E C (1977)
"A Method for The Direct Identification of Vibration Parameters from the Free Response", The Shock and Vibration Bulletin, Bulletin 47, September 1977, pp183-198

Ibrahim S R (1978)
"Modal Confidence Factor in Vibration Testing", J of Spacecraft and Rockets (AIAA), Vol.15, Sept.-Oct. 1978, pp313-316

Ibrahim S R and Pappa R S (1982)
"Large Modal Survey Testing Using the Ibrahim Time Domain Identification Technique", J of Spacecraft and Rockets (AIAA), Vol.19, No.5, Sept.-Oct. 1982, pp459-465

Jackson P A (1990)
"The Global and Local Behaviour of Bridge Deck Slabs", J of The Inst of Structural Engineers, Vol.68, No.6, March 1990

Jeary A P and Ellis B R (1984)
"Non-Destructive In-situ Testing using Dynamic Techniques", Proc of the Third Int Conf on Tall Building, 10-15 Dec., 1984, Hong Kong and Guangzhou, China.

Ju F D, Akgun M, Wong E T and Lopez T L (1984)
"Modal Method in Diagnosis of Fracture Damage in Simple Structures", Random Vibrations, AMD-Vol.65, The Winter Annual Meeting of ASME, December 1984, pp113-125

Ju F D and Mimovich M E (1987)
"Experimental Diagnosis of Fracture Damage in Structures by the Modal Frequency Method", Modal Testing and Analysis, DE-Vol.3, The ASME Design Technology Conferences - 11th Biennial Conf on Mechanical Vibration and Noise, September 1987, pp29-36

Ju J H and Xu Z D (1989)
"The Multi-Terms Sensitivity Analysis of Structure Modification", Proc of the Seventh Int Modal Analysis Conf, 1989, pp584-588

Juang J N and Pappa R S (1984)
"An Eigensystem Realization Algorithm (ERA) for Modal Parameter Identification", JPL Workshop on Identification and Control of Flexible Space Structures, Pasadena, CA, June 1984, pp299-318

Kato M and Shimada S (1986)
"Vibration of PC Bridge During Failure Process", J of Structural Enginering, ASCE, Vol 112, No. 7, July 1986

Kenley R M and Dodds C J (1980)
"West Sole WE Platform : Detection of Damage By Structural Response Measurements", Twelve Annual Offshore Technology Conf, Houston, Texas, May 5-8, 1980.

Kennedy C C and Pancu C D P (1947)
"Use of Vectors in Vibration Measurement and Analysis", J of Aeronautical Sciences, Vol.14, No.11, 1947, pp603-625

Kim J H, Jeon H S and Lee C W (1992)
"Applications of the Modal Assurance Criteria for Detecting and Locating Structural Faults", Proc of the Tenth Int Modal Analysis Conf, February 1992

Kinnier K H and McKeel W T Jr. (1965)
"Substructure Influence on Dynamic Stress Response of Superstructures in Composite Bridges", Highway Research Record Number 103, Bridges and Structures, Highway Research Board, 1965

Lauer K R (1991)
"State of the Art Report: The use of Damage Classification Systems for Concrete Structures", Proc of the Int RILEM-IMEKO Conf on Diagnosis of Concrete Structures, ed. T. Jávaor, Expertcentrum Czechoslovakia, 1991

Law S S, Li X, Shi G B, Chen R Z, Liao H L and Ward H S (1990a)
"Destructive Test of a Model Reinforced Concrete Tee-Beam Bridge Deck and Dynamic Measurements in the Different Stages of Damage", Research Report, Civil & Structural Engg Department, Hong Kong Polytechnic, August 1990

Law S S, Li X and Ward H S (1990b)
"A Vibration Diagnosis Technique for Structural Stiffness Identification", Proc of the Int Conf on Vibration Problems in Engg, June 1990, Wuhan-Chongqing, China

Law S S, Shi G B, Chen R Z and Ward H S (1990c)
"Full Scale Dynamic Tests on 29 Simply Supported Reinforced Concrete Bridge Decks and Study on Vibrational Parameters for Damage Assessment", Research Report, Civil & Structural Engg Department, Hong Kong Polytechnic, June 1990

LAW S S and Kai C K (1991)
"On the Development of Two Datalogging Programmes", Proc of the Fourth Int Congress on Material Strength and Reliability, Beijing, October 1991

Law S S, Shi G B, Chen R Z and Ward H S (1991a)
"Full Scale Destructive Test of Reinforced Concrete Bridge - Rong Xing Bridge and Dynamic Measurements in the Different Stages of Damage", Research Report, Civil & Structural Engg Department, Hong Kong Polytechnic, September 1991

Law S S, Ward H S, Waldron P and Taylor C A (1991b)
"Condition Monitoring of a Model Reinforced Concrete Bridge Deck in its Failure Process", Int Workshop on Technology for Hong Kong Infrastructure Development, Hong Kong, December 1991

LAW S S (1992)
"User's Manual of A Dual Channel Spectral Analysis Programme", Research Report, Civil & Structural Engg Department, Hong Kong Polytechnic, January 1991

Leonard D R (1974)
"Dynamic Tests on Highway Bridges - Test Procedures and Equipment", TRRL Laboratory Report 654, 1974.

Li G H and Si D (1987)
"Transverse Load Distribution Computation of Highway Bridge Deck", (in Chinese), Second edition, People's Transportation Publisher, 1987

Liang R Y, Hu J L and Choy F (1992)
"Theoretical Study of Crack-Induced Eigenfrequency Changes on Beam Structures", J of Engg Mech, ASCE, 118 (2), 1992, pp384-396

Lim T W (1991a)
"Structural Damage Detection Using Modal Test Data", AIAA Journal, Vol.29, No.12, 1991, pp2271-2274

Lim T W (1991b)
"Analytical Model Improvement Using Measured Modes and Submatrices", AIAA Journal, Vol.29, No.6, June 1991

Lock G P D and Jones A W (1976)
"The Detection of Failures in Off-shore Structures by Vibration Analysis, A Feasibility Study", IMech E Conf Publications 1976-2, The Interpretation of complex Signals from Mechanical System, 24 Feb., The Institution of Mechanical Engineers, 1976

Luk Y W (1987)
"Identification of Physical Mass, Stiffness and Damping Matrices Using Pseudo-Inverse", Proc of the Fifth Int Modal Analysis Conf, Vol.1, London, England, 1987

Mannan M A and Richardson M H (1990)
"Detection and Location of Structural Cracks using FRF Measurements", Proc of the Eighth Int Modal Anal Conf, Vol.1, 1990, pp652-657

Masri S F, Miller R K, Saud A F and Caughey T K (1987a)
"Identification of Nonlinear Vibrating Structures: Part I-Formulation", J of Applied Mech, Trans of ASME, Vol.54, No.4, 1987, pp918-922

Masri S F, Miller R K, Saud A F and Caughey T K (1987b)
"Identification of Nonlinear Vibrating Structures: Part II-Applications", J of Applied Mech, Trans of ASME, Vol.54, No.4, 1987, pp923-929

Mazurek D F and DeWolf J T (1990)
"Experimental Study of Bridge Monitoring Technique", J of Structural Engg, ASCE, Vol.116, No. 9, 1990

McClure R M and West H H (1984)
"Full-scale Testing of a Prestressed Concrete Segmental Bridge", Canadian J of Civil Engg Vol.11, 1984, pp505-515

McLamore V R, Hart G C and Stubbs I R (1971)
"Ambient Vibration of Two Suspension Bridges", J of the Structural Division, ASCE, ST10, Oct., 1971.

Minami T (1987)
"Stiffness Deterioration Measured on a Steel-Reinforced Concrete Building", Earthquake Engg and Structural Dynamics, Vol.15, No.6, August 1987

Ministry of Communications (1986)
"*Technical Specification for Highway Maintenance, JTJ073-85, 1986*", (in Chinese), The People's Communication Publishing House, Beijing, 1986

Mitsuru I, Fu K S and Yao T P J (1983)
"*Rule-Base Damage Assessment System for Existing Structures*", Solid Mech Archieves, Vol.8, 1983 pp99-118

Moody J R and Mansell D S (1980)
"*Dynamics Interaction of Bridge Bearings, Superstructure and Loads*", Proc of Australia Conf on the Mech of Structures and Materials, Nedlands, May 12-14, 1980.

Natke H G and Yao T J P (1988)
"*System Identification Approaches in Structural Safety Evaluation*", Structural Safety Evaluation Based on System Identification Approaches, Vieweg, Braunschweig, FRG, 1988, pp460-473

Natke H G and Cempel C (1991)
"*Fault Detection and Localisation in Structures: A Discussion*", Mech. Systems and Signal Processing 1991, 5(5), pp345-356

Oehler L T (1957)
"*Vibration Suspectibilities of Various Highway Bridge Types*", J of the Structural Division, ASCE, Vol.83, ST4, July 1957.

Orr M F Jr (1990)
"*Eigenvector Derivatives for Analytical Model Improvement*", Proc of the Eighth Int Modal Analysis Conf, Vol.2, 1990

Otnes R K and Enochson L (1978)
"*Applied Time Series Analysis*", Wiley and Sons, New York, 1978

Pandey A K, Biswas M and Samman M M (1991)
"*Damage Detection from Changes in Curvature Mode Shapes*", J of Sound and Vibration (1991) 145(2), 321-332

Papaeconomou N and Dimarogonas A (1989)
"*Vibration of Cracked Beams*", Computational Mech, Vol.5, 1989, pp88-94

Park Y S, Park H S and Lee S S (1988)
"*Weighted-Error-Matrix Application to Detect Stiffness Damage by Dynamic-Characteristic Measurement*", Int J of Analytical and Experimental Modal Analysis Vol.3, No. 3, July 1988, pp101-107

Project Report (1986)
"*Report on Load Test of Yuan Dun Bridge*", (in Chinese), Transport Department of Guangdong Province of China and Chongqing Institiute of Transport, June 1986

Qi G Z, Yang J C S, Kan C D and Bedewi H E (1990)
"A New System Identification Technique for On-Line Nondestructive Evaluation", Intelligent Structures, K.P. Chong, et. (ed). Elsevier Applied Science 1990, pp368-387

Qian G L, Gu S N and Jiang J S (1990a)
"A New Approach for Vibration Monitoring and Fault Diagnosis", (in Chinese), Acta Mechanica Solida Sinica, Vol.11, No. 3, September, 1990, pp217-228

Qian G L, Gu S N and Jiang J S (1990b)
"The Dynamic Behaviour and Crack Detection of a Beam with a Crack", J of Sound and Vibration, Vol.138, No. 2, 1990, pp233-243

Report YC4-4/1978 (1982)
"Testing Method on Long Span Reinforced Concrete Bridge Deck", (in Chinese), Ministry of Transport, The People's Republic of China, 1982

Richardson J A and Douglas B M (1987)
"Identifying Frequencies and Three-Dimensional Mode Shapes from a Full Scale Bridge Test", Proc of the Fifth Int Modal Analysis Conf, Vol.1, London, England, 1987

Rizos P F and Aspragathos N (1990)
"Identification of Crack Location and Magnitude in a Cantilever Beam from the Vibration Modes", J of Sound and Vibration, Vol.138, No. 3, 1990, pp381-388

Roemer M J and Mook D J (1990)
"Robust Time-Domain Identification of Mass, Stiffness, and Damping Matrices", Proc of the Eighth Int Modal Analysis Conf, Vol.2, 1990

Rowe R E (1962)
"Concrete Bridge Design", C.R. Books, 1962

Salane H J, Baldwin J W Jr and Duffield R C (1981)
"Dynamics Approach for Monitoring Bridge Deterioration", Transportation Research Record 832, 1981

Salane H J and Baldwin J W (1990)
"Changes in Modal Parameters of a Bridge During Fatigue Testing", Experimental Mech, June 1990

Samman M M, Biswas M and Pandey A K (1991)
"Employing Pattern Redognition for Detecting Cracks in a Bridge Model", Int J of Analytical and Experimental Modal Analysis 6(1) pp35-46, Jan.1991, pp35-44

Sanayei M and Onipede O (1991)
"Damage Assessment of Structures Using Static Test Data", AIAA Journal, Vol.29,No.7, July 1991, pp1174-1179

Sanayei M and Scampoli S F (1991)
"Structural Element Stiffness Identification from Static Test Data", J of Engg Mech, ASCE, Vol.117, No.5, May 1991, pp1021-1036

Scanlon A and Mikhailovsky L (1987)
"Full-Scale Load Test of Three-Span Concrete Highway Bridge", Canadian J of Civil Engg, Vol.14, 1987

Schiff A J (1972)
"Identification of Large Structure Using Data from Ambient and Low Level Excitations", System Identification of Vibrating Structures, Mathematical Models from Test Data, 1972 Winter Annual Meeting of The ASME

Shahrivar F and Bouwkamp J G (1980)
"Damage Detection in Offshore Platforms using Vibrations Information", Proc of 3rd Offshore Mech and Arctic Engg Symposium Vol.2, New Orleans Louisiania 1980, ASME

Springer W T, Lawrence K L and Lawley T J (1988)
"Damage Assessment Based on the Structural Frequency-Response Function", Experimental Mech Vol.28, No. 1, March 1988, pp34-37

Staalduinen P C and Brederode P J (1987)
"Dynamic Testing of Offshore Structures", Proc of Internatinal Conf on Structural Faults and Repairs Vol.1, 7-9 July 1987, University of London

Stahle C V Jr (1962)
"Phase Separation Techniques for Ground Vibration Testing", Aerospace Engg, 1962, pp56-57 and 91

STANDARD JT/GQB011-73 (1973)
"Standard Drawing on Highway Structures - Precast Concrete Tee-Beam Bridge", (in Chinese), The First Highway Engg Design Office, Ministry of Transport, The People's Republic of China, September 1973

STANDARD JTJ023-85 (1985)
"Design Standard on Reinforced and Prestressed Concrete Highway Structures", (in Chinese), Ministry of Transport, People's Republic of China, May 1985

Stroud R C (1985)
"Excitation, Measurement and Analysis Methods for Modal Testing Combined Experimental/Analytical Modelng of Dynamic Structural Systems", presented at the Joint ASCE/ASME Mech Conf, Albuquerque, New Mexico, sponsored by The Applied Mech Division, ASME, AMD-Vol.67, June 24-26, 1985, pp49-78

Stubbs N (1985)
"A General Theory of Non-Destructive Damage Detection in Structures", Structural Control, Proceedings of the Second Int Symposium on Structural Control, Nijhoff, Dordrecht, The Metherlands, 1985, pp694-713

Stubbs N and Osegueda R (1990)
"Nondestructive Construction Error Detection in Large Space Structures", AIAA Journal, Vol.28, No. 1, January 1990, pp146-152

Tai W H, Kung D N and Yang J C S (1988)
"Application of System Identification Technique to Damage Detection and location in Offshore Platform", Proc of the Seventh Int Conf on Offshore Mech and Arctic Engg, Houstonk Texas, February 1988

Tilly G P (1990)
"Evaluation of Bridges - European Perspective", Bridge Evaluation, Repair and Rehabilitation, ed. Andrzej S. Nowak, Kluwer Academic Publishers, 1990

Toner W (1992)
"Private Communication with S S Law", University of Bristol, April 1992

Tongi University (1980)
"Bridge Superstructures", (in Chinese), People's Transportation Publishing House, Beijing, 1980

Tsai T, Yang J C S and Chen R Z (1985)
"Detection of Damages in Structures by the Cross Random Decrement Method", Proc of the Third Int Modal Analysis Conf, Orlando, Florida 1985, Vol.2

Vandeurzen U, Leuridan J and Doucet Y (1987)
"Structure Monitoring Using a Diagnosis Technique Based on Combined Use of FEA and Test", Proc of the Fifth Int Modal Analysis Conf, Vol.2, London, England, 1987

Vandiver J K (1975)
"Detection of Structural Failure on Fixed Platforms By Measurement of Dynamic Response", Seventh Annual Offshore Technology Conf in Houston, Texas, May 5 8, 1975.

Vold H and Rocklin G E (1982)
"The Numerical Implementation of a Multi-Input Modal Estimation Method for Minicomputers", Proc of the First Int Modal Analysis Conf, pp542-548, Orlando, Florida, 1982

Wang B P (1991)
"Improved Approximate Methods for Computing Eigenvector Derivatives in Structural Dynamics", AIAA Journal, Vol.29, No. 6, 1991

Wang W J and Zhang A (1987)
"Structural Failure Diagnosis and Monitoring by Sensitive Vibration Characters", (in Chinese), Astronautica Sinica, Vol.8, No. 3, March 1987, ppA138-A144

Wang W J (1987)
"Sensitivity Analysis in Fault Vibration Diagnosis of Structures", Proc of the Fifth Int Modal Analysis Conf, Vol.1, London, England, 1987, pp496-501

Ward H S (1984)
"Traffic Generated Vibration and Bridge Integrity", J of Structural Engg, ASCE, Vol.110, No. 10, Oct., 1984.

Ward H S, Law S S, Shi G B and Chen R Z (1987)
"Dynamic Bridge Characteristics from Traffic Loading", Proc of the First National Structural Engg Conf 1987 Melbourne 26-28 August 1987

Watstein D (1953)
"Effect of Straining Rate on the Compressive Strength and Elastic Properties of Concrete", J of the American Concrete Inst, Vol.24, No.8, April 1953.pp729-744

Wojnarowskim E, Stiansen S G and Reddy N E (1977)
"Structural Integrity Evaluation of a Fixed Platform using Vibration Criteria", Proc of the Ninth Annual Offshore Technology Conf in Houston, Texas, May 2-5, 1977

Wolf W L (1987)
"Eigenvalue Sensitivity Derivatives for General Structural Systems", Proc of the Fifth Int Modal Analysis Conf, Vol.2, London, England, 1987

Wolf W L (1988)
"Eigenvalue and Eigenvector Derivatives for General Structural Systems", Proc of the Sixth Int Modal Analysis Conf, 1988

Wolff T and Richardson M (1989)
"Fault Detection in Structures from changes in Their Modal Parameters", Proc of the Seventh Int Modal Analysis Conf, 1989, pp87-94

Zhang J L, Jiang J S, He C A and Gu S N (1990)
"A Structural Fault Vibration Diagnosis Method", (in Chinese), Chinese J of Applied Mech, Vol.7, No.1, March 1990, pp74-82

Zhang S D (1984)
"Design Theory on Bridge Beams - Transverse Load Distribution, Curve Bridge, Effective Width and Shear Lag", (in Chinese), People's Transportation Publishing House, , Beijing, 1984

APPENDIX 5.1

THE EFFECTIVE WIDTH OF A BRIDGE BEAM IN A GRID STRUCTURE

A5.1.1 SECTIONAL PROPERTIES OF A TEE-BEAM SECTION

Notation of cross-section parameters is given in Fig.A5.1.

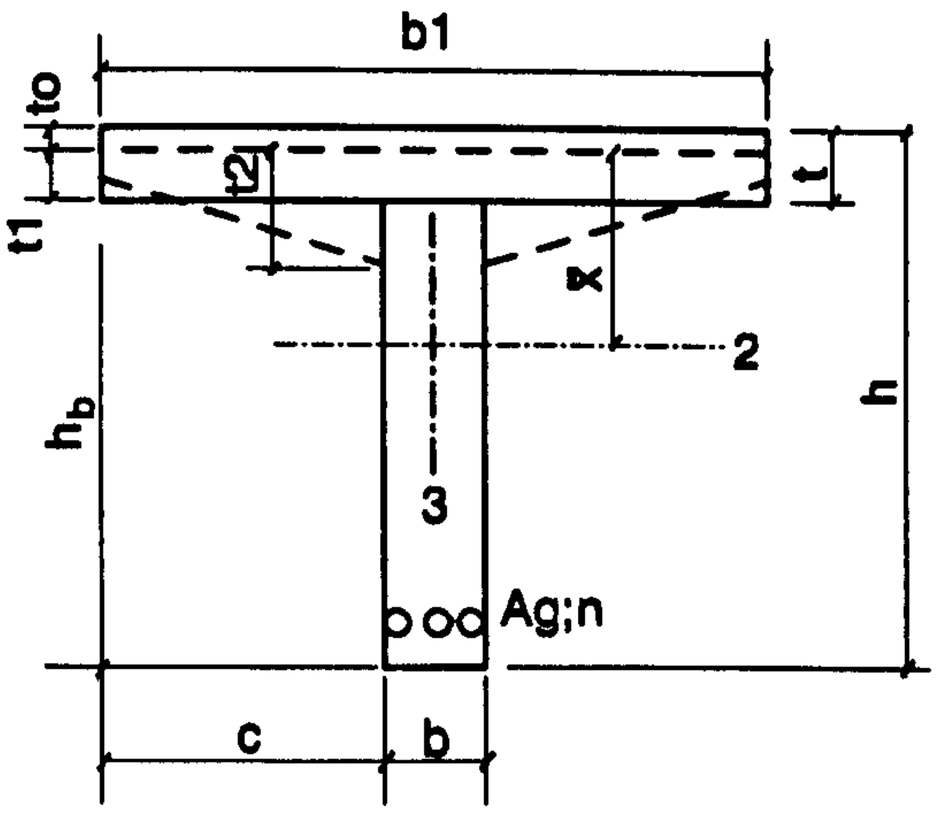

FIG.A5.1-Notation for the Cross-section Parameters

Axial area $$A_1 = b_1 t + b(h-t) + n A_g \qquad \text{(A5.1.1)}$$

where n is the modular ratio

Shear area $$S_2 = S_3 = \frac{A_1}{K} \qquad \text{(A5.1.2)}$$

$$\text{where } K = \frac{12 + 11\mu_1}{10\ (1 + \mu_1)} \qquad \text{(A5.1.3)}$$

and μ_1 is the Poisson's Ratio

Neutral Axis depth

$$\bar{x} = \frac{1}{2} \cdot \frac{(b_1 - b)t^2 + bh^2 + 2nA_g h_b}{(b_1 - b)t + bh + nA_g} \qquad \text{(A5.1.4)}$$

Moment of Inertia

$$I_2 = \frac{b_1 \bar{x}^3}{3} - \frac{(b_1-b)(\bar{x}-t)^3}{3} + \frac{b(h-\bar{x})^3}{3} + nA_g(h_b-\bar{x})^2 \qquad \text{(A5.1.5)}$$

$$I_3 = \frac{tb_1^3}{12} + \frac{(h-t)b^3}{12} \qquad \text{(A5.1.6)}$$

Ignoring the effect of reinforcement, the torsional Moment of Inertia is

$$I_t = C_1 b_1 t^3 + C_2 (h-t) b^3 \qquad \text{(A5.1.7)}$$

where $C_1 = \frac{1}{3} \cdot [1-0.630\ (\frac{t}{b_1}) + 0.052\ (\frac{t}{b_1})^5]$ (A5.1.8)

$$C_2 = \frac{1}{3} \cdot [1-0.630\ (\frac{b}{h-t}) + 0.052\ (\frac{b}{h-t})^5] \qquad \text{(A5.1.9)}$$

Section Modulus

at centroid of tension steel $W_2 = \frac{I_2}{h_0 - x}$ (A5.1.10)

at edge of flange $W_3 = \frac{I_3}{(b_1/2)}$ (A5.1.11)

A5.1.2 CALCULATION OF EFFECTIVE WIDTH OF BEAM

The calculation for the effective width b_1 of the flange in the Tee-beam is as follows. Details on the theory can be found in Zhang (1984) and Rowe (1962).

Let L′ be the distance between the ribs of two adjacent beams, b_1' the distance between adjacent diaphragms, and c the overhang of the flange of the precast beam as shown in Fig.A5.1, given by

$$c = 0.5\ (b_1' - b) \qquad \text{(A5.1.12)}$$

Calculate the ratio c/L' from which the value of λ can be found from Table 3.2 taken from Tongji (1980).

The effective width of the flange in a Tee-beam is

$$b_1 = 2\lambda + b \qquad \text{(A5.1.13)}$$

The effective width calculated by this method is close to the values given by the Chinese Design Standard JTJ023-85 (1985) and British Bridge Design Standard BS5400:Part4 (1984). The appropriate clauses are listed in A5.1.3.

A5.1.3 REFERENCE STANDARDS

Standard JTJ023-85: Clause 4.50

The width of the Tee-beam to be used in calculation should be the smallest of the following three values:

1. One-third of the design span of beam.
2. Distance between centroid of adjacent beams.
3. b + 2c + 12t

   where b is the thickness of web,

   c is the horizontal distance of haunch in beam

   t is the thickness of flange

BS5400: Part 4: Clause 6.3.1.2

In the absence of any more accurate determination the effective flange width for a Tee-beam should not exceed the lesser of:

the width of the web plus one-fifth of the distance between the points of zero moment, or the actual flange width.

For an L-beam, the effective flange should not exceed the lesser of:

the width of the web plus one-tenth of the distance between points of zero moment, or the actual width of the flange.

The effective width calculated by Eqn.(A5.1.13) is used in this Thesis.

Table 3.2 Parameter λ in Effective Width Calculation

from Tongji (1980)

c/L′	λ/c
0.05	0.983
0.10	0.936
0.15	0.867
0.20	0.789
0.25	0.710
0.30	0.635
0.35	0.568
0.40	0.509
0.45	0.459
0.50	0.416

APPENDIX 6.1

LIMITING DESIGN REQUIREMENTS FOR A BRIDGE DECK TO CODE OF PRACTICE JTJ023-85

A6.1.1 THE STRENGTH CRITERION

Clauses 4.1.6 and 4.1.7 of the Bridge Design Standard JTJ023-85 (1985) give a formula for the calculation of the moment capacity of a rectangular or Tee-beams at the ultimate limit state. The moment of resistance is calculated by the following formula:

$$M_j \leq \frac{1}{\gamma_c} R_a b \bar{x} (h_o - \frac{\bar{x}}{2}) + \frac{1}{\gamma_s} R'_g A'_g (h_o - a'_g) \qquad \text{(A6.1.1)}$$

The neutral axis position is calculated by

$$R_g A_g - R'_g A'_g = R_a b \bar{x} \qquad \text{(A6.1.2)}$$

The depth of compression of concrete has to satisfy the following:

$$\bar{x} \leq \xi_{jg} h_o \qquad \text{(A6.1.3)}$$

$$\bar{x} \geq 2 a'_g \qquad \text{(A6.1.4)}$$

where

M_j is the moment resistance to ultimate strength requirement;

R_a is the compressive strength of concrete;

R_g is the tensile strength of tension reinforcement;

A_g is the area of tension reinforcement;

R'_g is the compressive strength of compression reinforcement;

A'_g is the area of compression reinforcement;

γ_c is the safety factor on concrete, taken as 1.25;
γ_s is the safety factor on reinforcement, taken as 1.25;
b is the width of section or rib of Tee-beam;
$\bar{x}$ is the neutral axis depth;
h_o is the effective height of section;
ξ_{jg} is a factor on compression zone of section, taken as 0.55 for Class II and III reinforcement;
a'_g is the distance between compression reinforcement and the top of section.

A6.1.2 THE DEFLECTION CRITERION

Clauses 4.2.1 to 4.2.3 give the requirements for the moment capacity under the limiting deflection condition. A maximum vertical deflection of 1/600th of the span is specified. The flexural stiffness of the structure is taken as $0.85\ E_h I_{o1}$ where E_h is the elastic modulus of concrete and I_{o1} is the moment of inertia of the cracked section at the ultimate limit state about the neutral axis.

A6.1.3 THE CRACK WIDTH CRITERION

Clauses 4.2.5 and 4.2.6 give the requirements for the calculation of moment capacity at the limiting cracking condition. The maximum crack width of rectangular, Tee or I beams is calculated by the following formula. A maximum crack width of 0.2 mm is specified.

$$\delta_{f_{max}} = C_1 C_2 C_3 \frac{\sigma_g}{E_g} \left(\frac{30 + d}{0.28 + 10\mu}\right) \qquad \text{(A6.1.5)}$$

where
C_1 is a factor on surface condition of reinforcement, taken as 1.4 for plain steel and 1.0 for high yield bars;
C_2 is a factor on load duration, taken as 1.0 for short-term loading;
C_3 is a factor on shape of bending element, taken as 1.0

for member with ribs and 1.15 for slab;

E_g is the elastic modulus of tension reinforcement;

d is the equivalent diameter of tension reinforcement in mm;

μ is the steel percentage calculated by

$$\mu = \frac{A_g}{bh_1 + (b_i - b)h_i} \quad \text{for} \quad 0.006 \leq \mu \leq 0.02 \qquad \text{(A6.1.6)}$$

b_i is the width of flange on tension edge;

h_i is the thickness of flange on tension edge;

h_1 is the distance between tension reinforcement to compression edge;

σ_g is the service stress on tension reinforcement calculated by the following formula;

$$\sigma_g = \frac{M}{0.87A_g h_1} \qquad \text{(A6.1.7)}$$